# Modelling Amyloidosis in Mice

By
Ivana Slamova

A thesis submitted in fulfilment of the requirements for the degree of Doctor of Philosophy

Centre for Amyloidosis and Acute Phase Proteins
Division of Medicine
University College London
2016

# Declaration

I, Ivana Slamova confirm that the work presented in this thesis is my own. Where information has been derived from other sources, I confirm that this has been indicated in the thesis. No portion of the work referred to in this thesis has been submitted in support of an application for another degree or qualification of this or any other university or institute of learning.

# Abstract

Amyloidosis is a group of disorders in which specific soluble proteins convert into insoluble extracellular fibrillar deposits. Certain mutations in amyloid-prone proteins result in aggressive forms of the disease.

$\beta_2$-microglobulin (β2m), a cell surface protein and transthyretin (TTR), a normal plasma protein, are inherently amyloidogenic. In patients undergoing long-term dialysis, ineffective clearance of β2m from the plasma results in sustained increase of its concentration and its deposition as amyloid. Wild-type TTR is the amyloid precursor in senile systemic amyloidosis, a cause of heart failure in the elderly, and various different mutations in the human TTR gene cause the autosomal dominant conditions familial amyloid polyneuropathy and familial amyloid cardiomyopathy.

The D76N β2m variant causes highly penetrant hereditary systemic amyloidosis. Similarly, the S52P TTR variant also causes aggressive amyloidosis which is characterised by prominent cardiac ATTR deposits. Animal models for Aβ2m amyloidosis and ATTR amyloidosis have long been sought to enable a better understanding of disease mechanisms and for validation of diagnostic methods and treatments, but previous attempts to model these diseases *in vivo* have met with limited or no success. The aims of this project were to generate mouse models of: (1) Aβ2m amyloidosis and (2) cardiac ATTR amyloidosis by transgenic expression of these highly amyloidogenic variants.

In the work presented here, hβ2m$^{D76N}$ transgenic mice and hTTR$^{S52P}$ transgenic mice were generated. Despite expressing high plasma concentrations of the amyloidogenic proteins, the mice did not spontaneously develop amyloidosis. After priming amyloid deposition with pre-formed amyloid fibrils, the hβ2m$^{D76N}$ transgenic mice failed to develop amyloid deposits. It is notable that most of the β2m circulates bound in a complex, potentially limiting the availability of free β2m monomers for conversion into fibrils. In the hTTR$^{S52P}$ transgenic mice, priming of amyloid deposition with amyloid fibrils led to consistent and reproducible development of cardiac ATTR amyloidosis.

# Acknowledgements

Firstly I would like to thank my supervisors, Dr Paul Simons and Dr Raya Al-Shawi who have led me through a very exciting research project over the last few years. They have been great mentors, providing encouragement, help and inspiration whenever it was needed. I would like to thank them not only for providing excellent scientific stimulation and support but also for guiding me through a very important part of my life. We have been through laughs and tears, and words cannot express enough how grateful I am that they have been in my life.

I would also like to thank my colleagues in the Centre for Amyloidosis and Acute Phase Proteins and staff in the National Amyloidosis Centre in the Royal Free Hospital – Michal Golos for his great help with never-ending genotyping and for giving me a hand with lots of other laboratory tasks, to Dr Stephan Ellmerich for his help with some animal work, Dr Patrizia Mangione and Prof Vittorio Bellotti for providing not only recombinant proteins and other experimental materials but mainly for their scientific ideas, support and discussions. I am also very grateful to Janet Gilbertson for her time, patience and discussions while sitting at the microscope with me and teaching me what is and what is not amyloid. I would also like to thank Nicola and Karen for their help and useful tips with tissue sectioning and immunohistochemistry, and to the Transgenic Unit staff for animal husbandry. I am also grateful to Prof Philip Hawkins and Prof Sir Mark Pepys for their support. It has always been a pleasure and fun to work with all these people.

Lastly, I express my warmest gratitude and love to my family and friends. To my mum, my dad and Verka for their love, support and for their incredible patience with me while I was busy and did not have time to see them. To my sister who has always been on the other side of the phone for me, day or night. To my Maida Vale friends for fun times and for help when some was needed (and for their not-so-funny jokes about my speed of writing). To Gid, whose friendship, great personality and delicious home-made Italian food often waiting for me in the kitchen after long days in the lab, have been a lifesaver. To Charlie, whose love, excitement for what I do, his belief in me and his support have been a driving force that has kept me going.

# Table of content

# List of Figures

# List of Tables

# Abbreviations

| | |
|---|---|
| AA | Serum amyloid A amyloid fibril protein |
| AApoAI | Apolipoprotein A-I amyloid fibril protein |
| AApoAII | Apolipoprotein A-II amyloid fibril protein |
| Ab | Antibody |
| Aβ2m | $\beta_2$-microglobulin amyloid fibril protein |
| AD | Alzheimer's disease |
| AEF | Amyloid-enhancing factor |
| AFib | Fibrinogen A α-chain amyloid fibril protein |
| AL | Immunoglobulin light chain amyloid fibril protein |
| ApoAI | Apolipoprotein A-I |
| ApoAII | Apolipoprotein A-II |
| ATTR | Transthyretin amyloid fibril protein |
| α2M | $\alpha_2$-macroglobulin |
| BSA | Bovine serum albumin |
| B2M | β2-microglobulin gene |
| β2m | β2-microglobulin |
| $\beta2m^{D76N}$ | β2-microglobulin variant with substitution of aspartate (D) residue at the position 76 of the mature protein with asparagine (N) residue |
| CIP | Calf intestine phosphatase |
| CPHPC | (R)-1-[6-[(R)-2-carboxy-pyrrolidin-1-yl]-6-oxo-hexanoyl] pyrrolidine-2-carboxylic acid (drug) |
| CSF | Cerebro-spinal fluid |
| CysC | Cystatin C |
| DNA | Deoxyribonucleic acid |
| DRA | Dialysis-related amyloidosis |
| dNTP | Deoxynucleoside triphosphate |
| DTT | Dithiothreitol |
| $dH_2O$ | Distilled water |
| ECL | Enhanced chemiluminescence |
| ELISA | Enzyme-linked immunosorbent assay |
| ERAD | Endoplasmic reticulum-associated degradation |
| FACS | Fluorescence-activated cell sorting |

| | |
|---|---|
| FAP | Familial amyloid polyneuropathy |
| FCS | Fetal calf serum |
| FcRn | IgG-Fc receptor |
| FITC | Fluorescein isothiocyanate |
| GAG | Glycosaminoglycan |
| GAPDH | Glyceraldehyde-3-phospate dehydrogenase |
| GS | Goat serum |
| hβ2m | Human β2-microglobulin |
| hCG | human chorionic gonadotropin |
| HS | Horse serum |
| hTTR | Human transthyretin |
| hTTR-MS | Fragment of human transthyretin gene |
| hTTR-NS | Fragment of human transthyretin gene |
| HRP | Horse radish peroxidase |
| H&E | Heamotoxylene and Eosin |
| IAPP | Islet amyloid polypeptide |
| $^{125}$I | Radioisotope of iodine |
| $^{125}$I-hSAP | $^{125}$I-labelled human serum amyloid P component |
| KO | Knock-out |
| L | Immunoglobulin light chain |
| mβ2m | Mouse β2-microglobulin |
| MCS | Multiple cloning site |
| MRI | Magnetic resonance imaging |
| MHC | Major histocompatibility complex |
| MT | Mouse metallothionein-I |
| mRNA | Messenger RNA |
| mTTR | Mouse transthyretin |
| NAC | National Amyloidosis Centre |
| NBF | Neutral buffered formalin |
| NK cells | Natural killer cells |
| ΔN6β2m | $\beta_2$-microglobulin fragment lacking the first six N-terminal residues |
| PBS | Phosphate buffered saline |
| PBST | Phosphate buffered saline with tween 20 |

| | |
|---|---|
| PCR | Polymerase chain reaction |
| PFA | Paraformaldehyde |
| PMS | Pregnant mare's serum |
| PVDF | Polyvinylidene difluoride |
| RBP | Retinol-binding protein |
| RE | Restriction enzyme |
| RNA | Ribonucleic acid |
| RT-PCR | Reverse-transcription polymerase chain reaction |
| SAA | Serum amyloid A protein |
| SAP | Serum amyloid P component |
| SD | Standard deviation |
| TMB | Tetramethylbenzidine |
| TTR | Transthyretin |
| $TTR^{S52P}$ | Transthyretin variant with substitution of aspartate serine (S) residue at the position 52 of the mature protein with proline (P) residue (applies to other TTR variants accordingly) |
| TAP | Transporter associated with antigen processing |
| $T_3$ | 3,5,3'-triiodothyronine |
| $T_4$ | Thyroxine |
| TBG | Thyroxine-binding globulin |
| WT | Wild-type |
| $^{99m}Tc$ | Nuclear isomer of an isotope of technetium |
| $^{99m}Tc$-DPD | 99m-Technetium labelled 3,3-diphosphono-1,2- propanodicarboxylic acid |

# 1 Introduction

## 1.1 Amyloidosis

The biological functions of proteins are directly linked to their specific three-dimensional structures. Normally, incorrectly folded proteins trigger complex biological responses causing degradation of such proteins. However, failure of these systems can cause a loss of protein function or overabundance and aggregation of misfolded proteins, resulting in protein misfolding disorders. Amyloidoses represent the largest group of misfolding diseases where specific proteins convert from their soluble functional state into amyloid, a highly organised insoluble fibrillar material, deposited in extracellular spaces causing the disruption of tissue structure and function *(Sipe et al., 2014)*.

More than 30 proteins have been identified to form amyloid in humans *(Sipe et al., 2014)*, with the number increasing every year. Classification of the amyloidoses is based on the precursor protein that forms the amyloid fibrils and the distribution of amyloid deposition *(Sipe et al., 2014)*. Amyloidosis can be local, where the amyloid is restricted to a particular organ or tissue of precursor protein synthesis, or systemic with the amyloid present in any viscera, blood vessel walls and connective tissue. These two can be further grouped into acquired or hereditary amyloidoses *(Pepys, 2006)*. Acquired amyloidosis is often a complication of a pre-existing primary disease that produces an amyloidogenic abnormal protein (e.g. the monoclonal immunoglobulin light (L) chains of AL amyloidosis) or prolonged production of a normal protein that is capable of being converted into amyloid (e.g. serum amyloid A (SAA) protein in AA amyloidosis). Hereditary amyloidosis is caused by mutant genes encoding variant proteins whose structure makes them particularly amyloidogenic (e.g. mutations in the gene for transthyretin (TTR) in ATTR amyloidosis).

In amyloidosis, the presence of amyloid deposits is the cause of the clinical manifestations of the disease. Protein misfolding into amyloid also

accompanies other disease, e.g. Aβ peptide within the brain in Alzheimer's disease *(Glenner and Wong, 1984, Lu et al., 2013, Haass and Selkoe, 1993)*, islet amyloid polypeptide (IAPP) in the pancreatic Islets of Langerhans in type 2 diabetes mellitus *(Melato et al., 1977, Jurgens et al., 2011)*; but these are not classified as amyloidosis, because it is not established that amyloid causes these diseases.

## 1.2 Amyloid and amyloid fibrils

Amyloid refers to a highly organised, insoluble fibrillar material that is deposited mainly in the extracellular spaces of organs and tissues as a result of changes in protein folding *(Pepys, 2006)*. Amyloid can form from disordered proteins that lack a well-defined tertiary structure or from partial unfolding of proteins that normally have well-defined tertiary structure *(Chiti and Dobson, 2006)*. Once amyloid deposition has been initiated, and with continued production and abundance of the precursor protein, amyloid fibrils formation persistently progresses. Amyloid deposits are remarkably stable and inert, and natural clearance mechanisms are very inefficient *(Pepys, 2001, Gillmore et al., 2001)*. However, amyloid deposits are in a state of dynamic turnover and can regress if new fibril formation is halted *(Tan and Pepys, 1994, Hawkins et al., 1993)*. Mechanisms of natural regression are unknown.

The identification of amyloid depends on its ability to bind the dye Congo red and exhibit green, yellow or orange birefringence when the stained deposits are viewed under polarised light *(Puchtler H, 1962)*. The optical effect is a result of alignment of the dye molecules along the fibrils. Congo red staining is not a very sensitive test and requires an adequate amount of amyloid, technically correct staining, high quality microscope and adequate observer experience.

Isolated amyloid fibrils can be imagined *in vitro* using transmission electron microscopy or atomic force microscopy. These imaging techniques revealed that all amyloid fibrils are straight, rigid, non-branching and consist of a number (usually 5 or 6) of protofilaments, each of which is about 2-5 nm in diameter *(Serpell et al., 2000)*. These protofilaments twist together to form rope-like fibrils that are 7-13 nm wide *(Serpell et al., 2000)*. X-ray diffraction analyses have shown that in each protofilaments, the protein molecules are arranged so that the peptide chain forms β-strand that run perpendicularly to the fibril long axis, regardless of the protein from which they are formed *(Sunde et al., 1997)*. A schematic picture of an amyloid fibril is shown in figure 1.1. Apart from Congo red, the amyloid fibrils also bind thioflavin T but this binding is less specific *(Nilsson, 2004)* and other detection techniques are under investigation *(Sjolander et al., 2016)*.

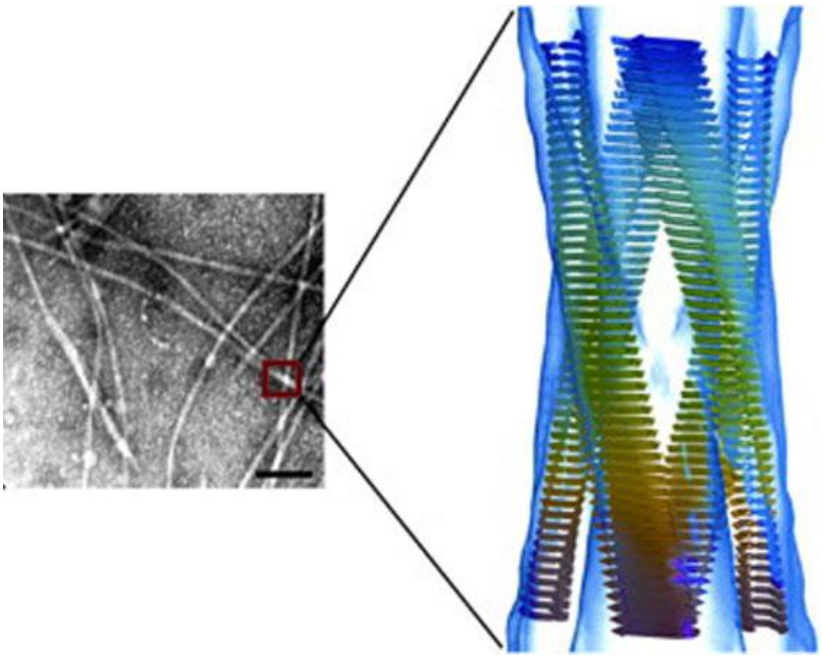

***Figure 1.1: Amyloid fibrils***

*Amyloid fibrils viewed under electron microscope (left) and their schematic structure (right). The mature amyloid fibril is formed from twisted protofilaments. Each protofilament is formed of β-strand peptide chain running perpendicularly to the fibril long axis.*

The amyloidoses differ in the protein precursors aggregating into amyloid fibrils, the tissue and organs involved in amyloid deposition and consequently in the clinical features. Different amyloidoses (as defined by precursor protein) have different characteristic patterns of deposition. In systemic amyloidosis, the damage mostly occurs at tissue distant from the site of the precursor protein synthesis *(Pepys, 2006)*. The process of fibril formation in extracellular spaces results in displacement of parenchymal tissue by amyloid deposits, causing tissue damage and organ dysfunction *(Pepys, 2006)*.

### 1.2.1 Amyloid fibril formation

Amyloid formation *in vivo* occurs with normal wild-type proteins and with genetically variant amyloidogenic proteins. However, amyloid deposits do not appear immediately in any case and amyloidosis is extremely rare in children and young adults *(Pepys, 2006)*. There is always a lag phase, often of many years, before the deposition of clinically significant amyloid *(Pepys, 2006)*. The lag phase is believed to be the time required for formation of “nuclei” or “seeds” which then act as templates for amyloid-fibril growth *(Serio et al., 2000, Kisilevsky, 2000)*. Once the seeds are formed, a process which occurs stochastically *in vivo*, amyloid formation is autocatalytic and progressive, given the continued supply and/or abundance of the precursor protein. In animal models of amyloidosis, the lag phase can be greatly shortened by administration of an amyloid-containing tissue extract *(Baltz et al., 1986a, Hol et al., 1986)* or by isolated amyloid fibrils *(Liu et al., 2007, Johan et al., 1998)*. *In vitro*, purified proteins can be converted into amyloid-like fibrils without any additional biological molecules, although the conditions under which this conversion happens are usually not physiological and require e.g. low pH, high temperature and/or organic solvents, which promote the proteins partial unfolding *(Myers et al., 2006b, Picotti et al., 2007, Lashuel et al., 1998, Verdone et al., 2002)*. The possibility to form amyloid fibrils *in vitro* has led to

extensive experiments of protein fibrillogenesis studying the underlying mechanisms of such processes. From the outcomes of such experiments, it is generally believed that the conversion of a soluble monomeric peptide into insoluble mature amyloid fibrils involves a partially unfolded intermediate that is thermodynamically unfavourable and rapidly progresses to the stable amyloid form *(Litvinovich et al., 1998, Kelly, 1998, Teplow, 1998, Quintas et al., 2001)*. The studies on kinetics of this transition then proposed the above mentioned nucleation dependent model, when a heterogeneous “nucleus” is formed consisting of oligomeric misfolded protein. Such seed then acts as a template in the polymerization step when normally folded monomeric polypeptides bind to the nucleus forming wide variety of structures from small soluble oligomers to large amyloid fibrils *(Kisilevsky, 2000)*. Seeding with natural or synthetic pre-formed fibrils accelerates fibrillogenesis *in vitro (Myers et al., 2006a)*.

During the fibril formation, several multimeric or polymeric non-fibrillar structures have been identified. These include very early species called oligomers (dimers, trimers, teteramers) and later beaded-like structures up to 200 nm in length called protofibrils *(Walsh et al., 1999, Harper et al., 1997, Walsh et al., 1997, Ionescu-Zanetti et al., 1999)*. These are believed to be soluble intermediates in the formation of mature, insoluble amyloid fibres.

### 1.2.2 Amyloid associated molecules

Each type of amyloid is characterised by the amyloid-precursor protein that forms the core. Irrespective of the amyloid protein, there are common additional non-fibrillar constituents found in all amyloid deposits *in vivo* but their function in not fully understood. These minor constituents include glycosaminoglycans *(Pras et al., 1971)*, serum amyloid P *(Baltz et al., 1986b)*, apolipoprotein E *(Wisniewski and Frangione, 1992)*.

*Glycosaminoglycans* (GAGs) are linear polysaccharides ubiquitously present in all mammalian organs and tissues, mostly in extracellular spaces and on the cell surface. GAGs – mostly heparan sulphate, chondroitin sulphate and dermatan sulphate have been co-purified and ultrastructurally co-localised with various amyloid fibrils *(Nelson et al., 1991, Magnus et al., 1992)*. They may contribute to amyloid fibrillogenesis and stabilization of the fibril structure *(Pras et al., 1971, Nelson et al., 1991, Madine et al., 2013)*.

*Serum amyloid P* component (SAP), a normal circulating plasma protein, is a member of the pentraxin protein family, that is secreted and catabolised by hepatocytes *(Hutchinson et al., 1994)*. SAP reversibly binds to all amyloid deposits *in vivo* and accounts for up to 15% of their mass *(Pepys et al., 1979)*. It has been shown that SAP stabilizes amyloid fibrils and protects them from degradation by proteases and phagocytic cells *in vitro (Tennent et al., 1995)* and contributes to amyloidogenesis *in vivo (Botto et al., 1997)*. The occurrence of SAP in all types of amyloid and the binding of SAP to amyloid has found its use in diagnosis and quantitative monitoring of amyloid deposits by intravenous injections of radioactively labelled SAP (SAP scintigraphy) *(Hawkins et al., 1990a)*, which is introduced below.

### 1.2.3 Pathogenicity of amyloid

The physical presence of amyloid deposits in extracellular spaces results in displacement of parenchymal tissue causing a disruption of tissue structure and function, and organ dysfunction. Increasing amyloid load increases the severity of the disease and stabilization or regression of amyloid deposits is associated with clinical stability or improvement of amyloidosis patients *(Pepys, 2006)*.

Recently, the cytotoxicity of amyloid fibrils and pre-fibrillar amyloid deposits has been debated. It has been suggested by *in vitro* studies that pre-fibrillar intermediates have a cytotoxic effect on cells of the affected tissue inducing

oxidative stress and cell apoptosis *(Bucciantini et al., 2004, Lorenzo et al., 1994, Reixach et al., 2004, Walsh et al., 2002)*. In a mouse model, the site of amorphous TTR aggregates coincided with an increase of oxidative stress in the tissue which may be caused by cytotoxic effects of the TTR aggregates on surrounding cells *(Sousa et al., 2002)*. Thus, although amyloid is inert, and amyloidosis is defined by the presence of mature amyloid deposits, cytotoxic pre-fibrillar material may in some cases contribute to clinical disease.

## 1.3 Epidemiology of amyloidosis

Although more than 30 different amyloid proteins cause amyloidosis, 5 types of amyloidosis account for ~95 % of all amyloidoses *(Wechalekar et al., 2016, Takahashi et al., 2016, Aguirre et al., 2016)* – immunoglobulin light chain (AL) amyloidosis, serum amyloid A (AA) amyloidosis, transthyretin (ATTR) amyloidosis, β2-microglobulin (Aβ2m) amyloidosis and fibrinogen A α-chain (AFib) amyloidosis. Characteristics of the common types of amyloidoses are shown in Table 1.1. Death certificates from the UK indicate that amyloidosis is a cause of death in 0.58 per 1000 individuals *(Pinney et al., 2013a)*. The incidence of amyloidosis in the UK is ~0.4 per 100 000 population with the incidence peak at age 60-79 years *(Pinney et al., 2013a)*.

Patterns of referrals have changed considerably over the last 20 years in the National Amyloidosis Centre (NAC) in the UK *(Wechalekar et al., 2016)* – the frequency of AL amyloidosis has remained stable (67 % of all cases – as a proportion of total referrals per year), a substantial decrease has been seen in AA amyloidosis (from 32 % to 6.8 % of all cases) which probably reflects improvement of treatment of inflammatory arthropathies, whereas wild-type ATTR amyloidosis-related cardiomyopathy has increased greatly (from 0.2 % to more than 6.4 %) *(Wechalekar et al., 2016)*.

| Fibril protein | Precursor protein | Acquired or Hereditary | Patients seen in the UK-NAC | Underlying disorder | Main target organs |
|---|---|---|---|---|---|
| **AL** | Immunoglobulin light chain (L) | Acquired | 4067 (68%) | Plasma cell dyscrasia | H, K, L, PN |
| **AA** | Serum amyloid A (SAA) | Acquired | 633 (12%) | Inflammatory disorders | K, (late – L, H) |
| **ATTR** | Transthyretin (TTR), wild-type | Acquired | 168 (3.2%) | Not known | H |
| | Transthyretin (TTR), variants | Hereditary | 339 (6.6%) | Mutations in TTR gene | PN, H |
| **AFib** | Fibrinogen A (Fib), variants | Hereditary | 87 (1.7%) | Mutations in Fib gene | K |
| **ALect2** | Leukocyte chemotactic factor-2 (Lect2) | Acquired | 16 (0.3%) | Not known | K, L |
| **AApoAI** | Apolipoprotein AI (ApoAI), variants | Hereditary | 40 (0.8%) | Mutations in ApoAI gene | K, L |
| **ALys** | Lysozyme (Lys), variants | Hereditary | 17 (0.3%) | Mutations in Lys gene | L, K |
| **AGel** | Gelsolin (Gel), variants | Hereditary | 4 (0.1%) | Mutations in Gel gene | PN |
| **Aβ2m** | $\beta_2$-microglobulin (β2m), wild-type | Acquired | 93 (1.8%) | Long-term dialysis | MS system |
| | $\beta_2$-microglobulin (β2m), variant | Hereditary | - | Mutation in β2m gene | PN, A, S, L, H |

***Table 1.1: Characteristics of the common types of systemic amyloidoses***

*Frequency of different amyloid types among 5100 individuals with amyloidosis assessed in the National Amyloidosis Centre (NAC) in the UK from 1987 to 2012. Amyloid fibril protein is designated letter A and followed by the abbreviation of the precursor protein name. H=heart, K=kidney, L=liver, PN=peripheral nervous system, MS=muscular-skeletal system, A=adrenal, S=spleen. (Amended from Wechalekar et al., 2016.)*

## 1.4 Types and clinical features of systemic amyloidoses

Amyloidoses are heterogeneous affecting multiple organs and the clinical features of systemic amyloidosis are rarely specific to one type of amyloidosis. Moreover, some types of amyloidoses invariably affect a specific organ (e.g. wild-type ATTR amyloidosis always affects the heart) whereas involvement of a specific organ ranges from absent to severe in other types of amyloidosis *(Wechalekar et al., 2016)*. In this section, the involvement of major organs in different types of amyloidoses is introduced.

Heart is the most common organ involved in amyloidosis and cardiac amyloidosis is the most prominent cause of morbidity and mortality in amyloidosis *(Wechalekar et al., 2016, Takahashi et al., 2016)*. The most common forms of cardiac amyloidosis are the AL and ATTR types. In AL amyloidosis, cardiac amyloid occurs in ~50 % of patients *(Merlini, 2012, Patel and Hawkins, 2015)*. Cardiac involvement is the dominant feature in wild-type ATTR amyloidosis and some hereditary ATTR amyloidoses *(Patel and Hawkins, 2015)*, although in some TTR variants cardiac amyloid is uncommon (e.g. V30M) or not reported *(Connors et al., 2003)*. Amyloid in the heart is also a common feature in apolipoprotein A-I (ApoAI) amyloidosis *(Patel and Hawkins, 2015)*. Amyloid deposition in the heart results in progressive thickening of ventricular walls, increases myocardial stiffness and ventricular filling pressure, which leads to atrial enlargement and atrial fibrillation and can cause systemic embolic events *(Feng et al., 2007)*. The most common types of death in cardiac amyloidosis are progressive heart failure and arrhythmia *(Selvanayagam et al., 2007)*.

The kidneys are most commonly involved in AA, AL, AFib and ApoAI amyloidoses *(Lachmann et al., 2007, Merlini et al., 2014, Wechalekar et al., 2016, Gregorini et al., 2005, Stangou et al., 2010)* and renal amyloid is often a source of morbidity. The clinical manifestation of renal amyloid is proteinuria or renal dysfunction, with varying degrees of renal insufficiency. Amyloid can be found anywhere in the kidney but deposition in the glomeruli predominates *(Dember, 2006)*. Renal impairment tends to progress more rapidly when the amyloid is deposited in the glomeruli of the kidney than in the interstitium of the kidney tubules *(Dember, 2006)*.

Autonomic and peripheral nerves are another major sites involved in AL amyloidosis, some hereditary forms of ATTR amyloidosis, ApoAI amyloidosis and hereditary β2m amyloidosis *(Wechalekar et al., 2016, Sousa et al., 1993, Valleix et al., 2012, Adams, 2001)*. Peripheral neuropathy is usually axonal and begins with loss of sensation of cold and heat and with feeling of pins and needles. The sensory neuropathy is followed by motor neuropathy with loss of

extensor function of toes and feet causing unstable walking *(Carr et al., 2016)*. Autonomic neuropathy is manifested by urinary incontinence, sweat abnormalities, diarrhoea alternating with constipation, erectile dysfunction, orthostatic hypotension *(Gertz et al., 2015)*.

Carpal tunnel syndrome is a common complication of ATTR amyloidosis and acquired β2m amyloidosis *(Kopec et al., 2011, Sekijima et al., 2011)*. It results from compression of median nerve and its entrapment in the carpal tunnel by amyloid deposits.

Amyloid deposits in the liver are very common in AL amyloidosis, in later stages of AA amyloidosis, in ApoAI amyloidosis and AFib amyloidosis *(Lachmann et al., 2007, Wechalekar et al., 2016, Janssens et al., 2010)*. The clinical manifestations of hepatic amyloid are mild. Accumulation of amyloid may increase the rigidity of the liver parenchyma resulting in higher liver stiffness *(Janssens et al., 2010)*. Amyloid is also commonly found in spleen in systemic amyloidosis but usually asymptomatic. An atraumatic rupture of amyloidotic spleen has been reported but is extremely rare *(Renzulli et al., 2009)*.

Gastrointestinal involvement is common in systemic amyloidosis and about 30-60 % of patients develop gastrointestinal symptoms *(Friedman and Janowitz, 1998, Petre et al., 2008)*. Amyloid in the tongue is a characteristic of AL amyloidosis and is present in 10-23 % patients with AL amyloidosis *(Kyle and Gertz, 1995)*. Hereditary ATTR amyloidosis often manifests with gastrointestinal symptoms but these may occur due to autonomic polyneuropathy.

Amyloid deposits in fat tissue are almost universal but asymptomatic *(Westermark and Stenkvist, 1973)*.

Although the amino acid sequence of proteins and the sustained supply of the relevant protein dictate the potential of a protein to form amyloid, the mechanisms that influence the preferential site of amyloid deposition are not yet understood. Genetic and/or environmental factors also play an important role in susceptibility to amyloid formation. This is apparent for example in

cases when the same V30M variant TTR, responsible for familial amyloid polyneuropathy has a later onset and lower penetrance in the Swedish form of the disease *(Sousa et al., 1993, Hellman et al., 2008)* than in the Portuguese and Japanese populations, in which the onset is much earlier and the penetrance is much higher *(Tawara et al., 1983, Plante-Bordeneuve et al., 2003)*.

## 1.5 Diagnosis of amyloidosis

Amyloidoses are complicated to diagnose because of different organs systems involvement and the localisation of amyloid deposits varies according to the amyloidogenic protein. They are often diagnosed in advanced stage of the disease because amyloidosis is only considered when the various more common causes of the symptoms have been ruled out. The diagnosis of amyloidosis includes careful clinical evaluation, confirmation of amyloid deposition, identification of amyloid type, assessment of the underlying amyloidogenic disorder, and evaluation of the extent of amyloidotic organ involvement. Family history is also important for diagnosis of hereditary amyloidosis.

The diagnosis of amyloid relies on histological analysis of affected organ biopsies stained with the dye Congo red after which the amyloid appears red under bright field illumination and turns orange, yellow or green with polarised light (Figure 1.2). Biopsy of subcutaneous fat is often used for histological diagnosis of amyloid *(Westermark and Stenkvist, 1973)*.

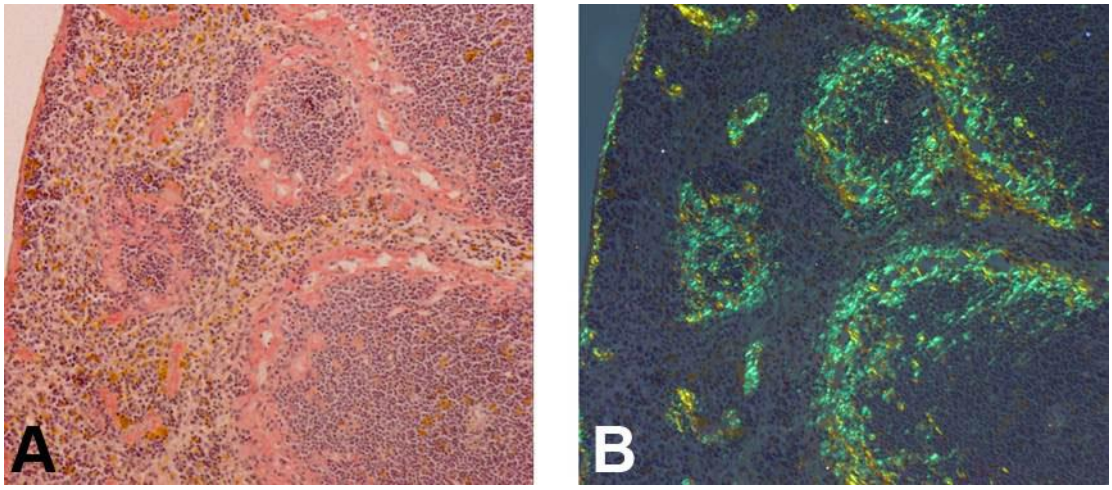


***Figure 1.2: Identification of amyloid by Congo red***

*Amyloid in a tissue specimen binds the dye Congo red. In a light microscope, the amyloid appears red under bright field (A) and turns green/orange when a polarization filter is applied (B). AA amyloid in mouse spleen.*

---

Immunohistochemical staining of tissue containing amyloid is the most widely available method to identify the specific amyloid fibril protein *(Schonland et al., 2012)*. Mass spectrometry of amyloidotic material is now also used for fibril typing. This analysis involves laser microdissection and capture of Congo red-positive material from fixed tissue section with a laser-capture microscope. Computer algorithms then match the material to a protein reference database *(Vrana et al., 2009, Gilbertson et al., 2015)*. This is technically challenging and requires validation in each laboratory before routine clinical use *(Wechalekar et al., 2016)*. When hereditary systemic amyloidosis is suspected, gene sequencing is performed.

In AL and AA amyloidoses, identification of the underlying disorder is an important step in diagnosis. Measurement of free immunoglobulin light chain in serum is required to detect monoclonal protein underlying AL amyloidosis *(Palladini et al., 2009)* and is informative in 95 % of cases *(Lachmann et al., 2003)*. In AA amyloidosis, identification of the underlying inflammatory

disorder responsible for elevated levels of the amyloidogenic serum amyloid A (SAA) protein is needed. However, sometimes the cause of elevated SAA levels is not known.

SAP scintigraphy, a non-invasive method using radiolabelled SAP as a specific tracer for amyloid, is used to evaluate the amyloid load *in vivo (Hawkins et al., 1988, Hawkins et al., 1990a)*. SAP, a normal plasma protein, binds avidly to all amyloid of human systemic amyloidoses and becomes concentrated at the sites of amyloid deposition. The fact that there is constant equilibrium between the circulating and the amyloid-bound SAP and that the amount of amyloid-bound SAP correlates with the quantity of amyloid present in the tissues *(Baltz et al., 1986b)* led to the development of a specific and quantitative *in vivo* tracing method for systemic amyloid deposition *(Hawkins et al., 1990a)*. This clinical method uses intravenously administered radiolabelled $^{125}$I-human SAP ($^{125}$I-hSAP) which is distributed between the plasma and the amyloid deposits. $^{125}$I-hSAP which retains in the body bound to amyloid then enables screening of the amyloid burden in amyloidosis patients (Figure 1.3). It has been shown that SAP scintigraphy is a safe and non-invasive technique providing information on the presence, distribution, extent and regression of amyloid deposits of all types which can be used repeatedly *(Hawkins et al., 1993)*. Major limitation of this technique is that it is unable to image amyloid in the moving heart. SAP scintigraphy is only available in NAC in London and in the University of Groningen in the Netherlands *(Wechalekar et al., 2016)*.

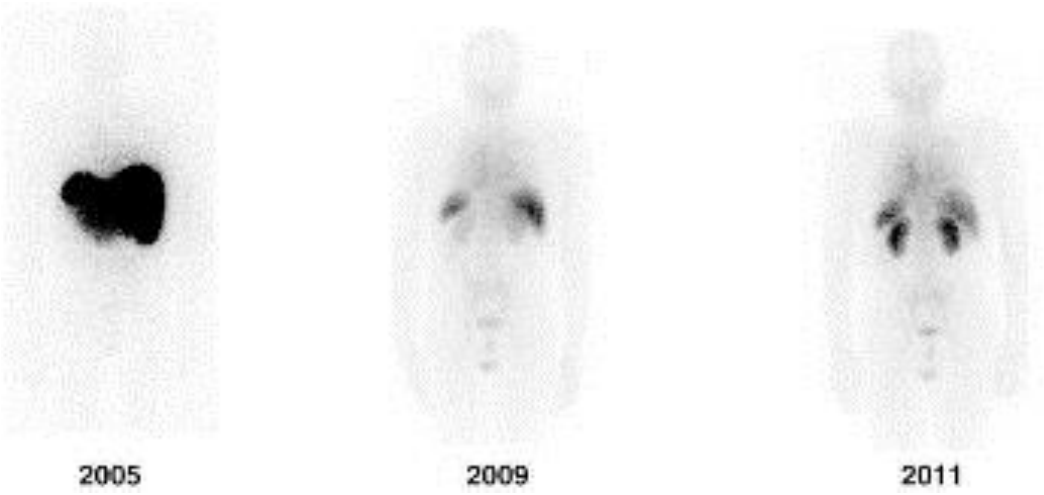


***Figure 1.3: SAP scintigraphy scans from a patient with AL amyloidosis***

*SAP scintigraphy scans from a patient with AL amyloidosis. In 2005, heavy amyloid deposits were seen on the scan in liver and spleen. In 2009, after a good response to treatment, a considerable regression of the deposits were observed. In 2011, the scan showed a relapse with amyloid deposits in the kidneys (Pepys et al., 2012).*

---

Cardiac amyloidosis is commonly assessed by echocardiography revealing ventricular wall thickening and diastolic dysfunction. Cardiac magnetic resonance imaging (MRI) is more precise and reproducible than echocardiogram *(Maceira et al., 2005)*. Cardiac MRI can give accurate anatomical information, including the wall thickness and allows quantification of the myocardial interstitial volume fraction, which is greatly expanded in amyloidosis *(Banypersad et al., 2013)*. Recently, it has been observed that scintigraphy with 99m-technetium ($^{99m}$Tc) labelled phosphate derivatives used commonly as a bone nuclear tracer, detects amyloid in some cases. Interestingly, the bone tracer is highly sensitive for ATTR amyloid and some AL amyloid *(Puille et al., 2002)*. This method has been studied in order to validate its use for evaluation of cardiac amyloid *(Perugini et al., 2005, Puille et al., 2002, Hutt et al., 2014)*.

## 1.6 Treatment of amyloidosis

Supportive care to maintain organ function is crucial for all types of amyloidosis. Liver transplantation to remove the hepatic source of the genetically variant amyloidogenic protein has been performed in selective patients with ATTR, AApoAI and AFib amyloidoses *(Wechalekar et al., 2016)*.

To date, the most effective treatment of systemic amyloidosis is focused on the reduction in the supply of the amyloid fibril precursor protein so that amyloid deposition ceases and regression of existing amyloid deposits can occur *(Pepys, 2006)* However, this is not yet possible for some types of amyloidosis *(Wechalekar et al., 2016)*. The treatment of the most common types of amyloidoses is briefly introduced.

Treatment of AL amyloidosis involves chemotherapy that targets the underlying clonal plasma cell dyscrasia which leads to a rapid reduction in production of amyloidogenic light chains by the B-cells, limiting progressive damage to amyloidotic organs *(Comenzo et al., 2012)*. However, treatment toxicity on amyloidotic organs with reduced function requires frequent assessment and a possible rapid change in treatment. Although the survival in patients with AL amyloidosis has increased over the past few years, nearly 25 % of all patients still die of disease-related complications within a few months of diagnosis *(Wechalekar et al., 2016)*. Chemotherapy followed by autologous stem cell transplant has shown very good results leading to improvement in organ function and survival of AL amyloidosis patients *(Dispenzieri et al., 2013, Cibeira et al., 2011)*. No particular treatment combination has yet been shown to reduce early cardiac deaths in AL patient with advanced progression of the disease *(Wechalekar et al., 2013)*.

In AA amyloidosis, the crucial step in management of the disease is a reduction of SAA production with treatment of the underlying inflammatory disorder causing the elevated concentrations of circulating SAA *(Lachmann et al., 2007)*.

Other promising strategies in treatment of systemic amyloidosis which are in development are based on the prevention of amyloid formation. This may be achieved by stabilization of the fibril precursor protein in order to inhibit its misfolding which is of particular interest in transthyretin amyloidosis and this strategy is discussed in transthyretin amyloidosis chapter together with RNA-inhibiting therapies targeting the synthesis of TTR. Tetracyclines, and in particular Doxycycline have been shown to inhibit fibril formation and disrupt amyloid fibrils *in vitro (Giorgetti et al., 2011, De Luigi et al., 2008)* and experiments in animal models suggested similar effects *in vivo (Aitken et al., 2010, Cardoso and Saraiva, 2006)*. On the basis of these studies, clinical trials designed to evaluate the efficacy, tolerability and safety of doxycycline are under investigation showing beneficial effects on stabilization of the disease progression in ATTR amyloidosis *(Obici et al., 2012)*, AL amyloidosis *(Wechalekar et al., 2015)* and pain relief in Aβ2m amyloidosis *(Montagna et al., 2013)*.

Another approach in treatment of amyloidosis is interfering with the interactions between amyloidogenic protein and additional molecules contributing to fibril aggregation. Inhibition of the interaction between GAGs and amyloid fibrils *(Kisilevsky et al., 2007)* is a possible approach to treatment of amyloidosis, and Eprodisate which acts in this way has been reported to slow the decline of renal function in AA amyloidosis *(Dember et al., 2007)*.

Recently, a novel immunotherapeutic approach of directly targeting amyloid deposit for removal has been reported *(Bodin et al., 2010)*. This strategy uses antibody that targets SAP, a common non-fibrillar component of amyloid deposits which binds to all amyloid fibrils *(Pepys et al., 1979)*. The use of SAP as the target means that the same treatment is, in principle, suitable for all types of amyloid. In order to prevent immune complex formation between circulating SAP and the therapeutic antibody, the circulating SAP protein is depleted using the drug CPHPC *(Pepys et al., 2002, Gillmore et al., 2010)*. CPHPC cross-links the SAP pentamers to form decamers that are rapidly cleared by the liver *(Pepys et al., 2002)* SAP remaining in the amyloid then

provides a specific target for the antibody. In mouse models of AA amyloidosis, this treatment approach resulted in activation of complement on the deposits thereby attracting and engaging macrophages which then fused to multinucleated giant cells capable of engulfing and rapidly clearing amyloidosis masses *(Bodin et al., 2010, Simons et al., 2013)*. These results led to human phase I clinical trial of anti-SAP antibody treatment, which has reported extremely promising results with rapid reduction in liver amyloid deposits *(Richards et al., 2015)*. Data on efficacy in cardiac and renal disease are awaited *(Richards et al., 2015, Wechalekar et al., 2016)*.

# 1.7 $\beta_2$-microglobulin amyloidosis

## 1.7.1 $\beta_2$-microglobulin

$\beta_2$-microglobulin (β2m) is a 11.7 kDa protein ubiquitously expressed by all nucleated cells. It was first described in 1968 by Bergaard and Bearn who isolated the protein from urine of patients with renal proximal tubular disorders *(Berggard and Bearn, 1968)*. Subsequent amino-acid sequence studies of β2m revealed its similarity with an immunoglobulin polypeptide chain *(Peterson et al., 1972)* leading to a discovery that β2m is an integral part of histocompatibility antigens on a cell surface *(Grey et al., 1973, Peterson et al., 1974)*. Evidence was then provided that murine histocompatibility antigen also contains a polypeptide subunit analogous to its human β2m counterpart *(Rask et al., 1974)*. β2m and its role in immune system as a part of major histocompatibility complex (MHC) class I molecules expressed by all nucleated cells has been since well characterised.

### 1.7.1.1 $\beta_2$-microglobulin and MHC class I

MHC class I is a plasma membrane heterodimer capable of binding and presenting peptides from intracellular proteins to cytotoxic $CD8^+$ T-lymphocytes. Peptides derived from normal cellular self-proteins are ignored by the $CD8^+$ T-lymphocytes *(Jardetzky et al., 1991)*, whereas peptides derived from mutated proteins or from pathogenic proteins trigger an adaptive immune response trough binding to $CD8^+$ T-cells presented by MHC class I. MHC class I also play an important role in innate immunity through natural killer (NK) cells. NK cells have the ability to recognize and non-specifically kill cells lacking self MHC class I molecules, e.g. tumour cells *(Bessoles et al., 2014, Kim et al., 2005)*.

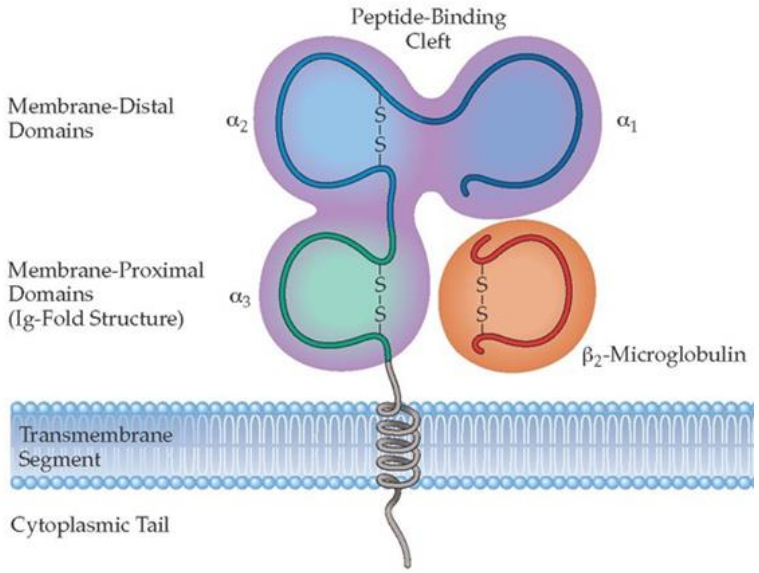


***Figure 1.4: MHC class I molecule***

*MHC class I molecules are present on the membrane distant surface of all nucleated cells. The complex consists of two polypeptide chains – heavy chain made of three domains ($\alpha_1$, $\alpha_2$, $\alpha_3$) and a non-covalently associated light chain, $\beta_2$-microglobulin. The heavy chain binds the peptide fragment and so determines the antigen specificity, $\beta_2$-microglobulin stabilizes the complex on the cell surface.*

---

The MHC class I molecule is a heterodimer composed of a 47 kDa heavy chain glycoprotein and a non-covalently associated 11.7 kDa β2m protein. The complex folds and assembles in the endoplasmatic reticulum (ER), where the newly synthesized heavy chain interacts with β2m protein through the assistance of chaperones calnexin *(Diedrich et al., 2001, Degen et al., 1992)*, calreticulin *(Sadasivan et al., 1996)*, tapasin *(Ortmann et al., 1997)* and the thiol oxidoreductase ERp57 *(Morrice and Powis, 1998)*. These chaperones together with the heavy chain, β2m and a transporter protein TAP *(Ortmann et al., 1994)* form a MHC class I loading complex *(Cresswell et al., 1999)*. The release of the MHC class I dimer from the loading complex is induced when an antigenic peptide binds to the peptide-binding side of the MHC class I *(Knittler et al., 1999, Jackson et al., 1994)*.

The peptides presented by MHC class I come from defective ribosomal translation products *(Yewdell et al., 1996)* and from functional mature proteins *(Colbert et al., 2013)*, both degraded by proteasomes in cytosol. The peptides are actively transported from the cytosol into the ER by the Transporter Associated with antigen Processing (TAP) (Shepherd et al., 1993). TAP interacts with MHC class I loading complex, allowing peptides to reach the MHC class I peptide-binding groove *(Sadasivan et al., 1996)*.

The fully assembled peptide-MHC class I complex then leaves ER via the Golgi apparatus to the plasma membrane where the bound peptide is exposed extracellularly, accessible to $CD8^+$ T-lymphocytes *(Swain, 1983)*. β2m bound to the heavy chain domain stabilizes the complex on the cell surface but is not directly involved in the interaction with the MHC-bound peptide fragment *(Otten et al., 1992)* (Figure 1.4).

The importance of β2m in the MHC class I assembly and transport to the cell surface was shown in transgenic mice with disrupted β2m gene. These mice lack MHC class I antigens on the cell surface and are deficient in $CD4^-$ $CD8^+$ T-cells *(Zijlstra et al., 1990, Koller et al., 1990)*.

The type of bound peptide, the binding affinity of such peptides and interactions with T-cells, play a role in MHC class I turnover *(Tsomides et al., 1991, Eberl et al., 1996)*. After the dissociation of the peptide from the MHC class I on the cell surface, the complex is destabilised, β2m is released into the circulation and the membrane-bound heavy chains are endocytically internalised and destroyed in lysosomes *(Cresswell et al., 1974, Machold and Ploegh, 1996)*.

#### 1.7.1.2 $\beta_2$-microglobulin associated with other membrane molecules

Similar to its function in MHC class I, β2m is non-covalently bound to a CD1 heavy chain and is essential for processing and the surface transport of CD1 complex *(Bauer et al., 1997)*. CD1 molecules comprise a group of

transmembrane glycoproteins expressed on thymocytes and antigen presenting cells including dendritic cells, epithelial cells and B-cells *(Calabi and Milstein, 1986, Small et al., 1987)* which present antigenic lipids for natural killer T cells *(Beckman et al., 1994)*. The assembly of CD1 complex takes place in the ER with the assistance of chaperones also involved in the formation of MHC class I loading complex – calnexin, calreticulin and ERp57 *(Kang and Cresswell, 2002)*.

β2m is also a part of an IgG-Fc receptor (FcRn). Similarly to MHC class I, β2m is a light chain non-covalently bound to a FcRn-heavy chain *(Simister and Mostov, 1989)*. FcRn is involved in the transfer of temporary passive immunity from mother to the foetus *(Story et al., 1994, Israel et al., 1995)* and binds IgG and albumin and rescues both from degradation by an intracellular recycling mechanism *(Junghans and Anderson, 1996, Chaudhury et al., 2003)*. In β2m knock-out mice, new born pups show lower IgG serum levels at birth than their littermates expressing the endogenous β2m *(Israel et al., 1995)* and adult β2m knock-out mice have a higher IgG turnover, resulting in lower IgG levels than wild-type controls *(Junghans and Anderson, 1996, Ghetie et al., 1996, Spriggs et al., 1992)*.

β2m is necessary for expression of the HFE protein on the cell surface *(Bhatt et al., 2007)*. HFE-deficiency causes hemochromatosis, an iron overload disorder associated with mutation in the HFE gene. The HFE gene is related to MHC class I family and was originally named HLA-H *(Barton et al., 2015, Feder et al., 1996)*. Mice lacking the endogenous β2m were shown to develop iron overload confirming that β2m is essential for the function of the hemochromatosis protein *(Bhatt et al., 2007, Rothenberg and Voland, 1996)*.

### 1.7.1.3 $\beta_2$-microglobulin in biological fluids

β2m is expressed on the cell surface as a part of complexes with immunological functions. When the complexes dissociate, most of β2m is shed from the cell surface into circulation. β2m is normally present in low

concentrations in all body fluids – serum, urine, cerebro-spinal fluid, saliva *(Berggard and Bearn, 1968, Evrin et al., 1971)*.

The concentrations of β2m in healthy people are 1-3 mg/l in serum, 1.7 mg/l in cerebro-spinal fluid and 1.1 mg/l in saliva *(Berggard and Bearn, 1968, Evrin et al., 1971)* and are kept constant by renal catabolism. In all body fluids, β2m is present in its free form *(Plesner and Bjerrum, 1980)*. In human serum, beside the free form, 2% of the protein was found to be associated with MHC class I heavy chains *(Plesner and Bjerrum, 1980)*.

More than 99.9% of the circulating β2m is cleared through the kidney glomeruli into the kidney tubules where it is reabsorbed by the proximal tubular cells and degraded, thus only 0.1% of the kidney filtered β2m enters urine in normal, healthy individuals *(Peterson et al., 1969, Karlsson et al., 1980)*. The function, if any, of free β2m in the body fluids is unknown.

### 1.7.1.4 Pathophysiology of $\beta_2$-microglobulin

Increased serum β2m is associated with several pathologies. β2m levels rise despite normal kidney function when β2m production is elevated, e.g. in chronic inflammatory conditions *(Yilmaz et al., 2014)*, in some viral infections *(Cooper et al., 1984)* and in malignancies of the hematopoetic system *(Nakao et al., 1981)*. Serum β2m increases in patients with impaired kidney function because of inefficient clearance and catabolism of the protein in renal failure, even though production of β2m is normal. Increased urine β2m concentration indicates renal proximal tubule impairment causing insufficient reabsorption of β2m. Concentration of β2m in cerebro-spinal fluid reflects immune activation and lymphoid cell turnover in the central nervous system *(Hansen et al., 1992)*.

One of the most serious pathophysiological properties of β2m is its ability to form amyloid. Aβ2m amyloidosis can be acquired or genetic *(Gejyo et al., 1986b, Valleix et al., 2012)*.

### 1.7.2 Wild-type $\beta_2$-microglobulin amyloidosis

In 1985, Gejyo et al. identified $\beta_2$-microglobulin as the protein forming amyloid fibrils isolated from amyloid-containing tissue in patients undergoing chronic dialysis *(Gejyo et al., 1985)*. This finding started a new approach of research of β2m as one of the proteins able to form amyloid *in vivo*.

The acquired systemic wild-type Aβ2m amyloidosis is also referred to as dialysis-related amyloidosis (DRA) because it is a serious complication for patients undergoing long-term dialysis. As β2m is cleared and catabolized only by the kidney and is poorly cleared by dialysis membranes, its circulating concentrations in end-stage renal failure patients rise up to ~50 µg/ml *(Floege et al., 1991)*. As a consequence of the β2m elevated levels in the serum, and by mechanisms that are currently poorly understood, wild-type β2m forms amyloid fibrils that target the cartilage of osteoarticular tissue, initially on the surface of the cartilage, subsequently extending to the synovia, joint capsules and tendons.

Epidemiology of wild-type Aβ2m amyloidosis

The incidence and prevalence of Aβ2m amyloidosis in dialysis patients is not known. In 1997, post-mortem examination revealed that the prevalence of histologically detectable Aβ2m amyloid already reaches 21 % within 2 years of the onset of haemodialysis, 50 % at 4-7 years and rises to >90 % beyond 7 years of dialysis *(Jadoul et al., 1997)*. In comparison, clinical studies have reported 50 % prevalence at 12 years of hemodialysis and almost 100 % at 20 years *(Koch, 1992, Kopec et al., 2011, Jadoul, 1998)*. Over the last years, the incidence of wild-type Aβ2m amyloidosis has decreased by ~50 % due to improved dialysis methods *(Hoshino et al., 2016, Schiffl, 2014)*. However, wild-type Aβ2m amyloidosis remains a disabling condition in patients who undergo long-term dialysis over 10 years, despite the advanced dialysis technology *(Schiffl, 2014)*.

Clinical manifestations of wild-type Aβ2m amyloidosis

The clinical manifestations of wild-type Aβ2m amyloidosis are erosive and destructive osteoarthropathies, destructive spondyloarthropathy and carpal tunnel syndrome. The typical sites of involvement are sternoclavicular joints, hips, knees, shoulders, wrists and spine *(Bardin et al., 1987, Jadoul et al., 1997)*. The pathological features in osteoarthropathies are joint destructions and dislocations, bone lesions of amyloid that can lead to pathologic fractures, shoulder and wrist tendons thickening and fluid collection in the joints *(Kiss et al., 2005)*. In spondyloarthropathy, Aβ2m amyloid deposits are found in intervertebral discs and the spinal ligaments causing erosion of the vertebral body and severe narrowing of the intervertebral disc space *(Marcelli et al., 1996)*. As the disease progresses, the vertebrae collapse and the patients may develop severe neurologic complications *(Marcelli et al., 1996)*. Carpal tunnel syndrome is induced by the amyloid deposition around synovium in the carpal tunnel causing compression of the nerves *(Kiss et al., 2005)*.

Rare cases of visceral dialysis-related amyloid have also been reported – organs involved include spleen, heart, gastrointestinal tract, blood vessels, lung *(Gal et al., 1994, Jimenez et al., 1998, Takayama et al., 2001)*, but typically the amyloid deposits are restricted to osteoarticular structures.

Diagnosis and treatment of wild-type Aβ2m amyloidosis

The diagnosis of DRA involves the use of imaging techniques – radiography, sonography and MRI *(Kiss et al., 2005)*. A tissue biopsy for histological confirmation is almost always required but not always possible.

The treatment of DRA focuses mainly on the prevention of Aβ2m fibrils deposition and on relief of the symptoms caused by Aβ2m amyloid deposits. Improved dialysis methods help to reduce the circulating β2m *(Nakai et al., 2001)* and thus delay the onset of the disease *(Schiffl, 2014)*. Suppression of inflammation is also beneficial for the prevention of amyloid deposition

*(Floege et al., 1992)*. Steroidal or non-steroidal inflammatory drugs are prescribed to relieve pain *(Yamamoto and Gejyo, 2005)*. Surgical intervention is necessary when the amyloid deposits induce severe osteoarticular symptoms *(Yamamoto and Gejyo, 2005)*. Renal transplantation has been shown to stop the further progression of the disease *(Floege et al., 1992)*, although in many case, a successful renal transplantation failed to achieve the regression of bone cysts induced by wild-type Aβ2m amyloidosis *(Mourad and Argiles, 1996)*.

### 1.7.3 Hereditary systemic amyloidosis due to D76N variant $\beta_2$-microglobulin

In 2012, Valleix et al. described the first naturally occurring amyloidogenic variant of β2m. This extremely amyloidogenic β2m variant is responsible for a highly penetrant autosomal dominant hereditary systemic amyloidosis in a French family *(Valleix et al., 2012)*. All clinically affected members of the family were heterozygous for a single nucleotide mutation, c.286G→A (GAT/AAT) in the B2M gene, encoding a substitution of a negatively charged aspartate residue at the position 76 of the mature protein with an uncharged asparagine residue (D76N) *(Valleix et al., 2012)*.

The clinical manifestations of the $A\beta2m^{D76N}$ amyloidosis are progressive bowel dysfunction and weight loss, persistent sicca syndrome, sensorimotor axonal polyneuropathy and severe orthostatic hypotension. The onset of the symptoms in one member of the family was noticed at the age of 48. Histological analysis and SAP scintigraphy revealed extensive amyloid deposits in spleen, liver, heart, salivary glands, nerves, colon and adrenal glands *(Valleix et al., 2012)*.

In contrast with the DRA, plasma β2m concentration in the $A\beta2m^{D76N}$ amyloidosis patients remained in normal range throughout the course of the disease (1.5 µg/ml) and renal function was also normal *(Valleix et al., 2012)*.

### 1.7.4 $\beta_2$-microglobulin amyloid fibrils

Since it was established that β2m is able to form amyloid *in vivo*, β2m protein structure and its fibrillogenesis have been intensively studied *in vitro*.

Soon after the amyloidogenic ability of β2m was described, *in vitro* fibrillogenesis of the wild-type β2m protein was achieved *(Connors et al., 1985)*. However, the *in vitro* fibrillogenesis of wild-type β2m is critically dependent on low pH (pH < 4) and high ionic strength of the solution to enable partial unfolding and subsequent aggregation into fibrils *(McParland et al., 2000, Eichner et al., 2011)*, which are conditions that do not mimic physiological environment.

When amyloid fibrils isolated from tissue of DRA patients were characterised, it was shown that the main constituent of the natural amyloid fibrils is the full-length intact β2m and a minor part of the natural fibrils consists of a β2m fragment lacking the first six N-terminal residues (ΔN6β2m) *(Linke et al., 1987, Stoppini et al., 2005)*. In contrast to the wild-type full length β2m, ΔN6β2m is less stable and forms amyloid-like fibrils in physiological conditions *(Eichner et al., 2011)*. Moreover, ΔN6β2m catalyzes the oligomerization of wild-type β2m in solution under physiological conditions, suggesting that this may play an important role in the pathogenesis of the disease *(Piazza et al., 2006, Eichner et al., 2011)*.

When $\beta2m^{D76N}$ variant was described, *in vitro* studies identified that the full-length $\beta2m^{D76N}$ protein incubated in physiological solution with mild shaking converts into fibrils at the highest rate ever reported for a globular amyloidogenic protein under physiological conditions – $\beta2m^{D76N}$ formed fibrils within a few hours whereas under the same conditions wild-type β2m remained natively folded and soluble *(Mangione et al., 2013)*. Although the variant can transform wild-type β2m into insoluble fibrils in a mixed solution *in vitro*, and at much higher rate than ΔN6β2m *(Mangione et al., 2013)*, it is notable that there was no wild-type β2m protein found in the amyloid fibrils

isolated from a tissue of Aβ2m$^{D76N}$ amyloidosis patient. These purely consisted of the full-length β2m$^{D76N}$ variant protein *(Valleix et al., 2012)*.

# 1.8 Transthyretin amyloidosis

## 1.8.1 Transthyretin

Transthyretin (TTR) is a protein found in plasma and cerebro-spinal fluid (CSF). Discovered in the 1940's, it was first named pre-albumin due to its migration before albumin in electrophoretic experiments on the biological fluids. In 1958, pre-albumin was demonstrated to bind thyroid hormone thyroxine *(Ingbar, 1958)* and ten years later, it was shown that pre-albumin also binds retinol-binding protein 4 (RBP) in the plasma *(Kanai et al., 1968)*. In 1981, in accordance with nomenclature clarification, pre-albumin was renamed to transthyretin, a name indicating its function – transport of thyroxine and retinol-binding protein *(Nomenclature-Committee, 1981)*.

TTR is a 55 kDa homotetramer composed of 4 identical subunits of 127 amino acids each *(Blake et al., 1978)*. TTR is secreted mostly by hepatocytes and by the choroid plexus of the brain *(Dickson et al., 1985, Holmgren et al., 1991)* and minor synthesis has also been identified in the retinal and ciliary pigment epithelia of the eye, visceral yolk sac, placenta and other organs *(Cavallaro et al., 1990, Soprano et al., 1986, McKinnon et al., 2005, Soprano et al., 1985)*. TTR concentration in human plasma is 170-350 mg/l and about 10-fold less in CSF *(Smith and Goodman, 1971)*. Most of TTR is degraded by the hepatic parenchymal cells and some TTR is also degraded in the muscle, skin and other organs *(Makover et al., 1988)*.

### 1.8.1.1 Functions of transthyretin

One of the functions of TTR is transport of thyroid hormone thyroxine ($T_4$). Thyroid hormones are essential for proper development of the central nervous system, metabolism, bone growth and for other regulatory functions during development and in adult life. Thyroid hormones exist in two main forms – thyroxine ($T_4$) and 3,5,3'-triiodothyronine ($T_3$). $T_4$ and a small amount

of $T_3$ are produced from an enzymatically cleaved thyroglobulin synthesized by the follicles of thyroid gland *(Tong et al., 1951)*. The thyroid hormones are distributed from the thyroid gland via circulation. After reaching the target tissue, $T_4$ requires a conversion by 5'-deiodinases to more biologically active form $T_3$ *(Braverman et al., 1970, Jennings et al., 1979).* $T_3$ binds to nuclear thyroid hormone receptor which then binds to thyroid hormone-responsive elements located in the promoter regions of thyroid-responsive genes and affects gene transcription *(Lavin et al., 1988)*. More than 99 % of $T_4$ circulates in the biological fluids bound to thyroid hormone transporting proteins: thyroxine-binding globulin (TBG), TTR and albumin *(Robbins and Rall, 1955, Ingbar, 1958)*. In humans, about 70 % of plasma $T_4$ is transported by TBG and 15 % by TTR *(Woeber and Ingbar, 1968)*. In rodents, TTR is the main carrier of plasma $T_4$ *(Norlund et al., 1997)*. In CSF, TTR is the main $T_4$ carrier for both, humans and rodents *(Larsson et al., 1985, Hagen and Elliott, 1973, Davis et al., 1970)*. However, studies on transgenic mice have revealed that thyroid hormone-carrier proteins are not essential for $T_4$ tissue uptake or distribution. Mice lacking TTR have decreased amounts of total plasma $T_4$ and $T_3$ but normal free plasma hormones levels compared to wild-type mice and their development is not affected, the mice are healthy and viable and thyroid hormones access and are distributed within the mouse brain *(Episkopou et al., 1993, Palha et al., 2002)*. Recently, the possibility of $T_4$ being able to activate thyroid hormones-responsive genes in tadpoles has suggested that $T_4$ may also adopt thyroid hormone-signalling activity and act directly on tissue *(Maher et al., 2016)*. TTR, together with other plasma carrier proteins is responsible for the maintenance of a large pool of the hormones in the circulation but its function in the hormones uptake in the tissue is not fully understood.

TTR also functions as a transporter of RBP-retinol complex *(Kanai et al., 1968)*. Retinol, or vitamin A, is a precursor of visual pigment chromophore in photoreceptors of retina mediating transduction, in which the light is translated into nervous signal, and thus ensuring optimal vision *(Hubbard and*

*Kropf, 1959, Arshavsky et al., 2002)*. Retinol is also a precursor of retinoic acid that binds to transcription factors in various tissues and regulates expression of many genes *(Piskunov et al., 2014)*. Transport of retinol from the liver to the peripheral tissue takes place in the plasma, where the retinol binds to RBP and subsequently retinol-RBP complex binds to TTR in the circulation *(Kanai et al., 1968)*. When not bound to TTR, RBP and retinol are quickly filtered by the kidney and lost in urine *(van Bennekum et al., 2001)*. In the target tissue, retinol-RBP complex binds to an RBP membrane receptor called STRA6 which also mediates the cellular uptake of vitamin A *(Kawaguchi et al., 2007)*. Although almost 50 % of circulating TTR is used to deliver retinol bound to RBP to targeted tissues *(Liz et al., 2010)*, TTR knock-out mice do not show any symptoms of vitamin A deficiency despite having very low circulating levels of vitamin A and RBP (<6 % and 3% of wild-type mice levels, respectively) *(Episkopou et al., 1993)*. The TTR knock-out mice can therefore utilize stored retinol from the liver despite a defective retinol transport *(Episkopou et al., 1993)*.

Besides the plasma carrier function, TTR has a proteolytic activity. It was shown that 1-2 % of TTR circulates in association with high density lipoproteins (HDL) through binding to apolipoprotein A-I (ApoAI) *(Sousa et al., 2000)*. In *in vitro* experiments, TTR cleaved ApoAI which affected cholesterol transport and increased ApoAI amyloidogenicity, features associated with atherosclerosis development *(Liz et al., 2004, Liz et al., 2007)*. TTR has also been reported to cleave Aβ peptide, an amyloidogenic peptide associated with pathobiology of Alzheimer's disease (AD), be capable of clearing Aβ, degrade aggregated forms of Aβ, and thus could have a protective role in AD *(Costa et al., 2008, Buxbaum et al., 2008)*. It was also suggested that the proteolytic activity of TTR plays a role in nerve regeneration *(Liz et al., 2009)*.

TTR is a negative acute-phase protein – transcription of TTR is down-regulated in the liver following inflammation or trauma leading to decreased concentration of TTR in the blood. However, the TTR synthesis in liver and choroid plexus is regulated independently *(Dickson et al., 1986)*.

## 1.8.2 Types of transthyretin amyloidosis

Transthyretin amyloidoses include two main types: wild-type ATTR amyloidosis (previously referred to as age-related senile systemic amyloidosis) with the wild-type TTR as the amyloid fibril precursor *(Westermark et al., 1990)*, and hereditary systemic ATTR amyloidosis caused by a mutation in the TTR gene. Wild-type ATTR amyloidosis is characterised by cardiac involvement. Hereditary systemic ATTR amyloidosis presents with familial amyloid polyneuropathy, in which the amyloid fibrils are mainly deposited in the peripheral nervous system, or familial amyloid cardiomyopathy, in which the major site of amyloid deposits is the heart.

While most amyloidogenic TTR mutations are associated with familial amyloid polyneuropathy, and amyloid in the heart may or may not present, cardiac amyloidosis is the predominant clinical feature in wild-type ATTR amyloidosis and in patients with V122I mutation in the TTR gene in which the amyloid polyneuropathy is rare *(Connors et al., 2003, Dungu et al., 2012)*.

### 1.8.2.1 Wild-type ATTR amyloidosis

Non-hereditary wild-type ATTR amyloidosis is referred to as senile systemic amyloidosis due to its late age of onset, usually after the seventh decade of life. The heart is generally the only organ affected, with carpal tunnel syndrome being sometimes the other clinical manifestation of the disease *(Pitkanen et al., 1984, Sekijima et al., 2011)*. In wild-type ATTR amyloidosis, amyloid deposits are derived from wild-type TTR and no genetic predisposition has been identified *(Westermark et al., 1990)*.

Epidemiology of wild-type ATTR amyloidosis

In non-hereditary wild-type ATTR amyloidosis, the prevalence of the disease increases with age. In post-mortem analyses, wild-type TTR cardiac amyloid was found in 25 % of individuals over the age of 85, with moderate or severe deposits in >5 % *(Tanskanen et al., 2008)*. The incidence of wild-type ATTR

amyloidosis is much greater in men than women and the median survival from the time of diagnosis is less than 4 years *(Connors et al., 2011, Pinney et al., 2013b)*.

Clinical manifestations and diagnosis of wild-type ATTR amyloidosis

Clinical manifestations of wild-type ATTR amyloidosis are atrial fibrillation and breathlessness with echocardiogram and MRI showing increased ventricular wall thickness and stiffness *(Rapezzi et al., 2009, Pinney et al., 2013b)*. Carpal tunnel syndrome can be an early sign of wild-type ATTR amyloidosis, preceding cardiac manifestation by 8 to 10 years, as wild-type TTR amyloid deposits are found in almost 30 % of elderly people undergoing carpal tunnel decompression *(Sekijima et al., 2011)*. Diagnosis of wild-type ATTR amyloidosis is confirmed by histological analysis of cardiac tissue biopsy and TTR gene sequencing showing no mutations. If cardiac biopsy is not possible, abdominal fat aspirate or rectal biopsy may be helpful. However, amyloid may not be found in these tissues *(Connors et al., 2011)*. Recently a new method of using $^{99m}$Tc-DPD scintigraphy for cardiac amyloid detection is being evaluated, showing remarkable sensitivity of amyloid localisation in the heart, especially in respect with ATTR amyloid *(Hutt et al., 2014, Puille et al., 2002)*.

### 1.8.2.2 Hereditary systemic ATTR amyloidosis

Hereditary ATTR amyloidosis is a dominantly inherited systemic amyloid disease that results from a mutation in the TTR gene. More than 100 variants of TTR gene have been identified to date, with >80 of these variants being amyloidogenic *(Connors et al., 2003)*. The TTR variants present a clinical heterogeneity but majority of the amyloidogenic variants are associated with familial amyloid polyneuropathy, a fatal disease characterized by extracellular ATTR amyloid deposits mainly in peripheral nervous system, including the autonomic nerves. Some mutations present with familial amyloid polyneuropathy (e.g. TTR$^{V30M}$) *(Saraiva et al., 1984)*, with a combination of

familial amyloid polyneuropathy and familial amyloid cardiomyopathy (e.g. $TTR^{R34T}$) *(Patrosso et al., 1998)*, with cardiomyopathy only (e.g. $TTR^{V122I}$) *(Jacobson et al., 1990)* and some mutation may also present with vitreous TTR deposition (e.g. $TTR^{V30M}$) *(Saraiva et al., 1984)* or leptomeningeal amyloid deposits (e.g. $TTR^{I84S}$) *(Dwulet and Benson, 1986)*.

FAP was first described in 1952 in Portugal *(Andrade, 1952)*, subsequently reported in Japan *(Araki et al., 1968)* and Sweden *(Andersson, 1976)*. It was then shown that Portuguese, Japanese and Swedish patients carry the same variant $TTR^{V30M}$ *(Saraiva et al., 1984)*. Some TTR variants have been well represented by extensive kindreds ($TTR^{V30M}$, $TTR^{T60A}$, $TTR^{V122I}$), whereas most of the mutations have been found in one family or a single individual.

Epidemiology of hereditary ATTR amyloidosis

The prevalence of familial amyloid polyneuropathy is estimated at 100.000 individuals in Europe *(Ando et al., 2013)*. The most common variant presenting with polyneuropathy is $TTR^{V30M}$, which has the highest prevalence in Sweden, Portugal and Japan reaching 1 in 1000 in endemic areas *(Ando et al., 2005, Hawkins et al., 2015)*. However, the penetrance varies between populations – for example in the $TTR^{V30M}$ carriers, the penetrance is low in Sweden with 11 % of carriers having clinical disease at 50 years of age *(Hellman et al., 2008)* but high in Portugal with 80 % of carriers being symptomatic by 50 years of age *(Plante-Bordeneuve et al., 2003)*. The progression of the disease can be fast following the onset of symptoms but the mean duration of disease from onset to death is approximately 10 years and may vary depending on endemic region, symptoms, genotype and other factors not yet known *(Ando et al., 2013)*.

Cardiac involvement is common in FAP, and has been reported in over half of the variants *(Connors et al., 2003)*. The two most common encountered genetic variants in familial amyloid cardiomyopathy are $TTR^{V122I}$ and $TTR^{T60A}$. $TTR^{V122I}$ is the most common type with 3-4 % of people of Afro-Caribbean descent carrying the V122I allele *(Buxbaum et al., 2010, Yamashita et al.,*

*2005)*. It is estimated that about 1.5 million African Americans carry the $TTR^{V122I}$ mutation and are at risk of development of ATTR cardiac amyloidosis, although the penetrance is uncertain *(Ruberg et al., 2012)*. $TTR^{T60A}$ is the most common variant in the UK *(Dungu et al., 2012)*.

Clinical manifestation and diagnosis of familial amyloid cardiomyopathy is similar to wild-type ATTR amyloidosis as it was described in the previous section.

Clinical manifestations of familial amyloid polyneuropathy

Familial amyloid polyneuropathy is characterized by severe peripheral and autonomic neuropathy. The first symptoms can occur in patients in their early 30s and progress substantially in the next two decades, but late onset of the disease is also common. The amyloid neuropathy is usually symmetrical ascending length-dependent sensorimotor axonal neuropathy. It usually starts with loss of sensations of heat and cold in lower limbs progressing into upper limbs *(Gertz et al., 2015)*. Within a few years, the sensory neuropathy is followed by motor neuropathy with loss of extensor function of toes and feet causing unstable walking and progressing over the next 10-20 years. The autonomic neuropathy is manifested by urinary incontinence, sweating abnormalities, diarrhoea alternating with constipation, erectile dysfunction and orthostatic hypotension *(Gertz et al., 2015)*. Carpal tunnel syndrome is also common.

In peripheral nerve biopsies, amyloid deposits are characteristically found in the endoneurium and around nerve blood vessels. As the disease progresses, nerve fibre density and viability is reduced and endoneurial blood vessels are frequently destroyed by the amyloid *(Plante-Bordeneuve and Said, 2011)*. No intracellular ATTR amyloid deposits were detected in the axons or neuronal cell bodies *(Adams and Said, 1996)*. ATTR amyloid deposits are also found in stomach, gastric and rectal walls but not particularly in the enteric nervous system *(Anan et al., 2001)*.

Diagnosis of familial amyloid polyneuropathy

Familial amyloid polyneuropathy is diagnosed histologically on tissue biopsy. Nerve, skin, fat, salivary gland or rectal biopsies may be used *(Foli et al., 2011, Gertz et al., 2015)* but negative result for the presence of amyloid does not exclude ATTR amyloidosis. Immunohistochemistry and mass spectrometry of laser-captured amyloid are used to confirm the amyloid protein and TTR gene sequencing is used to screen for TTR mutation. Scintigraphy with radiolabelled SAP reveals the amyloid burden of affected tissues.

### 1.8.2.3 Treatment of ATTR amyloidosis

The first-line treatment of hereditary systemic amyloidosis includes transplantation of failing amyloidotic organ or liver transplantation as the major site of TTR synthesis to replace the mutant amyloidogenic protein with normal non-mutated TTR *(Ando et al., 2013)*. The concentration of variant TTR has been decreased by 98 % in patients following liver transplantation *(Adams et al., 2000)* and this procedure has been shown to increase patient survival significantly *(Yamashita et al., 2012)*. However the presence of cardiac amyloid deposits is a limiting factor in liver transplantation as wild-type TTR can still be deposited as amyloid on the pre-existing amyloid template in the heart *(Barreiros et al., 2010)*. Cardiac transplantations in $TTR^{V122I}$ patients with cardiomyopathy seem to have promising long-term outcomes *(Dubrey et al., 2004, Thenappan et al., 2014)*.

New therapies are under development for ATTR amyloidosis. One strategy for treatment of ATTR amyloidosis focuses on developing molecules that bind to the plasma TTR tetramer to stabilize the native tetrameric structure of TTR molecule. By stabilizing the tetramer, TTR does not dissociate into monomers and misfolding and deposition of TTR monomers is inhibited. In 2006, Diflunisal, a non-steroidal inflammatory was reported to stabilise TTR tetramers against dissociation into monomers *(Sekijima et al., 2006, Miller et*

*al., 2004, Berk et al., 2013)*. Tafamidis, a novel TTR stabilizer, has been developed and tested in medical trials resulting in a slower progression of the disease and has received a marketing approval by the European Medicine Agency *(Johnson et al., 2012, Coelho et al., 2012)*. However, it was reported in a post-approval trial by the French Network for familial amyloid polyneuropathy that neurological impairment worsened in 55 % of patients with advanced $ATTR^{V30M}$ amyloidosis after one year of Tafamidis treatment, showing that Tafamidis was not able to stop progression of the disease in these patients *(Lozeron et al., 2013)*.

Another strategy of treating ATTR amyloidosis uses TTR RNA-inhibiting approaches – small interfering RNA (siRNA) therapy and anti-sense oligonucleotide (ASO) therapy *(Kurosawa et al., 2005, Benson et al., 2006)* which are now in clinical development. Preliminary data from clinical trials using TTR-targeting siRNA showed >80 % reduction in TTR levels without major toxic effects *(Coelho et al., 2013)*. ASOs are short synthetic oligonucleotides that bind directly to TTR mRNA, leading to its degradation by RNase H *(Benson et al., 2006)*. Studies using this interfering approach have shown rapid reductions in plasma TTR in transgenic mice expressing human TTR *(Benson et al., 2006)* and in non-human primate model *(Ackermann et al., 2012)*. Clinical trials in healthy volunteers and in ATTR amyloidosis patients are ongoing *(Hawkins et al., 2015)*.

### 1.8.3 Transthyretin amyloid fibrils

Familial amyloid polyneuropathy was first described in 1952 in Portuguese patients and in 1978, evidence was presented that the amyloid deposits in Portuguese patients with familial amyloid polyneuropathy have TTR (then pre-albumin) as a major constituent *(Costa et al., 1978)*. In 1981, it was shown that Swedish and Japanese familial amyloid polyneuropathy are also caused by amyloid deposits consisting of TTR *(Benson, 1981, Tawara et al., 1981)*. In 1983, studies on the primary structure of purified amyloid fibril protein of

Portuguese familial amyloid polyneuropathy patients revealed that there is a methionine for valine substitution at the position 30 of mature protein in comparison with normal plasma TTR and the variant TTR was also detected in the plasma of familial amyloid polyneuropathy patients together with normal wild-type TTR *(Saraiva et al., 1984)*. The V30M substitution was then confirmed in Swedish and Japanese familial amyloid polyneuropathy patients *(Dwulet and Benson, 1984, Tawara et al., 1983)*. In the next few years, other mutations in the TTR sequence were described and the exchange of a single amino acid residue in the TTR protein was thought to be making the TTR protein prone to amyloidogenesis *(Pras et al., 1983, Nakazato et al., 1984, Wallace et al., 1986, Dwulet and Benson, 1986)*. In 1988, amyloid fibrils isolated from heart of wild-type ATTR amyloidosis patients were identified as TTR with normal amino acid sequences showing that wild-type TTR is also amyloidogenic *(Cornwell et al., 1988)*. To date, more than 100 mutations in the TTR gene have been identified, most of which are associated with amyloid formation (http://amyloidosismutations.com/ attr.html).

Since the TTR and its involvement in amyloidosis have been discovered, the amyloidogenicity of the protein has been intensively studied *in vitro*. Native TTR is a tetramer. The amyloid aggregation of TTR requires dissociation of the tetramer into monomers and partial unfolding and refolding of such monomers into amyloidogenic intermediates with self-association into soluble oligomers and subsequently into insoluble amyloid fibrils *(Lai et al., 1996)*.

The native tetramers of TTR variants that are associated with amyloidosis are less stable *in vitro* than the wild-type TTR and it has been accepted that tetramer dissociation and partial denaturation of the released monomers is a crucial step for the formation of amyloid fibrils *(Colon et al., 1996)*. On the other hand, $TTR^{T119M}$ mutation, a common non-pathogenic variant in the Portuguese population, is more stable and when combined with an amyloidogenic TTR variant, inhibits fibrils formation both *in vitro* and *in vivo* in the carriers *(McCutchen et al., 1995, Alves et al., 1997)*. However, it is not

known what triggers TTR tetramer dissociation and monomer misfolding *in vivo*.

TTR is normally a very stable protein that does not thermally denature at temperatures <80 $^{o}$C, and its dissociation into monomers *in vitro* requires low pH or high concentration of denaturants *(Lashuel et al., 1998)*. However, it has been shown *in vitro* that monomeric subunits in the TTR tetramers exchange under native conditions showing that the TTR dissociates releasing a monomer and re-associates into a native tetramer again *(Schneider et al., 2001)*.

Amyloid fibrils isolated from hereditary ATTR amyloidosis patients heterozygous for a TTR mutation showed that the deposits consist of mutated as well as wild-type TTR and the mutated protein makes up for about two thirds of the ATTR amyloid deposits *(Dwulet and Benson, 1986, Thylen et al., 1993)*. Moreover, a major component of *ex vivo* ATTR amyloid fibrils is a 49-127 C-terminal fragment of the TTR monomer, regardless of the presence or position of any amyloidogenic mutation *(Thylen et al., 1993, Bergstrom et al., 2005)*. These findings and follow up *in vitro* experiments suggested that a proteolytic cleavage may have an important role in destabilizing the tetramers and releasing truncated monomers that are highly amyloidogenic *(Marcoux et al., 2015)*.

S52P variant TTR is the least stable variant and causes the most aggressive known phenotype of ATTR amyloidosis *(Mangione et al., 2014)*. *In vitro*, full-length hTTR$^{S52P}$ did not form amyloid fibrils under stirring in physiological conditions, same as wild-type human TTR and other TTR variants. However, amyloid fibrils were rapidly formed when trypsin was added into the hTTR$^{S52P}$ protein solution. The main component of the fibrillar material was identified as 49-127 fragment of hTTR$^{S52P}$, the same fragment as seen in *ex vivo* isolated ATTR amyloid fibrils *(Mangione et al., 2014)*. Also the S52P variant was shown to be much more susceptible to proteolytic cleavage compared to wild-type TTR and other TTR variants. Further experiments suggested that TTR composed of wild-type TTR and TTR$^{S52P}$ monomers may circulate as a

tetramer even if one subunit is cleaved. The 49-127 fragment is released from the tetramer under certain conditions leading to its rapid incorporation into amyloid fibrils *(Marcoux et al., 2015)*.

The effect of amyloid deposition on biochemical function of affected tissue has never been clearly confirmed and toxicity of non-fibrillar TTR aggregates has been studied. In asymptomatic carriers of V30M variant TTR, TTR was already aggregated in non-fibrillar form, negative for Congo red staining *(Sousa et al., 2001)*. Non-fibrillar TTR was also present in later stages of ATTR amyloidosis together with ATTR amyloid fibrils in the affected tissue. It was reported that the fibrillar ATTR deposits do not cause cellular damage but the non-fibrillar aggregates may be toxic to the cells inducing oxidative and inflammatory stress and cell apoptosis *(Sousa et al., 2001, Andersson et al., 2002)*.

## 1.9 Aims of this thesis

Amyloid formation of various precursor proteins has been extensively studied *in vitro* shedding light on the attributes of protein folding and misfolding and on the conditions of accelerating or inhibiting fibril formation. However, amyloid accumulation *in vivo* is a much more complicated process involving multiple components which may play more or less important roles in amyloidogenesis.

Animal models have been very useful in elucidating mechanisms of diseases and in translational research. Transgenic mouse models for some types of amyloid have been successfully generated – e.g. pancreatic amyloid deposition of IAPP *(Janson et al., 1996)*, Aβ peptide deposition in the brain *(Hsiao et al., 1996, Sturchler-Pierrat et al., 1997, Rockenstein et al., 2001)*. The only mouse models of systemic amyloidosis closely mimicking the human disease have been generated for systemic AA amyloidosis – mice with AA amyloid deposits have been produced by inducing inflammation, thus increasing the concentrations of circulating SAA *(McAdam and Sipe, 1976, Skinner et al., 1977)* or by transgenic overexpression of the plasma SAA *(Simons et al., 2013)*. These mice have been very informative in understanding the mechanisms of the disease.

Moreover, modelling AA amyloidosis in mice has enabled the discovery of principles and further development of the non-invasive SAP scintigraphy diagnostic method which has now been used in the clinic for diagnosing and imaging amyloidosis in patients *(Pepys et al., 1979, Baltz et al., 1986b, Hawkins et al., 1990a, Hawkins et al., 1990b, Hawkins et al., 1993)*. As introduced in the previous section, a novel immunotherapy directly targeting amyloid deposits has been developed and tested using AA amyloidosis mouse models *(Bodin et al., 2010, Simons et al., 2013)*. This immunotherapy is in clinical trials now showing very promising results *(Richards et al., 2015)*.

Although the animal models of systemic AA amyloidosis have been well established, different types of amyloidoses have different characteristic

patterns of amyloid deposition and different mechanisms preceding the precursor protein misfolding. Notably, there is no good animal model of cardiac amyloidosis. The prevalence of AA amyloidosis has been decreasing over the last decade *(Wechalekar et al., 2016)* which most likely reflects better management of underlying inflammatory disorders in AA amyloidosis patients. On the other hand, the number of patients diagnosed with cardiac ATTR amyloidosis has increased over the last decade *(Wechalekar et al., 2016)* and Aβ2m amyloidosis remains a disabling condition in many patients undergoing long-term dialysis *(Schiffl, 2014).* Despite many attempts to model Aβ2m amyloidosis and ATTR amyloidosis in mice, none have been successful to date.

Against this background, the aims in this thesis were to generate mouse models of Aβ2m amyloidosis and of cardiac ATTR amyloidosis by transgenic expression of highly amyloidogenic variants of these proteins.

# 2 Materials and methods

## 2.1 Materials

### 2.1.1 Standard buffers, solutions and media

Buffers and solutions routinely prepared in the laboratory are listed below.

**0.07 M Barbitone – Calcium (BC) buffer**

| | | |
|---|---|---|
| Na-Barbitone | 60.3 | mM |
| Barbitone | 9.7 | mM |
| $NaN_3$ | 0.1 | % |
| Ca-Lactate ($4H_2O$) | 0.58 | g/l |

**0.1 M Carbonate – Bicarbonate buffer**

| | | |
|---|---|---|
| $Na_2CO_3$ | 0.02 | M |
| $NaHCO_3$ | 0.07 | M |
| pH 9.0 | | |

**2 x Freezing medium**

| | | |
|---|---|---|
| Glycerol | 30 | % |
| in LB broth | | |

**Homogenisation buffer**

| | | |
|---|---|---|
| NaCl | 140 | mM |
| Tris | 10 | mM |
| EDTA | 10 | mM |
| $NaN_3$ | 0.1 | % |
| PMSF | 1.5 | mM |
| 1 tablet of Complete Mini Protease Inhibitor (Roche) | | |
| pH 8.0 | | |

**MES-SDS buffer**

| | | |
|---|---|---|
| MES | 50 | mM |
| Tris | 50 | mM |
| EDTA | 1 | mM |
| SDS | 0.1 | % |
| pH 7.3 | | |

**10% Neutral buffered formalin (NBF)**

| | | |
|---|---|---|
| Formaldehyde (37-40%) | 100 | ml |
| $NaH_2PO_4$ | 4 | g |
| $Na_2HPO_4$ (anhydrous) | 6.5 | g |
| $dH_2O$ | 900 | ml |

**4 % Paraformaldehyde (PFA)**

| | | |
|---|---|---|
| PFA | 4 | % |
| in PBS | | |

**PBS**

| | | |
|---|---|---|
| NaCl | 140 | mM |
| KCl | 2.7 | mM |
| $Na_2HPO_4$ | 8.1 | mM |
| $KH_2PO_4$ | 1.5 | mM |
| pH 7.4 | | |

**PBST**

| | | |
|---|---|---|
| Tween 20 | 0.1 | % |
| in PBS | | |
| (unless otherwise stated) | | |

**Saturated alcoholic Congo red solution**

| | | |
|---|---|---|
| NaCl | 0.35 | M |
| Congo Red | 2 | g/l |
| in 80 % ethanol | | |

**Saturated alcoholic NaCl solution**

| | | |
|---|---|---|
| NaCl | 0.35 | M |
| in 80 % ethanol | | |

**TAE buffer**

| | | |
|---|---|---|
| Tris base | 40 | mM |
| EDTA | 1 | mM |
| Glacial acetic acid | 0.114 | % |

**Tail digest buffer**

| | | |
|---|---|---|
| Sodium acetate | 0.3 | M |
| Tris-EDTA | 10 | mM |
| SDS | 1 | % |
| Proteinase K | 0.2 | mg/ml |

**TE buffer**

| | | |
|---|---|---|
| Tris-HCl | 10 | mM |
| EDTA | 0.1 | mM |
| pH 7.5 | | |

## 2.1.2 Primers

Oligonucleotide primers were designed using NCBI/Primer-BLAST online software (http://www.ncbi.nlm.nih.gov/tools/primer-blast). Primers were synthesized by Sigma-Aldrich (UK), provided lyophilized. 100 µM stock solutions were made by adding appropriate amounts of sterile nucleases-free $dH_2O$ and stored at -20 °C. Stock solutions of oligonucleotides were further diluted in $dH_2O$ to 10 µM working solution. All primers used are listed in Tables 2.1 and 2.2. Annealing temperatures of primers were calculated using the online ThermoScientific Tm calculator tool:

(http://www.finnzymes.fi/tm_determination.html).

| Use of primer pairs | Name | Sequence |
|---|---|---|
| **hβ2m amplification** | hβ2m4-For | 5′ - TTGCACTACTGGGAGATAAAGC |
| | hβ2m4-Rev | 5′ - TCAGAGTATCATCCCCCAATTT |
| **hβ2m mutagenesis** | B2m-mut-A | 5′- CACTGAAAAAA**A**ATGAGTATGCCTGCCGTGTGAACC |
| | B2m-mut-B | 5'- CGGCAGGCATACTCATTTTTTTCAGTGGGGGTGAATTCAG |
| **hβ2m transgenics screening** | hβ2m-F1 | 5′ - ACTGAATTCACCCCCACTGA |
| | hβ2m-R2 | 5′ - ATGGGATGGGACTCATTCAG |
| **hβ2m Ligation sites sequencing** | T7F primer | 5′ - GTAATACGACTCACTATAGGGC |
| | T3 primer | 5′ - CCCTTTAGTGAGGGTTAATT |
| **hβ2m Exon1 sequencing** | B2m-seq1 | 5' - GTGGGAGGCTCTCTCTTGTG |
| | B2m-seq2 | 5′ - CTTGGAGAAGGGAAGTCACG |
| **hβ2m Exon2+3 sequencing** | B2m-seq3 | 5′ - CGCAATCTCCAGTGACAGAA |
| | B2m-seq4 | 5′ - CAGTTCCTTTGCCCTCTCTG |
| **hβ2m Exon4 sequencing** | B2m-seq5 | 5′ - GGAATTGATTTGGGAGAGCA |
| | B2m-seq6 | 5′ - AAGGGGTCCTGAAACCAATC |
| **hβ2m RT-PCR** | hβ2m RT-PCR 5′ | 5′ - CGAGACATGTAAGCAGCATCA |
| | hβ2m RT-PCR 3′ | 5′ - GAGCTACCTGTGGAGCAACC |

***Table 2.1: List of hβ2m primers***

*Oligonucleotide primes used for cloning, mutagenesis, Gibson assembly, sequencing and RT-PCR of DNA sequences of the human B2M gene.*

| Use of primer pairs | Name | Sequence |
|---|---|---|
| **hTTR-NS amplification** | hTTR-NS-4-For | 5’ - TGTTTCCTGTTGACTGGGCATA |
| **(Exon 1 fragment)** | hTTR-NS-4-Rev | 5’ - AGAGGACACTTGGATTCACCG |
| **hTTR-MS amplification** | hTTR-SM-10-For | 5’ - AGCAACTGTTCTCAGGGGAC |
| **(Exon 2+3+4 fragment)** | hTTR-SM-10-Rev | 5’ - TCCTGGAGAATCCTGGTTGGA |
| **hTTR Exon1 sequencing** | hTTR-NS-seq1F | 5’ - TTGGTTGTTTTGTTTTGGTGA |
| | hTTR-NS-seq1R | 5’ - CTGGGTACCCTTGCCCTAGT |
| **hTTR Exon2 sequencing** | hTTR-SM-seq2F | 5’ - TCGCTCCAGATTTCTAATACCA |
| | hTTR-SM-seq2R | 5’ - TGATGTGAGCCTCTCTCTACCA |
| **hTTR Exon3 sequencing** | hTTR-SM-seq3F | 5’ - GTGTTAGTTGGTGGGGGTGT |
| | hTTR-SM-seq3R | 5’ - TGAGTAAAACTGTGCATTTCCTG |
| **hTTR Exon4 sequencing** | hTTR-SM-seq4F | 5’ - GCTTGCCAGCATATTTGAGC |
| | hTTR-SM-seq4R | 5’ - GTAAAGAAGTGGGCCCTTGG |
| **hTTR mutagenesis** | TTR_S52P_mut_For | 5’ - AGTGAG**C**CTGGAGAGCTGCATGGGCTC |
| | TTR_S52P_mut_Rev | 5’ - GCAGCTCTCCAG**G**CTCACTGGTTTTCCTATAAGGTG |
| **Gibson assembly:** | | |
| **Alb e-p For** | TTRass6 | 5’ - GCGCGCTTGGCGTAATCA |
| **Alb e-p Rev** | TTRass1 | 5’ - GGGGTTGATAGGAAAGGTG |
| **Exon 1 For** | TTRass2 | 5’ - ctttcctatcaaccccCAGAAGTCCACTCATTCTTG |
| **Exon 1 Rev** | TTRass3 | 5’ - aacgtaagtGTCGACAATTAATGAGCTTC |
| **Exon 2-4 For** | TTRass4 | 5’ - ttgtcgacACTTACGTTCCTGATAATGGG |
| **Exon 2-4 Rev** | TTRass5 | 5’ - ttacgccaagcgcgcACGCGTGGCAGATAAAAC |
| **hTTR transgenics screening** | hTTRg-3U | 5’ - ACCCAAGGCTTTTGCCTAAT |
| | hTTRg-3D | 5’ - ATTGCTTCCCATTTGACTGC |
| **hTTR RT-PCR** | hTTR RT-PCR 5’ | 5’ - GCTCTGGGAAAACCAGTGAG |
| | hTTR RT-PCR 3’ | 5’ - GCCGTGGTCGAATAGGAGTA |
| **GAPDH RT-PCR** | msGAPDHf | 5’ - CATTTCCTGGTATGACAATGAATACG |
| | msGAPDHr | 5’ - GGATAGGGCCTCTCTTGCTC |

***Table 2.2: List of hTTR primers***

*Oligonucleotide primes used for cloning, mutagenesis, Gibson assembly, sequencing and RT-PCR of DNA sequences of the human TTR gene.*

## 2.1.4 Antibodies

| Primary Ab | Host | Reactivity | Conjug. | Manufacturer | Use |
|---|---|---|---|---|---|
| β2-microgobulin 14H3 | Mouse | Human | | University of Pavia (Stoppini et al., 1997) | WB, ELISA |
| β2-microgobulin | Rabbit | Human | | Dako (A0072) | WB, ELISA, IHC |
| β2-microgobulin B2M-01 | Mouse | Human | FITC | Bioscience (ABX172) (Hilgert et al., 1984) | WB, FC, IF |
| CD45 | Rat | Mouse | APC | Biolegend | FC |
| CD16/CD32 (Fc-block) | Rat | Mouse | | BD Bioscience (553142) | FC |
| ApoAII | Rabbit | Mouse | | Provided by Dr.Higuchi (*) | IHC |
| mSAA1 | Goat | Mouse | | R&D (AF2948) | IHC |
| α2-macrogobulin | Rabbit | Human | | Dako (Q0102) | WB, IP |
| TTR (Prealbumin) | Rabbit | Human | | Dako (A0002) | WB, IH, RIE |
| TTR | Sheep | Human | | Binding site | WB |
| SAA | | Mouse | | Binding site (a-SAA1-95) | ELISA |

| Secondary Ab | Host | Reactivity | Conjug. | Manufacturer | Use |
|---|---|---|---|---|---|
| IgG | Goat | Rabbit | HRP | Dako (P0048) | WB, ELISA |
| IgG | Rabbit | Sheep | HRP | Dako (P0163) | WB |
| IgG | Horse | Rabbit | HRP | Vector Lab. (MP7401) | IHC |
| IgG | Horse | Goat | HRP | Vector Lab. (MP7405) | IHC |
| Clean-Blot IP Detection | | | HRP | ThermoScientific (21230) | WB |
| SAA | | Mouse | Biotin | Binding site (aSAA1-96) | ELISA |
| Streptavidin | | Biotin | HRP | Sigma (S5512) | ELISA |

| Other Ab and stains | Host | Reactivity | Conjug. | Manufacturer | Use |
|---|---|---|---|---|---|
| Hoechst 33342 | | | | Sigma (B2261) | IF |
| Rabbit IgG | | | | Sigma (15006) | IP |

***Table 2.3: List of antibodies***

*Antibodies used for Western blot (WB), ELISA, immunohistochemistry (IHC), flow cytometry (FC), immunofluorescence (IF), immunoprecipitation (IP) and rocket immunoelectrophoresis (RIE).*

*(*) Antibody kindly provided by Dr. Keiichi Higuchi, Institute of Pathogenesis and Disease Prevention Shinshu University Graduate School of Medicine, Japan*

## 2.2 Molecular cloning methods

### 2.2.1 Polymerase chain reaction

The polymerase chain reaction (PCR) is an *in vitro* DNA cloning method which allows selective amplification of a desired DNA sequence. PCR requires heat-stable DNA polymerase, DNA template, DNA precursors (deoxynucleoside triphosphates – dATP, dTTP, dCTP, cGTP) and two oligonucleotide primers. The reaction consists of a series of cycles of three steps:

- Denaturation – melts the double helix DNA into single strands
- Annealing – enables the primers to bind to the complementary DNA sequence
- Extension – allows DNA polymerase synthesis of a new complementary DNA strand by adding dNTP to the primer.

PCR was used to amplify the wild-type human β2-microglobulin (hβ2M) and human TTR (hTTR) genes and/or fragments of these genes, to insert specific mutation into a gene by site-directed mutagenesis, to prepare DNA fragments for Gibson assembly, to genotype animals and to identify mRNA expression of genes of interest by RT-PCR.

Wild-type hβ2M and hTTR genes were both amplified from human genomic DNA using Phusion Hot Start II High-Fidelity DNA Polymerase (Thermo Scientific). hβ2M gene was amplified with *hβ2M4-For* and *hβ2M4-Rev* pair of primers ($T_m$ = 65.5 $^oC$). hTTR sequence was split into 2 fragments, hTTR-NS and hTTR-MS. These two fragments were amplified separately using *hTTR-NS-4-For* and *hTTR-NS-4-Rev* pair of primers ($T_m$ = 60.0 $^oC$) and *hTTR-SM-10-For* and *hTTR-SM-10-Rev* pair of primers ($T_m$ = 60.0 $^oC$), respectively. The PCR protocol followed the Thermo Scientific guidelines using 2 µl of template genomic DNA (50-250 ng), 200 µM dNTPs (each), 0.5 µM oligodeoxynucleotide primers and 1U of Phusion Hot Start II DNA polymerase in Phusion HF buffer to make up 50 µl reaction mix (Table 2.4). 25-cycle or

35-cycle PCR was run with the cycling conditions listed in Table 2.5. Amplifications were performed on a Techne TC-5000 gradient thermal cycler. After amplifications the PCR products were analysed by electrophoresis on an agarose gel. The conditions of PCR used as a part of other methods are specified in the sections describing such methods.

| Component | Volume per 50 µl reaction [µl] | Final concentration |
|---|---|---|
| $dH_2O$ | 31.5 | |
| 5x Phusion HF Buffer | 10 | 1x |
| 10mM dNTPs | 1 | 200 µM each |
| 10µM Primer For | 2.5 | 0.5 µM |
| 10µM Primer Rev | 2.5 | 0.5 µM |
| Phusion DNA polymerase | 0.5 | 1 U |
| Template DNA | 2 | (50-250 ng/50 µl reaction) |

***Table 2.4: Components of a PCR reaction mix***

| Cycle step | Temperature | Time | Cycles |
|---|---|---|---|
| **Initial denaturation** | 98 °C | 30s | 1 |
| | | | |
| **Denaturation** | 98 °C | 10s | |
| **Annealing** | [$T_m$] °C | 20s | 35 |
| **Extension** | 72°C | 15-30s/1kb of amplicon | |
| | | | |
| **Final extension** | 72°C | 7.5min | 1 |
| | 4°C | hold | - |

***Table 2.5: PCR cycling conditions***

## 2.2.3 Agarose gel electrophoresis

Agarose electrophoresis is a standard method for separating DNA fragments. According to the fragment size, 0.5 %, 0.8 % and 1 % agarose gels were used to separate fragments (generally larger than 1 kb). Powdered agarose (Sigma Aldrich, UK) was dissolved in TAE buffer (40 mM TRIS base, 1 mM EDTA, 0.114 % glacial acetic acid) by boiling in a microwave oven. When cooled down to 65 $^{o}$C, 20 ml of agarose was mixed with 1 µl of 10 mg/ml ethidium bromide and poured into a gel casting tray. Once the gel was set, 100 ml of TAE mixed with 5 µl of 10 mg/ml ethidium bromide was added into an electrophoresis gel tank to submerge the gel. Ethidium bromide is a fluorescent dye that binds to DNA by intercalating between the bases. It enables visualization of DNA fragments under UV light by absorbing this UV light and transmitting the energy as visible orange light.

5 µl of PCR product or restriction digest was mixed with 1 µl of 6x loading dye (Fermentas) and loaded into wells. 1 kb DNA ladder (Gibco BRL) or λ x *Hind*III were used as markers and run alongside the samples. 0.5 % agarose gel was run at 50 V for 90min. 1 % agarose gel was run at 65 V for 60-90min.

## 2.2.4 Restriction analysis

Restriction enzymes (RE) are bacterial enzymes capable of cleaving DNA in a specific DNA sequence. Restriction enzyme digests were used to:

1. Perform restriction mapping of PCR-amplified clones and potential recombinant plasmids.
2. Prepare DNA vectors.
3. Digest methylated parental DNA templates after a PCR mutagenesis.

All restriction enzymes were supplied by New England Biolabs (UK) unless otherwise stated. DNA was digested under conditions recommended by the manufacturer. Generally, 1 µl of DNA or PCR product was mixed with 9 µl of RE reaction mix (1-10 U of RE and 100 µg/ml BSA in recommended RE

buffer) and incubated at 37 $^{o}$C for 1 hour. The presence of restriction fragments was confirmed by electrophoresis using 0.8 % agarose gel for sufficient fragment separation. For digestion of methylated parental DNA templates after a PCR mutagenesis, 20 U of *Dpn*I enzyme was added to 25 µl of PCR product and incubated at 37 $^{o}$C for 2 hours.

### 2.2.5 Vectors

pBluescript II SK (-) is a 3.0 kb plasmid with ampicillin resistant gene and a multiple cloning site (MCS) with 21 restriction enzyme recognition sites. This polylinker interrupts a coding sequence for β-galactosidase. The vector was linearised with *EcoR*V (pBSIISK(-)x*Eco*RV), gel purified and stored at -20 $^{o}$C.
pLitmus38i is a 2.8 kb plasmid with ampicillin selectable marker. *Nhe*I, *Sal*I and *Mlu*I sites in the polylinker were used to cut the vector to prepare sticky ends for inserting hTTR fragments into the vector. The cut vector was treated with calf intestine phosphatase (CIP) to dephosphorylate the 5' and 3' ends to prevent re-ligation of the linearised plasmid. After treatment with CIP, both vectors pLitmus38ix*Nhe*Ix*Sal*I and pLitmus38ix*Sal*Ix*Mlu*I were gel purified and stored at -20 $^{o}$C.

### 2.2.6 Gel purification

Gel purification is used to isolate and purify desired DNA fragments based on their size. QIAquick Gel Extraction Kit and protocol were used for DNA purification:
DNA was run on a 0.8 % agarose at 50 V for 1 hour in the dark. Following electrophoresis, DNA band was viewed under long-wavelength UV and excised from the agarose gel with a sterile scalpel blade. Care was taken to minimise exposure of DNA to light to avoid DNA damage. The excised gel containing the DNA fragment was mixed with QG buffer (5.5 M guanidine thiocyanate, 20 mM Tris-HCl, pH 6.6) in a 1 : 3 volume ratio (100 mg ~ 100

µl), and incubated at 50 $^{o}$C for 10 min or until the gel was dissolved. 1 volume of isopropanol was added into the dissolved mixture if the DNA fragment was < 500 bp or > 4 kb. The sample was then applied to a QIAquick column, centrifuged for 1 min. The QIAquick columns have a silica membrane that binds DNA in the presence of high ionic-salt buffers. These buffers drive hydrogen bond formation between silica gel and DNA as the DNA passes through the column. After the centrifugation, the flow through was discarded and 500 µl of QG buffer was applied to the column and spun for 1 min. Two washes in 750 µl and 500 µl of PE buffer followed (10 mM Tris-HCl pH 7.5, 80 % ethanol). The alcohol based washes remove contaminants in the sample such as nucleotides, proteins, salts and other impurities. After the last wash, the column was transferred into a clean tube, centrifuged for 1 min to dry and transferred into a clean tube again. DNA is released from the silica membrane by eluting with a low-ionic solution. Such solution disrupts the hydrogen bonds that bind DNA to the silica. DNA was eluted in 50 µl of EB buffer (10 mM Tris-HCl, pH 8.5) and stored at -20 $^{o}$C.

### 2.2.7 Vector and insert ligation

Vector and insert ligation was performed using Quick Ligation Kit (New England Biolabs, UK) and the manufacturer's guidelines were followed: 12 ng of vector was combined with 3-fold or 10-fold molar excess of insert (3 : 1 and 10 : 1 of insert to vector ratio) and the volume was adjusted to 5 µl with $dH_2O$. 5 µl of 2x Quick Ligation Buffer (66 mM Tris-HCl, 10 mM $MgCl_2$, 1 mM DTT, 1 mM ATP, 7.5 % polyethylene glycol, pH 7.6) was mixed in before adding 1 µl (2000 U) of Quick T4 DNA Ligase. The reaction mix was mixed thoroughly, centrifuged briefly, incubated at room temperature for 5 minutes, chilled on ice and transformed.

Gel purified 10.1 kb hβ2M PCR product was inserted by blunt-end ligation into an pBSIISK(-)x*Eco*RV vector to form a hβ2M/pBSIISK(-) recombinant plasmid. The ligation was carried out at 3 : 1 and 10 : 1 insert to vector molar

ratio as described above and the plasmids were transformed into competent cells.

Gel purified 7 kb *Nhe*I-*Sal*I fragment of hTTR-NS PCR product was ligated with gel purified pLitmus38ix*Nhe*Ix*Sal*I vector at 3 : 1 insert to vector molar ratio to form hTTR-NS/pLitmus38i recombinant plasmid. Gel purified 7.7 kb *Sal*I-*Mlu*I fragment of hTTR-MS PCR product was ligated with pLitmus38ix*Sal*Ix*Mlu*I to form hTTR-SM/pLitmus38i recombinant plasmid. Ligated plasmids were then transformed into competent cells.

## 2.2.8 Transformation

NEB 5-alpha chemically competent *E.coli* high efficiency cells (NEB, UK) were used to transform the recombinant plasmids. Tubes with 50 µl of cells were thawed out on ice for 10 minutes. 2 µl containing 10-100 ng of recombinant plasmid DNA was added to the cells. Each tube was mixed with gentle flicking 3 times. The cell mixture was incubated on ice for 30 minutes, then exposed to a heat shock at exactly 42 $^{o}$C in a water bath for exactly 30 seconds and immediately placed back on ice for 5 minutes. 950 µl of SOC medium was added under aseptic conditions to the cell mixture and incubated at 37 $^{o}$C for 60 minutes in a shaking incubator for cell recovery and expression of antibiotic resistance. 50 µl and 200 µl of transformation mix were plated out onto warm and dry LB agar plates containing 100 µg/ml of ampicillin. Plates were incubated overnight at 37 $^{o}$C. When required, some plates were treated with 40 µl of 25 mg/ml X-gal and dried prior to cell plating. Cells with hTTR-NS recombinant plasmids were incubated at 30 $^{o}$C with 25-50 µg/ml of ampicillin.

## 2.2.9 Screening of transformed cells

To identify which cells contain the recombinant plasmid, two marker gene systems were used:

1. Antibiotic resistance gene: a host cell strain that is sensitive to ampicillin and a vector that carries a resistance gene to ampicillin were chosen.
2. β-galactosidase gene complementation: the host cell contains a fragment of the β-galactosidase gene, the vector carries a different fragment of β-galactosidase gene with a MCS polylinker in it and only after transformation the active β-galactosidase enzyme is produced and able to convert colorless substrate X-gal (5-bromo, 4-chloro, 3-indolyl β-D-galactopyranoside) to a blue product. When an insert is successfully cloned into the MCS of a vector, the β-galactosidase gene is inactivated. Thus in the presence of X-gal, cells transformed with a vector carrying the insert are colourless, while cells containing non-recombinant plasmid are blue.

### 2.2.10 Growth of bacterial cultures

Bacterial cultures for plasmid preparation were grown from a single colony. A single colony was inoculated into ~4 ml of LB broth (10 mg/ml Trypton, 5 mg/ml yeast extract, 10 mg/ml NaCl) containing 100 µg/ml ampicillin and grown overnight at 37 $^{o}$C in a shaking incubator. Cells with hTTR-NS recombinant plasmids were incubated at 30 $^{o}$C with 25-50 µg/ml of ampicillin.

### 2.2.11 DNA purification and quantification

To remove contaminants like enzymes, salts, unincorporated nucleotides or oil, QIAquick systems were used to clean DNA.

For DNA clean-up after PCR reaction, QIAquick Gel Extraction Kit Protocol was followed as described above. DNA was eluted in 50 µl of EB buffer (10mM Tris-HCl, pH 8.5) and stored at -20 $^{o}$C.

Plasmid DNA from bacterial cultures was harvested using QIAprep Spin Miniprep Kit: ~2 ml of culture were pelleted, supernatant was removed and the pellet was rinsed with 200 µl of 10 mM Tris-HCl (pH 8.0) and thoroughly resuspended in 250 µl of P1 buffer (50 mM Tris-HCl pH 8.0, 10 mM EDTA,

100 µg/ml RNase). 250 µl of buffer P2 (200 mM NaOH, 1 % SDS) was added and mixed gently to lyse the cells, followed by adding 350 ul of neutralising N3 buffer (4.2 M Guanidin-HCl, 0.9 M potassium acetate, pH 4.8). The high salt concentration causes denatured proteins, chromosomal DNA, cell debris and SDS to precipitate. Precipitated protein was removed by centrifugation for 10 min at 13000 RPM. The supernatant containing the plasmid DNA was applied to a QIAprep spin columns and centrifuged for 1 min at the top speed. The flow-through was discarded, the column was washed by adding 500 µl of buffer PB (5 M Guanidin-HCl, 30% isopropanol) and spun for 1 min. Two washes in 750 µl and 500 µl of PE buffer (10 mM Tris-HCl pH 7.5, 80 % ethanol) followed when the column was spun for 1 min after each wash. After the last wash, the column was transferred into a clean tube, centrifuged for 1 min to dry and transferred into a clean tube again. DNA was eluted in 50 µl or 30 µl of EB buffer (10 mM Tris-HCl, pH 8.5) and stored at -20 $^{o}$C.

After purification, DNA was quantified by running on an agarose gel alongside standards of known DNA concentrations. Different dilutions of DNA samples were visually compared to standards.

### 2.2.12 Storage of transformed cells

Long-term storage of desired bacterial colonies is possible in a freezing medium containing glycerol. 600 µl of bacterial culture grown in LB was mixed with 600 µl of 2 x freezing medium (sterile 30 % glycerol in LB broth) under aseptic conditions, mixed gently but thoroughly and stored at -80 $^{o}$C.

### 2.2.13 Site-directed mutagenesis

*In vitro* site-directed mutagenesis is a method of creating specific changes in a known DNA sequence. The specific mutation is introduced by designing a pair of primers, each of which carries the mutation, and uses PCR with a high

fidelity DNA polymerase. During PCR, the mutation is incorporated into the amplicon replacing the original sequence.

In hβ2m$^{D76N}$ variant, a single base substitution c.286G→A in the hβ2M gene encodes replacement of aspartate residue at position 76 of the mature protein with asparagine residue (D76N). This mutation was introduced into the wild-type hβ2m sequence with primers *B2m-mut-A* and *B2m-mut-B* (Figure 2.1) using hβ2M/pBSIISK(-) recombinant plasmid as a DNA template and Phusion Hot Start II DNA polymerase in a 50 µl PCR reaction. PCR with the overlapping primers results in a product that re-circularizes to form a doubly-nicked plasmid. After a 20-cycle PCR, 25 µl of the PCR product was mixed with 1 µl of *Dpn*I restriction enzyme to remove the methylated parental non-mutated plasmid. 3 µl of digested product was transformed into NEB 5-alpha chemically competent *E.coli* high efficiency cells which are able to perform nick repairs in the mutated hβ2M/pBSIISK(-) recombinant plasmids. 3 µl of the undigested PCR product was also transformed as a control for colony-growing density. 50 µl and 200 µl of the cell mixtures were plated out on LB agar plates and grown overnight as described above. The obtained transformants were tested for carrying the correct inserts by subjecting the purified mutated plasmid DNA to restriction digest with *Hind*III in a 10 µl reaction mix in 37 $^{o}$C for 60 min. 5 µl of the digest was analysed on 0.8 % agarose gel. Potentially mutated recombinant plasmids from single colonies were sequenced. The verified mutated hβ2M/pBSIISK(-) recombinant plasmid was named hβ2M$^{D76N}$/pBSIISK(-).

In hTTR$^{S52P}$ variant, a single base substitution c.214T→C in the hTTR gene encodes replacement of serine residue at position 52 of the mature protein with proline residue (S52P). This mutation was incorporated into the wild type hTTR sequence with *TTR_S52P_mut_For* and *TTR_S52P_mut_Rev* primers (Figure 2.1). 20-cycle PCR was run as described above using hTTR-SM/pLitmus38i recombinant plasmid as a template DNA, Phusion Hot Start II DNA polymerase and 5 % DMSO in 50 µl reaction. The PCR product was treated with *Dpn*I enzyme and transformed into NEB 5-alpha chemically

competent *E.coli* high efficiency cells as above. Purified mutated recombinant plasmid DNA of the transformants was digested with *Hind*III to test the correct restriction pattern of the mutated hTTR-SM/pLitmus38i recombinant plasmid before sequencing. The verified mutated hTTR-SM/pLitmus38i recombinant plasmid was named hTTR-SM$^{S52P}$/pLitmus38i.

***hβ2M mutagenesis primers:***

```
    B2m-mut-A   5′-CACTGAAAAAAATGAGTATGCCTGCCGTGTGAACC-3′    Tm = 78.78
                  ||||||||||||||||||||||||||||              Tm overlap = 72.2
3′-GACTTAAGTGGGGGTGACTTTTTTTACTCATACGGACGGC-5′  B2m-mut-B   Tm = 78.96
```

***hTTR mutagenesis primers:***

```
                    5′-AGTGAGCCTGGAGAGCTGCATGGGCTC-3′        Tm = 78.9
                      ||||||||||||||||||||                  Tm overlap = 65.4
3′-GTGGAATATCCTTTTGGTCACTCGGACCTCTCGACG-5′                  Tm = 78.0
```

***Figure 2.1: Primer design for site-directed mutagenesis***

*Primers for site-directed mutagenesis were designed using NCBI/Primer Blast online software. The single base substitution c.286G→A in the hβ2M gene, encoding replacement of aspartate residue at position 76 of the mature protein with asparagine residue (D76N), and the substitution c.214T→C in the hTTR gene, encoding replacement of serine residue at position 52 of the mature protein with proline residue (S52P), were introduced by designing a pair of primers, each carrying the desired mutation. When designing the primers, the guidelines were: the annealing temperature $T_m$ of such primers should be just over 78$^0$C, the mutation is at least 4 bases form the 5'end and 8 bases from the 3'end and 3'end of each primer has at least 8 non-overlapping bases. At least one G or C should be at the end of each primer (modified from OpenWetWare Site-directed mutagenesis protocol).*

## 2.2.14 Gibson Assembly

Gibson Assembly allows in a single reaction insertion of one or more DNA fragments into virtually any position of a linearized vector and does not rely on the presence of restriction sites within a particular sequence to be synthesized or cloned *(Gibson et al., 2009)*. This method requires DNA fragments with 15-25 nucleotides overlaps with adjacent DNA fragment. To achieve this, DNA fragments and a vector to be assembled are PCR amplified using specifically designed primers with appropriate nucleotide overlaps. *Dpn*I digested and gel purified PCR amplified fragments are then assembled together following the guidelines of Gibson assembly cloning kit (NEB, UK) protocol: 0.02 – 0.5 pmol of DNA fragments (2-10 µl), containing 25-100 ng of vector and 3-fold excess of inserts, were mixed with 10 µl of Gibson Assembly Master Mix (2x) and appropriate amount of $dH_2O$ to make up 20 µl reaction mix. The reaction mix was then incubated at 50 $^{o}$C for 15 min. After the incubation, 2 µl of the reaction mix was transformed into NEB 5-alpha competent *E.coli* following the transformation protocol. Cells were then plated out on agar plates with 25 µg/ml ampicillin and grown overnight at 30 $^{o}$C.

Gibson assembly was used to assemble hTTR gene sequence under the control of mouse albumin enhancer and promoter in pBSIISK(-) plasmid. First, the enhancer/promoter of mouse albumin inserted into pBSIISK(-) vector (Albe-p/pBSIISK(-) (Gorski et al., 1986, Pinkert et al., 1987) was PCR amplified with *TTRass6* and *TTRass1* primers ($T_m$ = 60.7 $^{o}$C), 75ng of hTTR-NS/pLitmus38ix*Nhe*I was amplified with *TTRass2* and *TTRass3* primers ($T_m$ = 56.3 $^{o}$C) and hTTR-SM$^{S52P}$/pLitmus38ix*EcoR*V was amplified with *TTRass4* and *TTRass5* primers ($T_m$ = 59.3 $^{o}$C) with addition of 5 % DMSO (Table 2.2). 20 or 35 cycle PCR was run with high-fidelity DNA polymerase as described in section 2.2.1. The PCR products were then digested with *Dpn*I enzyme, concentrated on a microcon column and gel purified. Such prepared 3 PCR fragments were assembled together following the Gibson assembly protocol as described above with 0.012 pmol of Albe-p/pBSIISK(-) (40 ng) and 3-fold

molar excess of hTTR fragments. Assembled recombinant plasmid was transferred into NEB 5-alpha competent *E.coli* and grown at 30 $^{o}$C for 36 h on agar plates with 25 µg/ml of ampicillin, subcloned and purified. After a *Hind*III digest to verify the correct assembly, the assembled sequence was verified by sequencing. The verified assembled plasmid was named Alb-hTTR$^{S52P}$/pBSIISK(-).

# 2.3 Generation of transgenic mice

## 2.3.1 Gene construct preparation

Prepared gene constructs were excised from recombinant plasmids with restriction enzymes, gel purified and quantified. The transgenes were then diluted to optimal concentration for microinjections 2 ng/µl in TE buffer.

10.1 kb hβ2M$^{D76N}$ gene construct was excised from hβ2M$^{D76N}$/pBSIISK(-) recombinant plasmid with *BamH*I and *Xho*I.

10.9 kb Alb-hTTR$^{S52P}$ gene construct was excised from Alb-hTTR$^{S52P}$/pBSIISK(-) recombinant plasmid with *BssH*II and *Not*I.

## 2.3.2 Microinjections

Microinjections and embryo transfers were performed by Dr Paul Simons and Dr Raya Al-Shawi. Briefly, young C57Bl/6J female mice (3 – 6 weeks old) were superovulated to increase the number of fertilized eggs used for microinjection. To induce superovulation, 5 IU of PMS (pregnant mare's serum) was intraperitoneally injected to induce ovarian follicular development and oocyte maturation. After 47 hours, injections of 5 IU of hCG (human chorionic gonadotropin) followed to induce ovulation and the females were then mated with C57Bl/6J stud males. Next morning, the females were checked for vaginal plugs before harvesting fertilized eggs. Microinjected

embryos were implanted by Dr Raya Al-Shawi into pseudopregnant CBA X C57BL/6 F1 recipient females.

### 2.3.3 Transgenic founders identification

DNA for genotyping of 6 weeks old mice was obtained from a tail tip. The tissue was digested in 300 µl of tail buffer (0.3 M sodium acetate, 10 mM Tris-EDTA, 1 % SDS, 0.2 mg/ml Proteinase K) at 43 $^{o}$C overnight. Tail lysates were vortexed, incubated on ice for 20 min and spun at 9000 g (IEC Micromax RF Centrifuge, Thermo Electron Corporation, USA) at 4 $^{o}$C for 10 min to remove tissue debris and precipitated SDS. 100 µl of supernatant was transferred into a clean tube, incubated on ice for another 10 min and centrifuged at 9000 g at 4 $^{o}$C for 10 min. 1 µl of supernatant was transferred into a PCR tube and covered with 30 µl of mineral oil. The PCR sample was spun for 15 s and subjected to a denaturation step at 98 $^{o}$C for 10 min. 49 µl of PCR mix (0.2 mM dNTPs, 0.3 µM oligonucleotide primers, 1.5 mM $MgCl_2$, 1.25 U Taq polymerase in $NH_4$ buffer, all from Bioline) was added to the sample immediately after the denaturation to make up 50 µl PCR reaction volume. Cycling conditions were: initial denaturation at 94 $^{o}$C for 5 min followed by 35 cycles of denaturation at 94 $^{o}$C for 30 s, annealing at 55 $^{o}$C for 30 s and extension at 72 $^{o}$C for 1 min. Final extension at 72 $^{o}$C lasted 5 min and samples were then held at 10 $^{o}$C.

hβ2M$^{D76N}$ transgenic animals were identified using *hβ2m-F1* and *hβ2m-R2* primers (Table 2.1) distinguishing positive and negative animals by amplifying a 662 bp fragment of the transgene.

hTTR$^{S52P}$ transgenic animals were identified using *hTTRg-3U* and *hTTRg-3D* (Table 2.2) distinguishing positive and negative animals by amplifying a 689 bp fragment of the transgene.

### 2.3.4 Establishment of transgenic lines

Mice positive for the transgene of interest born to the microinjected females were bred with C57Bl/6J mice to identify germ line transmitters. The animals that proved to transmit the transgene into the first generation were named the transgenic founders (G0) of separate lines. Transgenic offspring of the G0 for each line were bred further into subsequent generations to ensure the transgene did not segregate out. After a successful transgene transmission and a secure establishment of the lines, expression levels of transgenic mice were examined.

## 2.4 Biochemistry

### 2.4.1 Protein sample preparation

Serum was used to analyse the levels of expression of a protein of interest. Tissue homogenate was used to investigate the presence of soluble and insoluble proteins in the tissue.

#### 2.4.1.1 Tissue homogenization

After collection, mouse tissue samples were snap-frozen in liquid nitrogen and kept at -70 $^{o}$C until needed. The tissue was then placed on ice and processed as quickly as possible to avoid protein degradation. 10 µl of homogenization buffer was added per 1 mg of tissue and the sample was homogenized by 3 x 3 sec blasts with a shaft of a homogenizer (Ultra Turrax T25, J&K IKA-Labortechnik, Germany) while cooling the sample tube on ice. The sample was allowed to settle for 30 min on ice. An aliquot of the homogenate (~10%) containing the total protein composition (H) was removed and snap-frozen in liquid nitrogen. The rest of the sample was centrifuged at 13500 g at 4 $^{o}$C for 30 min. The supernatant (S1) was collected

and kept on ice. The same starting volume of homogenization buffer was added into the pellet, homogenized by 3 x 3 blasts while cooling the tube on ice and spun again at 13500 g at 4 $^{o}$C for 30 min. The supernatant after this second homogenization (S2) was collected and kept on ice. This homogenization step was repeated 2 more times, when supernatants S3 and S4 were collected. After the aspiration of S4, the pellet (P) was resuspended again in the same volume of homogenization buffer by a quick blast, aliquoted out and snap-frozen in liquid nitrogen.

#### 2.4.1.2 Sample preparation for denaturing protein gel electrophoresis

Mouse serum was mixed with 10x reducing agent (0.5 M DTT,Sigma) and 4x NuPAGE LDS sample buffer (Life Technologies, UK) to make up 10 µl or 20 µl loading sample.

For hβ2m$^{D76N}$ transgenic mice and their controls, 1 µl of serum in 10 µl total sample volume was prepared, denatured at 80 $^{o}$C for 10 min, chilled on ice for few minutes, span briefly and loaded onto a gel. For hTTR$^{S52P}$ transgenic mice and their controls, 0.2 µl of serum in 20 µl total sample volume was prepared, denatured in 95 $^{o}$C for 20 min, chilled on ice for few minutes, span and loaded onto a gel.

1 µl of tissue homogenate/tissue homogenate supernatants/tissue pellet were mixed with 5 µl of 4x NuPAGE LDS sample buffer, 0.8 µl of β-mercaptoethanol and 13.2 µl of $dH_2O$ to make up a 20 µl sample volume. The samples were then denatured at 95 $^{o}$C for 20 min, span briefly and loaded onto a gel.

### 2.4.1.3 Sample preparation for native protein gel electrophoresis

hβ2m$^{D76N}$ transgenic mouse serum for native gel electrophoresis was prepared by mixing 1 µl of serum with 2 µl of bromophenol blue loading dye and loaded in a well of 1 % agarose gel.

Native hβ2m$^{D76N}$ transgenic mouse serum was compared to denatured hβ2m$^{D76N}$ transgenic mouse serum on a native 1% agarose gel. The denatured serum was prepared by mixing 1 µl of serum with 2 µl of 9 M urea in 0.07 M Barbitone – Calcium buffer (60.3 mM Na-barbitone, 9.7 M Barbitone, 0.1 % $NaN_3$, 0.58 g/l Ca-lactate x $4H_2O$) and loaded onto a gel.

### 2.4.1.4 Protein deglycosylation

Peptide N-glycosidase F (PNGase F) is an enzyme that cleaves glycans from asparagine residue of glycoproteins. To test whether the hTTR in hTTR$^{S52P}$ transgenic mice is glycosylated, a deglycosylation of the protein was performed.

The manufacturer protocol was followed. Generally, 0.4 µl of serum of hTTR$^{S52P}$ transgenic mouse (~20 µg of total protein) was used for 20 µl reaction. Firstly, mouse serum was denatured in Glycoprotein Denaturing Buffer in 10 µl reaction mix at 100 $^{o}$C for 10 min. The test tubes were then quenched on ice, span briefly and a total reaction volume of 20 µl was made up by adding 2 µl of 10 x G7 reaction buffer, 2 µl of 10 % NP40, 4 µl of $dH_2O$ and 1 µl of PNGase F enzyme. The mixture was incubated at 37 $^{o}$C for 1 h and 24 h. A sample prepared without the addition of 1 µl of PNGase F enzyme was included as a control of the reaction conditions. 10 µl of the deglycosylated samples were then loaded onto an SDS-PAGE gel and electrophoresed or stored at -20 $^{o}$C.

## 2.4.2 Protein gel electrophoresis

SDS-PAGE electrophoresis

Separation of proteins under denaturing conditions was performed using SDS-PAGE electrophoresis. SDS present in the running buffer denatures the proteins into their linear structure and coats the proteins alongside the whole molecule with a uniform negative charge. The charge of the proteins is now dependent of their molecular weights and the proteins are separated accordingly as they run through the matrix of the gel in an electrical field. NuPAGE Novex 4-12 % Bis-Tris gels or 12 % Bis-Tris gels of 1 mm thickness were used. Protein samples were run alongside a pre-stained protein standard (SeeBlue Plus2, Life Technologies, UK) at 100 V for minimum of 90 min in ice-cold MES-SDS buffer (50 mM MES, 50 mM Tris base, 0.1 % SDS, 1 mM EDTA, pH 7.3).

Native gel electrophoresis

In native gel electrophoresis, non-denatured proteins run according to their charge in an electrical field. The proteins were separated in 1 % agarose gel prepared in 0.07 M BC buffer using medium electroendosmosis agarose (Pronadisa, Spain). After boiling, agarose was poured into a 1 mm thick warmed gel cast with Gel-bond hydrophilic polyester film (Amersham?). The gel was left to set overnight at 4 $^{o}$C in a humid chamber. 3 µl samples were loaded into a well template aligned ~ 2 cm from the edge of the gel. Once all the samples soaked into the gel, the well template was carefully removed and the gel was placed on a continuous cooling plate and run at 180 V for 4 hours.

Rocket immunoelectrophoresis

Rocket immunoelecrophoresis is used to determine concentration of a specific protein in a protein mixture. The samples to be compared are loaded and electrophoresed into an agarose gel containing a specific antibody for

protein of interest detection. In the presence of an excess antigen, soluble antigen-antibody complexes are formed. As the antigen moves further into the gel, more complexes are formed until a point of equivalence between the antigen and antibody concentration is reached. At this point, the complexes are insoluble and a precipitate in a shape of a rocket is formed. The quantitation is based on measuring the height of the precipitate peak.

Rocket immunoelectrophoresis was used to determine the concentration of human TTR in the serum of $hTTR^{S52P}$ transgenic mice. A 1% agarose was prepared in 0.07 M BC buffer using medium electroendosmosis agarose (Pronadisa, Spain). After boiling, agarose was held at 56 $^{o}$C water bath. 200 μl polyclonal rabbit anti-human prealbumin antibody (Dako, 3.9 g/l) was added into 20 ml of the agarose, mixed well and poured into a 1 mm thick warmed gel cast with Gel-bond hydrophilic polyester film (Amersham). The set gel was left overnight at 4 $^{o}$C in a humid chamber. 2 mm wells were punched out and the wells were then loaded with 2 μl sample and/or standard. Standards were prepared from recombinant human $TTR^{S52P}$ protein diluted in PBS and spiked with mouse TTR-KO serum to avoid the serum matrix interference in result quantitation. Serum samples were loaded either undiluted or diluted in PBS. Electrophoresis was carried out at 180 V for 6 h with continuous base-plate cooling in BC buffer. After electrophoresis, the gel was rinsed and washed overnight in 5 % NaCl containing 0.02 % $NaN_3$ at 37 $^{o}$C. After washing, the gel was rinsed with $dH_2O$ and pressed under wet filter paper for 15 min, dried and stained in Coomassie blue staining solution (0.1 % Coomassie brilliant blue R350, 20 % methanol, 10 % acetic acid). After rinsing in $dH_2O$, the gel was destained in destaining solution (30% methanol, 10 % acetic acid) until satisfying background to rocket ratio was achieved. The gel was then dried, scanned and rocket heights were measured using Photoshop software (Adobe). The rocket heights were plotted against TTR concentration of the standards.

### 2.4.3 Western blot

After SDS-PAGE electrophoresis, the gel was transferred to polyvinylidene difluoride (PVDF) membrane using iBlot™ Gel Transfer Stacks Mini (Thermo Fisher Scientific, UK) and iBlot™ Dry Blotting System at 20 V for 7 min according to manufacturer instructions. After native gel electrophoresis, a PVDF membrane was cut to the size of the gel, soaked in 100 % methanol for 1 min and rinsed and washed in PBS for 10 min. The gel was places onto a glass plate and placed in a tray with a small amount of $dH_20$. The rehydrated membrane was then placed on the gel followed by several layers of 3MM paper (Whatmann) wetted in $dH_2O$ and a glass plate with weights was placed on the top. The proteins were allowed to transfer from the gel to the membrane by capillary force overnight.

After blotting, the membrane was rinsed twice and washed twice for 10 min in PBST (0.1% Tween 20 in PBS) and incubated in Protein Free T20 (Pierce, UK) blocking buffer for 90 min to block non-specific antibody binding sites and minimise background. After the washes, the membrane was incubated with primary antibody diluted in blocking buffer either for 2 h at room temperature or overnight at 4 $^{o}$C, on an orbital shaker (antibodies used for Western blot are in Table 2.3). After the incubation, the membrane was rinsed 3 times and washed 3 times for 10 min in PBST and then incubated with horse radish peroxidase (HRP) conjugated secondary antibody diluted in blocking buffer for 60 min at room temperature on an orbital shaker. Antibodies used for western blot analysis are listed in table 2.3). After the secondary antibody incubation, the membrane was rinsed 3 times and washed 3 times for 10 min in PBST. The protein detection was achieved using ECL system (Amersham Biosciences, UK). When autoradiography was performed, the film (Amersham Hyperfilm, GE Healthcare, UK) was pre-sensitised by a flash to raise its absorbance and to increase the linear range of signal detection by the film, then the film was placed on the top of the membrane, exposed at different

time points and developed using an automatic X-ray film processor (Compact X4, Xograph).

## 2.4.4 ELISA

Enzyme-linked immunosorbent assay (ELISA) is a quantitative method used to determine concentrations of a particular protein in a sample. Sandwich ELISA is a format in which the target antigen is detected using two layers of antibodies: a capture antibody that is bound to a microtiter plate to create a solid phase, and a detection antibody that binds to a different epitope of the captured antigen of interest. Optimised in-house protocols or commercial kits were used to measure concentrations of several proteins.

### 2.4.4.1 Human β2m ELISA optimisation

96-well microtiter plate with a high protein-binding capacity (CL S3590-100EA, Corning) was coated with 100 µl capture mouse monoclonal 14H3 anti-hβ2m antibody (University of Pavia, Italy, (Stoppini et al., 1997)) diluted in 0.1 M Carbonate-Bicarbonate buffer (pH 9.0). The tested concentrations were 1 / 2 / 4 / 10 / 20 / 40 / 100 µg/ml. The antibody coated plate was incubated covered at room temperature for 8 hours. The coating solution was removed and wells were washed 3 times with 250 µl of PBST to remove any unbound material.

The remaining protein-binding sites in the coated wells were blocked with 250 µl of blocking buffer. Different blocking buffers were tested to determine which buffer gives the lowest background, does not interfere with other assay components and does not possess any enzymatic activity that would lead to false positive results. The blocking buffers tested were: 1% bovine serum albumin (BSA) in PBS, 10% horse serum (HS) in PBS, 10% goat serum (GS) in PBS, Pierce Protein-free buffer (Thermo Fisher Scientific, UK) and 1% fetal calf serum (FCS) in PBS. Covered plate was incubated overnight at 4 $^{o}$C and washed 3 times with washing buffer.

To determine the most dynamic detection range of antibody binding, 0 – 20 µg/ml of recombinant hβ2m diluted in appropriate blocking buffer was used to obtain a suitable standard curve. To avoid inaccuracy due to serum matrix interference, addition of serum of mice expressing endogenous β2m (WT) or of β2m knock-out mice (KO) into standards was also analysed. 100 µl of standard diluted in appropriate blocking buffer was added into wells in duplicates for accurate quantitation and incubated at room temperature for 2 hours. Wells were then washed 3 times with washing buffer to remove any unbound protein.

Polyclonal rabbit anti-hβ2m antibody (Dako, A0072) was used as a detection antibody and the concentrations tested were: 0.05 / 0.1 / 0.2 / 0.4 / 1 / 10 µg/ml diluted in appropriate blocking buffer. 100 µl was added into each well and incubated at room temperature for 1 hour (an example of an ELISA plate testing different concentrations of antibodies is in Figure 2.2). After washing, 100 µl of HRP conjugated secondary goat anti-rabbit antibody (Dako, P0448) at the concentration 0.25 µg/ml diluted in blocking buffer was added and incubated for 1 hour at room temperature. Horse radish peroxidase (HRP) is an enzyme that catalyzes the reduction of $H_2O_2$ to $H_2O$. In the presence of a chromogenic substrate which acts as a hydrogen donor for this reduction, the solution changes colour and the optical density of the solution can be measured using a spectrophotometer. After washing off the secondary antibody 3 times with washing buffer, 100 µl of tetramethylbenzidine (TMB) substrate (0.2 mg/ml of TMB with 0.01 % $H_2O_2$; Pierce 34021) was added into each well and incubated in the dark until sufficient colour developed (7-15 min). A blue product is generated in direct proportion to the amount of hβ2m present in the sample tested or the calibrator. The enzymatic reaction was stopped by adding 100 µl of 1 M HCl causing a colour change from blue to yellow. The sample absorbance in each well was measured at 450 nm using FLUOstar Omega plate reader (BMG Labtech, GmBH Germany). The unknown sample protein concentration was interpolated from the obtained standard curve and multiplied by the dilution factor.

| | 1 | 2 | 3 | 4 | 5 | 6 | 7 | 8 | 9 | 10 | 11 | 12 |
|---|---|---|---|---|---|---|---|---|---|---|---|---|
| | 0.05 µg/ml detection Ab | | | | | | 0.1 µg/ml detection Ab | | | | | |
| **Capture Ab µg/ml** | **1** | **1** | **10** | **10** | **100** | **100** | **1** | **1** | **10** | **10** | **100** | **100** |
| A | 0 | 0 | 0 | 0 | 0 | 0 | 0 | 0 | 0 | 0 | 0 | 0 |
| B | 0.2 | 0.2 | 0.2 | 0.2 | 0.2 | 0.2 | 0.2 | 0.2 | 0.2 | 0.2 | 0.2 | 0.2 |
| C | 1 | 1 | 1 | 1 | 1 | 1 | 1 | 1 | 1 | 1 | 1 | 1 |
| D | 5 | 5 | 5 | 5 | 5 | 5 | 5 | 5 | 5 | 5 | 5 | 5 |
| E | 0 | 0 | 0 | 0 | 0 | 0 | 0 | 0 | 0 | 0 | 0 | 0 |
| F | 0.2 | 0.2 | 0.2 | 0.2 | 0.2 | 0.2 | 0.2 | 0.2 | 0.2 | 0.2 | 0.2 | 0.2 |
| G | 1 | 1 | 1 | 1 | 1 | 1 | 1 | 1 | 1 | 1 | 1 | 1 |
| H | 5 | 5 | 5 | 5 | 5 | 5 | 5 | 5 | 5 | 5 | 5 | 5 |
| | 0.2 µg/ml detection Ab | | | | | | 0.4 µg/ml detection Ab | | | | | |

***Figure 2.2: Grid experiment for ELISA capture and detection antibody optimization***

*The 96-well plate was divided into 4 quadrants. The 6 columns in each quadrant represent capture antibody concentrations, the 4 rows in each quadrant represent standard curve points, each of the 4 quadrants represents a different detection antibody concentration. Each quadrant contains all the possible combinations of capture antibody at 1, 10 and 100 µg/ml and standard curve points of 0, 0.2, 1 and 5 µg/ml of recombinant hβ2m diluted in a blocking buffer, at a detection antibody concentration of 0.05, 0.1, 0.2 and 0.4 µg/ml. The capture antibody used is mouse monoclonal 14H3 anti-hβ2m. The detection antibody used is polyclonal rabbit anti-hβ2m.*

---

### 2.4.4.2 Human β2m ELISA

To determine the concentration of hβ2m in the serum of transgenic mice, the optimised protocol was as follows:

The microtiter plate wells were coated with 100 µl of 10 µg/ml mouse monoclonal 14H3 anti-hβ2m capture antibody diluted in 0.1 M Carbonate-Bicarbonate buffer for 8 h at room temperature, washed 3 times with PBST and blocked with 250 µl of Pierce protein-free blocking buffer overnight at 4 $^{o}$C. To obtain a standard curve, 100 µl of recombinant hβ2m$^{D76N}$ protein diluted in blocking buffer at concentrations: 0 / 0.31 / 0.625 / 1.25 / 2.5 / 5 / 10

µg/ml and spiked with 5 µl of WT or β2m-KO serum, according to the background of the mice analysed, was added into wells in duplicates. Mouse serum was diluted 1/20 in blocking buffer and 100 µl per well (in duplicates) was incubated at room temperature for 2 h. After 3 washes in PBST, 100 µl of polyclonal rabbit anti-hβ2m detection antibody diluted in blocking buffer was used at concentration 4.8 µg/ml and incubated for 1 h at room temperature. Any unbound material was washed off and wells were incubated for 1 h with HRP conjugated goat anti-rabbit antibody diluted in blocking buffer at concentration 0.25 µg/ml. After 3 washes, 100 µl of TMB was added into each well and incubated in the dark for 7-10 min. The reaction was stopped by adding 100 µl of 1M HCl and the plate was read at 450 nm within 15 min. The standard curve was obtained using Prism software and the unknown sample protein concentrations were interpolated and multiplied by the dilution factor.

### 2.4.4.3 Mouse SAA ELISA

96-well microtiter plate with a high protein-binding capacity (CL S3590-100EA, Corning) was coated with 100 µl of 1 µg/ml capture anti-mouse SAA antibody aSAA1-95 (Binding site, UK) diluted in 0.1 M Carbonate-Bicarbonate buffer and incubated covered at 4 $^{o}$C overnight. Next day, the plate was washed 3 times with PBST, blocked with 250 µl of 2 % BSA in PBST blocking buffer for 2 h at room temperature and washed. To obtain a standard curve, 50 µl of mouse SAA protein diluted in blocking buffer at concentrations: 0 / 0.156 / 0.078 / 0.31 / 0.625 / 1.25 / 2.5 / 5 µg/ml was added into wells in duplicates. Mouse serum was diluted 1/100 in blocking buffer (when normal levels of SAA were expected) and 50 µl per well in duplicates was incubated for 1 h at room temperature. After 3 washes with PBST, 100 µl of biotinylated detection anti-mouse SAA antibody aSAA1-96 (Binding site, UK) diluted at 2 µg/ml in blocking buffer was added into the wells and incubated for 1 h at room temperature. The detection antibody was washed off 3 times with PBST and 100 µl of HRP conjugated streptavidin (Sigma S5512) diluted 1/3000 in blocking buffer was added into wells and incubated for 1 h at room

temperature. After 3 washes in PBST, 100 µl of TMB substrate was added in the wells and incubated in the dark for 10 min. The reaction was stopped by 1 M HCl and absorbance was read at 450 nm using FLUOstar Omega plate reader (BMG Labtech, GmBH Germany). The unknown protein concentrations were interpolated from the standard curve as described above.

Biotinylation of aSAA1-96 antibody

The anti-mouse SAA antibody aSAA1-96 (Binding site, UK) was biotinylated using NHS-D-Biotin (Sigma H1759). The biotin was dissolved in DMSO immediately prior to use at concentration 5 mg/ml. 50 µl of such prepared biotin was mixed with 500 µl of antibody at concentration 2 mg/ml in 0.1 M Carbonate-Bicarbonate buffer and incubated for 30 min to 2 h at room temperature. After the incubation, 50 µl of 1 M glycine was added into the mixture to stop the reaction. The biotinylated IgG was eluted in 3.5 ml PBS and the absorbance at 280 nm was measured on a luminescence spectrophotometer (LS55, PerkinElmer Inc., MA).

#### 2.4.4.4 Mouse cystatin C ELISA

Cystatin C levels in the serum of transgenic mice and their littermate controls were measured using Cystatin C ELISA kit (Biovendor, R&D, Czech Republic). Manufacturer's instructions of the sandwich ELISA assay were followed and the unknown were interpolated from the standard curve as described above.

#### 2.4.4.5 Total thyroxine ELISA

To quantify the total thyroxine (T4) in mouse serum, a Thyroxine (T4) ELISA kit was used (Calbiotech, USA). The kit was a solid phase competitive ELISA when the T4 in the mouse serum competes with HRP-conjugated T4 for binding sites as they are added into streptavidin-coated wells at the same time together with anti-T4-biotin labelled antibody. Upon the addition of the

substrate, the intensity of the developed colour is inversely proportional to the concentration of T4 in the serum sample. A standard curve and the unknown were interpolated as described above.

### 2.4.5 Immunofluorescence

Immunofluorescence is a technique using fluorescent-labelled antibodies to detect specific target antigen. Direct immunofluorescence was performed on blood films.

Blood films were prepared manually on slides by spreading a drop of blood to obtain appropriate film thickness and length, air-dried at room temperature and processed within 24 hours. The films were fixed for 10 min either in 4 % PFA in PBS at room temperature or in 100 % methanol at -20 $^{o}$C. After fixation, samples were rinsed and washed 3 times in PBS and blocked for 30 min in 2 % BSA in PBS. After blocking, the slides were assembled into a sequenza rack and incubated for 1 hour with 100 µl of FITC-conjugated mouse monoclonal anti-human β2m antibody B2M-01 (ABX172, Source BioScience, UK) *(Hilgert et al., 1984)* diluted 1/200 in blocking buffer. The fluorescein isothiocyanate (FITC) is a fluorochrome prone to photobleaching, therefore incubation and subsequent steps were performed in the dark when possible. After rinsing in PBS, the samples were counterstained with Hoechst 33342 (B2261 Sigma-Aldrich, UK) diluted 1/10000 in PBS for 10 min. After 3 washes in PBS, slides were mounted in Citifluor (Citifluor Ltd., UK), overlaid with a coverslip, kept in the dark and analysed under UV microscope (Nikon TE300) within 24 hours.

### 2.4.6 Flow cytometry

Fluorescence-based flow cytometry enables sorting heterogeneous mixture of cells based upon the light scattering and fluorescence characteristics of each cell. Flow cytometry was used to analyse expression of hβ2m on cell surface of leucocytes of $h\beta2m^{D76N}$ transgenic mice.

25 µl of whole blood was mixed with 25 µl of 0.1 % EDTA to prevent clotting and the sample was kept on ice. Erythrocytes were lysed by adding 1 ml of erythrocyte lysing buffer (150 mM ammonium chloride, 10 mM sodium bicarbonate, 1 mM disodium EDTA) into each sample and gentle mixing for 20 min. Leucocytes were collected by spinning at 200 g for 10 min at 4 $^{o}$C. Cells were then fixed with 1 % PFA in PBS for 5 min and washed 3 times with FACS wash buffer (1 % FBS, 0.1% $NaN_3$ in PBS). After the last wash, cells were resuspended in 50 µl of FACS wash buffer and incubated with Fc-block (rat anti-mouse CD16/CD32, BD Bioscience, UK) to reduce non-specific Fc receptor-mediated binding by antibodies of interest. Cells were then stained with APC-conjugated anti-mouse CD45 antibody (Biolegend, CA) and FITC-conjugated anti-human β2m B2M-01 antibody (Source Bioscience, UK) for 1h in the dark on ice. After staining, cells were washed twice with 1.5 ml of FACS wash buffer, resuspended in 500 µl FACS wash buffer and analysed on FACSCalibur (BD Bioscience, CA) using the CellQuest software.

## 2.5 Reverse Transcription PCR

Reverse transcription PCR (RT-PCR) is a technique for detection of mRNA transcription. After RNA isolation from tissue, a single-stranded complimentary DNA (cDNA) is synthesized from single-stranded RNA template using a reverse transcriptase enzyme. The reverse transcription reaction product is then used as a template for PCR.

## 2.5.1 RNA purification

Total RNA was extracted from liver, kidney, spleen, heart, tongue, skeletal muscle and brain of transgenic animals and non-transgenic controls using RNeasy Plus Universal Mini Kit. After collection, 30 – 50 mg of mouse tissue was snap-frozen in liquid nitrogen and kept at -70 $^{o}$C until needed. The tissue was homogenized in 900 µl QIAzol lysis reagent using a stainless steel bead and TissueLyser (Qiagen) for 2 x 2 min at 20 Hz. The homogenate was collected and left for 5 min to promote dissociation of nucleoprotein complexes. 100 µl of gDNA Eliminator solution was added into each sample, shook vigorously for 15 s, followed by 180 µl of chloroform, shook again and left for 3 min before centrifugation at 12000 g for 15 min at 4 $^{o}$C. The upper, aqueous phase was collected and mixed with 1 volume of 70 % ethanol. This mixture was then applied to an RNeasy mini spin column and centrifuged at 8000 g for 15 s at room temperature. The membrane of the column was then washed by 700 µl of buffer RWT and span for 15 s at 8000 g at room temperature and then washed twice by 500 µl of buffer RPE and span for 15 s at 8000 g each time. The column was then dried by spinning for 1 min at 8000 g. The RNA was eluted from the membrane in 50 µl of RNase-free water. The amount of RNA in each sample was measured using 8 sample spectrophotometer Nanodrop ND-8000 (Labtech International).

## 2.5.2 Reverse transcription

QuantiTect Reverse Transcription kit from QIAgen was used and manufacturer's guidelines were followed. Firstly, genomic DNA (gDNA) contamination in the RNA samples was removed by incubating 500 ng purified RNA with 2 µl of gDNA wipeout buffer in 14 µl reaction volume for 2 min at 42 $^{o}$C. After this step, first strand cDNA synthesis was achieved by mixing the 14 µl reaction from gDNA elimination step with 4 µl of Quantiscript RT buffer, 1 µl of RT primer mix and 1 µl of reverse transcriptase on ice and incubating for 30 min at 42 $^{o}$C followed by 3 min incubation at 95 $^{o}$C to

inactivate the enzyme. The RT primer mix enables cDNA synthesis from all regions of RNA transcripts. Reverse transcriptase is an RNA-dependent DNA polymerase enabling transcription of cDNA from an RNA template with a hybrid-dependent exoribonuclease activity degrading an RNA strand in RNA-DNA hybrids. A reaction without the reverse transcription enzyme was prepared simultaneously for each sample as a negative control. cDNA prepared in the reverse transcription step was then used immediately in a PCR reaction as a template or stored at -20 $^{o}$C. The 20 µl PCR reaction mix consisted of 1 µl of cDNA, 0.2 mM dNTPs, 0.3 µM oligonucleotide primers, 1.5 mM $MgCl_2$ and 1.25 U Taq polymerase in $NH_4$ buffer. The PCR reaction mix was covered with 30 µl of mineral oil, denatured at 94 $^{o}$C for 5 min and followed by 25 cycles of denaturation at 94 $^{o}$C for 30 s, annealing at 55 $^{o}$C for 30 s and extension at 72 $^{o}$C for 1 min. Final extension at 72 $^{o}$C lasted 5 min and samples were then held at 10 $^{o}$C.

The primers used in the PCR reaction to obtain hβ2m mRNA were *hβ2m RT-PCR 5'* primer and *hβ2m RT-PCR 3'* primer amplifying a 240 bp PCR product (Table 2.1), PCR primers used for the identification of hTTR mRNA were *hTTR RT-PCR 5'* primer and *hTTR RT-PCR 3'* primer amplifying a 226 bp PCR product (Table 2.2). A control RT-PCR reaction was performed on glyceraldehyde 3-phosphate dehydrogenase (GAPDH), a house-keeping gene expressed in all tissues with primers ms*GAPDHf* and ms*GAPDHr* (Table 2.2) amplifying a 133 bp PCR fragment.

## 2.6 Histochemistry

### 2.6.1 Tissue sample preparation

The organs of euthanized mice were dissected out and fixed in 10 % NBF overnight at room temperature. The tissue was then dehydrated through a series of graded ethanol incubations to displace the water within the tissue and infiltrated with paraffin wax. The infiltrated tissue was then embedded into wax blocks.

Paraffin embedded blocks were sectioned on a microtome (Leica RM2135, Germany) using disposable microtome blades (Feather S35, Japan). Cut sections were placed on a surface of a 45 $^{o}$C paraffin section mounting bath (Barnstead, Electrothermal, UK), collected onto a Superfrost Plus microscope slide (Thermo Scientific) and dried at 37 $^{o}$C overnight. 3 µm sections were cut for immunohistochemistry and H&E staining, 6 µm for Congo red staining.

### 2.6.2 Histological staining

Sections were dewaxed through 2 baths of xylene (5 min each) and hydrated through baths of graded ethanol (3 x 100%, 1 x 90%, 1 x 75%, 1 x 50%, 2 min each) followed by 5 min bath in tap water.

For Congo red staining, sections were then immersed for 5 min in Mayer's haematoxylin (Pioneer Research Chemicals, UK) for nuclear counterstaining and then placed in tap water for 5 min. Following a rinse in $dH_2O$, the sections were incubated for 20 min in filtered saturated alcoholic NaCl solution (0.35 M NaCl in 80 % ethanol) with 0.01 % NaOH and then 20 min in filtered alcoholic Congo red solution (0.35 M NaCl, 2 g/l Congo red (Raymond Lamb, UK) in 80 % ethanol) with 0.01 % NaOH. Immediately after the staining, the sections were rinsed in 100 % ethanol and immersed into 2 baths of 100 % ethanol (2 min each) and cleared in 2 baths of xylene (5 min each) before

mounting with DPX (BDF, UK) or ClearVue mountant XYL (4212, Thermo Scientific) and covered with a coverslip.

For Heamotoxylene and Eosin (H&E) staining, rehydrated sections were immersed in Coles Haematoxylene (Pioneer Research Chemicals, UK) for 10 min, rinsed in tap water for 5 min and destained in 1 % acid alcohol (Pioneer Research Chemicals, UK). After rinsing in tap water for 5 min, section were stained in 1 % aqueous eosin (Pioneer Research Chemicals, UK) for 2 min, rinsed in tap water and immersed in 100 % ethanol, cleared in xylene (2 x 5 min), mounted with DPX or ClearVue mountant and covered with a coverslip.

### 2.6.3 Immunostaining

The localisation of specific proteins within a tissue was assessed by immunohistochemistry. All steps were performed at room temperature unless otherwise stated. The sections were rehydrated as described above and incubated in 0.6 % $H_2O_2$ (Sigma, UK) for 15 min to block the tissue endogenous peroxidase. After a rinse in PBS, the slides were assembled into a sequenza rack and washed with PBST. Any non-specific binding sites were blocked with 30 min incubation in 2.5 % normal horse serum (Vector Laboratories). The slides were then incubated with 100 µl of primary antibody diluted in Dako antibody diluent for 1 hour at room temperature or at 4 $^{o}$C overnight. Antibodies used for immunohistochemistry are listed in Table 2.3. Non-primary antibody controls were incubated with the antibody diluent only. The antibody was washed away by two washes in PBST followed by 30 min incubation with 100 µl of secondary antibody conjugated with HRP micropolymers (Vector Laboratories). Any excess stain was washed off by PBST. The slides were then rinsed in PBS and stained with DAB (Metal Concentrate, Thermo Scientific UK) diluted 1:10 in Stable peroxide solution (Thermo Scientific, UK). The DAB is bound by the substrate and oxidised by the peroxidase producing a brown alcohol-insoluble precipitate at the site of enzymatic activity. After sufficient brown colour was developed (incubation

time no more than 10 min), the reaction was stopped by PBST. The slides were then rinsed in tap water, counterstained with Mayer's haematoxylene (Pioneer Research Chemicals) for 30 s, destained in tap water for 5 min and dehydrated through 2 min baths of graded ethanol (1 x 50 %, 1 x 75 %, 1 x 90 %, 3 x 100%). The sections were then cleared in two 5 min immersions in xylene and mounted with DPX or ClearVue mountant.

Immunostaining for TTR protein required antigen retrieval. In this case, the slides were rehydrated and the endogenous peroxidase was blocked as described above, rinsed in $dH_2O$, incubated in 1 % sodium metaperiodate (Fisher Scientific, UK) for 10 min and rinsed and washed twice in $dH_2O$ for 5 min. Then the slides were incubated in 0.1 % sodium borohydrate (Fisher Scientific, UK) for 10 min and again washed twice in $dH_2O$ for 5 min for each wash. The slides were then rinsed in 0.9 % NaCl, placed into a moisture chamber and incubated covered with 6 M guanidine hydrochloride in 0.9 % NaCl for 4 h. After rinsing in 0.9 % NaCl, the slides were then assembled into a sequenza rack, washed in PBST and stained with antibodies as described above.

### 2.6.4 Microscopy

Histological examination of stained sections was performed using a light microscope (Leica, Germany) and photographs were taken using Leica IM50 software. Congo red stained sections were analysed with and without polarizer and under UV light.

Immunofluorescence was performed within 24 hours using Nikon TE300 light microscope with UV filters.

## 2.7 Whole body $^{125}$I-human SAP retention

SAP is universally present in all amyloid deposits and persists there for a prolonged period of time. Whole body $^{125}$I-hSAP retention method is based on

the ability of human SAP avidly bind to amyloid and is used as a specific and quantitative *in vivo* tracing tool for systemic amyloid deposition in mice and humans *(Hawkins et al., 1988)*.

$^{125}$I-radiolabelled human SAP was prepared in the National Amyloidosis Centre (UK) as described in *(Hawkins et al., 1988)*. The mice were injected intravenously with $10^6$ c.p.m. of high specific activity $^{125}$I-hSAP and counted 24h and 48h after the label administration in a gamma counter to obtain the retention of the tracer. The $^{125}$I-hSAP injections and the whole body counts were performed by Dr S. Ellmerich from the Centre for amyloidosis and acute phase proteins, UCL. To protect the animals from uptake of radiolabelled iodine by thyroid gland, the mice were given 0.006 % KI in drinking water at least 24 h prior to injections and were kept on the KI treated water for a week after the injections. In the absence of amyloid, there is a rapid whole body clearance of the radiolabelled SAP and by 48 h, less than 10 % of the tracer is detectable.

## 2.8 Preparation of AEF for seeding experiments

Amyloidosis can be accelerated in experimental animals by administration of amyloid-enhancing factor (AEF). To prime amyloidosis in hβ2m$^{D76N}$ and hTTR$^{S52P}$ transgenic mice, *in vitro*-prepared and/or *ex vivo*-isolated amyloid fibrils and/or extract of amyloidotic tissue were used in a number of experiments. Spontaneous and amyloid-seeded amyloid deposition in transgenic and control mice was investigated.

**Aβ2m$^{D76N}$ fibrils preparation**

*In vitro*-prepared human Aβ2m$^{D76N}$ fibrils were obtained from Dr P. Mangione (Centre for amyloidosis and acute phase proteins, UCL). The fibrils were resuspended in sterile endotoxin-free PBS at a concentration 1 mg/ml and

stored at -80 $^{o}$C. When needed, the fibril suspension was further diluted in PBS prior to a 100 µl intravenous (i.v.) injection.

Human *ex-vivo* Aβ2m$^{D76N}$ fibrils were isolated by Dr P. Mangione from a spleen of Aβ2m$^{D76N}$ amyloidosis patient with severe Aβ2m amyloid deposition. Isolated amyloid fibrils were resuspended in sterile endotoxin-free PBS at a concentration 100 µg/ml and stored at -80 $^{o}$C. Each mouse received a 100 µl injection equal to 10 µg of fibrils intravenously.

**ATTR$^{S52P}$ fibrils preparation**

Human *ex-vivo* ATTR$^{S52P}$ fibrils were isolated by Dr P. Mangione from a spleen of ATTR$^{S52P}$ amyloidosis patient with severe ATTR amyloid deposition. Isolated amyloid fibrils were resuspended in sterile endotoxin-free PBS at a concentration 100 µg/ml and stored at -80 $^{o}$C. Each mouse was injected with 10 µg of fibrils, i.e. 100 µl of the fibril suspension intravenously.

**Preparation of ATTR$^{S52P}$ AEF from a tissue extract**

Unfixed spleen from ATTR$^{S52P}$ amyloidosis patience with abundant infiltration of amyloid was provided by Dr G. Tennent (Centre for amyloidosis and acute phase proteins, UCL) from Amyloid Research Tissue bank. The spleen was thawed out from -80 $^{o}$C and briefly rinsed in ice-cold 10 mM Tris-HCl, 0.138 mM NaCl, 0.1 %NaN3, pH 8.0. 300 mg of tissue was teased, mixed with 15 ml of sterile PBS and shook vigorously for 10 min. The suspension was then centrifuged and the supernatant was used to inject experimental mice with 200 µl intravenously.

# 3 Generation and establishment of hβ2m$^{D76N}$ transgenic mouse lines

## 3.1 Introduction

Human $\beta_2$-microglobulin (hβ2m) is a protein expressed by all nucleated cells. The human B2M gene consists of 4 exons and 3 introns and the promoter of the β2M gene has been identified within a hundred base pairs upstream *(Gussow et al., 1987)*. β2m is a part of major histocompatibility complex (MHC) class I molecules on the cell surface presenting antigens to $CD8^+$ cytotoxic T-lymphocytes. The association of the MHC class I heavy chain and β2m is a prerequisite for cell-surface expression of the complex. β2m deficiency is rare and results in complex immunodeficiency.

One of the most serious pathophysiological properties of the β2m protein in humans is its ability to form amyloid, which can be acquired, or genetic. In healthy people, the range of serum β2m concentration is 0.7 – 2.7 µg/ml *(Berggard and Bearn, 1968, Greipp et al., 1988, Floege et al., 1991)*. β2m is catabolised by the kidneys and patients with impaired kidney function have increased β2m concentrations due to its insufficient clearance. Because of its size, β2m is not cleared by dialysis membranes and its plasma concentrations remain elevated. Majority of end stage renal failure patients on long term dialysis develop acquired Aβ2m amyloidosis (dialysis-related amyloidosis) *(Gejyo et al., 1986b)*. Hereditary systemic Aβ2m amyloidosis caused by a mutation in the β2m gene has also been described *(Valleix et al., 2012)*.

Mice transgenic for human β2m were successfully generated in the past to study expression of the human MHC class I complex on the cell surface *(Krimpenfort et al., 1987, Chamberlain et al., 1988)*. The β2M transgene used to produce transgenic mice for the MHC class I experiments contained the full length human β2m gene with 2.9 kb 5' flanking sequence and 1.5 kb of 3' flanking sequence and 120 bp of pEMBL9 bacterial vector DNA at the 3' end. These mice produced hybrid MHC class I antigens on the cell surface

consisting of murine MHC class I heavy chains in association with the human β2m. The tissue expression of the transgene in these mice was very similar to the tissue expression of the endogenous mouse β2m. The concentration of free circulating human β2m in the transgenic mice was not reported.

In 2010, hβ2m transgenic mice generated specifically to study Aβ2m amyloidosis were reported. The human β2m construct consisted of a 360 bp human β2m gene cDNA expressed under the control of cytomegalovirus immediate early gene enhancer (CMV-IE)/chicken β-actin promoter and rabbit β-globin poly(A) signal *(Zhang et al., 2010, Niwa et al., 1991)*. The wide-spread expression of the transgene driven by the house-keeping β-actin promoter was confirmed in those mice. Despite the reported high concentration of circulating human β2m, the transgenic mice did not develop Aβ2m amyloidosis *(Zhang et al., 2010)*.

In 2012, a single nucleotide mutation in B2M gene was discovered in one family which causes hereditary systemic Aβ2m amyloidosis *(Valleix et al., 2012)*. The highly amyloidogenic c.286G→A (GAT/AAT) mutation in the B2M gene encodes a substitution of aspartate at the position 76 of the mature protein with asparagine (D76N). Unlike in dialysis-related amyloidosis caused by sustained elevated concentrations of serum wild-type β2m, the patients carrying the D76N mutation develop Aβ2m amyloidosis despite normal serum levels of β2m variant (< 3 μg/ml) and normal renal function *(Valleix et al., 2012)*.

Therefore the hypothesis was that expression of this first naturally occurring highly amyloidogenic human $\beta2m^{D76N}$ ($h\beta2m^{D76N}$) variant in mice will lead to an animal model of Aβ2m amyloidosis.

The aim to support the hypothesis was to generate $h\beta2m^{D76N}$ transgenic mice by cloning the human B2M gene from human genomic DNA and introducing the D76N mutation by site-directed mutagenesis. The transgenic mice were characterised with respect to the $h\beta2m^{D76N}$ transgene expression, the $h\beta2m^{D76N}$ protein concentration in the circulation and cell surface expression of the D76N variant for both, $h\beta2m^{D76N}$ transgenic mice expressing the

endogenous mouse β2m and hβ2m$^{D76N}$ transgenic mice in which the endogenous β2m was knocked-out.

## 3.2 Results

Transgenic mice carrying a highly amyloidogenic variant D76N of human $\beta_2$-microglobulin (hβ2m) were generated to study the mechanisms of Aβ2m amyloidosis. The transgene was prepared by cloning a full length wild-type hβ2m gene from human genomic DNA, in which the single base substitution c.286G→A (GAT/AAT) was introduced, encoding replacement of aspartate residue at the position 76 of the mature protein with asparagine residue (D76N). The advantage of using human genomic sequence, including exons and introns, over cDNA-based constructs is that the levels of expression of cDNA constructs can be much lower than the expression levels obtained by genomic DNA sequence. It was shown that introns enhance the efficiency of gene expression and thus play a role in facilitating transcription of microinjected genes *(Brinster et al., 1988, Whitelaw et al., 1991)*. The human β2m gene own promoter and regulatory sequences within the 5' and 3' ends were used to drive the expression of the transgene to maintain the tissue-specific expression of the transgene *(Chada et al., 1985, Hammer et al., 1987)*.

### 3.2.1 Cloning of human $\beta_2$-microglobulin

The hβ2m gene was PCR-amplified from genomic DNA with *hβ2m4-For* and *hβ2m4-Rev* primers (Table 2.1) using Phusion Hot Start II High-Fidelity DNA Polymerase. This polymerase was chosen to minimise PCR-introduced errors into the cloned sequence. The amplified 10.1 kb fragment contained the 7.4 kb sequence of hβ2m gene with 2.1 kb 5' flanking sequence and 630 bp 3' flanking sequence to maintain the gene regulatory elements (Figure 3.1). The 10.1 kb fragment was then cloned into an *EcoR*V site of a 3 kb pBSIISK(-) vector by blunt-end ligation.

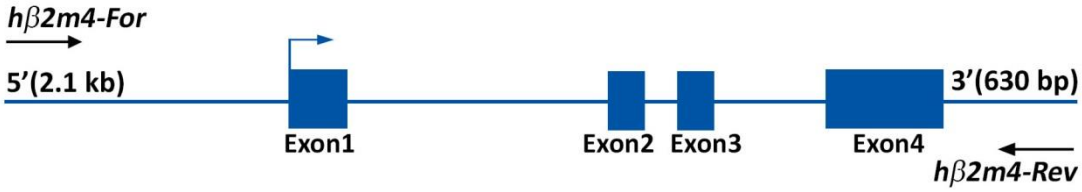


***Figure 3.1: Amplification of human $\beta_2$-microglobulin gene***

*10.1 kb hβ2m fragment containing the 7.4 kb sequence of hβ2m gene with its 4 exons and 3 introns, 2.1 kb 5' flanking sequence and 630 bp 3' flanking sequence, was PCR-amplified from human genomic DNA using hβ2m4-For and hβ2m4-Rev primers and ligated with pBSIISK(-)xEcoRV vector.*

---

After the hβ2m/pBSIISK(-) ligation product was transformed, plasmid DNA of 12 clones was purified by alkaline lysis and run on an agarose gel to assess the DNA size for each clone. The expected size of a correctly assembled recombinant plasmid was 13.1 kb and 9 of the 12 plasmids were recombinant (not shown). These recombinant plasmids were mapped by restriction analysis to verify the identity. *BamH*I and *Xho*I restriction sites are present in the multiple cloning site of the pBSIISK(-) vector but are missing in the sequence of the hβ2m gene (Figure 3.2). Restriction digest with these two enzymes results in cutting the insert out of the vector, producing two fragments of 10.1 kb (insert) and 3 kb (vector). In 8 plasmids, a 10.1 kb insert was cut out of the vector as shown in Figure 3.3 A. To further verify the identity of the cloned DNA, I used *Hind*III to map the clones as this enzyme has two recognition sites within the β2m gene. Because the β2m gene can be inserted in two different orientation into the plasmid, which contains a single *Hind*III site, two different restriction patterns of 3 fragments can be generated: 4.2 kb, 4.4 kb and 4.6 kb (Figure 3.2 B) or 7.2 kb, 4.4 kb and 1.6 kb (Figure 3.2 A). The restriction mapping suggested that 7 out of the 12 clones analysed (clones 1, 4, 5, 6, 10, 11, 12) carry one hβ2m gene insert(Figure 3.3 B).

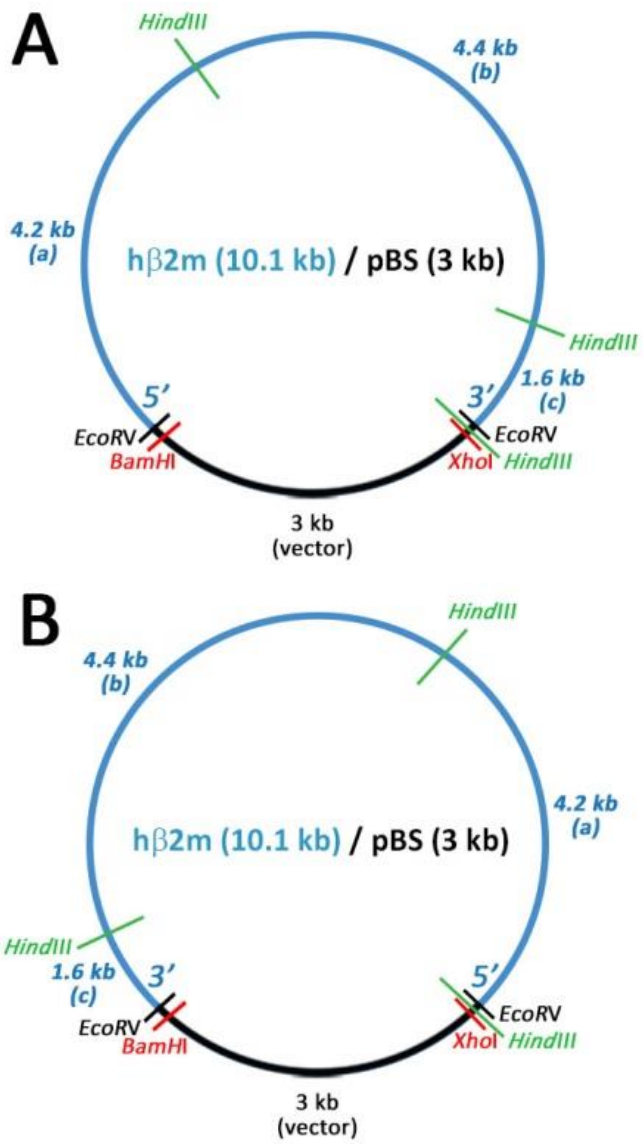


***Figure 3.2: hβ2m/pBSIISK(-) recombinant plasmid***

*Map of a 10.1 kb hβ2m fragment ligated into an EcoRV site of a 3 kb pBSIISK(-) vector. BamHI, XhoI and HindIII restriction enzymes were used for mapping of the sequence structure of recombinant plasmids. hβ2m insert can be bluntly cloned into the EcoRV linearised pBSIISK(-) vector in two directions. While cutting the insert out of the vector with BamHI and XhoI is not affected by the direction of insertion, HindIII digest distinguishes these two insertion possibilities by giving two different restriction patterns of 3 fragments: 7.2 kb (3 kb vector + 4.2 kb fragment a), 4.4 kb (fragment b), 1.6 kb (fragment c) with insertion 5' → 3' (Figure **A**) or 4.2 kb (fragment a), 4.4 kb (fragment b), 4.6 kb (3 kb vector + fragment c) with insertion 3' → 5' (Figure **B**).*

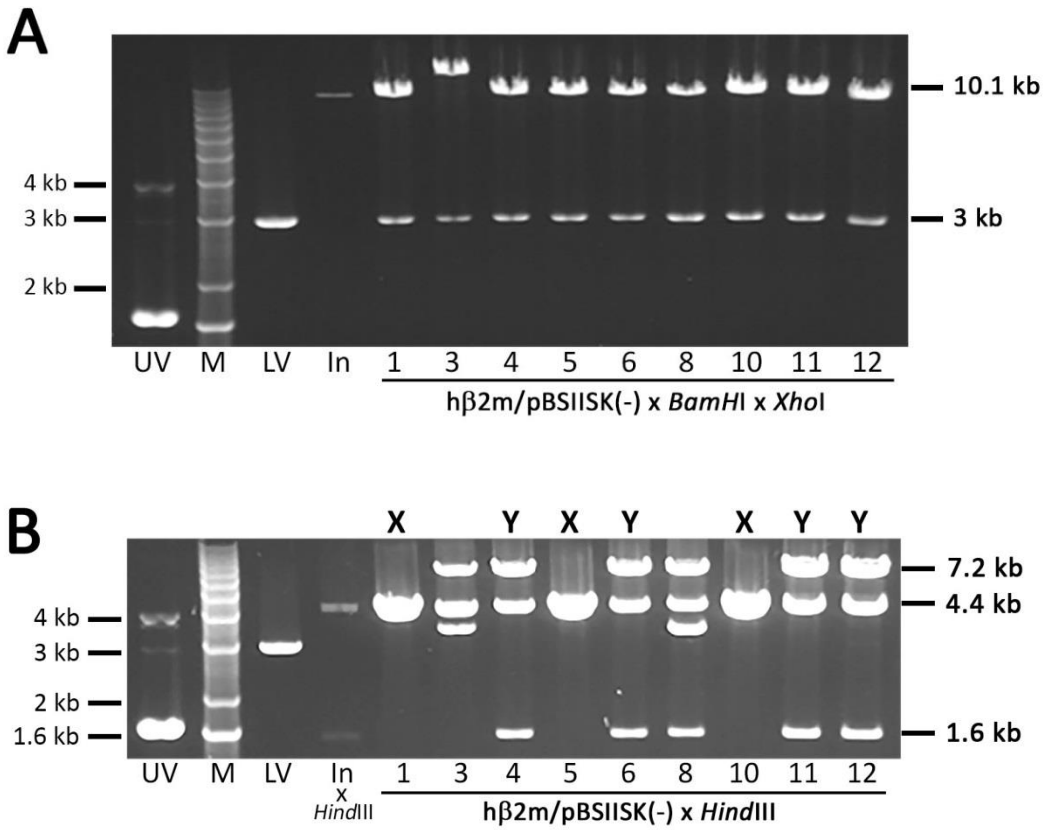


***Figure 3.3: hβ2m/pBSIISK(-) restriction analysis***

***A*** *– 9 clones were digested with BamH*I *and Xho*I*, enzymes that have their restriction sites in the polylinker of the vector but not in the genomic sequence of hβ2m, cutting the hβ2m insert (10.1 kb) out of the pBSIISK(-) vector (3 kb). 8 plasmids (1, 4, 5, 6, 8, 10, 11, 12) showed this restriction pattern. Uncut 3 kb vector (UV), linearised 3 kb vector (LV), 10.1 kb insert alone (In) and 1 kb marker (M) were run alongside the recombinant plasmids on an agarose gel.*

***B*** *– hβ2m/pBSIISK(-) recombinant plasmids 1, 3, 4, 5, 6, 8, 10, 11, 12 were analysed with HindIII enzyme. The hβ2m fragment can be bluntly inserted into the vector in two orientations. HindIII restriction digest distinguishes between the two orientations by producing two sets of restriction pattern: 7.2 kb, 4.4 kb and 1.6 kb fragments as seen in clones 4, 6, 11, 12 (lanes marked with Y) and 4.3 kb, 4.4 kb and 4.6 kb fragments seen in clones 1, 5 and 10 (lanes marked with X). Clones number 3 and 8 appeared to have the hβ2m insert but were not of the predicted size and were discarded. Uncut 3 kb vector (UV), linearized 3 kb vector (LV), 10.1 kb hβ2m insert cut with HindIII (In x HindIII; producing 3 fragments of 4.4 kb, 4.2 kb and 1.6 kb) and a 1 kb marker were run as controls alongside the samples.*

One hβ2m/pBSIISK(-) recombinant plasmid (clone 11) was sequenced by Source BioScience (UK) to exclude sequence alterations due to PCR-introduced errors. All 4 exons, exon-intron boundaries, 5' and 3' ends and ligation sites were sequenced to ensure that correct transcription and splicing of the transgene would be maintained as well as no alterations in the amino acid coding sequence were present. Primers for sequencing were designed using NCBI/Primer-BLAST online software and are listed in Table 2.1. The coding and regulatory sequences of the recombinant hβ2m/pBSIISK(-) clone (number 11) were identical to the reference sequence and this clone was used as a template for site-directed mutagenesis.

### 3.2.2 Mutagenesis of human $\beta_2$-microglobulin

The D76N mutation in the wild-type hβ2m gene was introduced by double primer site-directed mutagenesis. This method involves designing a pair of primers which are partly complimentary to one another and also to the DNA to be mutated except that they contain the desired mutation. *B2m-mut-A* and *B2m-mut-B* primers (Table 2.1) were designed so that the c.286G→A (GAT→AAT) substitution was present in the short oligonucleotide sequences priming a PCR amplification of the hβ2m/pBSIISK(-) recombinant plasmid (Figure 3.4). Recombinant plasmid number 11 as a DNA template and Phusion Hot Start II High-Fidelity DNA Polymerase were used in a 20-cycle PCR. The use of a high-fidelity polymerase is crucial to minimise the chances of unwanted mutations during the PCR and the hot-start formulation of the enzyme ensures that the primers are not degraded by the enzyme's exonuclease activity during the reaction set-up.

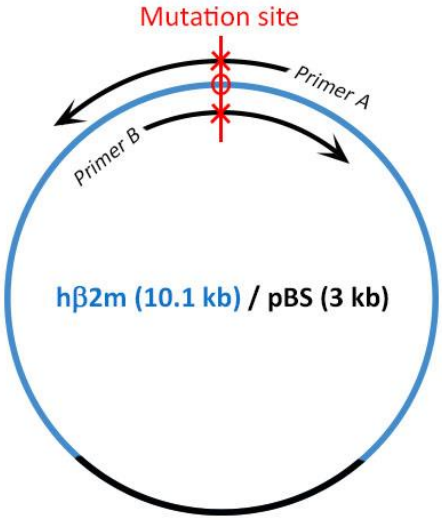


***B2m-mut-A*** 5′-CACTGAAAAAAATGAGTATGCCTGCCGTGTGAACC-3′

3′-GACTTAAGTGGGGGTGACTTTTTTTACTCATACGGACGGC-5′ ***B2m-mut-B***

***Figure 3.4: hβ2m$^{D76N}$ site-directed mutagenesis***

*B2m-mut-A and B2m-mut-B primers were designed which are partly complimentary to each other and to the targeted hβ2m gene, but containing C→A mutation causing the D76N substitution. In the first round of PCR reaction, the double stranded template hβ2m/pBSIISK(-) DNA denatures, the primers anneal to the template and new DNA strands are extended, resulting in plasmids with a single mismatch in the mutation site. Subsequent PCR cycles predominantly lead to double-stranded plasmids carrying the desired mutation on both strands.*

---

In the first round of PCR reaction, plasmids with a single mismatch at the mutation site in one strand are produced. As there is no DNA ligase in the mix, the new DNA strand is not covalently joined to the primer and there is a nick on the strand where the phosphodiester backbone of the DNA is not sealed. After several cycles of the PCR reaction, there will be a mixture of the original parental non-mutated plasmids and newly synthesized nicked plasmids which carry the mutation on both strands. To remove the parental non-mutated plasmids from the entire PCR product, the difference between DNA isolated from *dam*+ bacterial cells which is methylated and the newly

synthesized DNA from a PCR reaction which is not methylated was used. After the site-directed mutagenesis PCR reaction, *Dpn*I enzyme which cleaves DNA only when its recognition site (GATC) is *dam* methylated, was used to cut the parental DNA, leaving only the non-methylated mutated plasmids in the PCR product to be transformed into competent cells. *E.coli* can repair nicked DNA, as long as the nick is opposite an intact strand of DNA, so when the nicked mutated plasmids were transformed, they were repaired and able to replicate.

After transformation, plasmid DNA of 12 different clones was purified and mapped with *Hind*III restriction digest to establish which clones carry the hβ2m/pBSIISK(-) recombinant plasmid DNA and that the sequence of these plasmids has not been altered by major deletions or insertions. The mutation itself does not interfere with the restriction sites for *Hind*III and so the same pattern of 3 restriction fragments of 7.2 kb, 4.4 kb and 1.6 kb as in the template hβ2m/pBSIISK(-) clone number 11 was expected (Figure 3.2 A). The 7.2 kb, 4.4 kb and 1.6 kb bands were produced in 11 out of the 12 clones analysed (Figure 3.5).

These 11 clones were sequenced by Source BioScience (UK) using the *hβ2m-seq3 primer* (Table 2.1) to determine which clones carry the D76N mutation in the hβ2m sequence ($h\beta2m^{D76N}$). The mutation was confirmed in all 11 clones (Figure 3.6). One $h\beta2m^{D76N}$/pBSIISK(-) clone (plasmid number 4) was then sequenced further to exclude sequence alterations due to PCR-introduced errors. All 4 exons, exon-intron boundaries, 5' and 3' ends and ligation sites were verified to ensure that correct transcription and splicing of the transgene mRNA would be maintained and that no alterations in the amino acid coding sequence (except for the D76N substitution) were present. The same primers as for non-mutated hβ2m/pBSIISK(-) sequencing were used. No sequence alterations were detected in the coding and regulatory regions of the $h\beta2m^{D76N}$/pBSIISK(-) clone number 4 and the $h\beta2m^{D76N}$ transgene from this clone was prepared for microinjection.

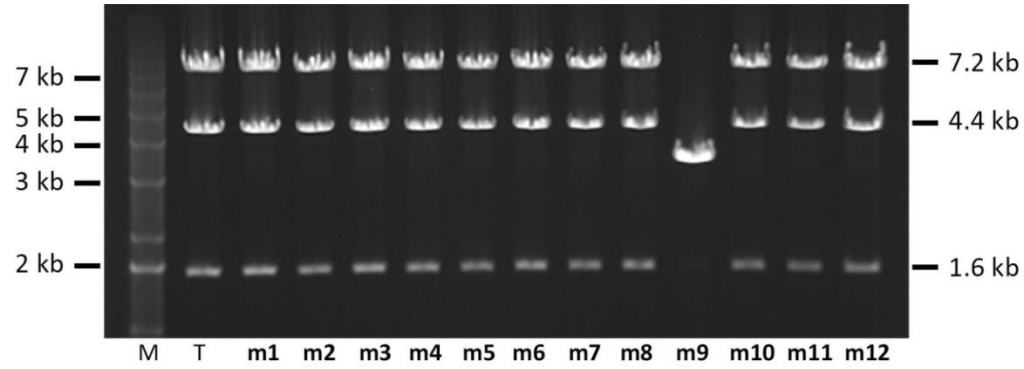


***Figure 3.5: Mutated hβ2m/pBSIISK(-) x HindIII***

*Because the desired D76N mutation in the hβ2m sequence does not change the HindIII restriction pattern of the hβ2m/pBSIISK(-) recombinant plasmids, the non-mutated template plasmid DNA (T) and the mutated hβ2m/pBSIISK(-) recombinant plasmids (m1 – m12) produce the same restriction fragments of 7.2 kb, 4.4 kb and 1.6 kb. 11 out of 12 clones analysed showed the predicted pattern of fragments indicating no gross alteration of the DNA structure.*

---

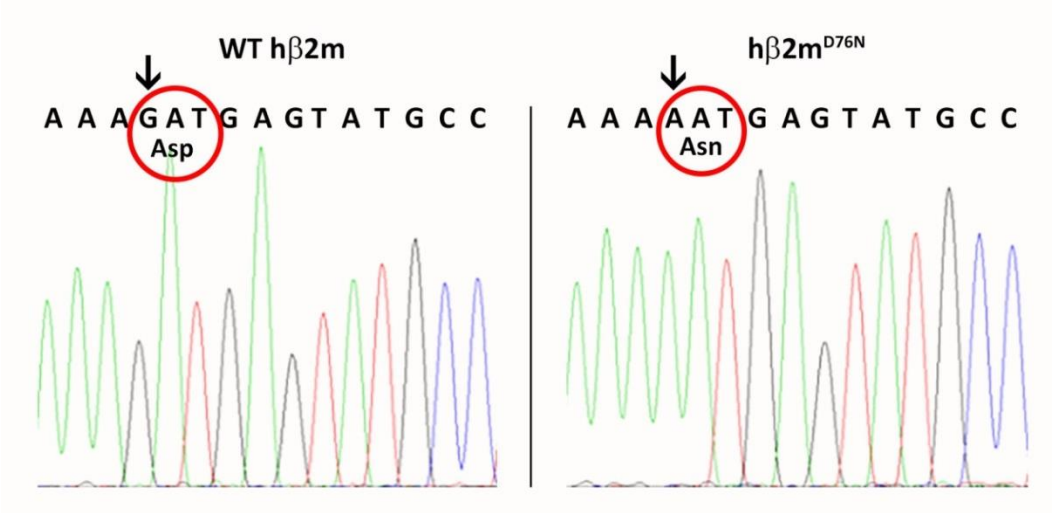


***Figure 3.6: Partial-sequence chromatograms of the B2M gene***

*Left – wild-type human β2m coding sequence; Right – amyloidogenic variant of human β2m. c.286G→A (GAT/AAT) single base substitution (arrows) encodes replacement of the negatively charged aspartate residue at the position 76 of the mature protein with an uncharged asparagine residue (D76N). The D76N mutation, introduced into the wild-type human β2m coding sequence by site-directed mutagenesis was confirmed in 11 out of 12 clones analysed.*

---

### 3.2.3 Generation of hβ2m$^{D76N}$ transgenic mice

The hβ2m$^{D76N}$/pBSIISK(-) was digested with *BamH*I and *Xho*I, cutting out a 10.1 kb hβ2m$^{D76N}$ fragment. The fragment was gel purified, quantified and used for pronuclear injection. The microinjections into C57Bl/6J embryos and embryo transfers into pseudo-pregnant recipient female mice were performed by Dr Raya Al-Shawi and Dr Paul Simons.

38 mice were born from the pronuclear microinjections. Ear and tail biopsies were collected and used for genotyping. Transgenic mice were identified by PCR using primers *hβ2m-sc-F1* and *hβ2m-sc-R2* (Table 2.1) that amplify a 662 bp fragment of the transgene. Five mice showed integration of the hβ2m$^{D76N}$ transgene - three males (mouse numbers 2, 4, 6) and two females (numbers 11 and 22), and the PCR clearly distinguished the transgenic mice from wild-type mice (Figure 3.7). All five transgenic mice were bred with C57Bl/6J mice to identify germline transmitters. Four mice proved to transmit the transgene to the first generation, establishing lines 2, 4, 6 and 11. Mouse number 22 died before producing any offspring.

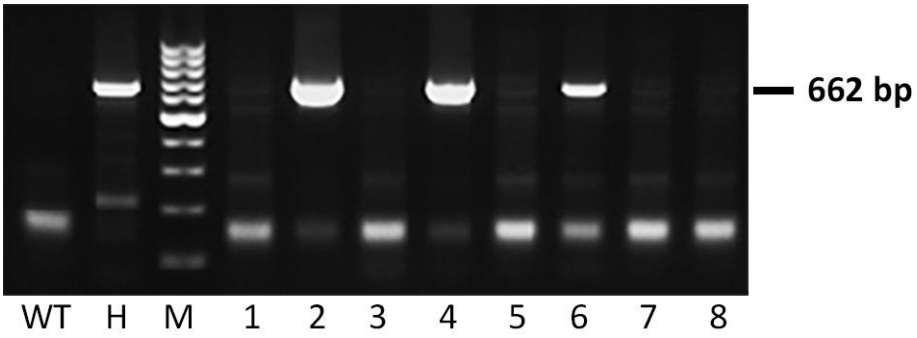


***Figure 3.7: Identification of hβ2m$^{D76N}$ transgenic mice by PCR***

*hβ2m$^{D76N}$ transgenic mice were identified by PCR using hβ2m-sc-F1 and hβ2m-sc-R2 primers. Mice positive for hβ2m$^{D76N}$ transgene (2, 4, 6) are distinguishable from their negative littermates (1, 3, 5, 7, 8) and a wild-type C57Bl/6J mouse (WT) by amplifying a 662 bp fragment. Human genomic DNA (H) used as a positive control and 100 bp marker (M) were run alongside the samples.*

Lines 2, 6 and 11 transmitted the transgene in a Mendelian fashion with approximately 50 % frequency of the transgene inheritance. In the first generation of line 4, 15/18 offspring were transgenic suggesting that the transgene in the genome of line 4 founder had more than one independently segregating integration site. All mice of all four lines were viable and fertile.

hβ2m$^{D76N}$ transgenic mice on C57Bl/6J background express the endogenous mouse β2m. Although the β2m sequence is 70 % identical between the human and mouse β2m, it was reported that mouse β2m is not amyloidogenic, unlike its human equivalent *(Ivanova et al., 2004, Eichner et al., 2011)*. Importantly, it has been reported that while ΔN6β2m, a truncated hβ2m found in amyloid deposits of dialysis-related amyloidosis patients, can aggregate *in vitro* into fibrillar material at physiological conditions (pH 7.2, 37 $^{o}$C while shaking at 200 RPM), addition of mouse β2m into the ΔN6β2m protein mixture abolishes the aggregation potential of the ΔN6β2m *(Eichner et al., 2011)*. For these reasons, the hβ2m$^{D76N}$ transgenic mice were also crossed with mouse β2m knock out (β2m-KO) mice (B6.129P2-B2m$^{tm1Unc}$/J, The Jackson Laboratory) to produce hβ2m$^{D76N}$ transgenic mice lacking the endogenous mouse β2m and to compare the effects of the murine β2m in the transgenic mice. All mice developed without any pathological abnormalities.

### 3.2.4 Expression of hβ2m mRNA in tissue of hβ2m$^{D76N}$ transgenic mice

β2m is a protein ubiquitously expressed by all nucleated cells. In the hβ2m$^{D76N}$ transgenic mice, the hβ2m transgene was expressed under the control of the gene's own promoter and own regulatory sequences. 2.9 kb and 1.2 kb of 5' and 3' flanking sequences of B2M gene were previously shown to regulate a pattern of hβ2m transgene expression in transgenic mice with a tissue-specific pattern very similar to that of endogenous mouse β2m *(Chamberlain et al., 1988)*. Liver, spleen, heart, kidney, tongue, skeletal muscle and brain of line 2 hβ2m$^{D76N}$ transgenic mice lacking the endogenous

mouse β2m were analysed for the transgenic hβ2m mRNA expression by reverse transcription PCR (RT-PCR).

RNA was isolated from mouse tissue and the samples were treated with DNase (gDNA wipe-out buffer, QIAGEN) to eliminate any contaminating genomic DNA. The obtained cDNA from the line 2 hβ2m$^{D76N}$ transgenic tissue was then PCR amplified using human β2m specific primers *hβ2m RT-PCR 5'* and *hβ2m RT-PCR 3'* primers (Table 2.1) which amplify a 240 bp PCR product. The primers were designed so that each primer is complementary to a short sequence on different exons. This enables to distinguish between PCR amplification of RNA and amplification of contaminating DNA which would contain the intron sequence. hβ2m mRNA was detected in all analysed tissue in the transgenic mice (Figure 3.8). The specificity of the human β2m primers was confirmed by RT-PCR of mRNA obtained from tissue of control β2m-KO mice, in which no amplification with *hβ2m RT-PCR 5'* and *hβ2m RT-PCR 3'* primers was produced (Figure 3.9).

As a positive control, RT-PCR of the ubiquitously present mouse house-keeping gene GAPDH was simultaneously performed. Using *msGAPDHf* and *msGAPDHr* primers (Table 2.2), a 133 bp PCR product was amplified from obtained cDNA in all analysed tissues of hβ2m$^{D76N}$ transgenic mice as well as of β2m-KO mice (Figure 3.8 and 3.9). This result confirmed that the extracted RNA is of a good quality and that no amplification of cDNA in the tissue with hTTR primers in the RT-PCR reactions is due to the fact that the gene of interest is not expressed and not due to lack of total RNA itself in the analysed samples or failure of cDNA synthesis.

To exclude the possibility of false positive signal by genomic DNA contamination, a control reaction prepared without the addition of reverse transcriptase enzyme into the RNA isolated from tissues of hβ2m$^{D76N}$ transgenic mice and β2m-KO mice was also performed. Using primers amplifying hβ2m cDNA and GAPDH cDNA (not shown), the PCR did not show any amplification of hβ2m and mouse GAPDH fragments, confirming

that the amplification of hβ2m and mouse GAPDH was specific to the extracted RNA from the mouse tissue (Figure 3.8).

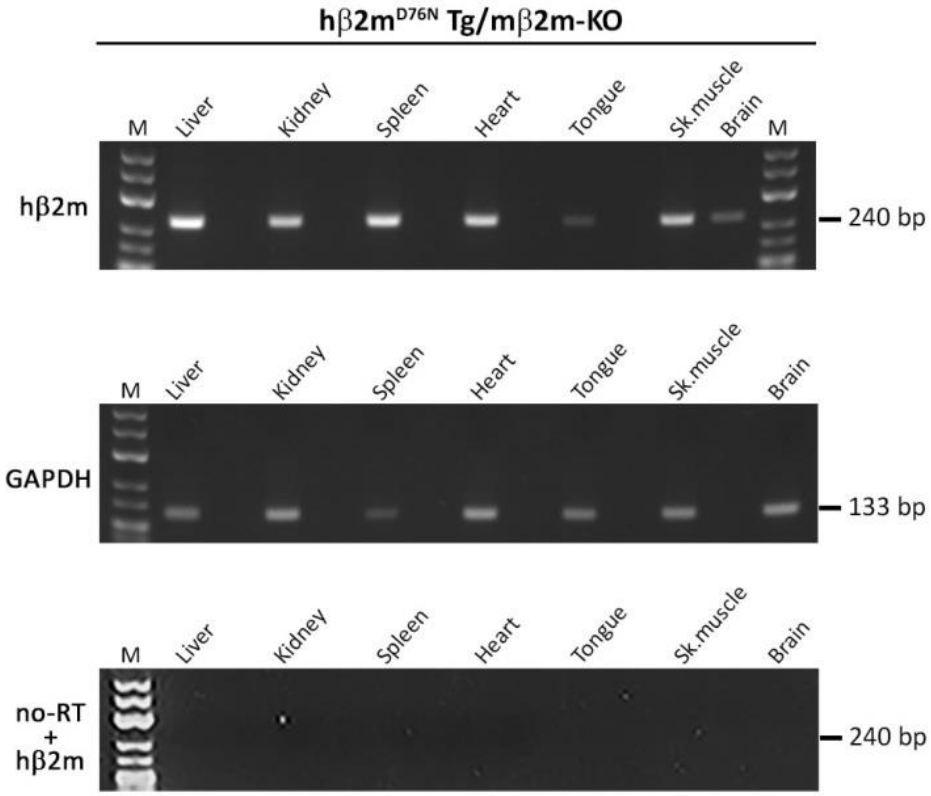


***Figure 3.8: Expression of transgene-encoded hβ2m mRNA***

*hβ2m transgene mRNA expression in tissue of hβ2m$^{D76N}$ transgenic mice on β2m-KO background was analysed by RT-PCR. RNA isolated from liver, kidney, spleen, heart, tongue, skeletal muscle and brain was used for cDNA synthesis using reverse transcriptase (RT) and a mixture of random primers and oligo-dT primers to ensure cDNA synthesis from all regions of RNA transcripts. The synthesized cDNA was then amplified by 25 cycle PCR using Taq polymerase. Primers specific for human β2m amplified a 240 bp fragment in all tissue analysed. Successful RNA extraction was confirmed by control RT-PCR reactions using primers specific for mouse GAPDH, an ubiquitously expressed gene, amplifying a 133 bp fragment in all tissue analysed. When no RT was added into the tissue RNA, PCR with hβ2m primers was not able to amplify a DNA fragment confirming that the signal was specific for the cDNA25 bp DNA ladder (M) was run alongside the samples.*

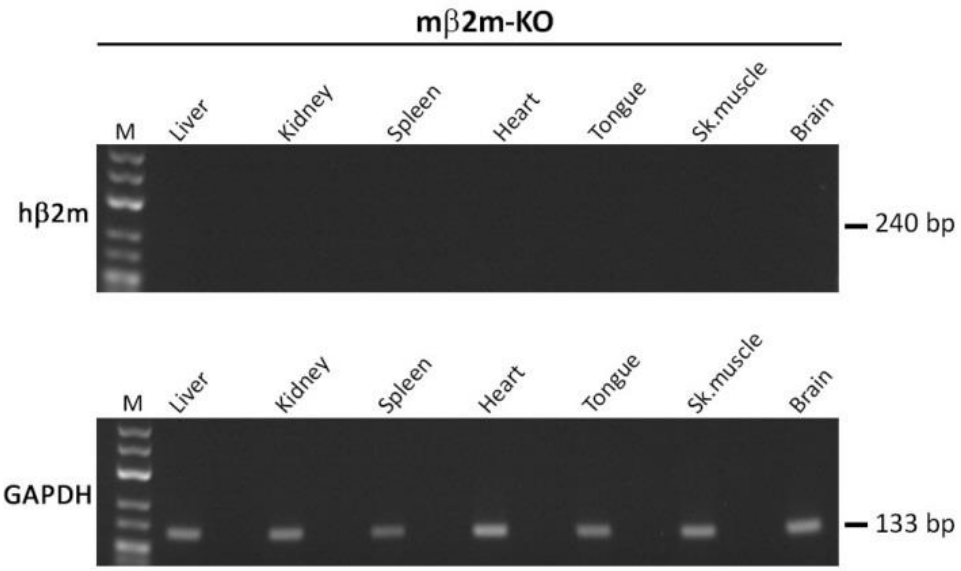


***Figure 3.9: Negative control RT-PCR of hβ2m transgene encoded mRNA***

*RNA isolated from liver, kidney, spleen, heart, tongue, skeletal muscle and brain of non-transgenic control mice lacking the endogenous mouse β2m (mβ2m-KO) was used for cDNA synthesis using reverse transcriptase and subjected to PCR amplification with mouse GAPDH primers detecting a ubiquitously expressed GAPDH house-keeping gene, and hβ2m primers. While the GAPDH primers amplified a 133 bp fragment, confirming successful extraction of RNA from the tissue as well as cDNA synthesis by reverse transcriptase, no amplification of hβ2m was detected confirming the specificity of hβ2m the primers to hβ2m transgene only.*

### 3.2.5 hβ2m in the serum of hβ2m$^{D76N}$ transgenic mice

Presence of hβ2m in the serum of the founders of hβ2m$^{D76N}$ transgenic lines 2, 4, 6 and 11 was evaluated by Western blot analysis. Recombinant purified hβ2m protein of known concentrations was used as a positive control of the protein migration and for estimation of the serum hβ2m concentration in the transgenic mice.

Three different anti-hβ2m antibodies were tested: Dako rabbit polyclonal anti-hβ2m antibody, Source Bioscience B2M-01 mouse monoclonal anti-hβ2m antibody and 14H3 mouse monoclonal anti-hβ2m antibody from University of Pavia (Table 2.3). 12 kDa band of the hβ2m protein was clearly detected in the serum of transgenic mice of lines 2, 4 and 11 but no hβ2m was detected in the serum of the founder of line 6. As expected, no such hβ2m signal was detected in the serum of C57Bl/6J mice and β2m-KO mice. When the intensity of hβ2m signal in the serum of transgenic mice was compared with the intensity of equivalent volume of human serum run together with the transgenic samples, the hβ2m concentration in all three lines appeared higher. From the signal intensity given by the known concentrations of the recombinant hβ2m protein, the estimated serum hβ2m concentration in line 11 was ~10 ng/µl and between 10 – 100 ng/µl in lines 2 and 4.

The Dako polyclonal antibody also strongly cross-reacted with denatured mouse β2m but both, the human and mouse proteins were distinguishable on an SDS-PAGE gel with mouse β2m migrating slightly slower (~13 kDa) than the 12 kDa human β2m protein. Both monoclonal B2M-01 and 14H3 antibodies were human β2m specific recognising the human β2m protein only. Because the monoclonal antibodies were both raised in mouse and anti-mouse secondary antibodies used for detection were strongly reacting with denatured IgG present in the mouse serum analysed, HRP-conjugated Clean-Blot IP Detection Reagent (Table 2.3) was used for detection of these antibodies as the Clean-Blot specifically binds to functional primary antibodies

(whole IgG) without binding to denatured IgG fragments. Western blots for all three tested antibodies are shown in Figure 3.10.

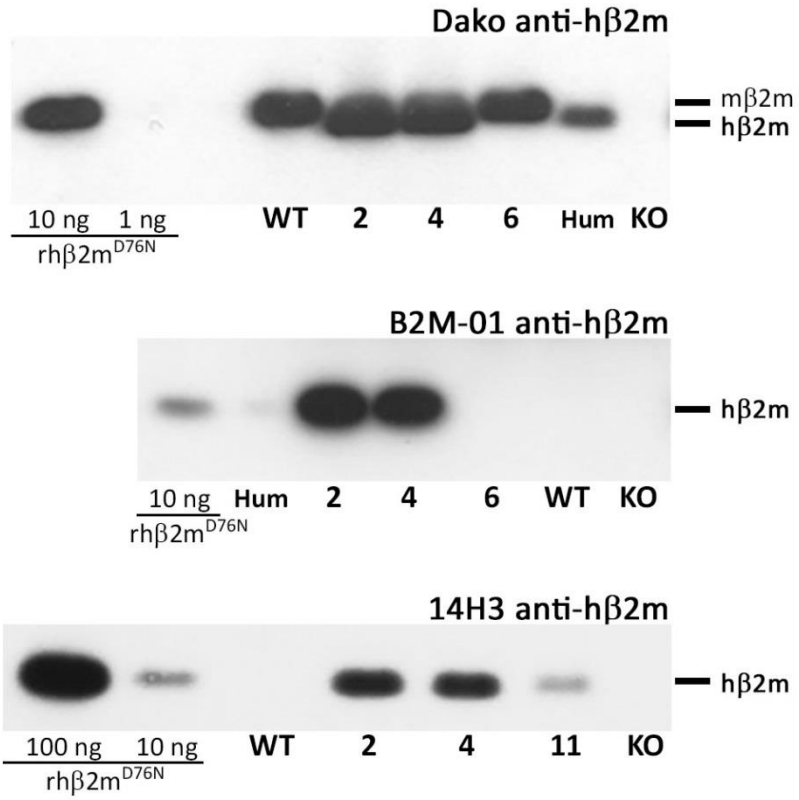


***Figure 3.10: hβ2m in serum of hβ2m$^{D76N}$ transgenic mice***

*Presence of hβ2m in serum of hβ2m$^{D76N}$ transgenic mice was analysed by Western blot. hβ2m was detected in serum of the transgenic founders of line 2, line 4 and line 11 and co-migrated with β2m protein in human serum (Hum). No hβ2m was detected in the serum of line 6 mouse. Three different antibodies were tested: Dako rabbit polyclonal anti-hβ2m, Source Bioscience B2M-01 mouse monoclonal anti-hβ2m and 14H3 mouse monoclonal anti-hβ2m. Both monoclonal antibodies were human β2m specific and no signal was detected in serum of C57Bl/6J (WT) and β2m-KO mice (KO). The Dako polyclonal antibody showed cross-reactivity with mouse β2m (mβ2m) but the mβ2m protein migrated slightly slower (~13 kDa) on an SDS-PAGE gel than the hβ2m (12 kDa). Recombinant purified human β2m$^{D76N}$ protein (rhβ2m$^{D76N}$) of known concentration was used for comparison. 1 µl of serum was loaded for each sample.*

### 3.2.6 Quantitation of hβ2m in serum of hβ2m$^{D76N}$ transgenic mice

Although commercial kits for measuring human β2m in serum are available, they are not suitable for detection of hβ2m in mouse serum due to cross-reactivity with mouse β2m. Further, the amounts of serum required are not possible to obtain by routine single blood sampling in mice. Therefore, to quantify the concentration of hβ2m in the serum of hβ2m$^{D76N}$ transgenic mice, a new sandwich enzyme-linked immunosorbent assay (ELISA) protocol for detection of hβ2m was developed and optimized.

#### 3.2.6.1 hB2m ELISA optimization

An ELISA protocol was developed to enable a specific detection and quantitation of hβ2m antigen in a mixture of mouse serum proteins including mouse β2m. In sandwich ELISA, the antigen is detected using two layers of antibodies: a capture antibody that is bound to a microtiter plate, and a detection antibody that binds to a different epitope of the captured antigen. HRP-linked secondary antibody is then applied to bind to the Fc-region of the detection antibody. In the last step, a chemical substrate is added, which is converted by the enzyme into a coloured product and its absorbance is measured. Test samples are then plotted against a standard curve obtained from absorbance measurement of standards.

Capture and detection antibody optimization

Monoclonal anti-hβ2m antibody 14H3 (Table 2.3) was used to coat the microtiter plate wells. The tested range of the antibody concentration was 1 - 100 µg/ml. Although 1 µg/ml of the anti-hβ2m capture antibody showed sufficient coating of the protein-binding site in the wells, 10 µg/ml was used for further optimisation and experiments to ensure that maximal coating was reached.

For detection of the hβ2m antigen captured by the monoclonal antibody in the wells, Dako rabbit polyclonal anti-hβ2m antibody (Table 2.3) was used as it can recognise different epitopes of the captured antigen. When the concentration of the detection antibody was lower than 1 µg/ml, not enough antibody was provided to bind to the captured antigen and no or very weak colour of the final product developed in each well regardless of the amount of antigen available, reading no or very low absorbance. The signal was improved with antibody concentration of 1 µg/ml and higher. The optimal signal to noise ratio was reached with 10 µg/ml of the detection antibody and was used in further steps of optimisation and experiments (Figure 3.11).

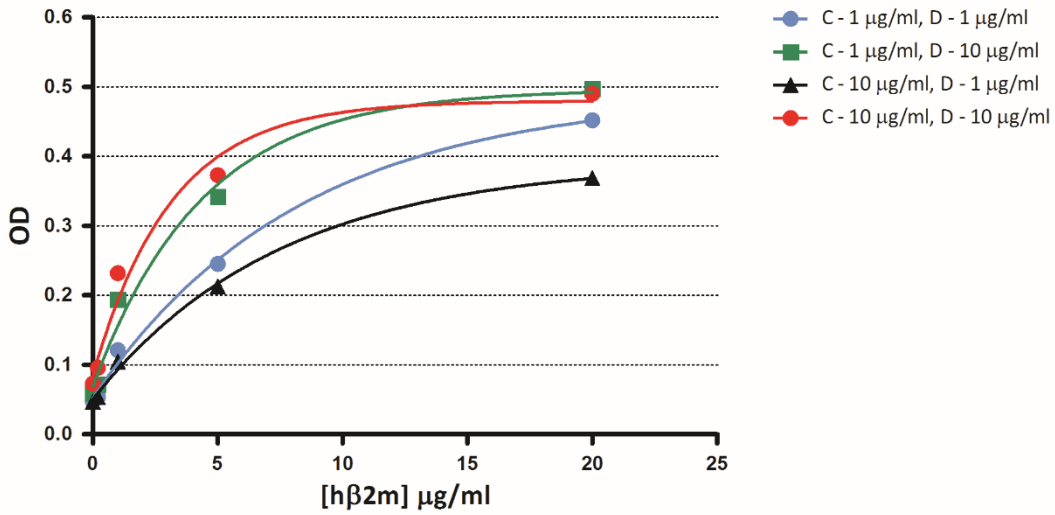


***Figure 3.11: Optimisation of capture and detection antibodies in hβ2m ELISA***
*To detect hβ2m antigen in mouse serum, different concentrations of capture and detection antibodies were compared by analysing the signal reached to obtain a standard curve. For antigen capture, monoclonal anti-hβ2m antibody 14H3 was used to coat the wells of a microtiter plate. To obtain a standard curve, 0.5, 5 and 20 µg/ml of recombinant hβ2m protein mixed with β2m-KO serum and β2m-KO serum alone as a blank were used. The antigen was then detected by Dako rabbit polyclonal anti-hβ2m antibody. The capture antibody (C) at concentrations 1 µg/ml and 10 µg/ml and detection antibody (D) at concentrations 1 µg/ml and 10 µg/ml were combined and obtained standard curves were compared. The best signal to noise ratio was reached when 10 µg/ml of capture antibody and 10 µg/ml of detection antibody were applied. 1% BSA was used as a blocking buffer.*

Blocking buffer optimisation

To improve the sensitivity of the assay by reducing non-specific binding and increasing the signal to noise ratio, 6 different blocking buffers were tested: PBST, 1 % bovine serum albumin in PBS, 10 % horse serum in PBS, 10 % goat serum in PBS, 1 % foetal calf serum in PBS and Pierce Protein-free T-20 buffer (Thermofisher Scientific). The optimised 10 µg/ml of capture antibody and 10 µg/ml of detection antibody were applied and recombinant hβ2m protein diluted in an appropriate blocking buffer was used to obtain standard curves. Insufficient blocking activity was observed for 1 % BSA, 10 % goat serum and 10 % horse serum. In contrast, PBST, Pierce Protein-Free buffer and 1 % foetal calf serum showed high sensitivity with low background (Figure 3.12) and these buffers were investigated further.

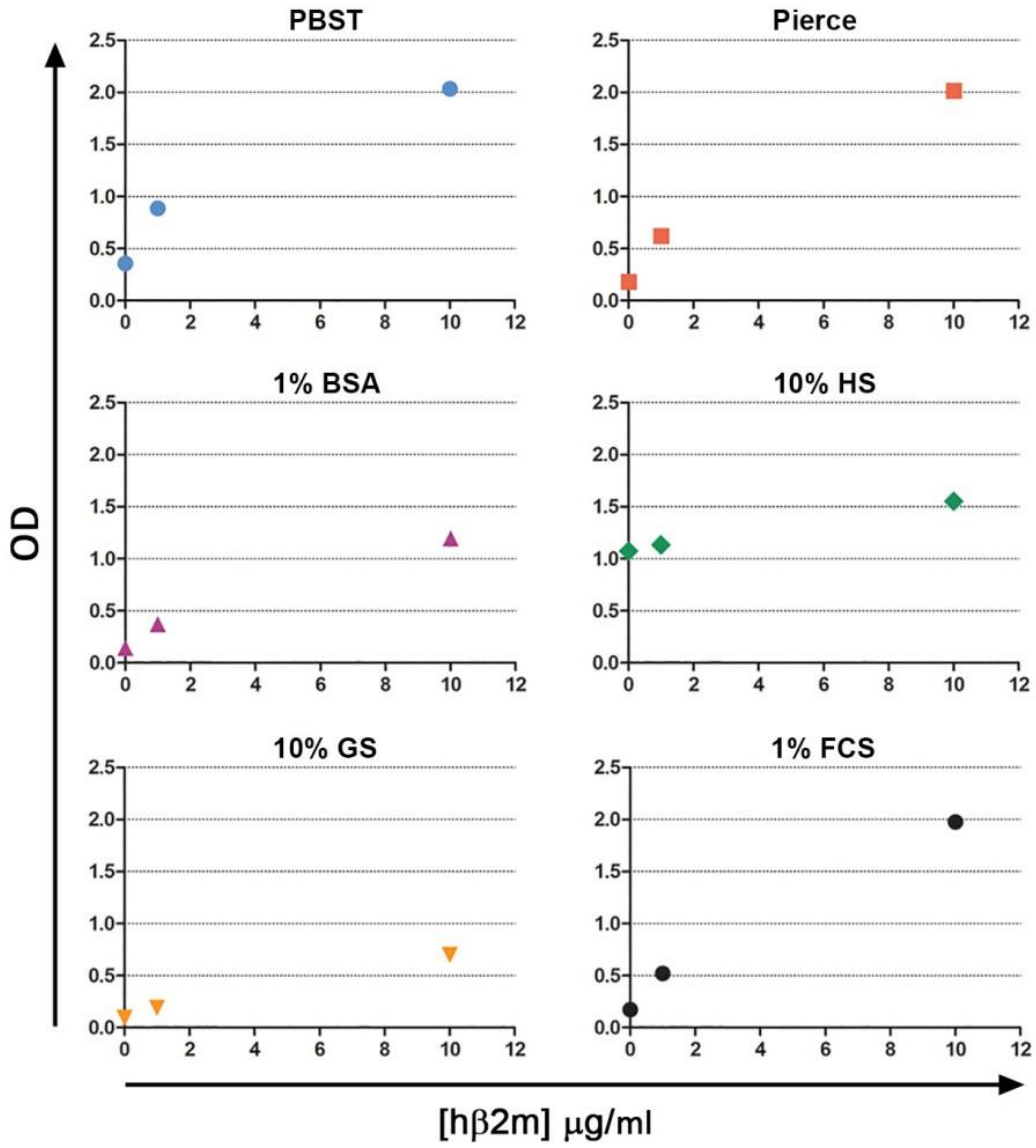


***Figure 3.12: Optimisation of blocking buffer in hβ2m ELISA***

*PBST, Pierce protein-free T-20 blocking buffer (Pierce), 1 % bovine serum albumin (BSA) in PBS, 10 % horse serum (HS) in PBS and 10 % goat serum (GS) in PBS and 1 % fetal calf serum (FCS) in PBS were tested to improve the hβ2m ELISA assay sensitivity. 0 µg/ml, 1 µg/ml and 10 µg/ml of recombinant hβ2m protein diluted in appropriate blocking buffer were used to compare the signal reached in the assay. Insufficient blocking was observed with 1 % BSA, 10 % HS and 10 % GS due to low sensitivity or high background. PBST, Pierce and 1 % FCS showed satisfactory blocking activity for their low background signal and high signal to noise ratio.*

Serum matrix interference

Naturally occurring proteins, heterophilic antibodies or other endogenous components of the serum can affect assay sensitivity and lead to inaccurate results. Interfering effect of the serum matrix on the measurement of hβ2m in the serum of transgenic mice was tested by spiking recombinant hβ2m protein used as a standard with different amounts of mouse serum. The effect of endogenous mouse β2m present in the wild-type serum was also compared to serum lacking the mouse β2m protein.

Addition of mouse serum decreased the signal obtained for each point of the standard curve. The more serum was added to the recombinant hβ2m protein, the more interference was observed and the lower optical density of the final product was measured (Figure 3.13). To ensure accurate measurements of hβ2m serum concentrations in the transgenic mice, each concentration of recombinant hβ2m protein used as a standard was mixed with control serum in a volume equivalent to the amount of analysed serum applied into wells.

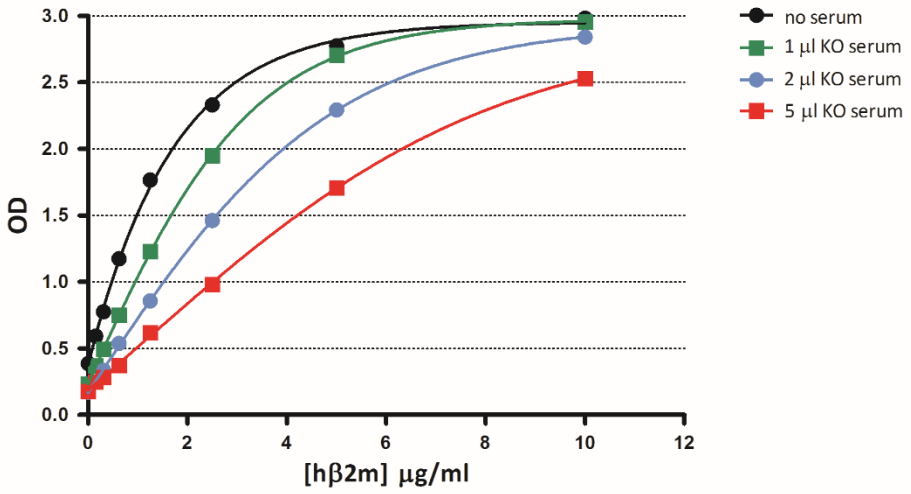


***Figure 3.13: The effect of serum matrix on hβ2m ELISA***

*The interfering effect of serum components on the measurement of serum levels of hβ2m in transgenic mice by ELISA was tested by spiking recombinant hβ2m protein of known concentration with 1 µl, 2 µl and 5 µl of mouse serum. The more serum was added to the recombinant hβ2m protein, the lower signal was detected. The same effect of serum matrix was observed for both, WT and β2m-KO serum.*

When the effect of endogenous mouse β2m present in the wild-type serum was compared to serum lacking the mouse β2m protein, only a minimal difference was observed confirming high specificity of the assay (Figure 3.14).

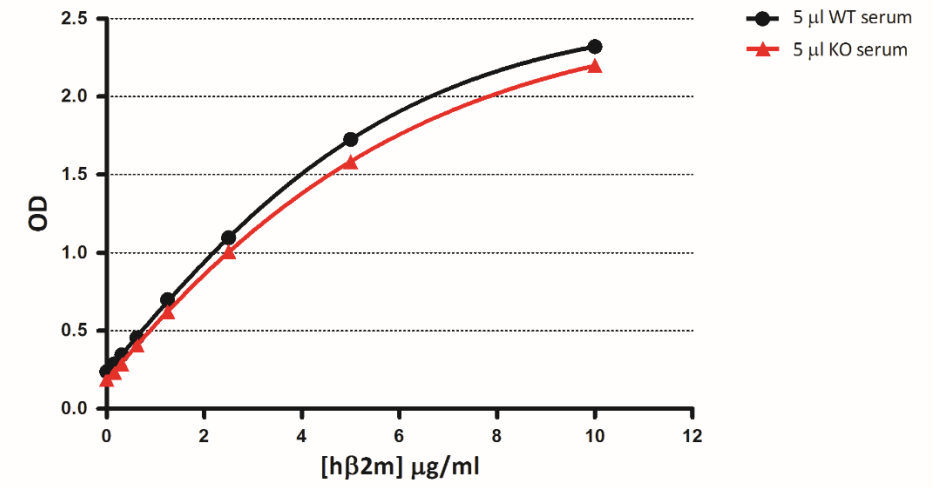


***Figure 3.14: The effect of endogenous mouse β2m in ELISA assay***

*The effect of endogenous mouse β2m present in the wild-type serum (WT) was compared to serum lacking the mouse β2m protein (KO). Only a minimal increase in signal was observed in serum containing the endogenous mouse β2m confirming assay specificity for human β2m protein in mouse serum matrix.*

---

The serum matrix interference in relation to different blocking buffers was also analysed. PBST, Pierce Protein-Free buffer and 1 % fetal calf serum were compared when the purified recombinant hβ2m protein was mixed with 5 µl of wild-type serum and 5 µl of β2m-KO serum. Pierce and PBST showed high sensitivity with low background for both, the β2m-KO as well as the wild-type serum matrix. The sensitivity of the assay decreased slightly with 1 % foetal calf serum used for blocking (Figure 3.15) and for this reason this blocking buffer was not used in further experiments.

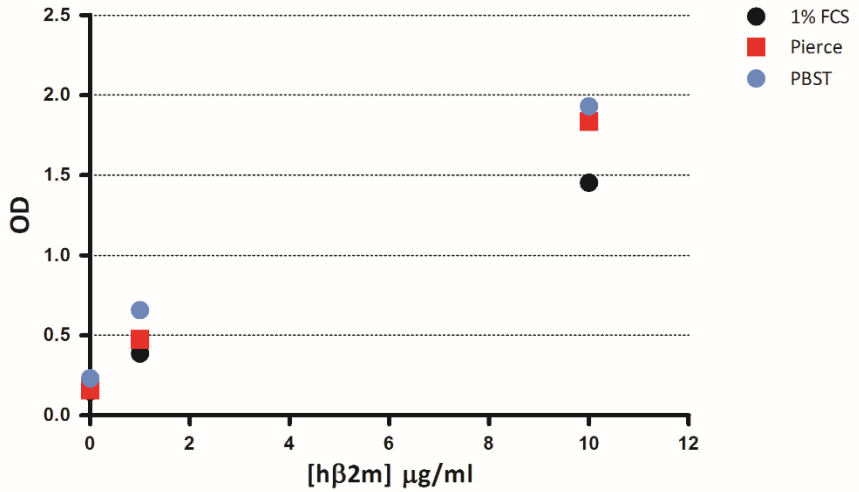


***Figure 3.15: Optimisation of blocking buffer for serum matrix interference***

*The effect of serum matrix interference and different blocking buffers on sensitivity of the ELISA assay was analysed by comparing the signal obtained when 5 µl of wild-type serum was mixed with recombinant hβ2m protein. While lower sensitivity was observed when 1 % fetal calf serum (FCS) in PBS was used for blocking, PBST and Pierce Protein-Free buffers showed good sensitivity and low signal to noise ratio.*

---

## hβ2m ELISA optimisation summary

After several optimisation steps, the hβ2m ELISA assay protocol to quantify the concentration of hβ2m in the serum of hβ2m$^{D76N}$ transgenic mice was as follows:

10 µg/ml of monoclonal anti-hβ2m antibody 14H3 was used to coat the wells of a microtiter plate to capture the hβ2m antigen in a mixture of serum proteins including endogenous mouse β2m. The remaining protein-binding sites in the wells were blocked with Peirce Protein-Free T20 buffer. 5 µl of mouse serum diluted in Peirce Protein-Free T20 blocking buffer was added to the wells and the captured antigen was detected by adding 10 µg/ml of rabbit polyclonal anti-hβ2m antibody (Dako). Known concentrations of recombinant hβ2m protein mixed with 5 µl of wild-type or β2m-KO mouse serum, depending on the genetic background of mice analysed, were used to obtain a standard curve for each plate assayed.

### 3.2.6.2 Concentrations of hβ2m in serum of hβ2m$^{D76N}$ transgenic mice

Three independent lines – line 2, line 4 and line 11 of transgenic mice that express the hβ2m$^{D76N}$ transgene have been established. The mice were generated on C57Bl/6J wild-type background (WT) in which the endogenous mouse β2m is also expressed. The three lines were also crossed on β2m knock-out background (β2m-KO) in which the mice lack expression of the endogenous mouse β2m.

The concentrations of hβ2m in the serum of hβ2m$^{D76N}$ transgenic mice on the WT background and on the β2m-KO background were quantified for each line by the optimised hβ2m ELISA assay. The values are shown as mean ± standard deviation (SD) for number of mice (n) analysed.

In healthy humans, plasma β2m concentration is 0.7 – 2.7 µg/ml *(Berggard and Bearn, 1968, Greipp et al., 1988, Floege et al., 1991)*. The highest serum concentration hβ2m was measured in line 2. In this line, the serum hβ2m in the transgenic mice on WT background (T/WT) was 18.82 ± 4.05 µg/ml (n=14), whereas in the transgenic mice on β2m-KO background (T/KO) the concentration was 35.33 ± 6.43 µg/ml (n=15). In line 11, the hβ2m concentration in T/WT mice was 6.31 ± 1.02 µg/ml (n=7) and in T/KO mice 3.70 ± 1.87 µg/ml (n=20). In line 4, hβ2m serum levels of T/WT mice were analysed but as the founder of this line had more than one integration site of the transgene, the hβ2m concentration varied among the offspring. A higher-expressing line 4 mouse of the first generation was crossed on β2m-KO background and its offspring were then analysed. In this line, the hβ2m concentration in T/KO mice was 9.46 ± 2.08 (n=11). The results are shown in Figure 3.16.

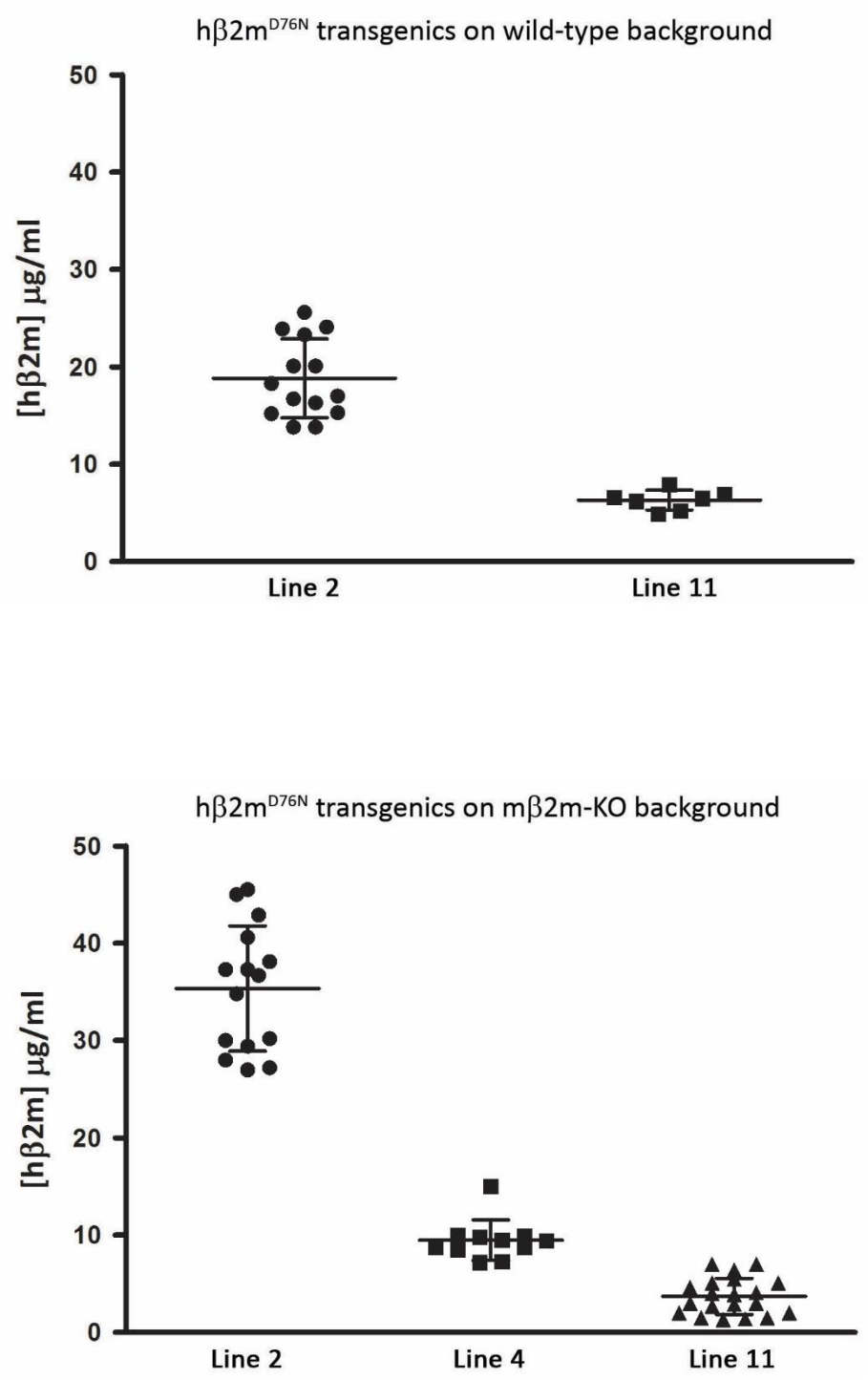


***Figure 3.16: Quantitation of serum hβ2m in hβ2m$^{D76N}$ transgenic mice***

*Concentrations of circulating hβ2m in the three established lines of hβ2m$^{D76N}$ transgenic mice on wild-type genetic background (top) and on mouse β2m-KO background (bottom) was quantified by ELISA.*

In all three lines, hβ2m$^{D76N}$ transgenic females on β2m-KO background had higher concentrations of serum hβ2m than transgenic males (Table 3.1). The sex difference was statistically significant in line 2 and line 11. Because the transgene in the line 4 was integrated into the genome of the founder in more than one site, smaller number of animals of one lineage was available to be grouped and analysed.

| [hβm] µg/ml | T/WT | | T/KO | |
|---|---|---|---|---|
| | Males | Females | Males | Females |
| **Line 2** | 18.3 ± 4.70 | 19.52 ± 3.59 | 32.20 ± 4.93 | 41.6 ± 4.05 |
| (n) | (5) | (6) | (10) | (5) |
| *P value* | *ns* | | *p = 0.012* | |
| | | | | |
| **Line 4** | N/A | N/A | 8.8 ± 1.4 | 9.7 ± 2.3 |
| (n) | | | (3) | (8) |
| *P value* | | | *ns* | |
| | | | | |
| **Line 11** | 6.55 ± 0.50 | 6.22 ± 1.21 | 2.84 ± 1.68 | 4.99 ± 1.38 |
| (n) | (2) | (5) | (12) | (8) |
| *P value* | *ns* | | *p = 0.012* | |

**Table 3.1: Serum hβ2m concentration in transgenic males and females**

*Plasma hβ2m concentrations in three lines of hβ2m$^{D76N}$ transgenic males and females mice. Values represent mean ± SD for number (n) of mice analysed. Mann-Whitney two-tailed test was used for statistical analysis.*

In humans and mice, endogenous β2m increases in blood with age *(Norlund et al., 1997, Smith et al., 2015)*. When young and 12-15 months old transgenic mice of line 2 on β2m-KO background were compared, increase in serum hβ2m was not observed, with concentrations 39.13 ± 5.33 µg/ml (n=8) for 3-6 months old transgenic mice and 35.62 ± 5.39 µg/ml (n=10) for 12-15 months old transgenic mice (Figure 3.17). The increase of plasma β2m in

humans is evident in from the sixth decade and in mice older than 18 months *(Norlund et al., 1997, Smith et al., 2015)*, and the hβ2m$^{D76N}$ transgenic mice may have been too young to notice a difference in the plasma concentrations of hβ2m.

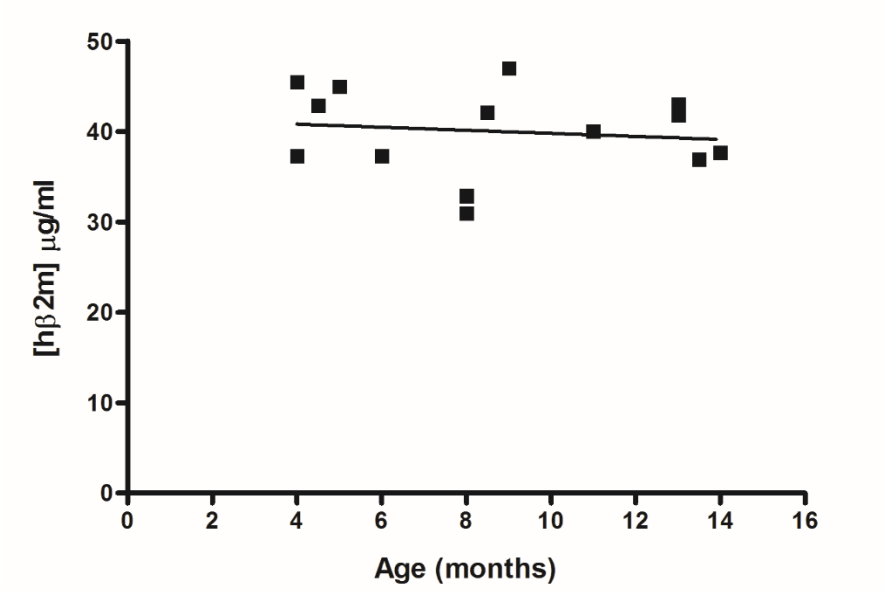


***Figure 3.17: Serum hβ2m in hβ2m$^{D76N}$ transgenic females in relation to age***

*Serum concentration of hβ2m in line 2 transgenic females on β2m-KO background was analysed in relation to age. The concentration in mice between 3 months and 15 months of age only slightly decreased with age (Pearson r = -0.1324)*

### 3.2.7 Cell surface expression of hβ2m in hβ2m$^{D76N}$ transgenic mice

The hβ2m$^{D76N}$ transgenic mice do not express human heavy chain of MHC class I complex, but it has been previously shown in human β2m transgenic mice that murine class I heavy chains associate with human β2m and such hybrid complexes are efficiently expressed at the cell surface *(Chamberlain et al., 1988)*. To determine whether the D76N variant hβ2m forms cell surface complexes with the mouse MHC I, leukocyte in blood films of transgenic and non-transgenic mice were stained with FITC-labelled anti-human β2m monoclonal antibody B2M-01. Specific staining was detected in the transgenic mice, except line 6 transgenics in which no immunofluorescence was observed confirming no transgene expression. No signal was detected in leukocytes of non-transgenic controls and β2m-KO mice (Figure 3.18).

To show that the immunofluorescent signal detected in the blood films of transgenic mice did not come from within the cells due to cell permeabilization, FACS analysis on living blood cells was performed to confirm the cell surface localization of the variant β2m. The cells were labelled with APC-conjugated anti-CD45, the leukocyte common antigen, and human β2m signal was analysed using FITC-labelled anti-human β2m monoclonal antibody B2M-01. The leukocytes of non-transgenic mice and β2m-KO mice gave indistinguishable pattern of background fluorescence whereas leukocytes of hβ2m$^{D76N}$ transgenic mice showed significantly higher signal confirming localisation of D76N variant β2m on cell surface (Figure 3.19).

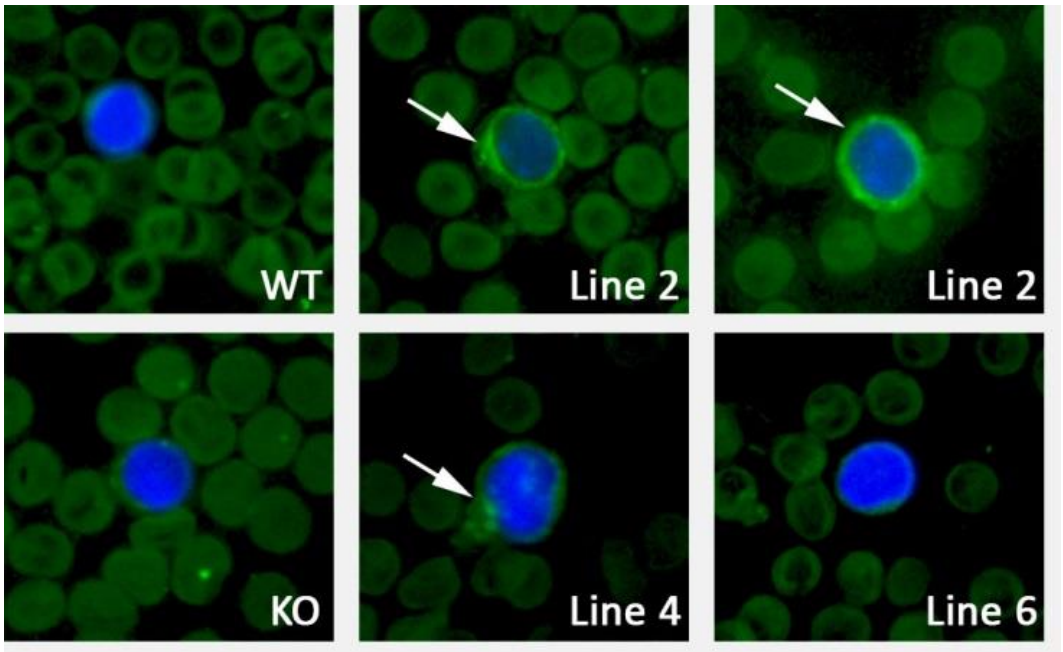


***Figure 3.18: hβ2m immunofluorescence of leukocytes of hβ2m$^{D76N}$ transgenic mice***

*Direct immunofluorescence staining of blood films using FITC-labelled monoclonal anti-hβ2m antibody B2M-01. The bright green fluorescence (white arrows) of leukocytes of hβ2m$^{D76N}$ transgenic mice confirmed the expression of human β2m in lines 2 and 4. No hβ2m immunofluorescence was observed in transgenic mice of line 6. No signal was detected on leukocytes of C57Bl/6J mice (WT) and β2m-KO (KO) mice. Nuclei of leucocytes were stained blue with Hoechst 33342. Erythrocytes appear green due to strong autofluorescence.*

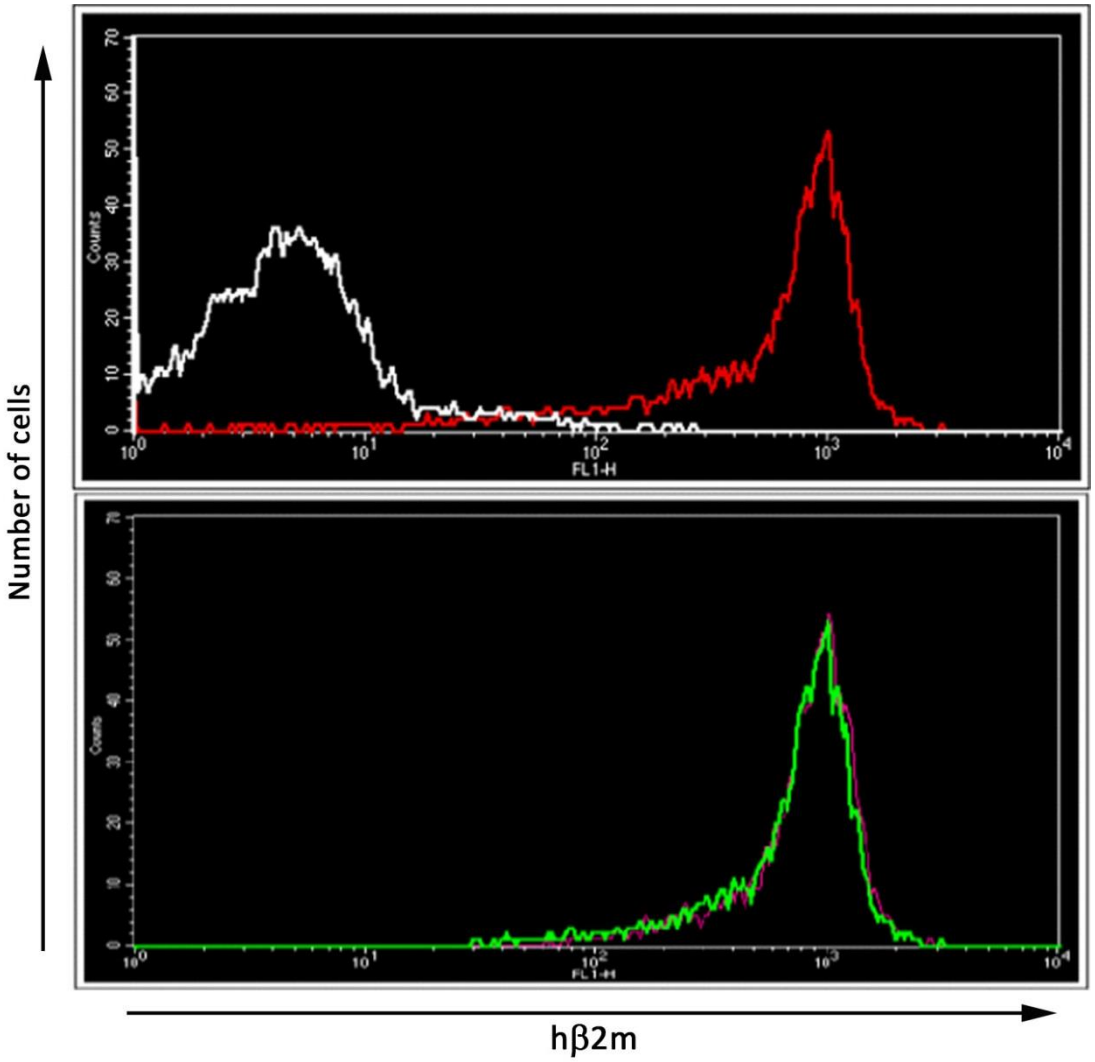


***Figure 3.19: hβ2m cell surface expression in hβ2m$^{D76N}$ transgenic mice***

*Peripheral blood leukocytes were analysed by FACS analysis to assess whether the D76N variant β2m was expressed on the cell surface.*

*Top - the signal of FITC-labelled anti-human β2m monoclonal antibody B2M-01 detected on leukocytes of hβ2m$^{D76N}$ transgenic mice (red) confirmed the localisation of the D76N variant hβ2m on the cell surface. Background levels of autofluorescence only were detected on the leukocytes of non-transgenic littermates and β2m-KO mice (white).*

*Bottom – no difference in signal of the cell surface D76N variant β2m was seen between line2 hβ2m$^{D76N}$ transgenics lacking the endogenous mouse β2m (green) and line 2 hβ2m$^{D76N}$ transgenics carrying mouse β2m allele (pink).*

## 3.3 Discussion

Although attempts have been made to model Aβ2m amyloidosis in mice, none have been successful to date. Here, transgenic mice expressing a highly amyloidogenic variant β2m$^{D76N}$ have been generated as a potential new model of Aβ2m amyloidosis.

β2m is expressed by all nucleated cells. To maintain the ubiquitous expression of the transgene, the hβ2M gene was cloned from genomic DNA and the gene's own promoter and regulatory sequences within the 2.1 kb of 5' flanking sequence and 630 bp 3' flanking sequence were used to drive the expression of the transgene. The advantage of using genomic sequence, including exons and introns, over cDNA-based construct is that the levels of expression of cDNA constructs can be much lower than the expression levels obtained by genomic DNA sequence because introns enhance the efficiency of gene expression and thus play a role in facilitating transcription of microinjected genes *(Brinster et al., 1988, Whitelaw et al., 1991)*. Furthermore, it was shown that own enhancer and promoter of a gene of interest maintains a tissue-specific expression of the transgene *(Chada et al., 1985, Hammer et al., 1987)*. Although the promoter of the B2M gene was identified *(Gussow et al., 1987)*, the regulatory sequences enhancing the B2M gene expression were not. Chamberlain et al. (1988) generated transgenic mice expressing hβ2m in which 2.9 kb and 1.2 kb of 5' and 3' flanking sequences, respectively, of the hB2M genomic sequence showed to regulate the hβ2m transgene expression with a tissue-specific pattern very similar to that of endogenous mouse β2m. Indeed, in the hβ2m$^{D76N}$ transgenic mice presented here, the hβ2m mRNA expression was confirmed in all tissues analysed. Moreover, the concentrations of the plasma human β2m in the three independent lines of the hβ2m$^{D76N}$ transgenic mice were similar or much higher than in healthy humans.

In healthy people, the range of serum β2m concentration is 0.7 – 2.7 μg/ml *(Berggard and Bearn, 1968, Greipp et al., 1988, Floege et al., 1991)* and

similar levels were measured in the line 11 of the hβ2m$^{D76N}$ transgenic mice. Aβ2m amyloidosis is a complication of patients with end stage renal failure whose circulating β2m levels rise up to 50-70 µg/ml and remain elevated for a long period of time *(Floege et al., 1991)*. In chronic kidney disease, serum β2m concentration increases up to ~20 µg/ml but Aβ2m amyloidosis is not present in the patients *(Sedighi et al., 2015)*. However, a patient with chronic kidney disease not on dialysis who developed Aβ2m amyloidosis was reported. In this patient the serum β2m concentration reached 32 µg/ml, which is higher than normally seen in chronic kidney disease patients *(Zingraff et al., 1990)*. Line 2 of the hβ2m$^{D76N}$ transgenic mice had measured plasma concentrations of the human β2m reaching to 40 µg/ml, which are concentrations at which Aβ2m amyloidosis may develop in people. On the other hand, patients carrying the highly amyloidogenic D76N variant β2m, causing hereditary systemic Aβ2m amyloidosis, had normal concentrations of serum β2m (1-3 µg/ml). Therefore, the concentrations of the highly amyloidogenic D76N variant β2m in the transgenic mice presented here should be sufficient for amyloid deposition.

In context with the plasma concentration of human β2m in transgenic mice, Zhang et al. (2010) generated a mouse model expressing wild-type human β2m and reported that the plasma concentrations of human β2m in those mice were ~190 µg/ml. To quantitate the human β2m plasma concentrations, they used semi-quantitative measurement by Western blot using Dako anti-hβ2m antibody, the same antibody used for detection of hβ2m in the hβ2m$^{D76N}$ transgenic mice presented here, and used plasma of wild-type mice expressing endogenous mouse β2m for comparison. However, there is a discrepancy in the literature about plasma concentration of the mouse β2m in mice. Zhang et al. (2010) reported that levels of plasma mouse β2m in C57Bl/6J mice are 113 µg/ml, similarly to Ivanova et al. (2004) who reported levels around 200 µg/ml. However, the data are either not shown by the authors or show a presence of the mouse β2m in mouse plasma without a comparable concentration estimate control *(Zhang et al., 2010, Ivanova et al.,*

*2004)*. On the other hand, Smith et al. (2015) reported and showed that levels of plasma mouse β2m in C57Bl/6J mice are <10 µg/ml *(Smith et al., 2015)*. Consistently with this, the data presented here show that the concentration of plasma mouse β2m in C57Bl/6J mice is higher than plasma β2m concentration in humans but not higher than 10 µg/ml. In the hβ2m transgenic mouse model generated by Zhang et al. (2010), the signal intensity of mβ2m in wild-type mice on an immunoblot used for quantitation of the β2m concentration was similar with hβ2m signal in the transgenic mice. Based on the observations described here, the levels of hβ2m in their transgenic mice are probably similar to levels seen in healthy humans, which are much lower than the concentrations reported.

β2m is essential for a correct assembly of MHC class I molecules in the ER and transport of the complex to the plasma membrane. It has been shown that β2m deficient mice lack MHC class I proteins and CD8+ T cells *(Zijlstra et al., 1990, Koller et al., 1990)*. On the other hand, in mice lacking endogenous β2m but expressing human β2m, murine class I heavy chains associate with human β2m and form functional hybrid complexes that are efficiently expressed at the cell surface *(Chamberlain et al., 1988)*. In hβ2m$^{D76N}$ transgenic mice presented here, the D76N variant human β2m protein was detected on cell surface of leukocytes in all three transgenic lines confirming the ability of the human variant to form functional MHC class I heterodimers with murine MHC class I heavy chains and present them on the cell surface. Interestingly, there was no difference observed in the signal of hβ2m$^{D76N}$ on the cell surface between hβ2m$^{D76N}$ transgenic mice expressing the endogenous mouse β2m and hβ2m$^{D76N}$ transgenic mice lacking the endogenous β2m protein. In cells cultured *in vitro*, cell surface murine MHC class I molecules exchange endogenous mouse β2m subunits with exogenous free human β2m or free bovine β2m molecules present in the culture medium *(Bernabeu et al., 1984)*. Both bovine and human β2m are equivalent in stabilizing the mouse MHC class I heavy chains and the heterodimers are able to present antigenic peptides. The affinity of murine

β2m for murine MHC class I heavy chain is much lower and the murine subunit exchange activity is much weaker compared to human β2m *(Shields et al., 1998, Pedersen et al., 1995)*. It is therefore possible that mouse/human MHC class I heterodimers are preferably formed in the hβ2m$^{D76N}$ transgenic mice or that β2m subunit exchange of assembled MHC class I on the cell surface favours the exchange of mouse β2m for the human β2m protein. The ratio of MHC class I with mouse β2m subunit and MHC class I with human β2m subunit on the cell surface of hβ2m transgenic mice is not known, nor is it known whether the presence of the hβ2m in transgenic mice has an effect on the total number of MHC class I formed and expressed on the cell surface.

In summary, three lines of transgenic mice expressing a highly amyloidogenic human β2m$^{D76N}$ variant have been successfully generated. In these mice, the plasma levels of the human β2m are similar or much higher than in Aβ2m$^{D76N}$ amyloidosis patients. Because the concentration of an amyloidogenic protein is an important prerequisite for priming formation of amyloid fibrils *in vivo*, the hβ2m$^{D76N}$ transgenic mice may have a high potential for developing Aβ2m amyloidosis.

# 4 Characterization of hβ2m$^{D76N}$ transgenic mice as a potential model of β2-microglobulin amyloidosis

## 4.1 Introduction

The previous chapter described generation and establishment of transgenic mice carrying the highly amyloidogenic D76N variant of β2m. The need for a transgenic model of Aβ2m amyloidosis arises from the fact, that although Aβ2m amyloidosis, a serious complication of the majority of patients undergoing long-term dialysis, has been known for over 30 years, the mechanisms of the disease are poorly understood. Although attempts have been made to model Aβ2m amyloidosis in mice, none has been successful to date.

Amyloid deposits in the dialysis-related Aβ2m amyloidosis are specific for the tissue of musculo-skeletal system despite the fact that the β2m protein is ubiquitously released from all nucleated cells of the body. The specificity of the deposition in joints, ligaments, cartilage and bones causes erosive and destructive osteoarthropathies, carpal tunnel syndrome, bone cysts and pathological fractures. Although in recent years the onset of this disease in patients undergoing dialysis has been significantly delayed due to advanced dialysis technology, dialysis-related amyloidosis remains a disabling complication in patients on long-term dialysis, with 50 % of patients after 13 years on dialysis still developing clinically severe manifestation of the disease *(Kopec et al., 2011, Hoshino et al., 2016)*.

Biochemical analyses showed that amyloid deposits present in Aβ2m amyloidosis patients consist of full-length non-mutated β2m and a truncated species of β2m missing the first six N-terminal residues (ΔN6β2m) *(Gorevic et al., 1986, Stoppini et al., 2005)* and fibrillogenesis of β2m *in vitro* has been extensively studied. It has been reported that while the truncated ΔN6β2m

can aggregate *in vitro* into fibrillar material at physiological conditions (pH 7.2, 37 $^{o}$C while shaking at 200 RPM), in fact the ΔN6β2m was able to convert full-length human β2m into amyloid-like aggregates under the physiological conditions under which full-length human β2m alone does not aggregate, addition of mouse β2m into the ΔN6β2m protein mixture completely abolished the aggregation potential of the ΔN6β2m *(Eichner et al., 2011)*. Furthermore, mouse β2m is not amyloidogenic *in vitro*, even in acidic conditions (pH 2.0) in which human β2m aggregates into fibrillar material *(Ivanova et al., 2004, Eichner et al., 2011)*. However, it is not known whether mouse β2m affects fibrillogenesis of human β2m *in vivo*.

In 2010, Zhang et al. generated transgenic mice expressing wild-type human β2m as a model of Aβ2m amyloidosis. Although the authors have reported that the mice have high plasma concentrations of the human β2m (~190 μg/ml), the actual plasma concentration may be much lower as it was discussed before. Nevertheless, the mice did not develop spontaneous Aβ2m amyloidosis up to 24 months of age, despite the fact that expression of the endogenous murine β2m was silenced in the transgenic mice *(Zhang et al., 2010)*. Priming of Aβ2m amyloid deposition with exogenous seeds of Aβ2m amyloid fibrils also failed and the transgenic mice lacking the mouse β2m did not develop Aβ2m amyloidosis *(Zhang et al., 2010)*.

In the previous chapter, generation and establishment of transgenic mice expressing the highly amyloidogenic β2m$^{D76N}$ variant were presented. The recently described first naturally occurring β2m$^{D76N}$ variant causes highly penetrant hereditary systemic Aβ2m amyloidosis in one French family with a severe phenotype of extensive visceral amyloid deposits with the onset in the fourth decade *(Valleix et al., 2012)*. The most disabling condition in the patients carrying this mutation is progressive bowel dysfunction caused by severe autonomic neuropathy *(Valleix et al., 2012)*. Amyloid deposits were also found in spleen, liver, heart, salivary glands, adrenal gland and colon but surprisingly no amyloid was found in bones, joins and ligaments typical for dialysis-related Aβ2m amyloidosis. Moreover, in contrast with dialysis-related

Aβ2m amyloidosis in which elevated β2m concentrations are one of the pre-requisites of developing Aβ2m amyloid deposits, the $\beta2m^{D76N}$ patients had normal levels of circulating β2m *(Valleix et al., 2012)*.

*In vitro* studies showed that the $\beta2m^{D76N}$ protein incubated in physiological solution at pH 7.4 with mild shaking rapidly converted into fibrils within a few hours, in contrast to wild-type β2m which remained natively folded and soluble under the same conditions *(Mangione et al., 2013)*. Moreover, the $\beta2m^{D76N}$ variant can transform wild-type β2m into insoluble fibrils in a mixed solution *in vitro* at much higher rate than ΔN6β2m *(Mangione et al., 2013)*. Interestingly, there was no wild-type β2m protein found in the amyloid fibrils isolated from a tissue of $A\beta2m^{D76N}$ amyloidosis patient, which purely consisted of the full length variant *(Valleix et al., 2012, Mangione et al., 2013)*.

In this project, transgenic mice carrying the recently discovered highly amyloidogenic D76N variant of β2m were generated. 3 independent transgenic lines were established which present with similar or higher concentrations of circulating $h\beta2m^{D76N}$ than concentrations seen in $\beta2m^{D76N}$ amyloidosis patients. Given the aggressive amyloidogenicity of the $\beta2m^{D76N}$ variant, the hypothesis was that these mice will develop Aβ2m amyloidosis.

The aims to support this hypothesis were to assess amyloid deposition in the transgenic mice in various tissues in which Aβ2m amyloid may occur, by histological analysis with Congo red staining and immunohistochemistry. $h\beta2m^{D76N}$ transgenic mice on both, wild-type mouse β2m and β2m-KO backgrounds were analysed to evaluate the effect of the mouse β2m on human β2m deposition and amyloid formation in the mice. The possibility of accelerating Aβ2m deposition by seeding the transgenic mice with pre-formed Aβ2m amyloid fibrils, a method commonly used in priming amyloid deposition in mouse models of AA amyloidosis *(Willerson et al., 1969, Simons et al., 2013)* and ApoAII amyloidosis *(Higuchi et al., 1998)* was also investigated.

## 4.2 Results

### 4.2.1 Assessment of spontaneous amyloid deposition in hβ2m$^{D76N}$ transgenic mice

The D76N variant β2m has been shown to be highly amyloidogenic and patients heterozygous for this mutation suffer from systemic amyloid deposits. The patients are clinically affected as early as in their fourth decade with heavy amyloid deposits in the viscera, involving especially spleen and adrenal glands. In a post-mortem examination of a 70 year old patient carrying the D76N mutation in the β2M gene, amyloid deposits were found in spleen, liver, heart, salivary glands, colon and nerves *(Valleix et al., 2012)*. In dialysis-related amyloidosis patients, persistent elevated levels of wild-type β2m are responsible for amyloid deposits in joints and bones.

In the hβ2m$^{D76N}$ transgenic mice, spontaneous amyloid deposition was assessed by Congo red staining of sections of wax embedded tissue and light microscopy with polarized light. Because of the wide-spread amyloid depositions in the Aβ2m$^{D76N}$ patients, the assessment involved a wide variety of tissues. The examined tissues included liver, kidney, spleen, heart, lung, stomach, gut, adrenal, sciatic nerve, salivary gland, tongue, skin, fat, eye and sternum cartilage in all three lines of the hβ2m$^{D76N}$ transgenics on both, wild-type and β2m-KO background. Because of the age-dependence in amyloid deposition typical for amyloidosis, the analysis was performed on mice 6 months old up to 24 months old. Age-matched non-transgenic wild-type and β2m-KO mice were also analysed as negative controls.

Despite the aggressively amyloidogenic character of the D76N variant of β2m and despite a thorough search of extensive tissue samples, no spontaneous deposition of Aβ2m amyloid was found in the transgenic mice. The number of animals analysed for each line and the outcome of the analysis is summarised in Tables 4.1 – 4.3.

Congo red positive staining exhibiting green birefringence under the polarised light typical for amyloid was detected in two 22 months old non-transgenic C57Bl/6J mice. In mice, two types of systemic amyloidoses associated with aging can naturally occur: AApoAII amyloidosis in which the amyloidogenic precursor is apolipoprotein A-II (ApoAII), an abundant protein in serum high-density lipoprotein *(Takeda et al., 1994, Higuchi et al., 1997)*, and AA amyloidosis associated with chronic inflammation in which serum amyloid A (SAA), an acute phase apolipoprotein, is the amyloidogenic precursor *(McAdam and Sipe, 1976, Eriksen et al., 1976, Higuchi et al., 1991b)*. Immunohistochemistry with antibodies against hβ2m, mouse ApoAII and mouse SAA confirmed that ApoAII was the amyloid protein in the tissue of the two 22 months old non-transgenic mice. No immunoreactivity was detected with anti-mouse SAA and anti-hβ2m antibodies in the Congo-red positive tissues (Figure 4.1).

| Line 2 | Spontaneous amyloid deposition | | | | | |
|---|---|---|---|---|---|---|
| | 6-12 months | | 12-18 months | | 18-24 months | |
| | T/WT | T/KO | T/WT | T/KO | T/WT | T/KO |
| Liver | 0/3 | 0/1 | - | 0/3 | 0/8 | 0/3 |
| Kidney | 0/3 | 0/1 | - | 0/3 | 0/8 | 0/3 |
| Spleen | 0/3 | 0/1 | - | 0/3 | 0/8 | 0/3 |
| Heart | 0/3 | 0/1 | - | 0/3 | 0/8 | 0/3 |
| Lung | 0/3 | 0/1 | - | 0/3 | 0/8 | 0/3 |
| Tongue | 0/3 | 0/1 | - | 0/3 | 0/8 | 0/3 |
| Salivary gland | 0/3 | 0/1 | - | 0/3 | 0/8 | 0/3 |
| Adrenal | 0/3 | 0/1 | - | 0/3 | 0/8 | 0/3 |
| Sciatic nerve | 0/3 | 0/1 | - | 0/3 | 0/8 | 0/3 |
| Gut | 0/3 | 0/1 | - | 0/3 | 0/8 | 0/3 |
| Stomach | 0/3 | 0/1 | - | 0/3 | 0/8 | 0/3 |
| Muscle | 0/3 | 0/1 | - | 0/3 | 0/8 | 0/3 |
| Fat | 0/3 | 0/1 | - | 0/3 | 0/8 | 0/3 |
| Skin | 0/3 | 0/1 | - | 0/3 | 0/8 | 0/3 |
| Eye | - | - | - | - | 0/7 | - |
| Optic nerve | - | - | - | - | 0/5 | - |
| Lacrymal gland | - | - | - | - | 0/5 | - |
| Cartilage | - | - | - | 0/1 | - | 0/3 |

**Table 4.1: Analysis of spontaneous amyloid deposition in hβ2m$^{D76N}$ transgenic mice**

*Summary of tissue analysed by Congo red in line 2 hβ2m$^{D76N}$ transgenic mice on wild-type background (T/WT) and on β2m-KO background (T/KO) at age groups 6-12, 12-18 and 18-24 months old. The samples are scored as number of mice with amyloid / number of mice analysed for each tissue.*

| Line 4 | Spontaneous amyloid deposition | | | | | |
|---|---|---|---|---|---|---|
| | 6-12 months | | 12-18 months | | 18-24 months | |
| | T/WT | T/KO | T/WT | T/KO | T/WT | T/KO |
| Liver | 0/2 | 0/3 | - | 0/3 | 0/4 | - |
| Kidney | 0/2 | 0/3 | - | 0/3 | 0/4 | - |
| Spleen | 0/2 | 0/3 | - | 0/3 | 0/4 | - |
| Heart | 0/2 | 0/3 | - | 0/3 | 0/4 | - |
| Lung | 0/2 | 0/3 | - | 0/3 | 0/4 | - |
| Tongue | 0/2 | 0/3 | - | 0/3 | 0/4 | - |
| Salivary gland | 0/2 | 0/3 | - | 0/3 | 0/4 | - |
| Adrenal | 0/2 | 0/3 | - | 0/3 | 0/4 | - |
| Sciatic nerve | 0/2 | 0/3 | - | 0/3 | 0/4 | - |
| Gut | 0/2 | 0/3 | - | 0/3 | 0/4 | - |
| Stomach | 0/2 | 0/3 | - | 0/3 | 0/4 | - |
| Muscle | 0/2 | 0/3 | - | 0/3 | 0/4 | - |
| Fat | 0/2 | 0/3 | - | 0/3 | 0/4 | - |
| Skin | 0/2 | 0/3 | - | 0/3 | 0/4 | - |
| Eye | - | 0/1 | - | 0/1 | 0/4 | - |
| Optic nerve | - | 0/1 | - | 0/1 | 0/4 | - |
| Lacrymal gland | - | 0/1 | - | 0/1 | 0/4 | - |

**Table 4.2: Analysis of spontaneous amyloid deposition in hβ2m$^{D76N}$ transgenic mice**

*Summary of tissue analysed by Congo red in line 4 hβ2m$^{D76N}$ transgenic mice on wild-type background (T/WT) and on β2m-KO background (T/KO) at age groups 6-12, 12-18 and 18-24 months old. The samples are scored as number of mice with amyloid / number of mice analysed for each tissue.*

| Line 11 | Spontaneous amyloid deposition | | | | | |
|---|---|---|---|---|---|---|
| | 6-12 months | | 12-18 months | | 18-24 months | |
| | T/WT | T/KO | T/WT | T/KO | T/WT | T/KO |
| Liver | 0/2 | 0/4 | - | 0/2 | 0/3 | - |
| Kidney | 0/2 | 0/4 | - | 0/2 | 0/3 | - |
| Spleen | 0/2 | 0/4 | - | 0/2 | 0/3 | - |
| Heart | 0/2 | 0/4 | - | 0/2 | 0/3 | - |
| Lung | 0/2 | 0/4 | - | 0/2 | 0/3 | - |
| Tongue | 0/2 | 0/4 | - | 0/2 | 0/3 | - |
| Salivary gland | 0/2 | 0/4 | - | 0/2 | 0/3 | - |
| Adrenal | 0/2 | 0/4 | - | 0/2 | 0/3 | - |
| Sciatic nerve | 0/2 | 0/4 | - | 0/2 | 0/3 | - |
| Gut | 0/2 | 0/4 | - | 0/2 | 0/3 | - |
| Stomach | 0/2 | 0/4 | - | 0/2 | 0/3 | - |
| Muscle | 0/2 | 0/4 | - | 0/2 | 0/3 | - |
| Fat | 0/2 | 0/4 | - | 0/2 | 0/3 | - |
| Skin | 0/2 | 0/4 | - | 0/2 | 0/3 | - |
| Eye | - | 0/4 | - | - | 0/2 | - |
| Optic nerve | - | 0/4 | - | - | 0/2 | - |
| Lacrymal gland | - | - | - | - | 0/1 | - |

**Table 4.3: Analysis of spontaneous amyloid deposition in hβ2m$^{D76N}$ transgenic mice**

*Summary of tissue analysed by Congo red in line 11 hβ2m$^{D76N}$ transgenic mice on wild-type background (T/WT) and on β2m-KO background (T/KO) at age groups 6-12, 12-18 and 18-24 months old. The samples are scored as number of mice with amyloid / number of mice analysed for each tissue.*

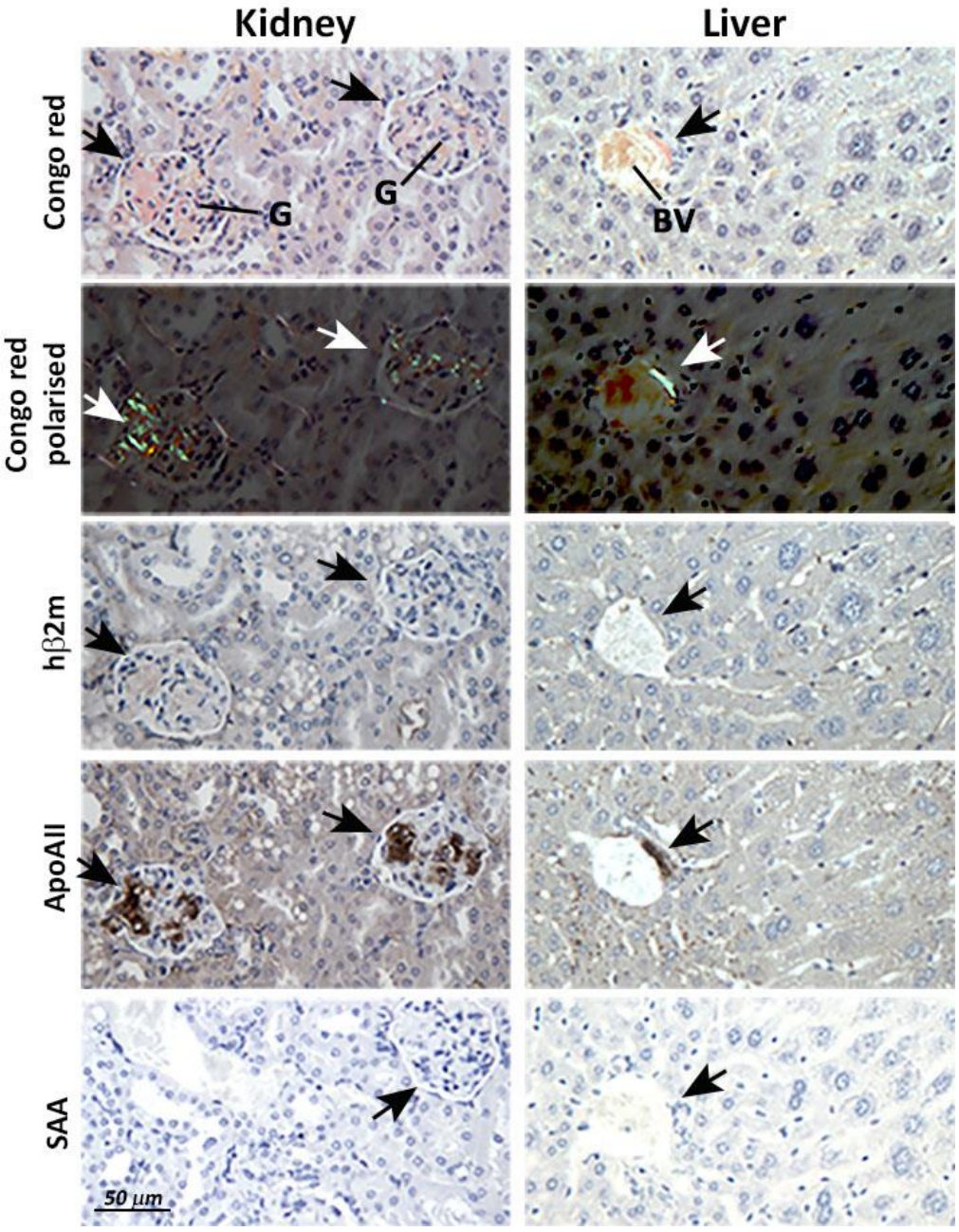


***Figure 4.1: Amyloid deposition in aged non-transgenic mice***

*Amyloid deposition in kidney and liver of a 22 months old non-transgenic wild-type control mouse was detected in Congo red stained section. Amyloid (black arrows) is stained red and exhibits green/orange birefringence under polarised light. The co-localisation of amyloid with mouse ApoAII protein in the tissue was confirmed by immunostatining with anti-mouse ApoAII antibody (1/4000), seen in dark brown. No co-localised signal was detected when the amyloidotic tissue was immunostatined with anti-mouse SAA antibody (1/100) and Dako anti-human β2m antibody (1/600). G – kidney glomerulus, BV – blood vessel in liver tissue.*

### 4.2.2 β2m deposition in hβ2m$^{D76N}$ transgenic mice

Because no amyloid was found in the hβ2m$^{D76N}$ transgenic mice, tissues of transgenic animals on both, wild-type and β2m-KO backgrounds were examined by immunohistochemistry with anti-human β2m antibody to analyse whether any extracellular accumulation of β2m, suggesting β2m deposition and aggregation, could be detected. Because β2m is expressed on all nucleated cells, indeed, the hβ2m expression in the hβ2m$^{D76N}$ transgenic mice was confirmed in all tissue analysed, and because free β2m is circulating in the blood, some β2m signal was expected in all transgenic tissue.

Because the Dako anti-human β2m antibody cross-reacted on Western blot with denatured mouse β2m, the specificity of Dako polyclonal anti-human β2m antibody (Table 2.1) to human β2m in fixed and wax embedded tissue was tested. Liver, kidney and spleen of 6-9 months old of 2 transgenic mice on wild-type background was immunostained together with tissues of 2 non-transgenic wild-type mice and 2 non-transgenic β2m-KO mice.

As expected, hβ2m signal was detected in the tissues of transgenic mice and no signal was detected in the tissue of non-transgenic β2m-KO mice. Only very weak background staining was detected in the tissues of non-transgenic wild-type mice expressing endogenous mouse β2m confirming the specificity of the antibody to human β2m (Figure 4.2).

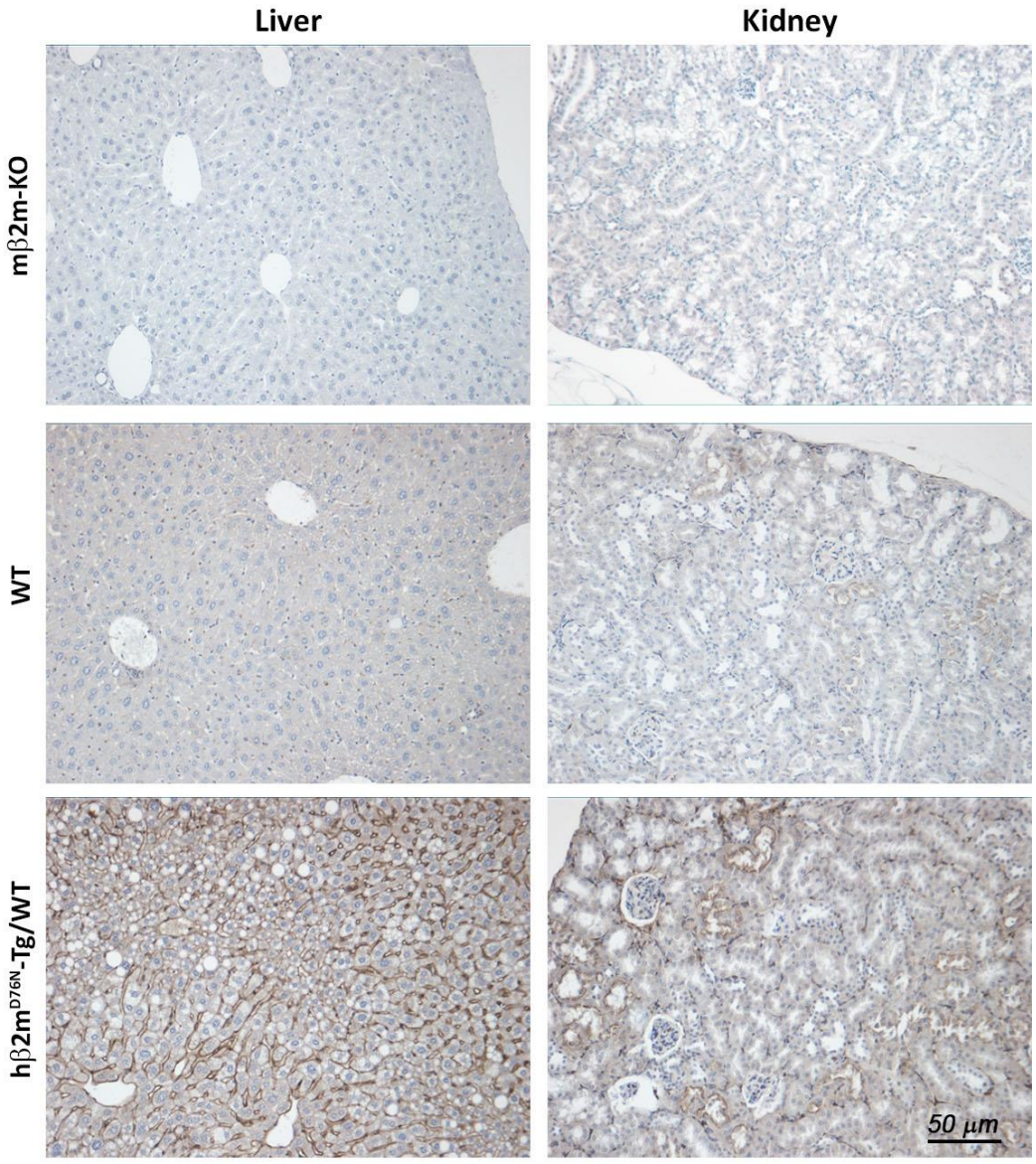


***Figure 4.2: Specificity of Dako anti-human $\beta_2$-microglobulin antibody***

*Under denaturing conditions of Western blot, Dako polyclonal anti-human β2m antibody cross-reacts with mouse β2m. In order to use the antibody in immunohistochemistry to evaluate the localisation of the variant human β2m in the tissue of hβ2m$^{D76N}$ transgenic mice, sections of fixed and wax embedded samples of β2m-KO mice (n=2), C57Bl/6J (WT) mice (n=2) and hβ2m$^{D76N}$ transgenic mice expressing also the endogenous mouse β2m (hβ2m$^{D76N}$-Tg/WT, n=2) were compared. The specificity of the antibody under native conditions was confirmed by giving a strong signal in the tissue of transgenic mice, whereas only very weak background staining was detected in the WT and β2m-KO mice. The figure shows representative images.*

Because amyloid deposition is time dependent, tissues of 4-week old hβ2m$^{D76N}$ transgenic mice on β2m-KO background (n=3) were compared to 18-months old hβ2m$^{D76N}$ transgenic mice on β2m-KO background (n=3). Transgenic mice on the β2m-KO background were chosen because of the possible inhibitory effect of mouse β2m on aggregation of human β2m reported in *in vitro* experiments *(Eichner et al., 2011)*, as discussed earlier. Two β2m-KO mice were used as negative controls. The tissues analysed included liver, kidney, spleen, heart, lung, stomach, gut, adrenal, sciatic nerve, salivary gland, tongue, skin, fat and sternum cartilage.

In the young, 4 weeks old mice, some β2m signal was observed in all tissue analysed as expected. Large amount of the human β2m protein was detected in the liver where the hβ2m appeared to be lining the sinusoids and radiating from the hepatic venules. Strong human β2m signal was also detected in the spleen, at the top of the villi of the intestine and in epidermis of the skin. Considerably more β2m signal was observed in liver, kidney, stomach, intestine, skin and tongue of the 18 months old mice when compared to the tissue of young mice. Representative images are shown in Figures 4.3 – 4.8. The hβ2m in the tissues of the old mice seemed to be accumulated extracellularly. With advancing age, the pattern of hβ2m signal became more widespread and more prominent suggesting deposition of hβ2m in the tissue, an observation consistent with pre-fibrillar aggregation. On the other hand, increasing expression of the transgene in older mice cannot be ruled out.

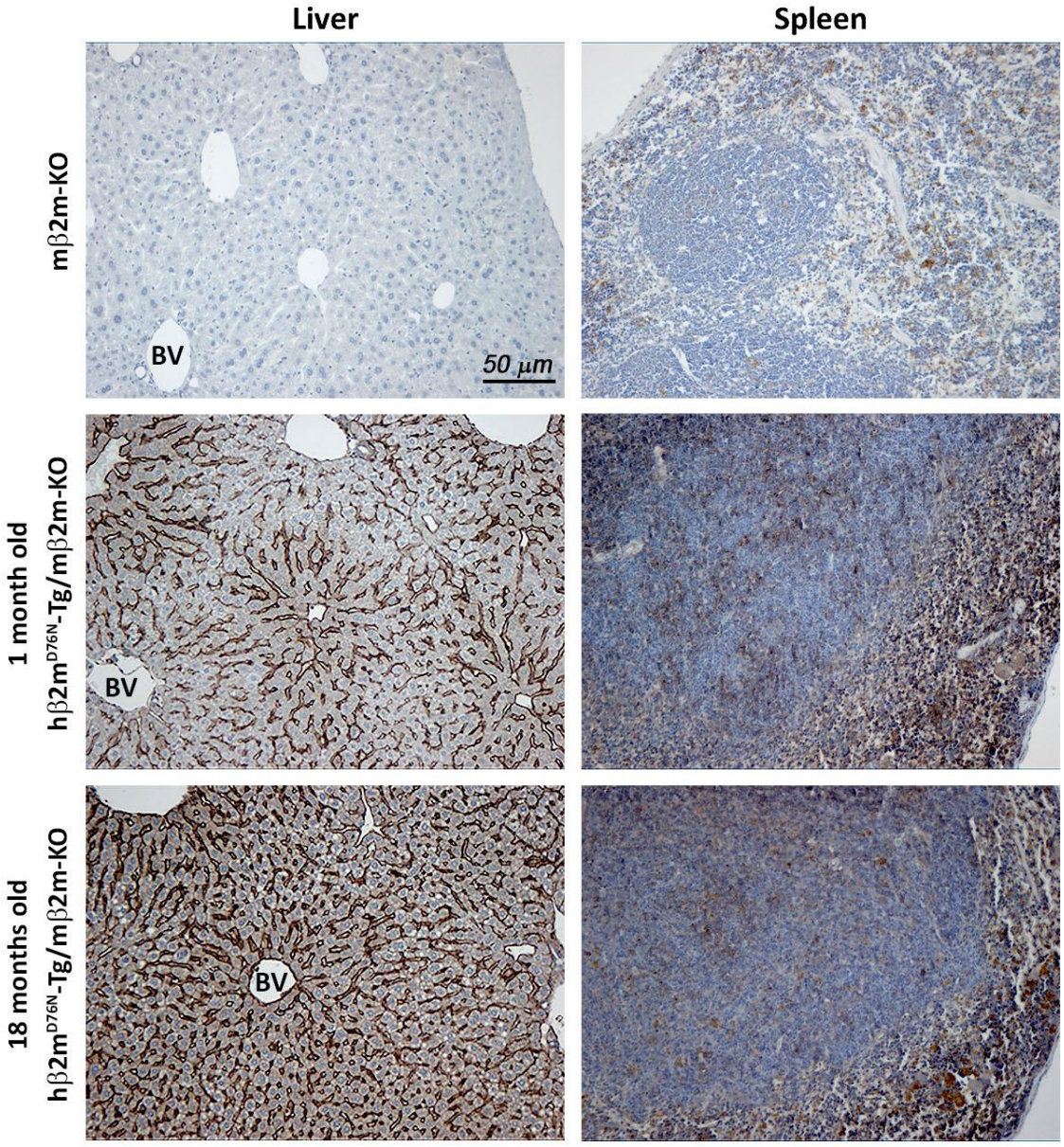


***Figure 4.3: Comparison of hβ2m localisation between young and old hβ2m$^{D76N}$ transgenic mice***

*Immunohistochemistry on liver and spleen of 1 month old (n=3) and 18 months old (n=3) hβ2m$^{D76N}$ transgenic mice on β2m-KO background (hβ2m$^{D76N}$-Tg/mβ2m-KO) stained with Dako anti-human β2m antibody. Strong β2m signal was observed in both, the liver and the spleen. More β2m was detected in the liver tissue of old mice than in the young mice. The localisation of β2m seemed extracellular, lining the sinusoids and surrounding the blood vessels (BV) suggesting increased β2m deposition with advanced age.*

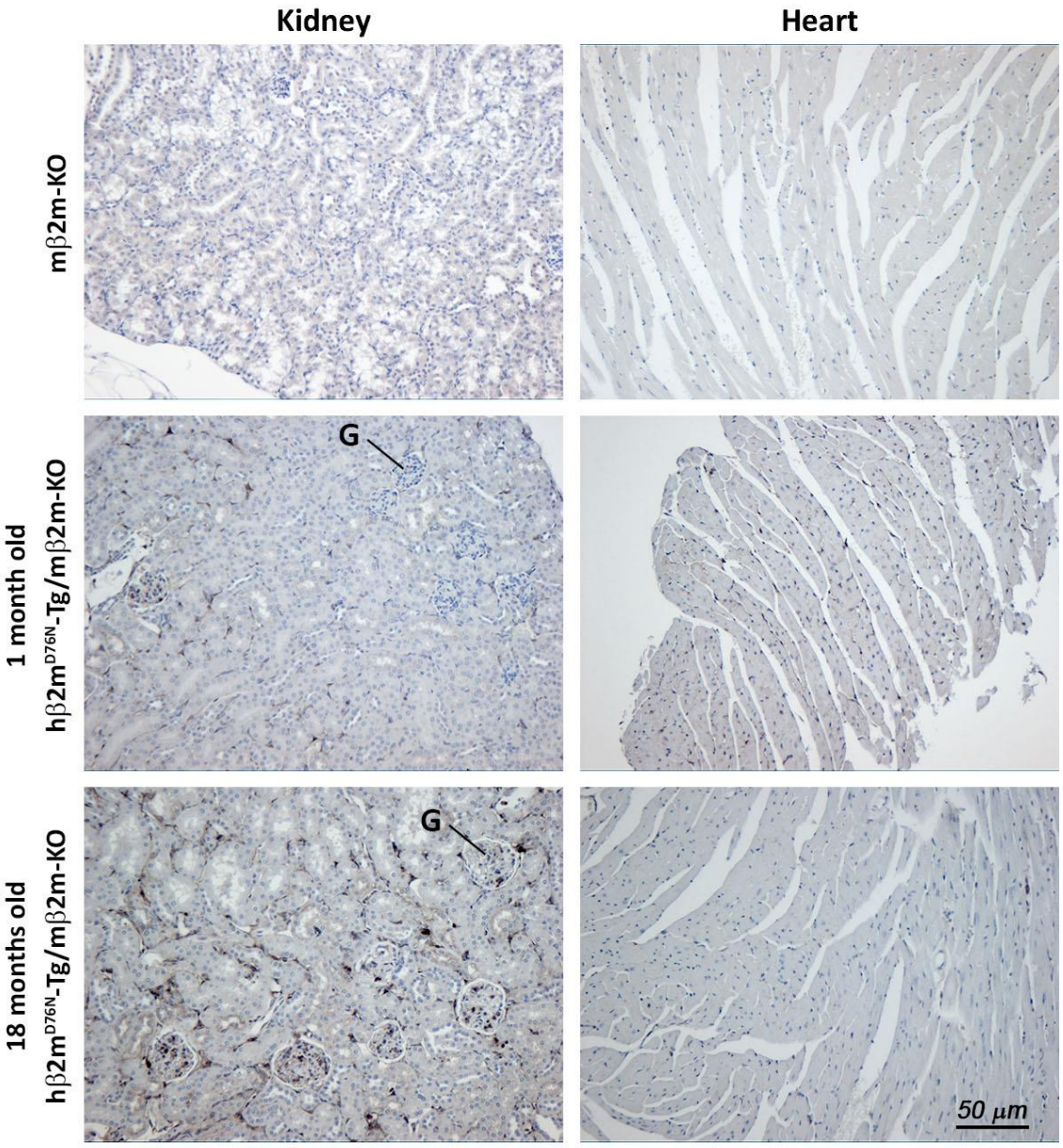


***Figure 4.4: Comparison of hβ2m localisation between young and old hβ2m$^{D76N}$ transgenic mice***

*Immunohistochemistry on kidney and heart of 1 month old (n=3) and 18 months old (n=3) hβ2m$^{D76N}$ transgenic mice on β2m-KO background (hβ2m$^{D76N}$-Tg/mβ2m-KO) stained with Dako anti-human β2m antibody. Very little β2m expression was observed in the tissue of the 1 month old mice. In the 18 months old mice, more β2m was detected in the kidney compared to 4 weeks old mice. β2m seemed to be localised in the sinusoids of the kidney, similarly to the liver, and in the glomeruli (G).*

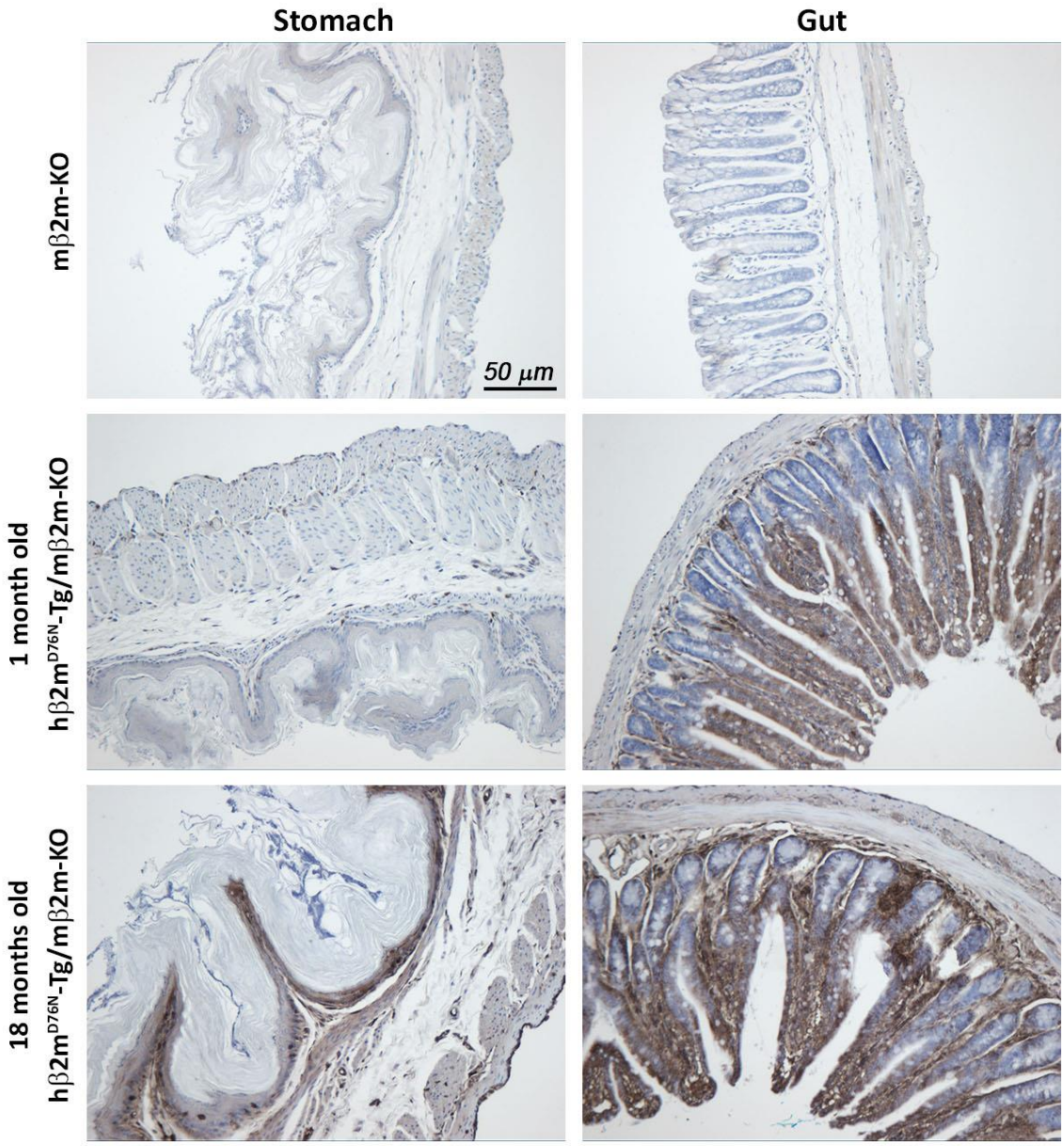


***Figure 4.5: Comparison of hβ2m localisation between young and old hβ2m$^{D76N}$ transgenic mice***

*Immunohistochemistry on stomach and gut of 1 month old (n=3) and 18 months old (n=3) hβ2m$^{D76N}$ transgenic mice on β2m-KO background (hβ2m$^{D76N}$-Tg/mβ2m-KO) stained with Dako anti-human β2m antibody. Strong β2m signal was detected in the villi and mucosa of the intestine, more so in the old mice compare to young transgenics. β2m in the stomach of young mice was not detected, whereas strong β2m signal was observed in the stomach submucosa of aged mice. β2m-KO mice were used as negative controls.*

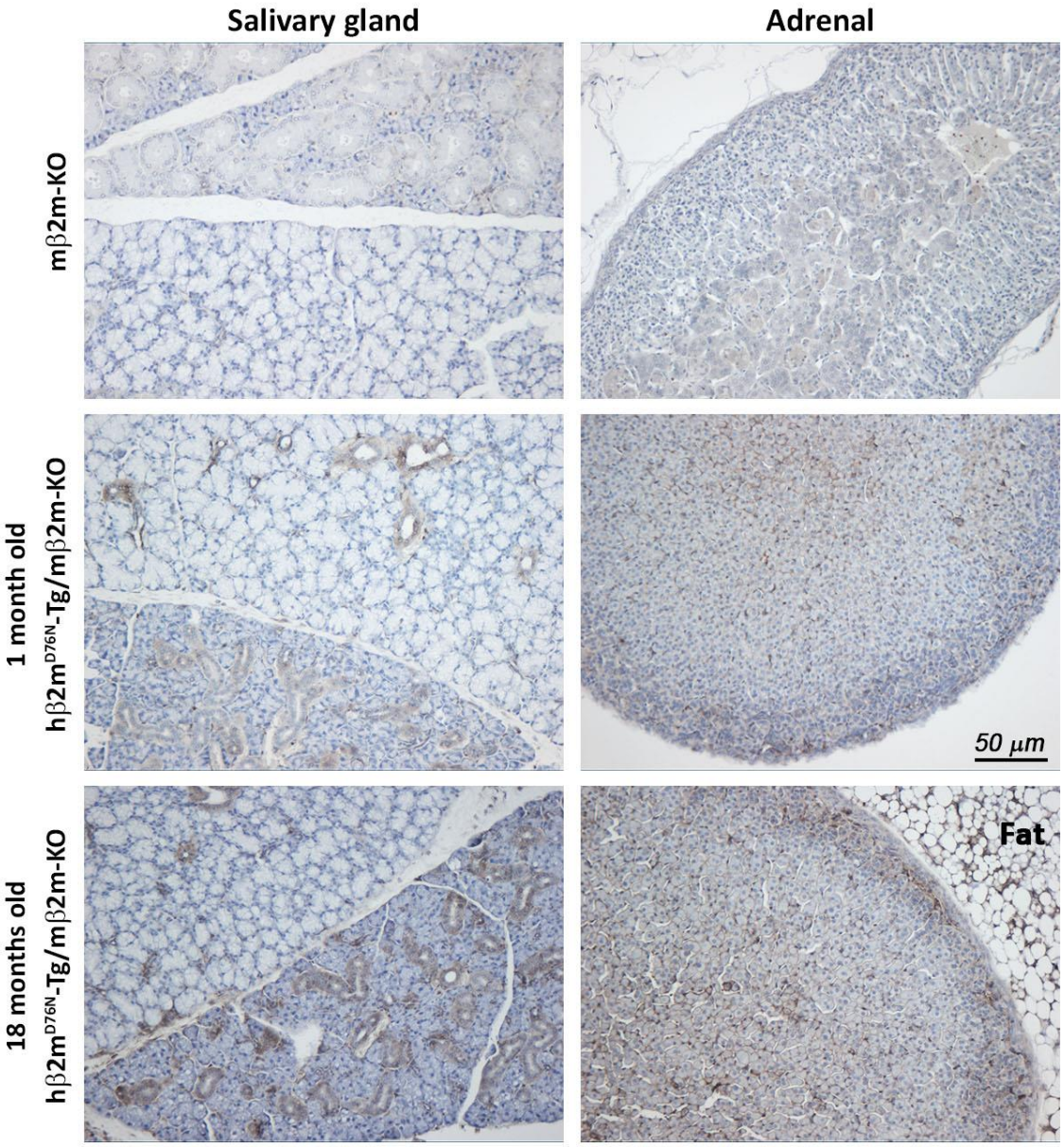


***Figure 4.6: Comparison of hβ2m localisation between young and old hβ2m$^{D76N}$ transgenic mice***

*Immunohistochemistry on salivary gland and adrenal of 1 month old (n=3) and 18 months old (n=3) hβ2m$^{D76N}$ transgenic mice on β2m-KO background (hβ2m$^{D76N}$-Tg/mβ2m-KO) stained with Dako anti-human β2m antibody. β2m was detected in both organs but no difference was observed between the young and old mice. β2m is also visible in the fat tissue surrounding the adrenal of the old transgenic mouse. β2m-KO mice were used as negative controls.*

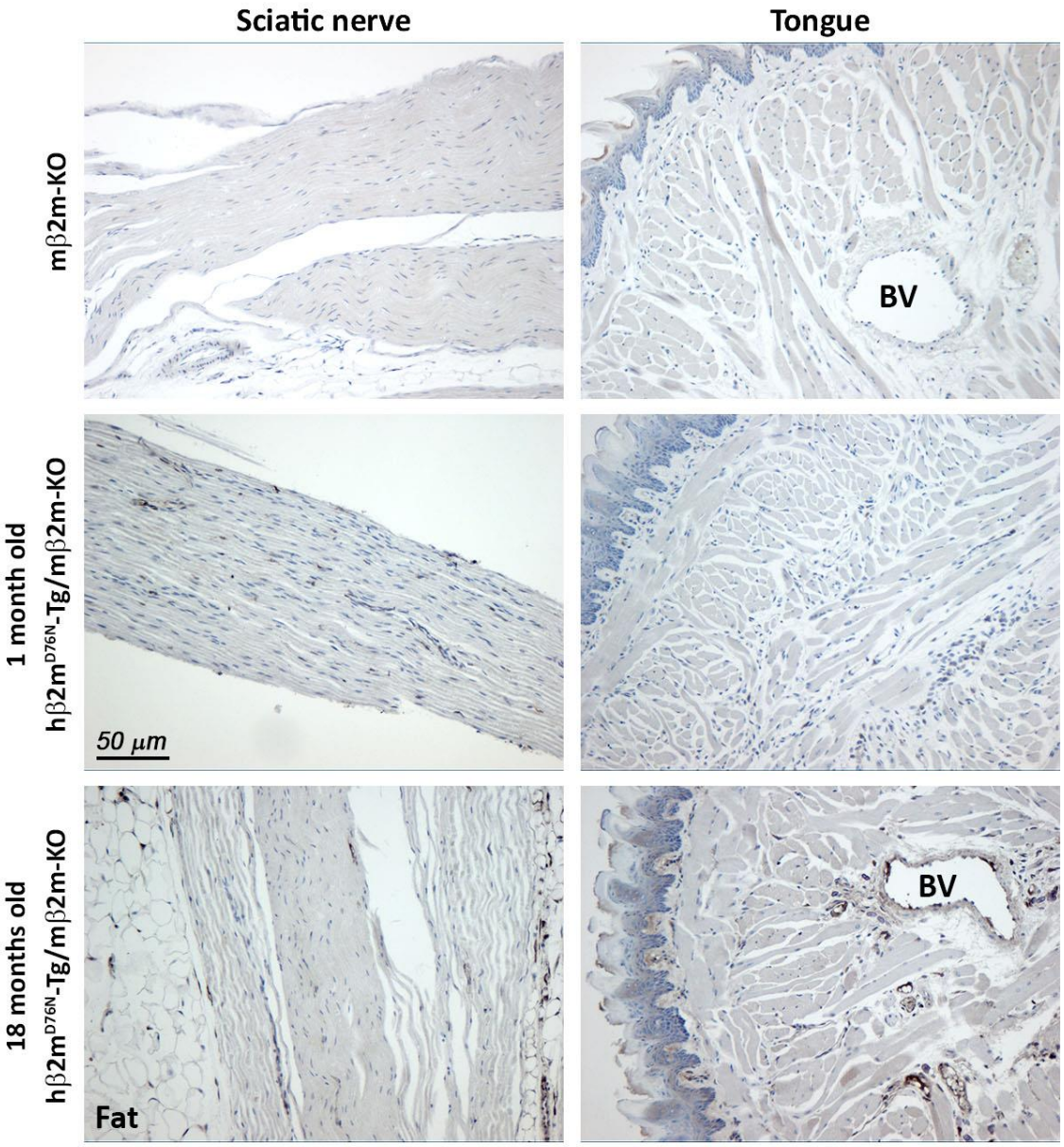


***Figure 4.7: Comparison of hβ2m localisation between young and old hβ2m$^{D76N}$ transgenic mice***

*Immunohistochemistry on sciatic nerve and tongue of 1 month old (n=3) and 18 months old (n=3) hβ2m$^{D76N}$ transgenic mice on β2m-KO background (hβ2m$^{D76N}$-Tg/mβ2m-KO) stained with Dako anti-human β2m antibody. Stronger β2m signal was detected in the tongue of old mice compared to young mice, concentrated around the blood vessels (BV). β2m in the fat tissue surrounding the sciatic nerve is seen in the picture of the old transgenic mouse.*

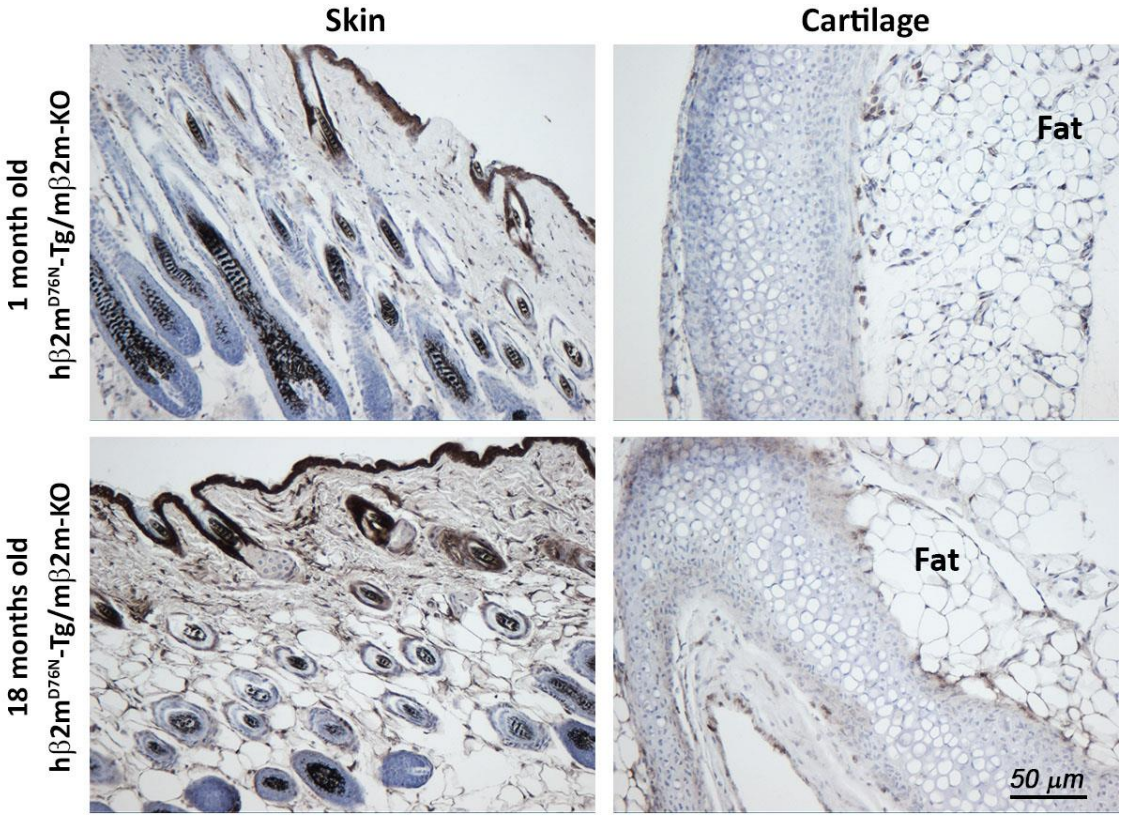


***Figure 4.8: Comparison of hβ2m localisation between young and old hβ2m$^{D76N}$ transgenic mice***

*Immunohistochemistry on skin and sternum cartilage of 1 month old (n=3) and 18 months old (n=3) hβ2m$^{D76N}$ transgenic mice on β2m-KO background (hβ2m$^{D76N}$-Tg/mβ2m-KO) stained with Dako anti-human β2m antibody. Age related increase in β2m was observed in the dermis and fat of the skin. β2m signal was detected in the fat surrounding the cartilage but the cartilage itself does not contain any β2m.*

### 4.2.3 Investigation of potential means to increase β2m concentration

Although high concentrations of the β2m variant circulate in the hβ2m$^{D76N}$ transgenic mice, especially in line 2, the mice did not develop spontaneous amyloid deposits. In dialysis-related amyloidosis, β2m circulating concentrations rise from ~1 μg/ml up to ~50 μg/ml due to chronic kidney disease and renal failure caused by insufficient clearance of the protein by the kidneys *(Floege et al., 1991, Sedighi et al., 2015).* After ~10 years of dialysis, the high concentrations of the plasma β2m result it Aβ2m amyloid fibril formation and deposition. I speculated whether inducing renal failure in mice would increase the circulating β2m variant and subsequently increase the chances of depositing the β2m variant as amyloid fibrils in the hβ2m$^{D76N}$ transgenic mice.

In mice, chronic kidney failure can be induced by administration of folic acid – administration of high-dose folic acid (~200 μg/g of body weight) leads to the folic acid undergoing glomerular filtration which is followed by widespread tubular damage, and reliably induces severe nephrotoxicity within days after the folic acid administration *(Koziolek et al., 2010, Long et al., 2008, Yuan et al., 2003)*. In patients with chronic kidney disease, serum β2m levels are elevated *(Liabeuf et al., 2012)*. However, in this mouse model of chronic kidney disease, β2m levels have not been reported.

Dr Jill Norman (Nephrology, UCL) and Dr James Tomlinson (MRC Clinical Sciences Centre, Hammersmith hospital site, Imperial College) kindly provided sera of C57Bl/6 mice collected at 2 days, 2 weeks and 12 weeks after folic acid administration *(Long et al., 2008)*, together with sera of control mice injected with vehicle only, for assessment of β2m concentration of the different groups. 1 μl of each sample was run on an SDS-PAGE gel and probed with Dako polyconal anti-hβ2m antibody that recognises mouse as well as human β2m. No increase in β2m concentration was observed between the control and the folic acid treated mice (Figure 4.9). Because folic

acid induced chronic kidney failure in the hβ2m$^{D76N}$ transgenic mice would not lead to a significant increase in the plasma β2m concentration, this experimental procedure was not investigated any further.

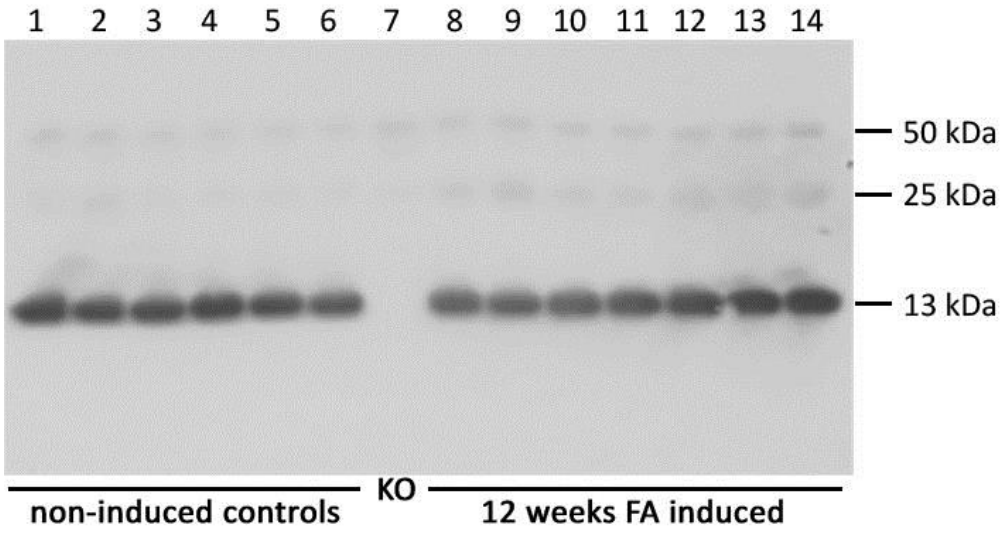


***Figure 4.9: β2m concentration in chronic kidney disease mouse model***

*1 µl of serum of non-induced C57Bl/6J mice (lanes 1 - 6) and of C57Bl/6J mice obtained 12 weeks after folic acid administration (lanes 8 – 14) was run on an SDS-PAGE gel and probed with Dako polyclonal anti-hβ2m antibody recognising 13 kDa mouse β2m. No difference in β2m concentration was observed between the non-induced and folic acid induced mice. β2m-KO serum (KO) was used as a negative control. Light and heavy chains of serum IgG were detected on the immunoblot.*

### 4.2.4 Monitoring kidney function in hβ2m$^{D76N}$ transgenic mice

In aged mice, the immunohistochemistry on the kidney revealed stronger signal of human β2m in the glomeruli, suggesting deposition of hβ2m. Although the kidney is not a site of amyloid deposition in Aβ2m amyloidosis patients, renal involvement is very common in systemic amyloidosis in humans and mice.

β2m together with cystatin C (CysC) have been proposed as markers for the detection of kidney function due to their ability to pass freely through the glomerular barrier and due to the fact that both proteins are produced at a relatively constant rate without being affected either by muscle breakdown nor tubular secretion (unlike creatinine) *(Randers et al., 1998, Randers et al., 2000, Bianchi et al., 2001)*. Both proteins have also been shown to predict cardiovascular event and mortality *(Shlipak et al., 2005, Joosten et al., 2014)*. In the folic acid-induced chronic kidney failure in mice discussed in the previous paragraph, plasma Cys C concentrations have been reported to rise *(Wang et al., 2011)*. To evaluate whether kidney function was compromised due to possible pre-fibrillar deposition in the hβ2m$^{D76N}$ transgenic mice reaching 1 year of age, CysC serum levels were analysed by ELISA.

The range of serum CysC concentration in C57Bl/6J mice is 0.6-0.8 μg/ml *(Xu et al., 2011, Sasabe et al., 2014)*. No significant difference was seen between 8-11 months old high expressing line 2 hβ2m$^{D76N}$ transgenic mice on wild-type background and aged-matched non-transgenic controls with CysC levels 0.586 ± 0.070 μg/ml (n=14) and 0.640 ± 0.069 μg/ml (n=6), respectively, suggesting normal renal function in the transgenic mice (Figure 4.10). The values are presented as mean ± standard deviation with numbers of mice (n) analysed.

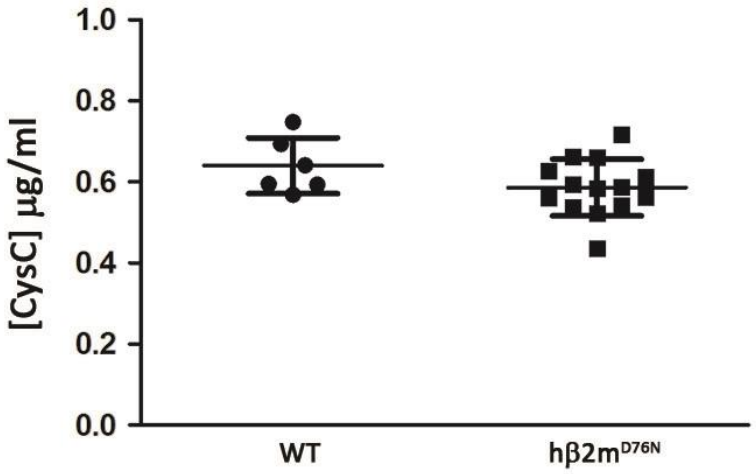


***Figure 4.10: Serum concentration of cystatin C in hβ2m$^{D76N}$ transgenic mice***
*Concentration of serum cystatin C (CysC) in 8-11 months old line 2 hβ2m$^{D76N}$ transgenic mice (n=14) and age-matched non-transgenic controls (WT, n=6) were determined by ELISA and analysed as mean ± SD for number (n) of mice by Mann-Whitney two-tailed test. No significant difference was found between the two groups showing no kidney impairment in hβ2m$^{D76N}$ transgenic mice.*

## 4.2.5 Amyloid fibril-induced amyloid deposition

Although no spontaneous Aβ2m amyloid deposition was observed in the hβ2m$^{D76N}$ transgenic mice despite the fact that the mice present much higher concentrations of the β2m$^{D76N}$ in the circulation than is seen in Aβ2m$^{D76N}$ patients, accumulation of β2m in various organs including the liver, spleen, stomach and gut, which are the sites of Aβ2m deposition in the β2m$^{D76N}$ patients, was observed. The β2m deposits may represent non-Congophilic pre-fibrillar aggregates of the amyloidogenic variant, a pre-amyloid stage of an amyloidogenic protein described in amyloidosis patients *(Sousa et al., 2001)*. In the process of amyloid formation, there is always a lag phase between the first appearance of the potentially amyloidogenic protein and the deposition of clinically significant amyloid. In mice, the lag phase can be significantly shortened by administration of an extract of tissue containing

amyloid, called amyloid-enhancing factor (AEF) *(Willerson et al., 1969, Baltz et al., 1986a)*. It has been shown in animals that administration of amyloid enhancing factor (AEF) acts as a seed for fibril formation and accelerates the appearance of amyloid fibrils. An extract of amyloidotic tissue and/or *ex vivo*-isolated or *in vitro*-prepared amyloid fibrils can act as AEF. *(Axelrad et al., 1982, Varga et al., 1986, Snel et al., 1989, Johan et al., 1998, Baltz et al., 1986a)*. To test, whether the β2m deposition could be accelerated which would result in amyloid formation, the mice were seeded with pre-formed Aβ2m$^{D76N}$ amyloid fibrils.

*In vitro*-prepared human Aβ2m$^{D76N}$ amyloid fibrils and *ex vivo*-isolated human Aβ2m$^{D76N}$ amyloid fibrils, both prepared by Dr Patrizia Mangione (Centre for amyloidosis and acute phase proteins, UCL), were used. Human *ex-vivo* Aβ2m$^{D76N}$ fibrils were isolated from spleen of an Aβ2m$^{D76N}$ amyloidosis patient with severe Aβ2m amyloid deposition. The availability of tissue of Aβ2m$^{D76N}$ amyloidosis patient was very limited and thus the amount of extracted fibrils for experimental work was limited. On the other hand, using *in vitro*-prepared Aβ2m$^{D76N}$ fibrils for seeding had the advantage of essentially unlimited availability of the fibrils for experimental induction of amyloidosis.

4 cohorts of amyloid fibril-seeded mice were set up to evaluate the possibility of accelerating amyloid deposition in hβ2m$^{D76N}$ transgenic mice:

***hβ2m$^{D76N}$ Cohort I*** was injected with 0.1 µg of *in vitro*-prepared human Aβ2m$^{D76N}$ amyloid fibrils,

***hβ2m$^{D76N}$ Cohort II*** was injected with 10 µg of *in vitro*-prepared human Aβ2m$^{D76N}$ amyloid fibrils,

***hβ2m$^{D76N}$ Cohort III*** was injected with 100 µg of *in vitro*-prepared human Aβ2m$^{D76N}$ amyloid fibrils,

***hβ2m$^{D76N}$ Cohort IV*** was injected with 10 µg of *ex vivo*-isolated human Aβ2m$^{D76N}$ amyloid fibrils.

Outline of the seeding experiments is shown in Figure 4.11.

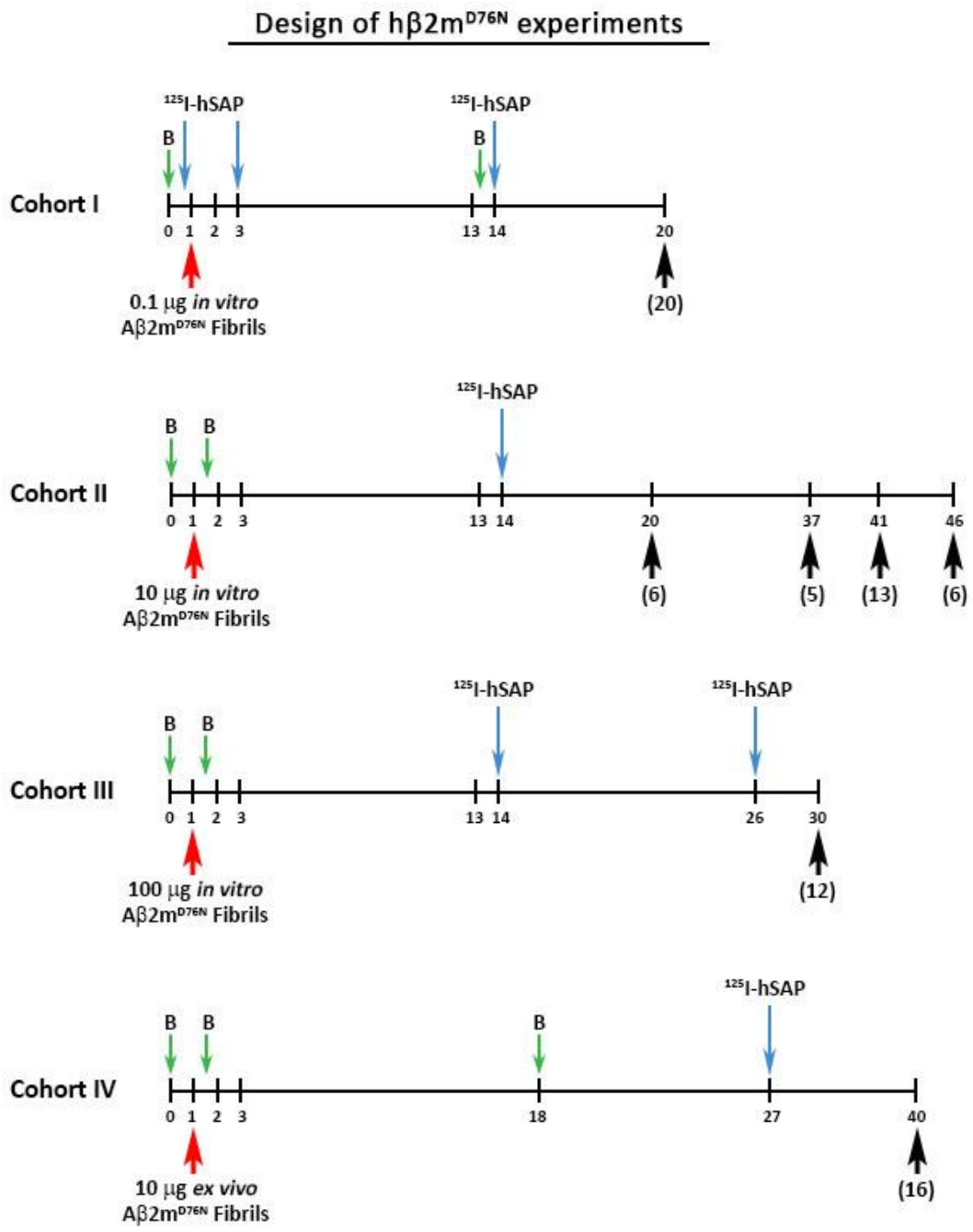


***Figure 4.11: Timeline of seeding experiments of hβ2m$^{D76N}$ transgenic mice***

*4 cohorts of hβ2m$^{D76N}$ transgenic and control mice were set up to prime amyloid deposition by injections with 0.1 µg (I), 10 µg (II) and 100 µg (III) of in vitro-prepared human Aβ2m$^{D76N}$ amyloid fibrils and 10 µg of ex vivo-isolated human Aβ2m$^{D76N}$ amyloid fibrils (IV). The timescale indicates number of weeks. Amyloid fibril injection (red arrow), blood sample collection (green arrow), $^{125}$I-human SAP whole body retention assay (blue arrow) and time-point when seeded animals were taken for analysis (black arrow) with the number of animals killed at each time point shown in brackets are indicated.*

### 4.2.5.1 Outcomes of preliminary seeding experiments

Monitoring an inflammatory response in fibril-seeded mice

Before seeding the experimental hβ2m$^{D76N}$ transgenic animals, different doses of *in vitro*-prepared human Aβ2m$^{D76N}$ amyloid fibrils were tested in C57Bl/6J mice. The reason for this was to test if any remaining endotoxins of fibrils prepared *in vitro* from *E.coli*-expressed variant β2m would cause an inflammatory response. In the presence of severe inflammation, circulating levels of serum amyloid A protein (SAA), an acute phase plasma protein, rise up to 1000-fold almost immediately and fall down to baseline when inflammation clears. In chronic inflammation, when SAA levels are persistently elevated, the SAA protein can deposit as amyloid causing AA amyloidosis *(Hoffman et al., 1984)*.

SAA levels were monitored prior to fibril injections and at 24 and 72 hours following intravenous injection of 0.2 µg, 2 µg and 20 µg of fibrils in 6 mice for each group. 6 mice injected with PBS only were used as a control group. The baseline level of SAA was < 20 µg/ml in all mice. 24 hours after injections, the SAA levels in PBS group and 0.2 µg group stayed < 20 µg/ml and increased in 2 µg group and 20 µg group reaching 498 ± 274 µg/ml and 1108 ± 348 µg/ml, respectively (mean ± SD, n=6). At 72 hours, acute inflammation diminished with SAA production regressed back to its normal level <20 µg/ml in all four groups (Figure 4.12). This result confirmed that administration of the fibrils is safe for the animals and that fibril injection did not cause chronic inflammation.

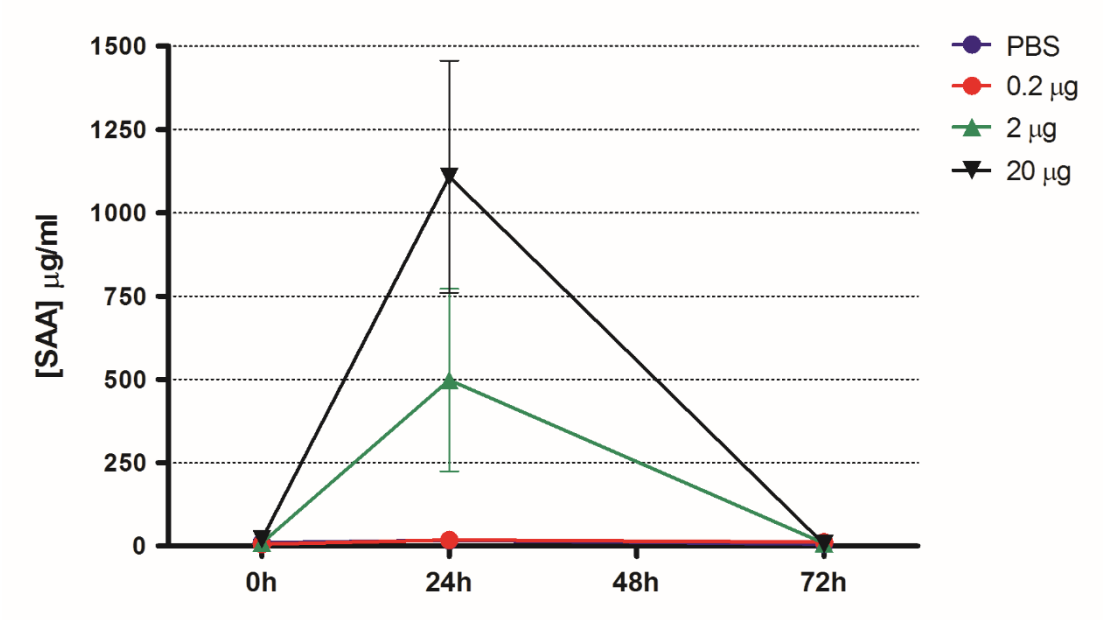


***Figure 4.12: Monitoring inflammatory response after fibril administration***

*Levels of serum SAA were monitored in C57Bl/6J mice to evaluate the inflammatory response following injections of in vitro-prepared human β2m$^{D76N}$ amyloid fibrils (0.2 µg, 2 µg, 20 µg) and PBS as a vehicle. Each group consisted of 6 mice. Blood samples were collected prior to the injection and 24 and 72 hours after the injection. Baseline serum SAA level was <20 µg/ml for each mouse. Acute inflammatory response was detected at 24 hours when > 2 µg of fibrils was administered but the SAA levels fell back to normal levels by 72 hours. The values are shown as mean ± SD (n=6).*

---

Evaluation of the seeding method

To evaluate the persistence of injected amyloid fibrils within the organism, 2 β2m-KO mice injected with 10 µg of *in vitro*-prepared human Aβ2m$^{D76N}$ amyloid fibrils and the mice were killed 72 hours after the seeding injections. At this time-point, Congo red positive stained material exhibiting green birefringence within liver, kidney, spleen, heart, lung and gut was not detected in the tissue sections. This result confirmed that any Congo red positive stained material exhibiting green birefringence in the experimental mice must be newly deposited material.

### 4.2.5.2 Monitoring amyloid deposition in vivo

SAP, a normal plasma protein, binds avidly to all amyloid of human systemic amyloidoses and becomes concentrated at the sites of amyloid deposition. The fact that there is constant equilibrium between the circulating and the amyloid-bound SAP and that the amount of amyloid-bound SAP correlates with the quantity of amyloid present in the tissues *(Baltz et al., 1986b)* let to a development of a specific and quantitative *in vivo* tracing method for systemic amyloid deposition in mice and humans *(Hawkins et al., 1988, Hawkins et al., 1990a)*. This clinical method uses intravenously administered radiolabelled $^{125}$I-human SAP ($^{125}$I-hSAP) which is distributed between the plasma and the amyloid deposits. $^{125}$I-hSAP which retains in the body bound to amyloid then enables screening of the amyloid burden in amyloidosis patients. In mice, whole body retention of intravenously administered radiolabelled $^{125}$I-hSAP in the whole body of a live animal enables to evaluate the amyloid laden in amyloidotic mice *in vivo* and can be repeated.

The injections and counts of radiolabelled material were performed by Dr Stephan Ellmerich (Centre for amyloidosis and acute phase proteins, UCL). The baseline level of $^{125}$I-hSAP retention 48 hours after injection of the radiolabelled tracer in untreated control mice was <10 %. Throughout the experiments, no change in $^{125}$I-hSAP retention was observed in any experimental groups suggesting that the mice were not heavily amyloidotic. However, the limiting sensitivity of the whole body count does not reveal the presence of small amounts of amyloid within the tissue.

### 4.2.5.3 hβ2m$^{D76N}$ Cohort I

3 – 6 months old mice were bled and tested for whole body $^{125}$I-hSAP retention prior to i.v. injection of 0.1 µg of *in vitro*-prepared human Aβ2m$^{D76N}$ amyloid fibrils. 9 hβ2m$^{D76N}$ transgenic mice on mouse β2m wild-type background (T/WT) and 3 non-transgenic controls (WT) were seeded, 5 T/WT mice and 3 non-transgenic mice were injected with vehicle only. All mice were

analysed with $^{125}$I-hSAP retention 3 and 14 weeks after fibrils administration with no animals showing amyloid deposition. The analysis of SAA concentration in the serum of the cohort I mice prior and 13 weeks after the fibril administration confirmed no chronic inflammation in the mice, with the SAA levels 26.6 ± 40.7 µg/ml (n=20) and 8.7± 10.0 µg/ml (n=20), respectively. 19 weeks after fibril injections, all mice (12 seeded, 8 non-seeded) were killed and tissues were collected for histological analysis. The genotypes and the lines of experimental mice, the tissues analysed and the outcome of the analysis is shown in Table 4.4. Congo red stained sections of wax embedded tissue were negative for presence of amyloid in all mice.

| **Cohort I** | **0.1 µg *in vitro* fibrils** | | | | **Non-seeded** | |
|---|---|---|---|---|---|---|
| | **Line 2 T/WT** | **Line 4 T/WT** | **Line 11 T/WT** | **Controls -ve/WT** | **Line 2 T/WT** | **Line 11 T/WT** |
| Liver | 0/4 | - | 0/5 | 0/3 | 0/3 | 0/2 |
| Kidney | 0/4 | - | 0/5 | 0/3 | 0/3 | 0/2 |
| Spleen | 0/4 | - | 0/5 | 0/3 | 0/3 | 0/2 |
| Heart | 0/4 | - | 0/5 | 0/3 | 0/3 | 0/2 |
| Lung | 0/4 | - | 0/5 | 0/3 | 0/3 | 0/2 |
| Salivary gland | 0/4 | - | 0/5 | 0/3 | 0/3 | 0/2 |
| Adrenal | 0/4 | - | 0/5 | 0/3 | 0/3 | 0/2 |
| Sciatic nerve | 0/4 | - | 0/5 | 0/3 | 0/3 | 0/2 |
| Gut | 0/4 | - | 0/5 | 0/3 | 0/3 | 0/2 |
| Stomach | 0/4 | - | 0/5 | 0/3 | 0/3 | 0/2 |
| Muscle | 0/4 | - | 0/5 | 0/3 | 0/3 | 0/2 |
| Fat | 0/4 | - | 0/5 | 0/3 | 0/3 | 0/2 |
| Skin | 0/4 | - | 0/5 | 0/3 | 0/3 | 0/2 |

***Table 4.4: Cohort I – lack of induction of amyloid deposition in seeded hβ2m$^{D76N}$ transgenic mice***

*Summary of tissue analysed by Congo red in hβ2m$^{D76N}$ transgenic mice on mouse β2m wild-type background (T/WT) seeded with 0.1 µg of in vitro-prepared human Aβ2m$^{D76N}$ amyloid fibrils. 4 transgenic mice were from line 2 and 5 transgenic mice were from line 11. 3 seeded non-transgenic littermates (-ve/WT) and 5 non-seeded age-matched transgenic mice injected with vehicle only were also analysed at the same time as controls. The samples are scored as number of mice with amyloid / number of mice analysed for each tissue.*

### 4.2.5.4 hβ2m$^{D76N}$ Cohort II

The second cohort consisted of 40 mice 2 – 5 months old at the start of the experiment. 20 hβ2m$^{D76N}$ transgenic mice on mouse β2m-KO background (T/KO) and 10 β2m-KO controls were injected with 10 µg of *in vitro*-prepared human Aβ2m$^{D76N}$ amyloid fibrils. 8 T/KO mice and 2 β2m-KO mice were also followed as non-seeded controls. All mice were bled prior to and 72 hours after fibril injection to monitor serum SAA concentration as an inflammation marker. The analysis of SAA concentration in the serum confirmed no prolonged inflammatory response after the injections, with SAA level 31.8 ± 39.5 µg/ml (n=38) prior to, and 22.1 ± 31.9 µg/ml (n=30) 72 hours after fibril injections. 12 weeks after fibril injections, all remaining mice were screened for whole body $^{125}$I-hSAP retention showing background levels of retention only.

Amyloid deposition was examined by analysing mice at 19 weeks (4 seeded T/KO and 2 seeded β2m-KO mice), 36 weeks (5 seeded T/KO mice and 3 T/KO and 2 β2m-KO non-seeded controls), 40 weeks (8 T/KO and 5 β2m-KO seeded mice, 3 T/KO and 2 β2m-KO non-seeded controls) and 46 weeks (3 T/KO and 3 β2m-KO seeded mice, 2 T/KO non-seeded controls) after fibril administration. Liver, kidney, spleen, heart, lung, salivary gland, tongue, adrenal, stomach, gut, sciatic nerve, skeletal muscle, skin and fat were fixed and embedded in wax blocks. No amyloid deposition was detected by Congo red staining in any tissues in all mice. The genotypes and the lines of experimental mice, the tissues analysed and the outcome of the analysis is shown in Table 4.5.

| Cohort II | 10 µg *in vitro* fibrils | | | | Non-seeded | |
|---|---|---|---|---|---|---|
| | Line 2 T/KO | Line 4 T/KO | Line 11 T/KO | Controls -ve/KO | Line 4 T/KO | Line 11 T/KO |
| Liver | - | 0/10 | 0/10 | 0/10 | 0/3 | 0/5 |
| Kidney | - | 0/10 | 0/10 | 0/10 | 0/3 | 0/5 |
| Spleen | - | 0/10 | 0/10 | 0/10 | 0/3 | 0/5 |
| Heart | - | 0/10 | 0/10 | 0/10 | 0/3 | 0/5 |
| Lung | - | 0/10 | 0/10 | 0/10 | 0/3 | 0/5 |
| Salivary gland | - | 0/10 | 0/10 | 0/10 | 0/3 | 0/5 |
| Adrenal | - | 0/10 | 0/10 | 0/10 | 0/3 | 0/5 |
| Sciatic nerve | - | 0/10 | 0/10 | 0/10 | 0/3 | 0/5 |
| Gut | - | 0/10 | 0/10 | 0/10 | 0/3 | 0/5 |
| Stomach | - | 0/10 | 0/10 | 0/10 | 0/3 | 0/5 |
| Muscle | - | 0/10 | 0/10 | 0/10 | 0/3 | 0/5 |
| Fat | - | 0/10 | 0/10 | 0/10 | 0/3 | 0/5 |
| Skin | - | 0/10 | 0/10 | 0/10 | 0/3 | 0/5 |
| Tongue | - | 0/10 | 0/10 | 0/10 | 0/3 | 0/5 |
| Eye | - | 0/10 | 0/10 | 0/10 | 0/3 | 0/5 |
| Optic nerve | - | 0/10 | 0/10 | 0/10 | 0/3 | 0/5 |
| Lacrymal gland | - | 0/10 | 0/10 | 0/10 | 0/3 | 0/5 |

***Table 4.5: Cohort II – lack of induction of amyloid deposition in seeded hβ2m$^{D76N}$ transgenic mice***

*Summary of tissue analysed by Congo red in hβ2m$^{D76N}$ transgenic mice on β2m-KO background (T/KO) seeded with 10 µg of in vitro-prepared human Aβ2m$^{D76N}$ amyloid fibrils. 10 transgenic mice of line 4, 10 transgenic mice of line 11 and 10 non-transgenic littermates (-ve/KO) were seeded and 8 age-matched transgenics were non-seeded. The samples are scored as number of mice with amyloid / number of mice analysed for each tissue.*

### 4.2.5.5 hβ2m$^{D76N}$ Cohort III

6 hβ2m$^{D76N}$ T/KO mice from line 2 and 6 β2m-KO mice were injected with 100 µg of *in vitro*-prepared human Aβ2m$^{D76N}$ amyloid fibrils at 4 months of age. Serum SAA levels 72 hours after fibril injection (56.6 ± 60.7 µg/ml, n=12) did not differ from concentrations prior to injections (49.8 ± 54.7 µg/ml, n=12), confirming no prolonged inflammation caused by the fibril administration. Whole body $^{125}$I-hSAP retention was performed at weeks 13 and 26 after fibril seeding with background levels of retention in all mice. All mice were terminated 29 weeks after seeding. Amyloid deposition was examined in liver, heart, kidney, spleen, colon and sciatic nerve embedded into wax blocks and stained with Congo red. No amyloid deposits were observed in any tissue analysed (Table 4.6).

| **Cohort III** | **100 µg *in vitro* fibrils** | | | |
|---|---|---|---|---|
| | **Line 2 T/KO** | **Line 4 T/KO** | **Line 11 T/KO** | **Controls -ve/KO** |
| Liver | 0/6 | - | - | 0/6 |
| Kidney | 0/6 | - | - | 0/6 |
| Spleen | 0/6 | - | - | 0/6 |
| Heart | 0/6 | - | - | 0/6 |
| Gut | 0/6 | - | - | 0/6 |
| Sciatic nerve | 0/6 | - | - | 0/6 |

***Table 4.6: Cohort III – lack of induction of amyloid deposition in seeded hβ2m$^{D76N}$ transgenic mice***

*Summary of tissue analysed by Congo red in line 2 hβ2m$^{D76N}$ transgenic mice on mouse β2m-KO background (T/KO) seeded with 100 µg of in vitro-prepared human Aβ2m$^{D76N}$ amyloid fibrils. The samples are scored as number of mice with amyloid / number of mice analysed for each tissue.*

### 4.2.5.6 hβ2m$^{D76N}$ Cohort IV

In the fourth cohort, 10 hβ2m$^{D76N}$ T/KO mice and 6 β2m-KO mice were seeded with 10 µg of *ex vivo*-isolated human Aβ2m$^{D76N}$ amyloid fibrils at 2 – 5 months of age. 4 age-matched hβ2m$^{D76N}$ T/KO were used as non-seeded controls. SAA concentrations of the experimental mice were 26.0 ± 46.8 µg/ml (n=18) prior to and 35.3 ± 53.6 µg/ml (n=18) 72-hours after the fibril injection, showing no significant difference between the injected and non-injected mice and confirming no prolonged inflammation after the seeding. 26 weeks after fibril injections, $^{125}$I-hSAP retention was performed. At 48 h after the tracer administration, the retention was at base-line level <10 % in all mice suggesting that there were no considerable amounts of amyloid in the mice. 39 weeks after seeding, all mice were analysed. Liver, kidney, spleen, heart, lung, tongue, salivary gland, adrenal, sciatic nerve, gut, stomach, muscle, fat and skin were collected into fix. Liver, kidney and spleen were also snap-frozen in liquid nitrogen and stored at -80 $^{o}$C. Congo red stained sections of wax embedded tissues did not reveal any amyloid in any mice (Figure 4.13). The genotypes and the lines of experimental mice, the tissues analysed and the outcome of the analysis is shown in Table 4.7.

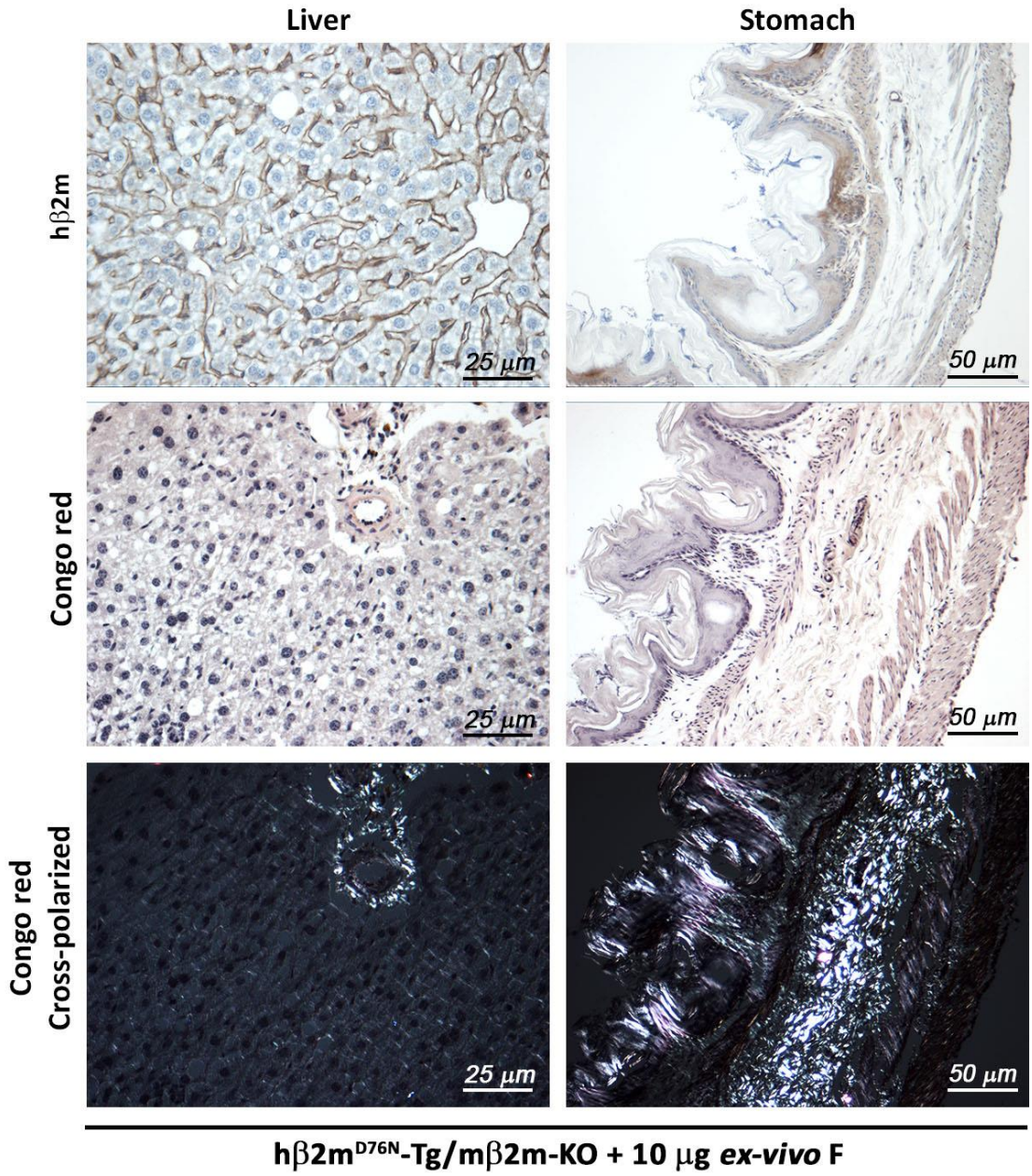


***Figure 4.13: Negative Congo red staining of tissue of Cohort IV seeded mice***

*hβ2m$^{D76N}$ transgenic mice on mβ2m-KO background were seeded with 10 µg of ex vivo-isolated human Aβ2m$^{D76N}$ amyloid fibrils at 2 – 5 months of age (Cohort IV) and taken for analysis 9 months after seeding. Staining of wax embedded tissue with Dako polyclonal anti-hβ2m antibody confirmed substantial amount of the hβ2m variant within the tissue. However, Congo red staining did not show any green birefringence that would indicate amyloid deposits under polarized light. Only white birefringence of collagen and connective tissue reacting with Congo red was detected under polarized light around blood vessel and in the submucosa of stomach.*

| Cohort IV | 10 µg *ex vivo* fibrils | | | | Non-seeded | |
|---|---|---|---|---|---|---|
| | Line 2 T/KO | Line 4 T/KO | Line 11 T/KO | Controls -ve/KO | Line 2 T/KO | Line 4 T/KO |
| Liver | 0/7 | 0/3 | - | 0/6 | 0/3 | 0/2 |
| Kidney | 0/7 | 0/3 | - | 0/6 | 0/3 | 0/2 |
| Spleen | 0/7 | 0/3 | - | 0/6 | 0/3 | 0/2 |
| Heart | 0/7 | 0/3 | - | 0/6 | 0/3 | 0/2 |
| Lung | 0/7 | 0/3 | - | 0/6 | 0/3 | 0/2 |
| Salivary gland | 0/7 | 0/3 | - | 0/6 | 0/3 | 0/2 |
| Adrenal | 0/7 | 0/3 | - | 0/6 | 0/3 | 0/2 |
| Sciatic nerve | 0/7 | 0/3 | - | 0/6 | 0/3 | 0/2 |
| Gut | 0/7 | 0/3 | - | 0/6 | 0/3 | 0/2 |
| Stomach | 0/7 | 0/3 | - | 0/6 | 0/3 | 0/2 |
| Muscle | 0/7 | 0/3 | - | 0/6 | 0/3 | 0/2 |
| Fat | 0/7 | 0/3 | - | 0/6 | 0/3 | 0/2 |
| Skin | 0/7 | 0/3 | - | 0/6 | 0/3 | 0/2 |
| Tongue | 0/7 | 0/3 | - | 0/6 | 0/3 | 0/2 |

***Table 4.7: Cohort IV – lack of induction of amyloid deposition in seeded hβ2m$^{D76N}$ transgenic mice***

*Summary of tissue analysed by Congo red in Cohort IV of hβ2m$^{D76N}$ transgenic mice on β2m-KO background (T/KO) seeded with 10 µg of ex vivo-isolated human Aβ2m$^{D76N}$ amyloid fibrils. 7 transgenic mice of line 2; 3 transgenic mice of line 4 and 6 non-transgenic littermates (-ve/KO) were seeded. 5 age-matched transgenic littermates were analysed as non-seeded controls. The samples are scored as number of mice with amyloid / number of mice analysed for each tissue.*

### 4.2.6 Search for amyloid in tissue homogenate

Despite high concentrations of the amyloidogenic variant β2m circulating in the blood and despite noticeable age-related accumulation of the variant in some tissue of the hβ2m$^{D76N}$ transgenic mice, no amyloid was detected by Congo red staining in the tissue sections of aged and amyloid-fibril seeded mice. However, the signal provided by Congo red bound to disperse amyloid deposits may not be visible by polarized light microscopy. To test whether any insoluble β2m could be detected in the tissue of the transgenic mice, suggesting the presence of insoluble fibrillar material within the tissue, liver and spleen of hβ2m$^{D76N}$ transgenic mice were homogenised and the homogenate was centrifuged to concentrate the insoluble material. The pellet was then washed four times to remove any soluble material and run on an SDS-PAGE gel and subjected to Western blot analysis with anti-hβ2m antibody 14H3. Two 10 months old non-seeded hβ2m$^{D76N}$ transgenic mice on β2m-KO background (T/KO) from the high-expressing line 2 were compared with two age-matched T/KO mice seeded with 10 µg of *ex vivo*-isolated human Aβ2m$^{D76N}$ amyloid fibrils. Soluble hβ2m was detected in the tissue homogenate and in the supernatant collected after pelleting the homogenised material in the transgenic mice, as expected. No hβ2m was detected in the last wash aspirated from the pellet confirming removal of all soluble material from the pellet. However, no insoluble β2m was detected in the pellet of the tissue suggesting absence of β2m amyloid fibrils in the tissue. No β2m signal was detected in liver and spleen homogenates of β2m-KO mice that were used as negative controls (Figure 4.14).

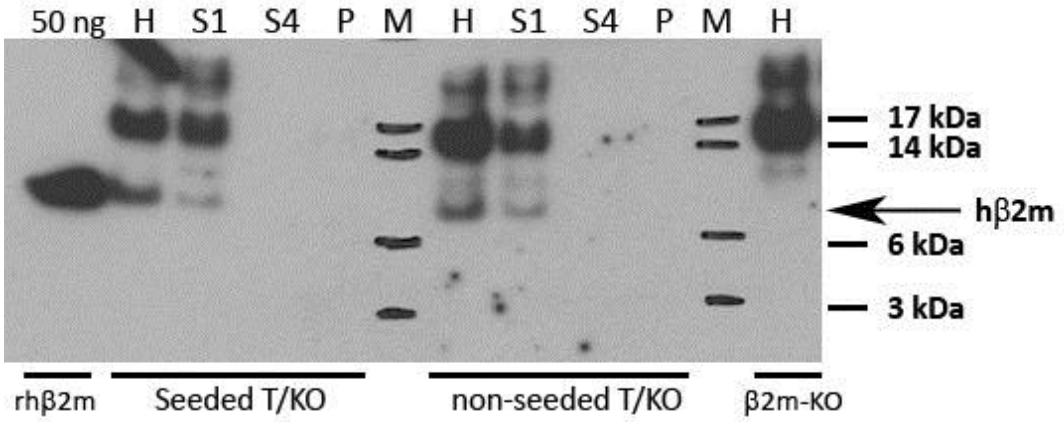


***Figure 4.14: hβ2m in the liver homogenate of hβ2m$^{D76N}$ transgenic mice***

*Liver tissue of 10 months old β2m-KO mouse, 10 months old non-seeded line 2 hβ2m$^{D76N}$ transgenic mouse on β2m-KO background (non-seeded T/KO) and 10 months old line 2 hβ2m$^{D76N}$ transgenic mouse on β2m-KO background seeded with 10 µg of ex-vivo isolated Ahβ2m$^{D76N}$ amyloid fibrils (seeded T/KO) were homogenised and the homogenate (H), supernatant (S1) aspirated from pelleted insoluble material, fourth wash of the pellet (S4) and the pellet (P) were run on an SDS-PAGE gel and probed with anti-hβ2m antibody 14H3. Only soluble hβ2m was detected in the liver homogenates and the supernatants S1 in transgenic mice. No insoluble hβ2m was detected in the pellet of the tissue. No β2m signal was detected in the liver homogenate of a β2m-KO mouse. 50 ng of purified recombinant hβ2m$^{D76N}$ protein (hβ2m, kindly provided by Dr Riccardo Porcari) and a size marker (M) were run alongside the samples.*

### 4.2.7 Native hβ2m in the serum of hβ2m$^{D76N}$ transgenic mice

In humans, β2m protein is released from the cell surface after the dissociation of the MHC I complex into the blood where it circulates as a monomer *(Gagnon et al., 1988)*. However, it has been reported that β2m protein circulates in a complex in mouse plasma *(Natori et al., 1976)* and further it was shown in rats that human β2m protein injected into the animals circulated not only as a free monomer but also complexed with a plasma glycoprotein *(Nguyen-Simonnet et al., 1982)*. In hemodialysis patients, proportion of plasma β2m was found to circulate in a complex with $\alpha_2$-macroglobulin (α2M), whereas no β2m-α2M complexes were observed in the healthy people *(Motomiya et al., 2003)*.

To analyse their native conformations, proteins can be run on an agarose gel in the absence of denaturing and reducing agents. Under the non-reducing and non-denaturing conditions, proteins run in the gel principally according to their native charge. In fact, the native wild-type human β2m protein and the native β2m$^{D76N}$ variant are distinguishable by their different electrophoretic mobilities with the wild-type β2m migrating faster than the variant *(Mangione et al., 2013)*. On a denatured SDS PAGE gel, the β2m$^{D76N}$ variant from the plasma of the transgenic mice ran as a full-length, non-glycosylated human β2m protein. However, the hβ2m$^{D76N}$ transgenic mice did not develop spontaneous or amyloid fibril-seeded amyloidosis. The reason for this could be that the β2m$^{D76N}$ variant does not circulate only as a free monomer but also in a complex which may be protecting the β2m$^{D76N}$ variant from misfolding.

I speculated that if: 1) native and denatured pure hβ2m co-migrate; 2) native and denatured pure hβ2m$^{D76N}$ co-migrate; 3) hβ2m$^{D76N}$ in denatured serum from hβ2m$^{D76N}$ transgenic mouse co-migrates with pure hβ2m$^{D76N}$ and 4) hβ2m$^{D76N}$ in native serum from hβ2m$^{D76N}$ transgenic mouse migrates

differently, this could imply that the β2m$^{D76N}$ variant in the hβ2m$^{D76N}$ transgenic mice circulates in a complex.

Therefore, serum of the high expressing line 2 hβ2m$^{D76N}$ T/KO mouse was denatured in 6 M urea to disrupt any complexes and run alongside the native serum sample of the same mouse on an agarose gel. Purified recombinant human β2m protein and purified recombinant human β2m$^{D76N}$ variant used as controls were also run on the gel in their native form as well as after denaturation in 6 M urea to confirm that the denatured proteins co-migrated with the native proteins for both the wild-type β2m and β2m$^{D76N}$ variant. β2m-KO and C57Bl/6J mouse sera were also treated with 6 M urea and run on the gel in denatured and native form. Native human serum was used a positive control. The gel was then blotted onto a membrane and probed with Dako polyclonal anti-hβ2m antibody which recognises both mouse as well as human β2m.

The native and denatured pure hβ2m$^{D76N}$ variant co-migrated on the gel as did the native and denatured pure hβ2m$^{D76N}$ variant confirming that the denaturation does not interfere with the mobility of the proteins. However, while the hβ2m$^{D76N}$ variant in the denatured serum from hβ2m$^{D76N}$ transgenic mouse co-migrated with the pure monomeric hβ2m$^{D76N}$ variant, the hβ2m$^{D76N}$ variant in the native serum from hβ2m$^{D76N}$ transgenic mouse migrated faster. Similarly in the serum of C57Bl/6J mouse, mouse β2m in the denatured serum was migrating much slower than mouse β2m in the native serum. In native human serum, only a band co-migrating with recombinant non-mutated human β2m was observed. These results are shown in Figure 4.15.

These results suggest that in mice, a β2m-binding component exists in the plasma and the majority of the circulating β2m is bound in a complex. Thus, only a small proportion of the hβ2m$^{D76N}$ variant in the transgenic mice may circulate as a free monomer available to convert into amyloid fibrils.

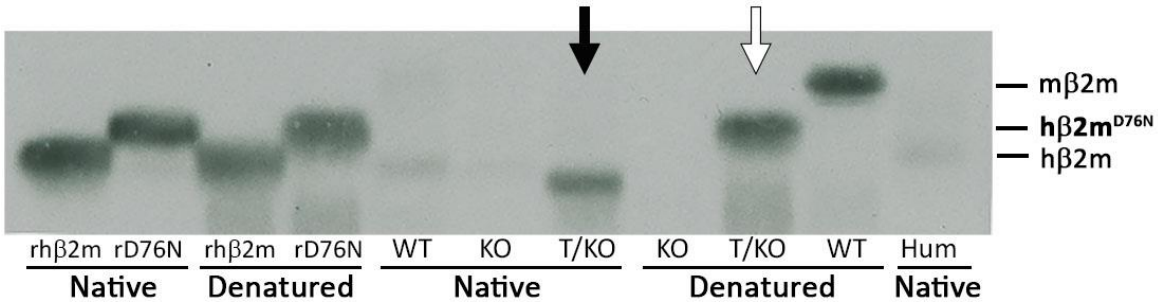


***Figure 4.15: The comparison of β2m in native and denatured serum***

*1 µl of native sera of C57Bl/6J (WT), β2m-KO (KO) and line 2 hβ2m$^{D76N}$ transgenic mouse on β2m-KO background (T/KO, black arrow) mice were run alongside 1 µl of 6 M urea-denatured serum of the same mice on 1% agarose gel and probed with Dako polyclonal anti-hβ2m antibody which recognises both human and mouse β2m. In the denatured serum, only monomeric proteins were detected - monomeric hβ2m$^{D76N}$ variant in the transgenic mouse (white arrow) and monomeric mouse β2m (mβ2m) in the serum of a WT mouse. Native hβ2m$^{D76N}$ and mβ2m from the serum of the transgenic and wild-type mouse, respectively, were migrating faster compared to their denatured equivalents. Native and denatured recombinant wild-type human β2m (rhβ2m) co-migrated as did the native and denatured recombinant hβ2m$^{D76N}$ (rD76N) confirming that the denaturation does not interfere with the protein mobility of the monomers. β2m in native human serum (Hum) co-migrated with recombinant wild-type human β2m (rhβ2m) confirming that β2m exists in human plasma as a monomer. 30 ng of each recombinant protein was loaded per well.*

## 4.3 Discussion

In this project, transgenic mice expressing the highly amyloidogenic D76N variant of β2m protein were generated. Surprisingly, despite the fact that the hβ2m$^{D76N}$ transgenic mice have high concentrations of the amyloidogenic protein exceeding the concentrations seen in Aβ2m$^{D76N}$ amyloidosis patients up to 35-fold, none of the mice developed spontaneous Aβ2m amyloid deposits even at the age of 2 years.

Amyloid fibril formation *in vivo* is a time-dependent process. Normally soluble proteins take decades to convert into clinically recognisable amyloid deposits. In this lag phase, first amyloid fibrils develop, forming the so called “seeds”, which is a process that occurs stochastically *in vivo (Jarrett and Lansbury, 1993, Kelly, 1998)*. The seeds then act as a template for further amyloid deposition. Once amyloid deposition has been initiated, and with continuous production and abundance of the precursor protein, amyloid fibril formation is autocatalytic and the clinical disease is progressing. *In vitro (Jahn et al., 2008)* and in experimental animals *in vivo (Willerson et al., 1969, Snel et al., 1989, Higuchi et al., 1998)* , amyloid deposition can be induced by exogenous seeding with pre-formed amyloid material. *In vitro*-prepared and *ex-vivo* isolated amyloid fibrils as well as crude extract from an amyloidotic tissue which has not been yet fully characterised but the active compound of which are amyloid fibrils, can all serve as AEF *(Axelrad et al., 1982, Baltz et al., 1986a)*. The hβ2m$^{D76N}$ transgenic mice presented here were therefore injected with *in vitro*-prepared and *ex vivo*-isolated Aβ2m$^{D76N}$ amyloid fibrils. However, Aβ2m amyloid deposits detectable by Congo red were not found in the seeded transgenic mice. In a transgenic mouse model expressing wild-type β2m, seeding of the transgenic mice with amyloid fibrils was also not sufficient in priming amyloid deposition *(Zhang et al., 2010)*. However, the concentration of the wild-type human β2m in the plasma of these transgenic mice may have been overestimated, as it was discussed in the previous

chapter, and thus the low concentration of the human β2m may have been the limiting factor in developing amyloid deposits.

In the dialysis related amyloidosis, Aβ2m deposits consist of wild-type human β2m protein and an isoform of the protein lacking the first six N-terminal residues (ΔN6β2m) *(Bellotti et al., 1998)*. *In vitro* experiments have shown that although wild-type hβ2m does not form amyloid fibrils under physiological conditions *(Calabrese and Miranker, 2009, Bellotti et al., 1998)*, ΔN6β2m forms amyloid fibrils and is capable of catalysing assembly of wild-type hβ2m into amyloid-like fibrils at physiological conditions *(Bellotti et al., 1998, Stoppini et al., 2005, Piazza et al., 2006)*. On the other hand, *in vitro* experiments showed that under conditions which are favourable for amyloid fibril formation of hβ2m, mβ2m does not form amyloid fibrils *(Ivanova et al., 2004, Eichner et al., 2011)*. Moreover, the aggregation potential of ΔN6β2m and the wild-type hβ2m was abolished in the presence of mouse β2m in the solution *(Eichner et al., 2011, Karamanos et al., 2014)*. To avoid the possible inhibiting effect of mβ2m on Aβ2m amyloid fibril formation, the hβ2m$^{D76N}$ transgenic mice were crossed with mouse β2m-KO mice to produce hβ2m$^{D76N}$ transgenics lacking the endogenous β2m. However, despite the lack of the murine β2m, spontaneous and amyloid-fibril seeded amyloid deposition was still not detected in the transgenic mice and thus the effect of the mouse β2m on amyloid-fibril formation could not be evaluated.

In dialysis-related amyloidosis, poor correlation between the plasma β2m concentration and the extent of Aβ2m amyloidosis suggests that additional factors are responsible for the initiation of β2m aggregation *(Gejyo et al., 1986a)*. These observations are consistent with *in vitro* studies that have shown that production of wild-type human β2m amyloid-like fibrils in the absence of detergents, solvents or other additional factors, under physiological conditions have not been achieved *(Myers et al., 2006a)*. *In vivo* models, in which human β2m was successfully expressed have been unable to demonstrate the deposition of typical Aβ2m amyloid fibrils *(Zhang et al., 2010, Diomede et al., 2012)*. Fukunishi et al. have reported a rat model

expressing human β2m, in which only rats with collagen-induced arthritis, but not untreated rats, developed some amyloid in the knee joints. However, the amyloid deposits were not typed and thus not known whether the rats developed Aβ2m amyloid. Also, the number of animals that developed amyloid was not specified and the amyloid deposition was not further investigated *(Fukunishi et al., 2007)*. On the other hand, *in vitro* biochemical studies showed that the human β2m$^{D76N}$ variant is highly amyloidogenic. The rapid fibrillogenesis occurs within a few hours in physiological buffer when enhanced by fluid agitation and exposure to a hydrophobic surface. In contrast, fibrillogenesis of the wild-type human β2m is extremely slow under the same conditions, being minimal or absent after 100 days of incubation *(Mangione et al., 2013)*. The fluid agitation relevance is explained by the similarity with the extracellular environment, a site of amyloid deposition in systemic amyloidosis, where interstitial fluid flows over the extensive surfaces of the fibrous network of elastin and collagen. The fibrous network provides these hydrophobic surfaces promoting unfolding of globular proteins. Indeed, elastin has been shown to promote amyloid fibrillogenesis of β2m$^{D76N}$ variant in solution *(Mangione et al., 2013)*. Moreover, the β2m$^{D76N}$ variant is a much more potent promoter of amyloid fibril formation by wild-type human β2m when compared to ΔN6β2m *(Mangione et al., 2013, Eichner et al., 2011)*. However, only full-length human β2m$^{D76N}$ variant is present in the amyloid deposits of hereditary Aβ2m$^{D76N}$ amyloidosis patients, with wild-type human β2m and ΔN6β2m being absent *(Valleix et al., 2012)*.

The failure of the hβ2m$^{D76N}$ transgenic mice to develop spontaneous and amyloid fibril-seeded Aβ2m amyloidosis despite the aggressive propensity of the β2m$^{D76N}$ variant to form amyloid, led to a question whether the human β2m$^{D76N}$ variant circulates in the system as a free monomer or whether it may be bound in a complex which would prevent the availability of the free β2m to form amyloid fibrils in the extracellular spaces. Indeed, electrophoresis of native non-denatured serum of hβ2m$^{D76N}$ transgenic mice revealed that the human β2m does not circulate as a free monomer in the serum of the mice.

Molecular chaperones are proteins involved in protein folding, unfolding and remodelling. They assist newly synthesized proteins to achieve their native fold, mediate assembly and disassembly of complexes and protect proteins from aggregation *(Bukau et al., 2006, Doyle et al., 2013)*. Extracellular chaperones and their function to contribute to proteome stability in the biological fluids by capturing and leading misfolded proteins for lysosomal proteolysis via endocytosis, have been recently identified – namely $\alpha_2$-macroglobulin (α2M) *(French et al., 2008)*, haptoglobin *(Yerbury et al., 2005)* and clusterin *(Humphreys et al., 1999)*.

α2M is best known for its ability to trap a range of proteases via a cage-like quaternary structure *(Sottrup-Jensen, 1989)*. It has been shown that α2M can form complexes with misfolded proteins and promote their removal from the extracellular spaces and therefore protect against pathogenic misfolded proteins *(Narita et al., 1997)*. α2M was identified as a potent chaperone of β2m – *in vitro* experiments showed that α2M binds β2m *(Gouin-Charnet et al., 1997, Gouin-Charnet et al., 2000)* and α2M-β2m complexes have been found *in vivo* in the serum of DRA patients *(Motomiya et al., 2003)*. Preliminary experiments investigating whether β2m circulates in the serum of hβ2m$^{D76N}$ transgenic mice bound to α2M suggest that α2M may not be the β2m-binding partner.

Another extracellular chaperon identified to bind β2m is haptoglobin *(Sultan et al., 2013)*, serum glycoprotein with main function to bind free haemoglobin. It has been shown *in vitro* that haptoglobin interacts with β2m oligomers, preventing Aβ2m amyloid fibril formation, however interaction with monomeric β2m was not observed *(Sultan et al., 2013)*. Characterisation of the chaperone activity of haptoglobin *in vivo* is very limited. Clusterin is also present in all extracellular fluids and has diverse biological functions. In terms of amyloid, clusterin has been most studied in association with Alzheimer's disease (AD) *(Boggs et al., 1996, Lacour et al., 2016, Calero et al., 2012)*. It has been shown that clusterin, similarly to haptoglobin, does not bind to native or fibrillar proteins but interacts with oligomeric species and plays a

role in the control of extracellular protein misfolding *(Kumita et al., 2007, Yerbury et al., 2007)*. No interactions of clusterin and β2m have been described. Other molecular chaperones may be involved in binding misfolded β2m in biological fluids and prevent its deposition in tissue as amyloid.

In the serum of wild-type mice, native endogenous β2m was also observed to circulate in a complex whereas in native human serum, only monomeric β2m was detected. It is therefore possible that a murine specific molecule may chaperone β2m in the mouse serum. Nevertheless, if β2m has a binding partner in mouse serum, its identification would give a possibility to cross the $h\beta2m^{D76N}$ transgenic mice with mice in which the gene coding for the specific protein has been knocked out. In such mice, the D76N variant β2m might be present in the serum as a monomer without the protection of its binding component, available to form amyloid fibrils in the extracellular spaces of the mice.

# 5 Generation and establishment of hTTR$^{S52P}$ transgenic mice

## 5.1 Introduction

Transthyretin (TTR) is one of the proteins that can misfold from its normal globular configuration and convert into insoluble amyloid fibrils. The main source of plasma TTR is the liver *(Holmgren et al., 1991)*, although TTR expression has been identified in the choroid plexus of the brain *(Dickson et al., 1985)* and retina *(Cavallaro et al., 1990)*. In blood, TTR circulates as a homotetramer where it functions as a transporter of thyroid hormone thyroxine ($T_4$) *(Woeber and Ingbar, 1968)* and retinol via retinol-binding protein (RBP) *(Kanai et al., 1968)*. Besides its transport functions, TTR is a protease *(Liz et al., 2004)*. The concentration of TTR in plasma of healthy humans is 170-400 µg/ml *(Smith and Goodman, 1971, Maetzler et al., 2012)*.

In pathological conditions, TTR is associated with wild-type ATTR amyloidosis, previously referred to as senile systemic amyloidosis, and with hereditary systemic ATTR amyloidosis caused by a mutation in the TTR gene. Wild-type ATTR amyloidosis is an under-recognised condition in the elderly that involves accumulation of the TTR as amyloid affecting predominantly the heart. Hereditary systemic ATTR amyloidosis presents with familial amyloid polyneuropathy and/or familial amyloid cardiomyopathy, in which the TTR amyloid fibrils are mainly deposited in the peripheral and autonomic nervous system and the heart, respectively. Over 100 TTR variants have been identified to date, with >80 of these variants causing amyloidosis (www.amyloidosismutations.com/attr.html).

Several transgenic mice carrying a human TTR gene, including wild-type TTR and V30M and L55P variants, have been generated to study ATTR amyloidosis. TTR$^{V30M}$ is one of the most common variants in Europe *(Ando et al., 2013)* associated with familial amyloid polyneuropathy affecting peripheral and autonomic nerves as the main symptom, with progression of the disease

at a later stage into cardiac amyloidosis. $TTR^{L55P}$ variant is an aggressively amyloidogenic variant with an early onset of neurological and cardiac involvement *(Jacobson et al., 1992)*.

The first transgenic mice carrying human TTR were generated shortly after the discovery that V30M variant TTR is the amyloidogenic protein responsible for familial amyloid polyneuropathy. In 1986, Sasaki et al. generated transgenic mice expressing human $TTR^{V30M}$. In an attempt to maximise the efficiency of the transgene expression, the human TTR gene was fused with a mouse metallothionein-I (MT) promoter, a promoter that contains sequence elements responsible for heavy metal inductions. Upon addition of $ZnSO_4$ into drinking water, the transgenic mice expressed about 10 µg/ml human TTR in the serum, levels more than an order of magnitude lower than in humans *(Sasaki et al., 1986)*. Amyloid deposition in these mice was not examined. A similar approach of MT-$hTTR^{V30M}$ transgene construct was conducted by Yi et al. The generated mice expressed 10-50 µg/ml of plasma human TTR and spontaneous amyloid deposition was observed from 12 months of age in gastrointestinal tract and kidneys with later deposition in heart, thyroid and possibly other organs in some animals *(Yi et al., 1991)*. However, neither number of mice nor the consistency of amyloid deposition was reported. Moreover, these transgenic mice were never reported again as a model of ATTR amyloidosis.

In order to examine the possibility of ATTR amyloid deposits in the nervous system, a different approach of generating human TTR transgenic mice was tested. To maintain the physiological sites of TTR expression, the TTR gene's own promoter and sequences enhancing expression of the TTR were investigated by Nagata et al. (1995). Two different lengths of sequences upstream of the transcription initiation site of the human $TTR^{V30M}$ gene, 0.6 kb and 6.0 kb, were compared to identify the position of regulatory elements upstream of the TTR gene. The 6.0-$hTTR^{V30M}$ gene showed appropriate tissue specific expression in the liver, choroid plexus and yolk sac, whereas the 0.6-$hTTR^{V30M}$ gene was not expressed in the choroid plexus. The liver

expression and plasma TTR concentration in mice carrying the 0.6-hTTR$^{V30M}$ gene were much lower than in mice carrying the 6.0-hTTR$^{V30M}$ transgene which had ~150 µg/ml of hTTR in the plasma *(Nagata et al., 1995)*. ATTR amyloid deposition was reported in some transgenic mice for both constructs in the gastrointestinal tract, kidney, heart and skin. Amyloid was also observed in liver and spleen in some animals however the amyloid protein was identified as SAA *(Takaoka et al., 1997)*. Interestingly, when these transgenic mice were moved to a different animal facility with a different health status, the mice did not develop amyloid deposits *(Sousa et al., 2002)* suggesting that, at least in part, the amyloid observed was AA amyloid as a consequence of inflammation.

Another two models of human TTR transgenic mice were simultaneously generated and compared, in which the mice carried 19.2 kb of genomic DNA of wild-type human TTR or of human TTR$^{L55P}$ *(Teng et al., 2001)*. Both strains showed transgene expression in tissues similar to humans. Mice carrying the L55P variant had low serum concentration of the human TTR (10-30 µg/ml) and no amyloid deposits were observed in these mice even at the age of 2.5 years. On the other hand, mice carrying 100 copies of the wild-type human TTR gene had concentration of the human TTR 100-fold higher than the mice expressing the L55P variant. Amyloid deposits were observed in the heart of 20 % of the transgenic mice at 18 months, increasing to 50 % at two years *(Teng et al., 2001)*. TTR immunoreactivity was also observed in the hearts but the data presented did not show co-localisation with the amyloid deposits. The hearts were negative for SAA immunoreactivity but the possibility of ApoAII amyloid was not addressed. Spontaneous ApoAII amyloidosis (including in the heart) is common in old mice *(Higuchi et al., 1991b, Higuchi et al., 1991a)*. Even if the amyloid in these mice was ATTR amyloid, the slow progression of the amyloid deposition in this model is not sufficiently consistent and robust for the use of the mice as a model of the disease.

L55P variant was also used by Sousa et al. to examine the cytotoxic activity of TTR deposits. The transgenic mice obtained by microinjection of TTR$^{L55P}$

cDNA under the control of sheep methallothionein promoter had plasma TTR concentration similar to humans (50-200 µg/ml). TTR deposition in the tissue of the transgenic mice was detected and progressed with age, however these deposits were non-Congophilic and TTR amyloid was not detected in these mice up to 2 years of age *(Sousa et al., 2002)*. Non-Congophilic non-fibrillar deposits of TTR in nerves were detected in patients in early stages of ATTR amyloidosis *(Sousa et al., 2001)*. Observations that non-Congophilic TTR deposits in the $TTR^{L55P}$ transgenic mice had a cytotoxic effect in sites related to TTR deposition in the $TTR^{L55P}$ transgenic mice *(Sousa et al., 2002)* suggest that pre-fibrillar deposits have pathological effect in the disease development.

Although these models have provided valuable insight into TTR gene expression, TTR protein interactions and TTR deposition, none of them have been able to provide a consistent model of ATTR amyloidosis.

In 1993, an extremely aggressive amyloidosis with very early onset caused by $TTR^{S52P}$ variant was reported in the UK *(Booth et al., 1993)*. This mutation is characterised by widespread ATTR amyloid deposits by the third decade with fatal cardiac involvement within just a few years *(Mangione et al., 2014, Gonzalez-Duarte et al., 2013)*. Recently, the S52P variant has been extensively studied *in vitro* and the biochemical analysis of the variant have provided new evidence that may play an important role in pathogenesis of ATTR amyloidosis. Cardiac TTR amyloid typically contains fragmented TTR, with the fragments being mostly cleaved between amino acids at the position 48-49 *(Bergstrom et al., 2005, Ihse et al., 2013)*. *In vitro* studies looking into proteolytic cleavage of TTR variants associated with cardiac amyloidosis showed that S52P variant is much more susceptible to cleavage in comparison with wild-type TTR, $TTR^{V122I}$ and $TTR^{L55P}$ *(Mangione et al., 2014)*. While *in vitr*o fibrillogenesis of wild-type TTR and other mutant forms of TTR require the use of very harsh conditions, not found in nature *(Colon and Kelly, 1992)*, the cleaved S52P variant very rapidly converts into amyloid fibrils in physiological conditions *in vitro*, whereas neither un-cleaved S52P nor other variants nor wild-type TTR formed amyloid under the same conditions

*(Mangione et al., 2014)*. Moreover, the fibrils produced *in vitro* from cleaved S52P TTR have the characteristic appearance of genuine amyloid fibrils in electron micrographs *(Mangione et al., 2014)*, in contrast with the insoluble material produced from wild-type TTR and other variants *(Hurshman et al., 2004, Bateman et al., 2011, Bonifacio et al., 1996)*.

These new insights into the possible mechanisms foregoing amyloid deposition and the susceptibility of the $TTR^{S52P}$ to cleavage which makes the S52P variant extremely amyloidogenic suggest that expression of human $TTR^{S52P}$ in mice may be a promising approach in generating a new model of cardiac ATTR amyloidosis.

The outcomes of TTR transgenic mice produced by other groups were assessed and, together with new ideas were used to design $TTR^{S52P}$ transgene. Similarly like in the $\beta_2$-microglobulin project, the genomic sequence, including exons and introns were used as it was shown that introns enhance the efficiency of gene expression and thus play a role in facilitating transcription of genes *(Brinster et al., 1988, Whitelaw et al., 1991)*. The clinical observations and results obtained from transgenic mice produced by other groups indicate that concentration of the precursor protein plays an important role in initiating amyloid deposition. To maximise the expression of the S52P variant but at the same maintain the main site of endogenous TTR expression, which is the liver, replacement of the TTR gene's own promoter with an albumin promoter was considered. Mouse albumin is abundantly expressed in the mouse liver *(Tilghman and Belayew, 1982)* and the mouse albumin enhancer/promoter has been well characterized showing that it is liver-specific and that it stimulates production of a transgene mRNA at levels comparable to mouse albumin *(Pinkert et al., 1987)*.

The aim of this part of the project was to generate transgenic mice expressing high concentrations of the highly amyloidogenic $hTTR^{S52P}$ protein towards the development of a model of cardiac ATTR amyloidosis.

## 5.2 Results

Transgenic mice carrying a highly amyloidogenic variant S52P of human transthyretin (hTTR$^{S52P}$) were generated as a transgenic model of ATTR amyloidosis. The transgene was prepared by cloning a full length wild-type hTTR gene from human genomic DNA, in which the single base substitution c.214T→C (TCT/CCT) was introduced, encoding replacement of serine residue at the position 52 of the mature protein with proline residue (S52P). To maximise the expression levels of the S52P variant in the liver, the transgene was expressed under the control of mouse albumin enhancer and promoter *(Pinkert et al., 1987)*.

### 5.2.1 Cloning of human transthyretin

The TTR gene was PCR amplified from human genomic DNA. Although several primer pairs were tested, attempts to amplify the entire 15.8 kb hTTR sequence containing the 7.3 kb TTR gene, 7 kb 5' flanking sequence and 1.5 kb 3' flanking sequence were not successful. For this reason, the 15.8 kb TTR sequence was split into two fragments, 8 kb hTTR-NS and 8 kb hTTR-SM and each fragment was cloned separately (Figure 5.1).

8 kb long hTTR-NS fragment contained 7 kb of 5' flanking sequence and exon 1 of the human TTR gene. This fragment was PCR-amplified from genomic DNA with *hTTR-NS-4-For* and *hTTR-NS-4-Rev* primers (Table 2.2). This primer pair was designed so that *Nhe*I and *Sal*I restriction sites were present within the amplified fragment.

8 kb long hTTR-SM fragment contained exons 2, 3 and 4, and 1.5 kb 3' flanking sequence of the human TTR gene. This fragment was PCR-amplified from genomic DNA using *hTTR-SM-10-For* and *hTTR-SM-10-Rev* primers (Table 2.2). The primer pair was designed to include the *Sal*I and *Mlu*I restriction sites within the amplified fragment.

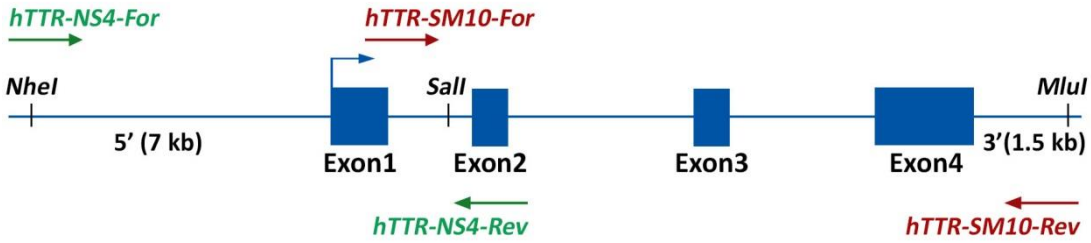


***Figure 5.1: Schematic representation of cloning of human transthyretin***

*Cloning of 15.8 kb hTTR containing the 7.3 kb hTTR gene with its 4 exons and 3 introns, 7 kb 5' flanking sequence and 1.5 kb 3' flanking sequence was split into two parts:*

*1) hTTR-NS fragment containing 7kb 5' flanking sequence, exon 1 and intron 1 was PCR amplified with primers hTTR-NS4-For and hTTR-NS4-Rev, cut with NheI and SalI and cloned into pLitmus38ixNheIxSalI.*

*2) hTTR-SM fragment containing exons 2, 3 and 4, introns and 1.5 kb 3' flanking sequence was PCR amplified with primers hTTR-MS10-For and hTTR-MS10-Rev, cut with SalI and MluI and cloned into pLitmus38ixSalIxMluI.*

*N.B. Primers are not drawn to scale.*

---

Both fragments were amplified using Phusion Hot Start II High-Fidelity DNA Polymerase. This thermostable polymerase has a proofreading capability and a very low error rate compared to other DNA polymerases. Purified *Nhe*I-*Sal*I fragment of hTTR-NS was then cloned into 2.8 kb pLitmus38ix*Nhe*Ix*Sal*I and *Sal*I-*Mlu*I fragment of hTTR-SM was cloned into pLitmus38ix*Sal*Ix*Mlu*I and the ligates were then transformed into competent cells.

The identity of the sequence for both recombinant plasmids was verified by restriction digest. hTTR-NS/pLitmus38i recombinant plasmid digested with *BamH*I enzyme gave the expected restriction pattern of 3 fragments of 4.1 kb, 3.7 kb and 2.0 kb (not shown). hTTR-SM/pLitmus38i digested with *Hind*III enzyme showed the expected 3 fragments of 6 kb, 2.6 kb and 1.8 kb (not shown).

Four hTTR-NS/pLitmus38i recombinant plasmids and two hTTR-SM/pLitmus38i recombinant plasmids were sequenced by Source BioScience (UK) to exclude sequence alterations due to PCR-introduced errors. All

exons, exon-intron boundaries, 5' and 3' ends and ligation sites were sequenced to ensure that correct transcription and splicing of the transgene would be maintained as well as no alterations in the amino acid coding sequence were present. Primers for sequencing were designed using NCBI/Primer-BLAST online software and are listed in Table 2.2. No mutations were detected in the coding and regulatory sequences of the recombinant plasmids and one hTTR-NS/pLitmus38i (plasmid number 8) and one hTTR-SM/pLitmus38i (plasmid number 1) were used for further work.

### 5.2.2 Mutagenesis of human transthyretin

The S52P mutation was introduced into the human TTR gene sequence by site-directed mutagenesis. Because the mutation site is in exon 3 of the hTTR gene, which is in the hTTR-SM fragment, hTTR-SM/pLitmus38i recombinant plasmid was used as a template for the site-directed mutagenesis. This method involves designing a pair of primers which are partly complimentary to one another and also to the DNA to be mutated except that they contain the desired mutation. *hTTR-S52P-mut-For* and *hTTR-S52P-mut-Rev* (Table 2.2) were designed so that the c.214T→C (TCT/CCT) substitution was present in the short oligonucleotide sequences priming a PCR amplification of the hTTR-SM/pLitmus38i recombinant plasmid (Figure 5.2). A 20-cycle PCR with the recombinant plasmid as a DNA template and Phusion Hot Start II High-Fidelity DNA Polymerase was run. The advantage of using the high-fidelity polymerase is the minimal chance of unwanted mutations during the PCR and the hot-start formulation of the enzyme which ensures that the primers are not degraded by the enzyme's exonuclease activity during the reaction set-up.

The site-directed mutagenesis PCR reaction produces plasmids which carry the mutation on both strands, as it is described in mutagenesis of hβM gene.

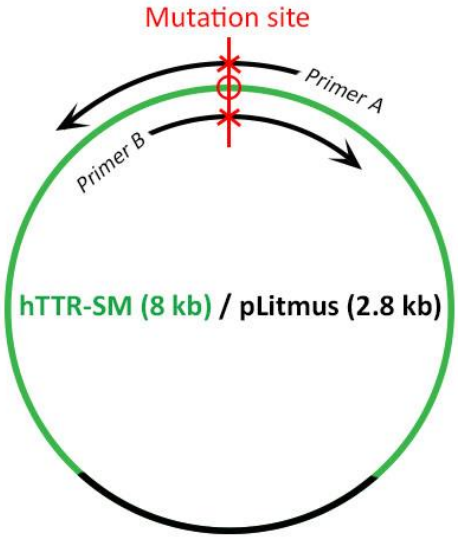


***hTTR-S52P-mut-For*** 5′-AGTGAGCCTGGAGAGCTGCATGGGCTC-3′

3′-GTGGAATATCCTTTTGGTCACTCGGACCTCTCGACG-5′ ***hTTR-S52P-mut-Rev***

***Figure 5.2: hTTRS52P site-directed mutagenesis***

*hTTR-S52P-mut-For and hTTR-S52P-mut-Rev primers were designed which are partly complimentary to each other and to the targeted hTTR gene, but containing T→C mutation causing the S52P substitution. In the first round of PCR reaction, the double stranded template hTTR-SM/pLitmus38i DNA denatures, the primers anneal to the template and new DNA strands are extended, resulting in a plasmid with a single mismatch in the mutation site. Subsequent PCR cycles predominantly lead to double-stranded plasmids carrying the desired mutation on both strands.*

*N.B. Primers are not drawn to scale.*

---

After transformation of the newly synthesized mutagenized plasmids, plasmid DNA of 8 different clones was purified and mapped with *Hind*III restriction digest to establish which clones carry the hTTR/pLitmus38i recombinant plasmid DNA and that the sequence of these plasmids has not been altered by major deletions or insertions. The mutation itself does not interfere with the restriction sites for *Hind*III and so the same pattern of 3 restriction fragments of 6 kb, 2.6 kb and 1.8 kb as in the hTTR-SM/pLitmus38i template DNA were

expected and confirmed in all 8 mutated recombinant plasmids tested (Figure 5.3).

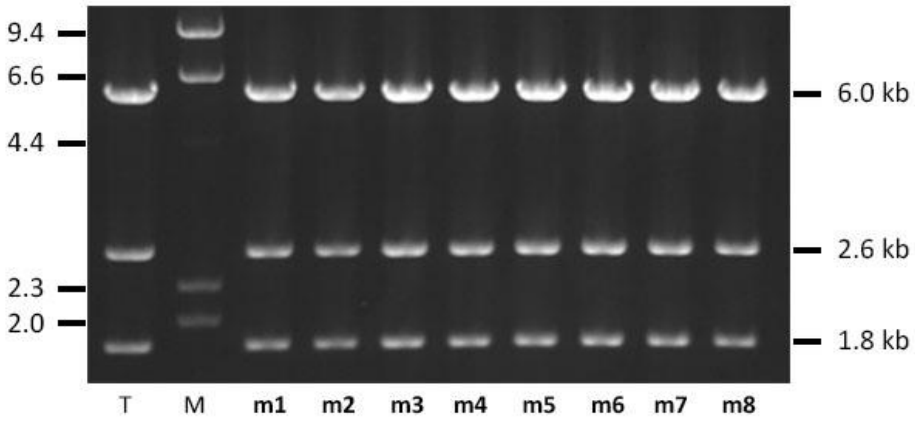


***Figure 5.3: Mutated hTTR-SM/pLitmus38i x HindIII***

*HindIII restriction analysis of mutated hTTR-SM/pLitmus38i recombinant plasmids (m1 – m8) showed 3 fragments of expected sizes 6.0 kb, 2.6 kb and 1.8 kb in all clones. Non-mutated template plasmid hTTR-SM/pLitmus38i digested with HindIII enzyme (T) was used as a control and run alongside the samples in which the same restriction pattern is obtained as the introduced mutation does not interfere with the HindIII restriction sites. λ-DNAxHindIII (M) was used as a size marker.*

---

5 of the 8 clones were sequenced by Source BioScience (UK) using the *hTTR-SM-seq3F and hTTR-SM-seq3R* primers (Table 2.2) to determine which clones carry the S52P mutation in the exon 3 of the human TTR sequence ($hTTR^{S52P}$). All 5 clones were confirmed to carry the mutation (Figure 5.4).

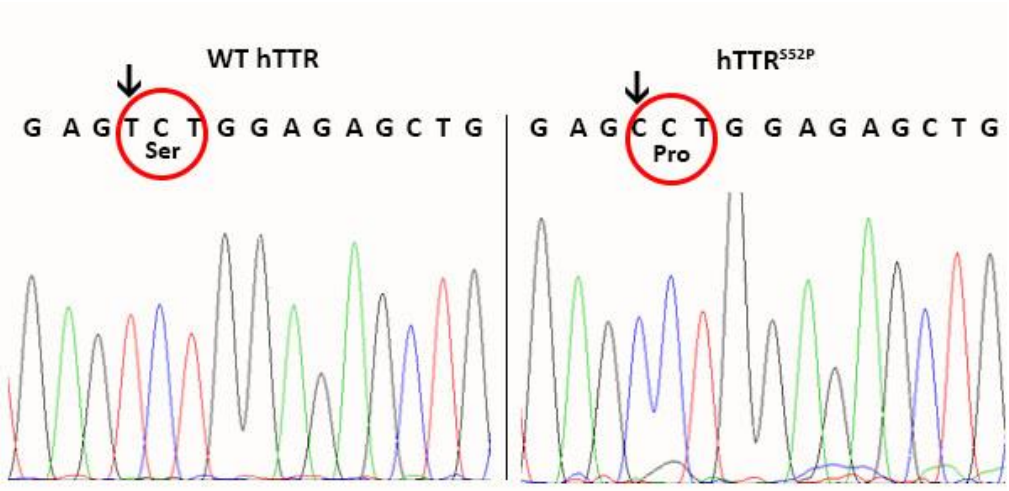


***Figure 5.4: Partial-sequence chromatograms of the human TTR gene***

*Wild-type human TTR coding sequence (WT hTTR) and amyloidogenic variant of human TTR (hTTR$^{S52P}$) show the c.214T→C single base substitution (arrows) which encodes replacement of a charged serine (TCT) residue at position 52 of the mature protein with a proline residue (CCT). The S52P mutation, introduced into the wild-type human coding sequence by site-directed mutagenesis was confirmed in all 5 clones analysed.*

---

One hTTR-SM$^{S52P}$/pLitmus38i clone (plasmid number 1) was then sequenced further to exclude sequence alterations due to PCR-introduced errors. All 3 exons of this fragment of the hTTR sequence, exon-intron boundaries, 3' end and ligation sites were verified to ensure that correct transcription and splicing of the transgene mRNA would be maintained and that no alterations in the amino acid coding sequence (except for the S52P substitution) were present. The same primers as for sequencing of the non-mutated hTTR-SM/pLitmus38i were used (Table 2.2). No sequence alterations were detected in the coding and regulatory regions of the hTTR-SM$^{S52P}$/pLitmus38i and this clone was used to assemble the full hTTR$^{S52P}$ transgene.

### 5.2.3 Gibson assembly of Alb-hTTR$^{S52P}$ transgene

The final step in the construct preparation was to join the mouse albumin enhancer and promoter, the hTTR-NS fragment carrying exon 1 of the hTTR gene and the hTTR-SM$^{S52P}$ fragment carrying exons 2, 3 and 4 of the hTTR gene with the S52P mutation in exon 3 to create the final Alb-hTTR$^{S52P}$ transgene. This was achieved by Gibson assembly.

Gibson Assembly allows in a single reaction insertion of one or more DNA fragments into virtually any position of a linearized vector and does not rely on the presence of restriction sites within a particular sequence to be synthesized or cloned *(Gibson et al., 2009)*. This method requires DNA fragments with 15-25 nucleotides overlaps with adjacent DNA fragment. To achieve this, DNA fragments and a linearised vector to be assembled are PCR amplified using specifically designed primers to generate fragments with overlapping ends. Exonuclease, DNA polymerase and DNA ligase enzymes combined in the Gibson assembly mastermix then create single stranded 3' overhangs to facilitate the annealing of fragments that are complimentary to one another, fill the gaps within each annealed fragment and anneal nicks in the assembled DNA, respectively.

The linearised mouse albumin enhancer/promoter in pBSIISK(-) vector *(Pinkert et al., 1987, Gorski et al., 1986)* was PCR amplified with *TTRass6* and *TTRass1* primers which created a 5.2 kb Alb/pBSIISK(-) fragment. *Nhe*I linearised hTTR-NS/pLitmus38i was amplified with *TTRass2* and *TTRass3* primers which created a 0.9 kb 5'-UTR – *Sal*I fragment of hTTR-NS carrying exon 1 of the hTTR gene. hTTR-SM$^{S52P}$/pLitmus38i linearised with *EcoR*V was PCR amplified with *TTRass4* and *TTRass5* primers which created a 7.7 kb *Sal*I – *Mlu*I fragment of hTTR-SM$^{S52P}$ carrying exon 2, exon 3 (with the S52P mutation), exon 4 and a 1.5 kb 3' flanking sequence of the hTTR gene. The PCR amplifications were performed using Phusion Hot Start II High-Fidelity DNA Polymerase. Each of the PCR amplified fragments had short sequence overlaps with the adjacent fragments (Table 2.2). These three

fragments were then joined together in Gibson assembly to make up the Alb-hTTR$^{S52P}$/pBSIISK(-) recombinant plasmid in which the mouse albumin enhancer/promoter is linked to the full length of hTTR$^{S52P}$ gene with 1.5 kb of 3' flanking sequence in pBSIISK(-) vector (Figure 5.5).

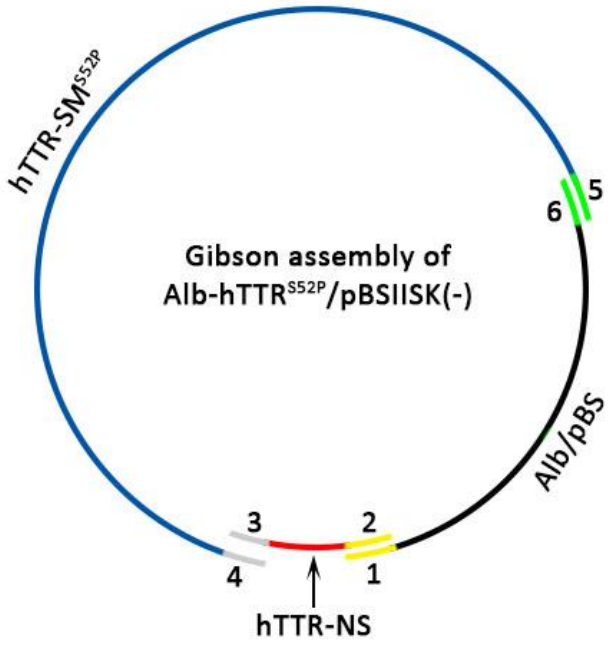


***Figure 5.5: Gibson assembly of Alb-hTTR$^{S52P}$ fragment in pBSIISK(-)***

*890 bp 5'UTR-SalI fragment of hTTR-NS, 7.7 kb SalI-MluI fragment of hTTR-SMS52P and mouse albumin enhancer/promoter in pBSIISK(-) were PCR amplified using specifically design primers with nucleotide overlaps (1-6). These fragments were then assembled together to make up Alb-hTTR$^{S52P}$ transgene in which the full length hTTR$^{S52P}$ gene with its 1.5 kb 3' flanking sequence is joined together with mouse albumin enhancer/promoter in pBSIISK(-) vector.*

---

The assembled reaction was then transformed into competent cells. The predicted size of correctly assembled Alb-hTTR$^{S52P}$/pBSIISK(-) recombinant plasmid was 13.7 kb (Figure 5.6). Five out of twelve analysed and linearised recombinant plasmids suggested the correct assembly. These five plasmids were digested with *Hind*III to verify the identity of the assembled clones and

all five recombinants showed the predicted fragments of 6.4 kb, 5.5 kb and 1.8 kb (Figure 5.7). Two of these five Alb-hTTR$^{S52P}$/pBSIISK(-) plasmids were sequenced by Source BioScience (UK) to verify all coding sequences, correct assembly of fragments and exon-intron boundaries of the construct to ensure that correct transcription and splicing of the transgene mRNA would be maintained and that no alterations in the coding sequence were present. After the sequences verification, one Alb-hTTR$^{S52P}$/pBSIISK(-) recombinant was used to prepared the Alb-hTTR$^{S52P}$ microinjection fragment (Figure 5.8).

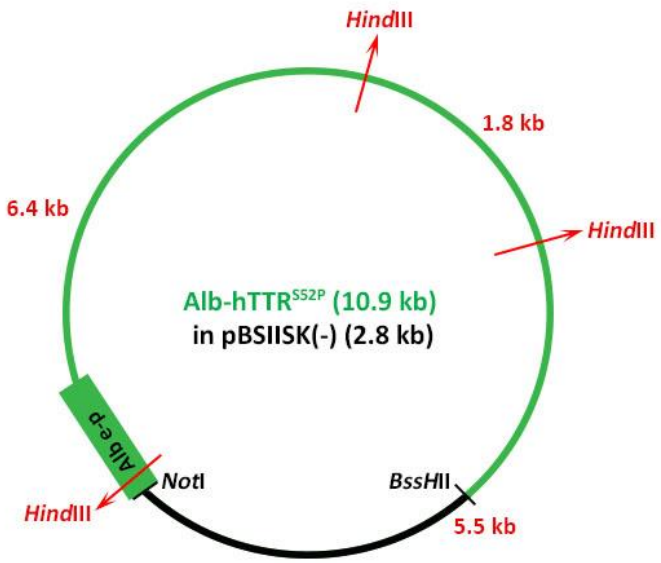


***Figure 5.6: Map of assembled Alb-hTTR$^{S52P}$ fragment in pBSIISK(-) vector.***
*HindIII, used for identification of recombinant plasmids obtained by Gibson assembly, cuts the 13.7 kb Alb-hTTR$^{S52P}$/pBSIISK(-) plasmid into 3 fragments of 6.4 kb, 5.5 kb and 1.8 kb. NotI and BssHI were used for excision of the 10.9 kb Alb-hTTR$^{S52P}$ microinjection fragment from the plasmid.*

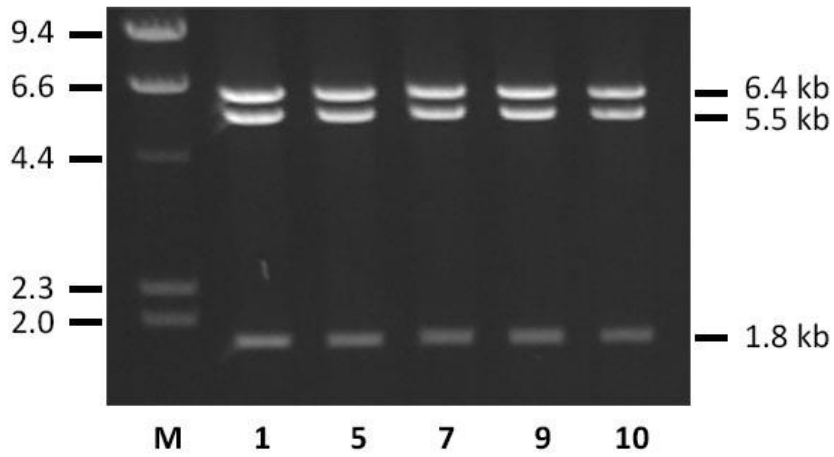


***Figure 5.7: HindIII restriction analysis of Alb-hTTR$^{S52P}$/pBSIISK(-)***

*HindIII restriction analysis of five assembled Alb-hTTR$^{S52P}$/pBSIISK(-) clones showed predicted restriction pattern of three fragments of 6.4 kb, 5.5 kb, 1.8 kb in all five clones (1, 5, 7, 9, 10). λ-DNAxHindIII was run alongside the samples as a size marker.*

---


***Figure 5.8: Schematic representation of the assembled Alb-hTTR$^{S52P}$ fragment***

*The 10.9 kb NotI – BssHI fragment excised from the Alb-hTTR$^{S52P}$/pBSIISK(-) was used for microinjections to generate hTTR$^{S52P}$ transgenic mice.*

---

## 5.2.4 Generation of hTTR$^{S52P}$ transgenic mice

The 10.9 kb Alb-hTTR$^{S52P}$ fragment was cut out of the circular Alb-hTTR$^{S52P}$/pBSIISK(-) plasmid with *BssH*II and *Not*I (Figure 5.8). The fragment was gel purified to remove the plasmid vector sequence, quantified and used for pronuclear injection. The microinjections into C57Bl/6J embryos and embryo transfers into pseudo-pregnant recipient female mice were performed by Dr Raya Al-Shawi and Dr Paul Simons.

27 pups were born from the pronuclear microinjections. Ear and tail biopsies were collected and used for genotyping at 5 weeks of age. Transgenic mice were identified by PCR using primers *hTTRg-3U* and *hTTRg-3D* (Table 2.2) that amplify a 689 bp fragment of the transgene. Two females showed integration of the hTTR$^{S52P}$ transgene, and the PCR clearly distinguished the transgenic mice from non-transgenic mice (Figure 5.9). Both transgenic females were bred with C57Bl/6J mice to identify germline transmitters. 1 female proved to transmit the transgene to the first generation, establishing line 5.

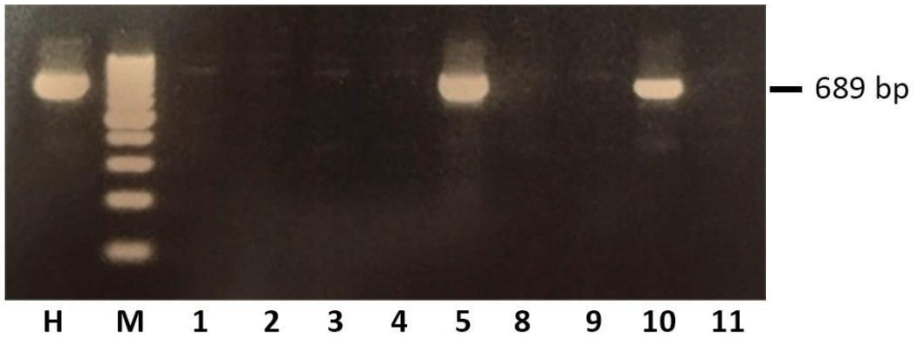


***Figure 5.9: Identification of hTTR$^{S52P}$ transgenic animals***

*hTTR$^{S52P}$ transgenic mice born from microinjected embryos were identified by PCR using hTTRg-3U and hTTRg-3D primers. Two transgenic animals (mice number 5 and 10) were distinguished from their negative littermates (mice numbers 1, 2, 3, 4, 8, 9, 11) by an amplification of a 689 bp fragment of the transgene. Human genomic DNA (H) was used as a positive control and run alongside the samples together with a 100 bp marker (M).*

In hTTR transgenic mice carrying L55P variant produced by Sousa et al. (2002) and Tagoe et al. (2007), a difference in deposition of human TTR protein was noticed between mice expressing the endogenous mouse TTR and mice in which the murine TTR gene was silenced (TTR-KO). Although no ATTR amyloid was detected in any $TTR^{L55P}$ transgenic mice, increased TTR deposition was observed in transgenic mice on TTR-KO background in comparison with transgenic mice with the murine TTR present *(Sousa et al., 2002, Tagoe et al., 2007)*. This observation suggested that the murine TTR may interfere with hTTR deposition in the hTTR transgenic mice. TTR is a homotetramer and presence of the murine TTR in hTTR transgenic mice leads to a formation of TTR heterotetramers composed of both, murine and human TTR monomers *(Tagoe et al., 2007)*. It was then shown that in the transgenic mice the murine/human TTR heterotetramers are more stable to denaturation *(Tagoe et al., 2007)* and *in vitro* experiments looking at the dissociation rates and kinetic stability of murine/human heterotetramers suggested that the presence of murine subunit in the murine/human TTR heterotetramers may prevent human TTR fibrillogenesis *(Reixach et al., 2008)*. For this reason, the $hTTR^{S52P}$ transgenic mice were bred on mouse TTR-KO background *(Episkopou et al., 1993)* as well as on mouse TTR wild-type background to evaluate the effect of the mouse endogenous TTR in the transgenic mice.

### 5.2.5 Expression of hTTR mRNA in the $hTTR^{S52P}$ transgenic mice

TTR is normally expressed mostly by hepatocytes and by the choroid plexus of the brain *(Dickson et al., 1985)* and minor synthesis has also been identified in the retinal and ciliary pigment epithelia of the eye, visceral yolk sac, placenta and other organs *(Soprano et al., 1985, Soprano et al., 1986, Cavallaro et al., 1990, McKinnon et al., 2005)*. In the $hTTR^{S52P}$ transgenic mice, the hTTR transgene is expressed under the control of mouse albumin

promoter which has been shown to be liver-specific *(Pinkert et al., 1987)*. Thus the transgene expression was expected exclusively in the liver.

Liver, spleen, heart, kidney, tongue, skeletal muscle and brain of hTTR$^{S52P}$ transgenic mice lacking the endogenous mouse TTR were analysed for the transgenic hTTR mRNA expression by reverse transcription PCR (RT-PCR).

RNA was isolated from mouse tissue and any contaminating DNA in the samples was eliminated by DNase (gDNA wipe-out buffer, QIAGEN). The isolated RNA was then transcribed into cDNA by reverse transcriptase using a mix of primers which ensured cDNA synthesis from all regions of RNA transcripts.

The obtained cDNA from the hTTR$^{S52P}$ transgenic tissues was PCR amplified using human TTR specific primers *hTTR RT-PCR 5'* and *hTTR RT-PCR 3'* (Table 2.2) each of which is complementary to a sequence from different exons. The PCR-amplified product was a 226 bp fragment. As expected, the hTTR mRNA was detected only in the liver (Figure 5.10 A). The specificity of the human TTR primers was confirmed by RT-PCR of mRNA obtained from tissue of control TTR-KO mice, in which no amplification with *hTTR RT-PCR 5'* and *hTTR RT-PCR 3'* primers was detected (Figure 5.11 A).

As a positive control, RT-PCR of the mouse house-keeping gene GAPDH which is ubiquitously expressed in all tissue was simultaneously performed. Using *msGAPDHf* and *msGAPDHr* primers (Table 2.2), a 133 bp PCR product was amplified from obtained cDNA in all analysed tissues of hTTR$^{S52P}$ transgenic mice as well as of TTR-KO mice (Figure 5.10 B and 5.11 B). This result confirmed that the extracted RNA is of a good quality and that no amplification of cDNA in the tissue with hTTR primers in the RT-PCR reactions is due to the fact that the gene of interest is not expressed and not due to lack of total RNA itself in the analysed samples or failure of cDNA synthesis.

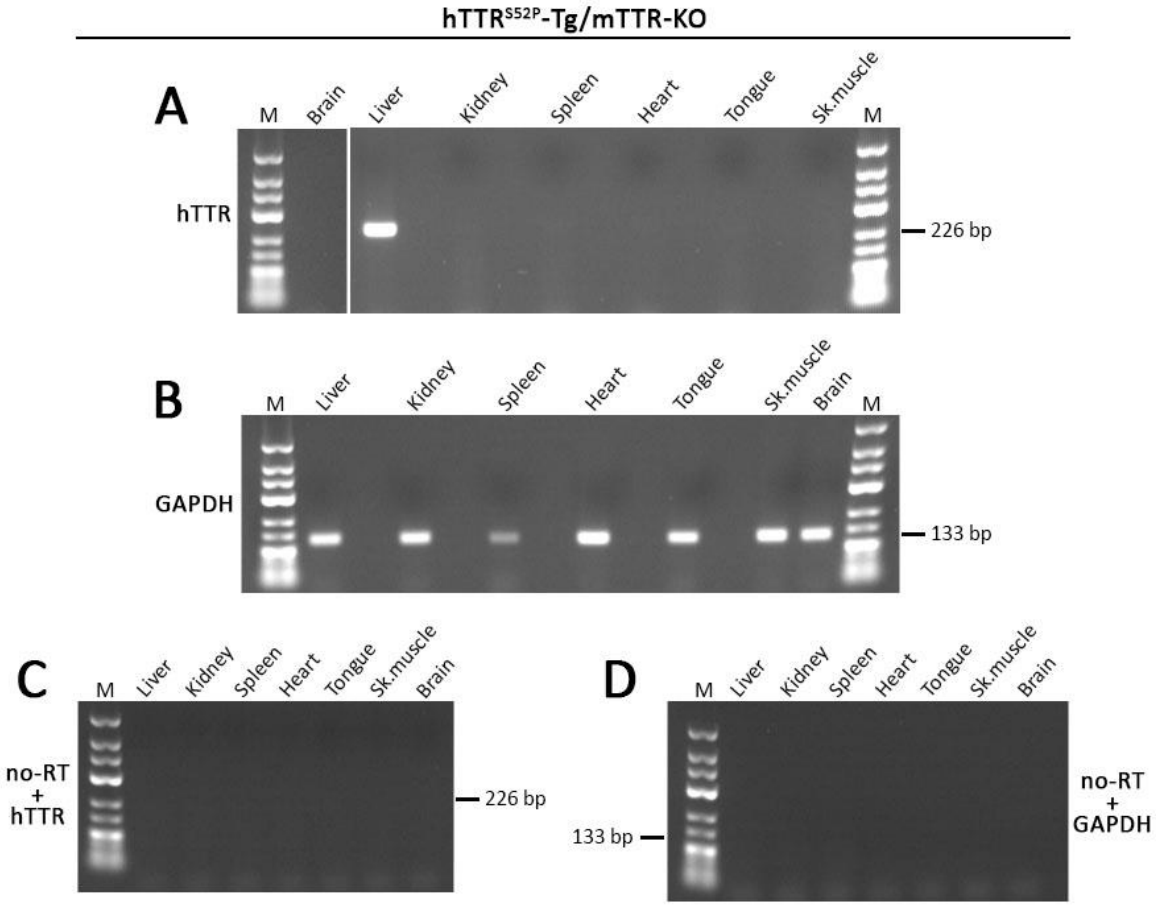


***Figure 5.10: Expression of transgene-encoded hTTR mRNA***

*hTTR transgene mRNA expression in tissue of hTTR$^{S52P}$ transgenic mice on TTR-KO background was analysed by RT-PCR. RNA isolated from liver, kidney, spleen, heart, tongue, skeletal muscle and brain was used for cDNA synthesis using reverse transcriptase (RT) and a mixture of oligo-dT primers and random primers to ensure cDNA synthesis from all regions of RNA transcripts. The synthesized cDNA was then amplified by 25 cycle PCR using Taq polymerase. hTTR expression (A) was detected as a 226 bp fragment in the liver only as expected as the transgene was under the control of liver-specific albumin promoter. Successful RNA extraction and cDNA synthesis was confirmed by control RT-PCR reactions using primers specific for mouse GAPDH, an ubiquitously expressed gene, amplifying a 133 bp fragment in all tissue analysed (B). When no RT was added into the tissue RNA, no PCR amplification was detected in any tissue with either hTTR (C) or GAPDH (D) primers confirming specificity of the PCR reaction to cDNA synthesized from the tissue-extracted RNA. 25 bp DNA ladder (M) was run alongside the samples.*

To exclude the possibility of false positive signal by genomic DNA contamination, a control reaction prepared without the addition of reverse transcriptase enzyme into the RNA isolated from tissues of hTTR$^{S52P}$ transgenic mice was also run. Using primers amplifying hTTR cDNA and GAPDH cDNA, no amplification after the PCR was detected, confirming that the amplification of hTTR and mouse GAPDH fragments was specific to the extracted RNA from the mouse tissue (Figure 5.10 C, D).

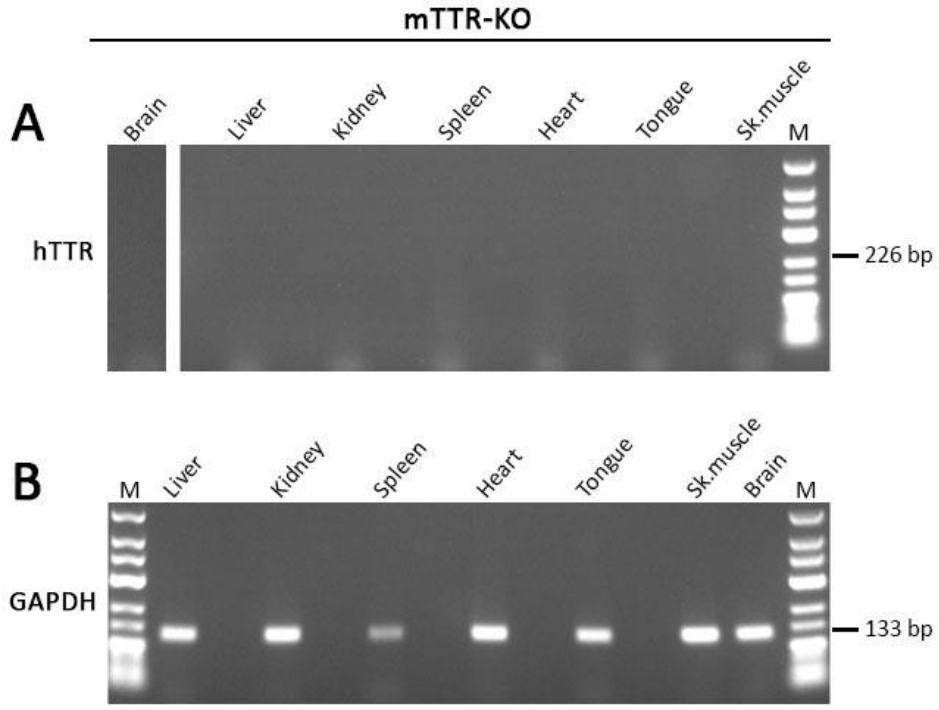


***Figure 5.11: Negative control RT-PCR of hTTR transgene-encoded mRNA***

*RNA isolated from liver, kidney, spleen, heart, tongue, skeletal muscle and brain of non-transgenic control mice lacking the endogenous mouse β2m (mβ2m-KO) was used for cDNA synthesis using reverse transcriptase and subjected to PCR amplification with hTTR primers (A) amplifying a 226 bp fragment in hTTR positive samples and mouse GAPDH primers (B) detecting a ubiquitously expressed GAPDH house-keeping gene. While the GAPDH primers amplified a 133 bp fragment, confirming successful extraction of RNA from the tissue as well as cDNA synthesis by reverse transcriptase, no amplification using the hTTR primers was detected confirming the specificity of the assay.*

### 5.2.6 hTTR in the serum of hTTR$^{S52P}$ transgenic mice

Presence of hTTR in the serum of hTTR$^{S52P}$ transgenic mice was evaluated by Western blot analysis. Human serum was used as a positive control of the protein migration and for estimation of the amount of the hTTR protein in the mouse serum.

0.2 µl of serum of hTTR$^{S52P}$ of transgenic mice, C57Bl/6J mice, TTR-KO mice, as well as 0.2 µl of human serum were separated on an SDS-PAGE gel and blotted onto a PVDF membrane which was probed with antibodies against human TTR. Two antibodies were tested: Dako rabbit polyclonal anti-human TTR and sheep polyclonal anti-human TTR from Binding site. Both antibodies recognized human TTR as a 14 kDa band migrating together with the TTR in the human serum. From the signal intensity given by the TTR in the human serum and hTTR signal in the transgenic mice, the hTTR concentration in the transgenic mice was equivalent to the concentration of the TTR in the human sample. Both antibodies also reacted with mouse TTR (mTTR) which migrated faster as a 13 kDa band and was clearly distinguishable from the human TTR protein in the serum of the transgenic mice carrying both alleles (T/WT) or one allele (T/Het) of the murine TTR. As expected, no signal was detected in the serum of TTR-KO mice. No difference in the hTTR signal was observed in the serum of T/WT and T/Het mice and in the serum of mice lacking the mouse TTR (T/KO). These results are shown in Figure 5.12.

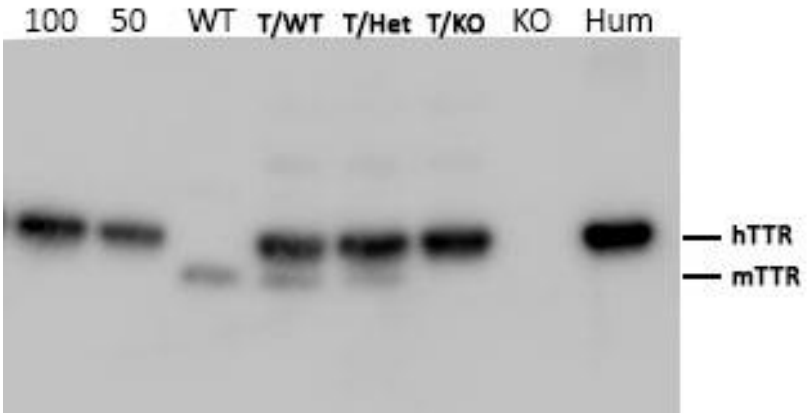


***Figure 5.12: hTTR in serum of hTTR$^{S52P}$ transgenic mice***

*Western blot analysis showing expression of human TTR in the serum of hTTR$^{S52P}$ transgenic mice carrying one (T/Het) or two (T/WT) alleles of endogenous mouse TTR and hTTR$^{S52P}$ transgenics on mouse TTR knock-out background (T/KO) using a sheep polyclonal anti-human TTR antibody (Binding site) recognising both, human and mouse TTR. Human TTR (14 kDa) is distinguishable from mouse TTR which migrates faster as a 13 kDa band. No signal was detected in mouse TTR knock-out serum (KO). Human serum was used as a positive control (Hum), wild-type C57Bl/6J serum as a negative control (Wt) and 100 ng and 50 ng of recombinant human TTR per well were used for a concentration estimate. 0.2 µl of serum was loaded per well for each sample analysed.*

---

## 5.2.7 Quantitation of serum hTTR in the hTTR$^{S52P}$ transgenic mice

To quantify the concentration of circulating hTTR in hTTR$^{S52P}$ transgenic mice, mouse serum was assayed by rocket immunoelectrophoresis.

No rocket was formed when sera of C57Bl/6J mice and TTR-KO mice were analysed, showing that the Dako anti-hTTR antibody, which recognizes both human and murine TTR in their denatured form, is specific for human TTR only in its native conformation. hTTR$^{S52P}$ transgenic mice carrying one or two alleles of the endogenous mouse TTR (T/Het or T/WT, respectively) showed higher measured concentration of serum hTTR in the rocket analysis than

transgenic mice lacking the endogenous murine TTR (T/KO) (Figure 5.13). Moreover, sex difference was observed in the serum levels of hTTR with males expressing higher levels than females.

The measured concentrations were 1736 ± 447 µg/ml (n=13) in T/WT males, 1231 ± 137 µg/ml (n=6) in T/WT females, 1109 ± 255 µg/ml (n=8) in T/Het males, 799 ± 98 µg/ml (n=7) in T/Het females, 596 ± 128 µg/ml (n=12) in T/KO males and 361 ± 175 µg/ml (n=9) in T/KO females (Figure 5.14).

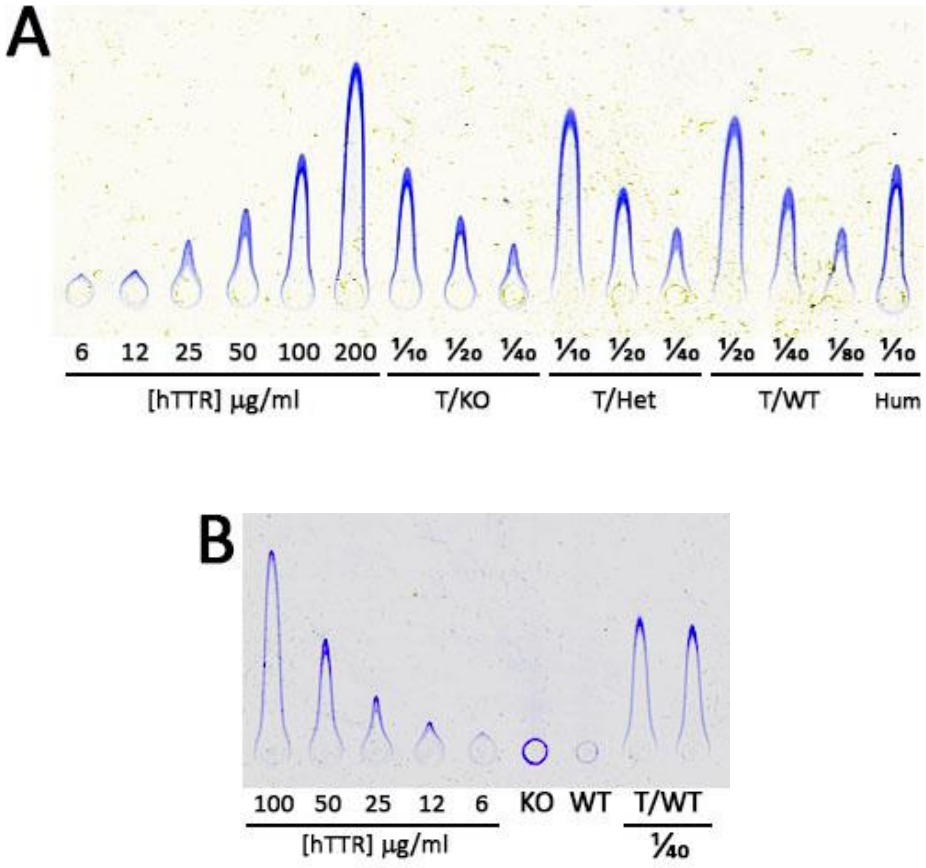


***Figure 5.13: Quantitation of serum hTTR by rocket immunoelectrophoresis***

*Serum of hTTR$^{S52P}$ transgenic mice was analysed by rocket assay. Human serum (Hum) was used as a positive control (panel A) and undiluted mouse sera of C57Bl/6J (WT) and mTTR-KO (KO) mice were used as negative controls (panel B). The assay is specific for hTTR. Note that different range of dilutions of transgenic sera were tested. Known concentrations of hTTR in human serum were used to prepare standard curve. The gels were stained with Coomassie blue.*

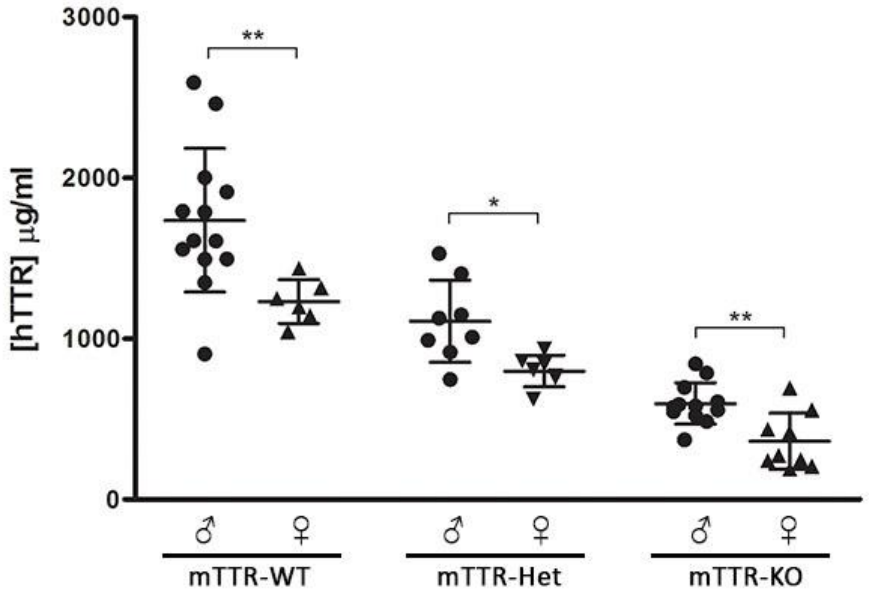


***Figure 5.14: Quantitation of serum hTTR in hTTR$^{S52P}$ transgenic mice***

*The concentration of human TTR in the serum of hTTR$^{S52P}$ transgenic mice was quantified using rocket immunoelectrophoresis. A difference between males and females was observed, with the serum levels of hTTR significantly higher in males than females. Native TTR is tetrameric – while in the hTTR$^{S52P}$ transgenic mice on mTTR-KO background the homotetramers are formed of human TTR only, heterotetramers between human and mouse TTR are formed in mice carrying one or two alleles of mouse TTR (mTTR-Het and mTTR-WT, respectively). The values are expressed as mean ± standard deviation for number of mice analysed (n). Mann-Whitney two-tailed test was used to analyse the differences between males and females with statistical significance showed as p<0.05 (*) and p<0.01 (**).*

---

Although a significant difference was seen in the serum hTTR concentrations between transgenic mice expressing or lacking murine TTR, such difference was not observed in the denatured serum run on an SDS-PAGE gel. Native TTR is tetrameric and it has been shown that in transgenic mice carrying human and mouse TTR, heterotetramers composed of human and murine subunits are formed *(Tagoe et al., 2007, Zhao et al., 2008)*. In hTTR$^{S52P}$ transgenic mice on mouse TTR-KO background, the TTR is a homotetramer formed only by the human subunits. In transgenic mice in which the murine

TTR is present, human/mouse TTR heterotetramers can be formed as it is illustrated in Figure 5.15. As no rocket was formed when serum of C57Bl/6J mice was analysed, the rocket analysis is human TTR specific. Thus, one or more human subunits present in a mouse/human TTR heterotetramer may react with the anti-human TTR antibody in the gel, contributing to the precipitate in the rocket. The concentration of tetramers containing at least one human TTR subunit in transgenic mice on wild-type background is higher than the concentration of homotetramers in transgenic mice on TTR-KO background. The concentrations of hTTR containing tetramers are intermediate in hTTR transgenics on mTTR heterozygous background. These considerations probably explain the apparent discrepancies between the concentrations measured by rockets in the serum of transgenic mice on knock-out background and those carrying the endogenous mouse TTR, given that no differences were observed by Western blotting.

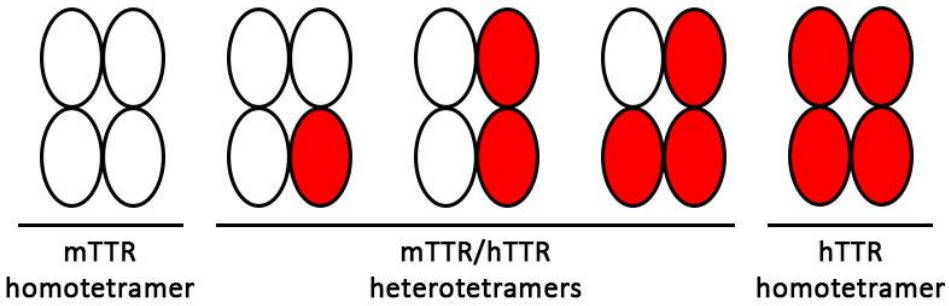


***Figure 5.15: TTR tetramers***

*Native TTR is a tetramer composed of four TTR monomers. In transgenic mice expressing human TTR (hTTR; red subunit) as well as mouse TTR (mTTR; white subunit), five different compositions of the TTR tetramer can occur: homotetramers when the TTR is composed of the same monomers, or heterotetramers when both, mouse and human TTR monomers are present.*

## 5.2.8 Body weight of hTTR$^{S52P}$ transgenic mice

A difference was observed between the transgenic and non-transgenic animals in the body weight and the size of the body, from birth and throughout their life span, regardless the presence of endogenous murine TTR. The hTTR$^{S52P}$ transgenic mice were smaller and had significantly lower body weight than their non-transgenic littermates (Table 5.2). No difference was seen in body weights between non-transgenic mice wild-type, heterozygous and knock-out for endogenous mouse TTR-KO throughout their life (Table 5.1).

| Non-transgenic control mice | | | | |
|---|---|---|---|---|
| **[Weight] g** | **Males** | **(n)** | **Females** | **(n)** |
| **mTTR Wild-type** | 19.81 ± 1.71 | (6) | 17.92 ± 1.31 | (6) |
| **mTTR Heterozygous** | 20.06 ± 2.38 | (12) | 18.24 ± 1.50 | (8) |
| **mTTR Knock-out** | 19.01 ± 2.18 | (10) | 19.17 ± 0.96 | (3) |
| **P value** | ns | | ns | |

***Table 5.1: Body weight of non-transgenic mice on different mTTR backgrounds***
*Comparison of weights of 5 weeks old non-transgenic males and females that are wild-type, heterozygous or knock-out for endogenous murine TTR (mTTR). Values are shown as mean ± SD for number (n) of mice analysed. One way ANOVA (Kruskal-Wallis test) was used for statistical analysis. Presence or absence of expression of mTTR did not affect the weights of the mice.*

| [Weight] g | Males | (n) | Females | (n) |
|---|---|---|---|---|
| **Non-transgenic controls** | 19.86 ± 2.23 | (28) | 18.29 ± 1.36 | (17) |
| **hTTR$^{S52P}$ transgenics** | 13.59 ± 2.58 | (20) | 14.44 ± 2.18 | (13) |
| **P value** | < 0.0001 | | < 0.0001 | |

***Table 5.2: Body weight of transgenic and non-transgenic mice***

*Weights of hTTR$^{S52P}$ transgenic mice at 5 weeks of age are shown as mean ± SD for number (n) of mice analysed. Mann-Whitney two-tailed test was used for statistical analysis. The difference in body weight between transgenic mice and the non-transgenic littermates was observed from birth and throughout the life span of the mice, regardless of presence of murine TTR.*

Such phenotype of the transgenic mice could be related to the expression of the TTR$^{S52P}$ transgene itself or it could be due to a position effect *(Al-Shawi et al., 1990)* of the randomly integrated transgene causing a disruption of a normal gene sequence in the mouse genotype. Because only one line of the hTTR$^{S52P}$ transgenic mice has been characterised so far, the position effect of the transgene has not been evaluated yet.

## 5.2.9 TTR$^{S52P}$ variant binds thyroxine $T_4$ in hTTR$^{S52P}$ transgenic mice

TTR is the main carrier of thyroxine hormone $T_4$ in rodents *(Davis et al., 1970)*. $T_4$ is synthesized exclusively in the thyroid gland and is distributed via circulation bound to $T_4$ carriers to target tissue where it is converted to biologically active $T_3$ form by 5'-deiodinase enzymes *(Balfour and Tunnicliffe, 1960, Braverman et al., 1970, Jennings et al., 1979)*. In TTR-KO mice, total $T_4$ levels in serum were reported to be almost 3-fold lower than in wild-type mice *(Episkopou et al., 1993)* but the mice are healthy and viable. To analyse the potential of hTTR$^{S52P}$ to bind $T_4$, total $T_4$ levels were measured in the hTTR$^{S52P}$ transgenic mice and non-transgenic controls by ELISA.

The concentration of total $T_4$ in wild-type mice was 0.049 ± 0.005 µg/ml (n=4), whereas in the TTR-KO mice, the concentration was 0.028 ± 0.009 µg/ml

(n=4). Lower levels of $T_4$ have been reported in transgenic mice in which the mouse TTR was knocked-out *(Episkopou et al., 1993, Zhao et al., 2008)*. In the $hTTR^{S52P}$ transgenic mice on mouse TTR knockout background, the presence of the $hTTR^{S52P}$ variant rescued the total $T_4$ in the plasma, with measured concentration 0.050 ± 0.011 µg/ml (n=9). The concentrations of $T_4$ in $hTTR^{S52P}$ transgenic mice on wild-type background (0.063 ± 0.027 µg/ml, n=4) were equivalent with non-transgenic wild-type controls. In the non-transgenic mice heterozygous for mTTR, the concentration of $T_4$ was intermediate between wild-type and TTR knock-out mice (0.037 ± 0.003 µg/ml, n=6), and the concentration increased in the presence of the $hTTR^{S52P}$ variant (0.062 ± 0.014 µg/ml, n=10). The results are shown in Figure 5.16. These results confirm that the S52P variant expressed in the transgenic mice forms functional tetramers able to bind $T_4$.

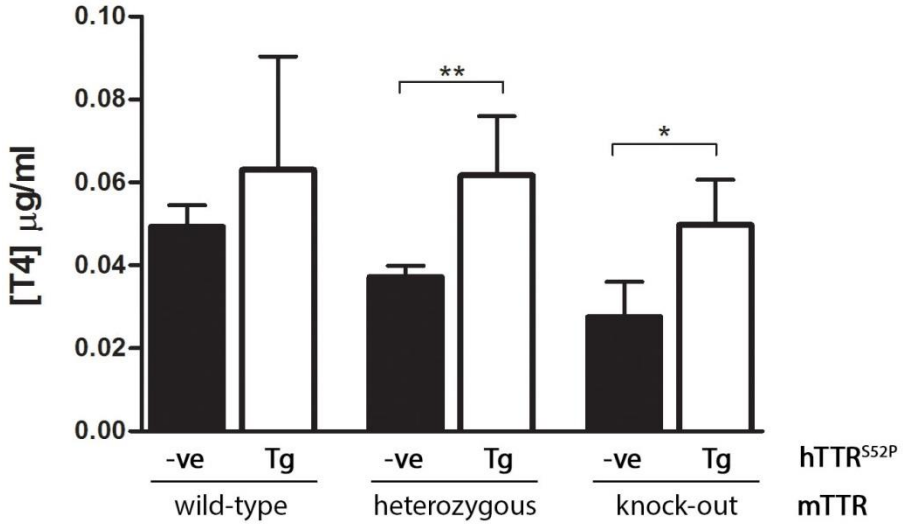


***Figure 5.16: Serum thyroxine (T4) levels in $hTTR^{S52P}$ transgenic mice***

*T4 concentration in the serum of $hTTR^{S52P}$ transgenic (Tg) and non-transgenic (-ve) mice with both alleles (wild-type), one allele (heterozygous) or no allele (knock-out) of mouse TTR (mTTR) was measured by ELISA. Mann-Whitney two-tailed test was used for result analysis with statistical significance of p<0.05 (*) and p<0.01 (**).*

### 5.2.10 Presence of glycosylated TTR in serum of hTTR$^{S52P}$ transgenic mice

In serum of all hTTR$^{S52P}$ transgenic mice tested, a slower migrating band was consistently detected on immunoblots in addition to the 14 kDa monomeric hTTR. This band was a minor component and was absent from the serum of non-transgenic mice and normal human serum. TTR is not normally secreted as a glycoprotein. However, presence of glycosylated TTR in plasma of carriers of the V30M variant of TTR was reported in both, humans and transgenic mice *(Teixeira and Saraiva, 2013)*.

To identify whether the slower migrating band seen in the serum of hTTR$^{S52P}$ transgenic mice was glycosylated TTR, serum of transgenic mice was treated with PNGase F, an enzyme that cleaves carbohydrate residues from N-glycoproteins. Indeed, the enzymatic treatment led to a loss of the slower migrating band on the immunoblot as documented in Figure 5.17.

The specificity of the enzymatic treatment under the reaction conditions was tested in serum samples of the same transgenic mice by subjecting the serum to the same reaction conditions but without the addition of PNGase F enzyme into the reaction. After this treatment, the slower migrating band was still detected in these samples confirming that the reaction conditions had no effect on the TTR in the serum and its mobility.

Non-treated transgenic serum and human serum were used as positive controls and serum of C57Bl/6J mice and TTR-KO mice were used as negative controls for detection of the human TTR.

Overall, these results confirm that a fraction of the human S52P variant circulating in the transgenic mice is N-glycosylated.

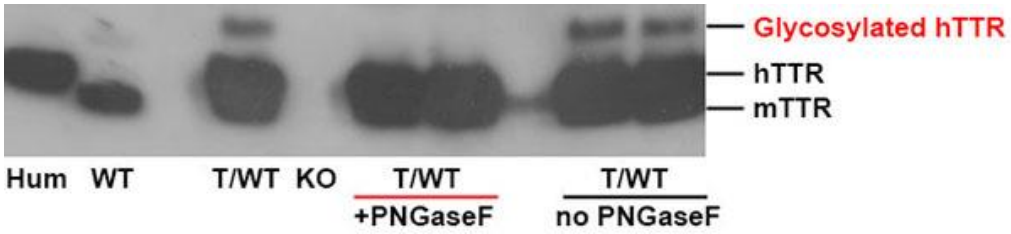


***Figure 5.17: Glycosylated TTR in the serum of hTTR$^{S52P}$ mice***

*Treating serum of hTTR$^{S52P}$ transgenic mice with PNGase F, an enzyme that cleaves carbohydrate residues from glycoproteins, results in a loss of a slower migrating band on western blot (+PNGase F), showing that a fraction of the human protein circulating in the transgenic mice is N-glycosylated. The deglycosylation reaction conditions had no effect on the serum TTR when no enzyme was added into the reaction mix (no PNGase F). Human TTR (hTTR) only was detected as a 14 kDa band in human serum (Hum). Mouse TTR (mTTR) only was detected as a 13 kDa band in serum of C57Bl/6J mouse. hTTR, mTTR and glycosylated hTTR were detected in non-treated serum of hTTR$^{S52P}$ transgenic serum (T/WT). No signal was detected in the serum of TTR-KO mice (KO). Sheep anti-hTTR antibody (Binding site, UK) was used for TTR detection. The film was deliberately over-exposed in order to show clearly the glycosylated TTR band.*

## 5.3 Discussion

Despite many attempts to model ATTR amyloidosis in mice, no or very little and inconsistent ATTR amyloid deposition has been achieved in the transgenic mice to date. hTTR$^{S52P}$ is the most highly amyloidogenic TTR variant described so far. Here, transgenic mice expressing hTTR$^{S52P}$ have been generated as a potential new model of ATTR amyloidosis. Although TTR is also synthesized in the choroid plexus of the brain, the liver is effectively the sole source of plasma TTR *(Holmgren et al., 1991)*. To maintain the liver as the physiological site of expression but at the same maximise the expression levels of the S52P hTTR variant in the transgenic mice, the hTTR$^{S52P}$ transgene was expressed under the control of mouse albumin enhancer-promoter, which has been well characterised *(Pinkert et al., 1987)*. Albumin in abundantly expressed in the liver and the concentration of albumin in plasma is about 100-times higher than of TTR in mice *(Champy et al., 2008)*.

Transgenic mice produced to study the control sequences located upstream of mouse albumin gene, transgenes with up to 12 kb of mouse albumin 5'-flanking sequences fused to human growth hormone gene were tested *(Pinkert et al., 1987)*. In those mice, 8.5 – 10.4 kb region located upstream of the albumin promoter acted as an enhancer essential for high levels of the transgene expression as well as determining the hepatic-specific expression, with the region in between -8.5 and -0.3 kb shown to be disposable *(Pinkert et al., 1987)*. This enhancer/promoter was successfully used *(Johnson et al., 1995, Heckel et al., 1990)*. Indeed, in the hTTR$^{S52P}$ transgenic mice presented here, the hTTR mRNA expression was confirmed exclusively in the liver as expected, consistent with the characterisation of the albumin enhancer-promoter used to drive the transgene expression. Moreover, the hTTR$^{S52P}$ transgenic mice have serum concentration of the human TTR higher than typical in healthy humans. The high concentration of circulating human TTR in the hTTR$^{S52P}$ transgenic mice, which is one of the highest reported in TTR

transgenic mice generated world-wide so far, is an important prerequisite for priming formation of amyloid fibrils. Although the data presented above relate to a single transgenic line, four new transgenic mice generated with the same construct have similarly high levels of expression showing that this construct contained all regulatory elements necessary for consistently high levels of liver-specific expression.

In this context, it is interesting to note that TTR knock-in transgenic mice generated by Zhao et al. (2008) by knock-in of human TTR cDNA with rabbit β-globin intron into the mouse TTR locus only gave 10 % of the TTR expression levels observed in the $hTTR^{S52P}$ transgenic mice presented here, using the same assay (data not shown). Although this allele has all of the 5' and 3' regulatory sequences in the chromosomal context of the mouse Ttr gene, the expression is low. Against this background, the data in this chapter show that the combination of using the genomic sequence, including the introns, and a strong liver-specific promoter is a successful strategy in driving high level liver-specific expression of human TTR.

The clinical disease of amyloidosis occurs when the rate of amyloid deposition exceeds its continuing rate of reabsorption by natural clearance mechanisms, resulting in accumulation of substantial amyloid deposits in various organs. Once the process of amyloid formation has begun, amyloid deposition and its progress depend only on a continuing supply of the respective amyloid fibril precursor protein. This was very clearly demonstrated in AA amyloidosis patients by Lachmann et al. (2007) and confirmed by Simons et al. (2013) in a transgenic mouse model of AA amyloidosis with a doxycycline-inducible system of expression of an amyloidogenic mouse SAA protein. In patients, AA amyloidosis derives from sustained overproduction of SAA associated with chronic inflammation. The plasma SAA concentration in healthy humans is 3 µg/ml, but the concentration can increase to more than 2000 µg/ml during acute phase inflammation response *(Ledue et al., 1998, Lachmann et al., 2007)*. Spleen, adrenal glands, gut and liver are affected with amyloid deposits in AA amyloidosis but the dominant feature is renal

dysfunction caused by amyloid deposits. Upon successful anti-inflammatory treatment which decreased the production of SAA, the amyloid deposits in the patients remained stable or regressed and the survival of the patients improved *(Lachmann et al., 2007)*. When the SAA transgenic mice were exposed to doxycycline in drinking water, SAA production dramatically increased to values only seen in severe inflammation in humans and the mice developed systemic amyloid deposits within 4-16 weeks. However, after the doxycycline withdrawal, the SAA transgene expression was switched off immediately leading to base-line, very low concentration of circulating mouse SAA and the amyloid load in the tissue of the amyloidotic transgenic mice slowly regressed *(Simons et al., 2013)*.

Therefore, the high serum concentration of the extremely amyloidogenic S52P variant TTR in the transgenic mice presented here should be sufficient for amyloid deposition.

Interestingly, the hTTR$^{S52P}$ transgenic males have almost twice as much of the TTR variant in the serum than transgenic females. Sex difference in TTR serum levels is also seen in humans with men having higher plasma levels of TTR than women although the difference is not so marked *(Maetzler et al., 2012, Smith and Goodman, 1971, Ingenbleek and De Visscher, 1979, Ingenbleek and Bernstein, 2015)*. Importantly, cardiac ATTR amyloidosis is almost exclusively seen in men *(Ng et al., 2005, Rapezzi et al., 2008, Pinney et al., 2013b)*. The sex-dependent mechanisms in male prevalence of ATTR cardiac amyloidosis are yet unexplained and the sex difference of TTR concentration in the hTTR$^{S52P}$ mice may be a useful characteristic for investigating the correlation between TTR concentration, sex hormones and amyloid deposition. There is no difference in albumin expression and albumin plasma concentration between men and women and between male and female mice suggesting that the activity of the albumin promoter used for the TTR$^{S52P}$ transgene expression is unlikely to explain the sex difference in TTR concentrations.

Although TTR is not secreted as a glycoprotein, fraction of the circulating hTTR was found to be N-glycosylated in the serum of $hTTR^{S52P}$ transgenic mice. N-glycosylation is a mainly co-translational, highly conserved process characterized by addition of a sugar complex to the nascent polypeptide chain as soon as it is translocated into ER, with functions such as accelerating protein folding *(Jitsuhara et al., 2002)*, increasing protein stability *(Culyba et al., 2011, Shental-Bechor and Levy, 2008)* and reducing aggregation by increasing solubility *(Sato et al., 2012)*. Proteins that are correctly folded and assembled pass the ER-quality control system and are trafficked to Golgi apparatus and their final destination through the secretory pathway. Proteins that are not folded correctly enter a process called endoplasmic reticulum-associated degradation (ERAD) *(Lippincott-Schwartz et al., 1988, McCracken and Brodsky, 1996)*. ERAD facilitates the translocation of proteins targeted for degradation from ER into cytosol, where these proteins enter the ubiquitin-proteasome machinery and are degraded *(Baldridge and Rapoport, 2016, Vembar and Brodsky, 2008)*. Most of secreted proteins are glycoproteins and the glycosylation pattern and N-glycan interactions play an important role in recognition of the protein folding status in the ER *(Liu et al., 1999, Helenius and Aebi, 2004, Kapoor et al., 2004)*. ER-quality control of non-glycosylated proteins is not that well characterised yet. Recently, studies done by Sato et al. on TTR as an example of non-glycosylated protein, whose pathological variants escape the ER-quality control and aggregate into amyloid fibrils in the extracellular spaces, provided an insight into the process of ER-quality control and ERAD of non-glycosylated proteins *(Sato et al., 2012)*. It was shown that unfolding of unstable TTR variants (D18G, V30M, L55P) exposes a cryptic N-glycosylation site near the C terminus at the asparagine side chain at the position 98 of TTR and that N-glycan is transferred to TTR post-translationally. The authors suggest that this may increase its solubility and prevent aggregation of the aggregation-prone variant in the ER in order to maintain cellular homeostasis *(Sato et al., 2012).* Further it was shown that post-translational N-glycosylation of TTR is the molecular switch that targets

the misfolded protein for degradation by proteasomes *(Sato et al., 2012)*. N-glycosylated TTR was detected in serum of the hTTR$^{S52P}$ transgenic mice presented in this project. In consistency with the finding presented here, it was recently reported that N-glycosylated TTR was detected in human plasma of TTR$^{V30M}$ carriers as well as in plasma of hTTR$^{V30M}$ transgenic mice *(Teixeira and Saraiva, 2013)*. Thus it seems that the TTR variants escape from the ER-quality control and ERAD systems with mechanisms not known yet.

In summary, transgenic mice expressing a highly amyloidogenic human TTR$^{S52P}$ have been successfully generated. These mice present with high plasma levels of the human TTR, one of the pre-requisites of amyloid formation *in vivo*. Moreover, fraction of the hTTR in serum of the transgenic mice was found to be N-glycosylated, a feature recently detected in human plasma of V30M variant carriers *(Teixeira and Saraiva, 2013)*, suggesting that a fraction of the human protein in these mice has escaped ER-associated degradation, a quality control mechanism that prevents secretion of misfolded proteins. This result indicates that TTR$^{S52P}$ in the transgenic mice has the propensity to misfold and potentially to form amyloid.

# 6 Assessment of amyloid deposition in hTTR$^{S52P}$ transgenic mice

## 6.1 Introduction

Cardiac involvement is the leading cause of morbidity and mortality in amyloidosis *(Falk, 2005, Dubrey et al., 1998)*. It is characterised by extracellular amyloid infiltration throughout the heart, with amyloid deposits occurring in ventricles and atria, within the vessels, in the valves and in the conduction system, causing restrictive cardiomyopathy and progressing to heart failure. Cardiac amyloidosis occurs in about 50 % of patients with AL amyloidosis *(Merlini, 2012)*, is a dominant feature in patients with wild-type ATTR amyloidosis and hereditary systemic ATTR amyloidosis, although in the most common type of hereditary systemic amyloidosis associated with TTR$^{V30M}$, cardiac involvement is not so common *(Rapezzi et al., 2006, Pinney et al., 2013b, Rapezzi et al., 2010)*, and is often found in AApoAI amyloidosis *(Mucchiano et al., 2001, Eriksson et al., 2009)*. In AA amyloidosis, amyloid cardiomyopathy is rare, affecting about 1 % of AA patients *(Lachmann et al., 2007)*.

In non-hereditary cardiac ATTR amyloidosis, which results from deposition of wild-type TTR as amyloid, the prevalence of the disease increases with age. In post-mortem analyses, wild-type TTR cardiac amyloid was found in 25 % of individuals over the age of 85, with moderate or severe deposits in >5 % *(Tanskanen et al., 2008)*. Such findings suggest that cardiac ATTR amyloidosis is much more common than is currently diagnosed and that many older people with cardiac ATTR amyloidosis are not identified, perhaps because the cause of heart failure is not thoroughly investigated.

In hereditary ATTR amyloidosis, associated with ~85 pathogenic TTR variants *(Benson and Kincaid, 2007, Dubrey et al., 2011)*, amyloid can occur in various organs and tissues. In most cases of hereditary ATTR amyloidosis, the hallmark is peripheral and autonomic nerve neuropathy associated with

clinical syndrome of familial amyloid polyneuropathy, in which cardiac amyloidosis can occur at a later stage of the disease *(Rapezzi et al., 2010)*. Some TTR variants are associated exclusively with familial amyloid cardiomyopathy. Among the TTR variants predominantly targeting the heart, $TTR^{V122I}$ is the most common type affecting 3-4 % of people of Afro-Caribbean descent *(Jacobson et al., 1997, Yamashita et al., 2005, Buxbaum et al., 2010)*. It is estimated that about 1.5 million African Americans carry the $TTR^{V122I}$ mutation and are at risk of development of ATTR cardiac amyloidosis *(Ruberg and Berk, 2012)*, which is clinically indistinguishable from the wild-type non-hereditary amyloidosis.

Diagnosis of cardiac amyloidosis is usually delayed but increasing availability of cardiovascular magnetic resonance imaging in recent years has led to a greater recognition of the disease *(Patel and Hawkins, 2015)*. Currently, about 100 new British patients per year are diagnosed in the NHS National Amyloidosis Centre (NAC) and the reported pattern of referral in the last 20 years showed that wild-type ATTR amyloidosis-related cardiomyopathy has increased greatly (from 0.2 % to more than 6.4 %) *(Wechalekar et al., 2016)*.

The prognosis for patients with cardiac amyloidosis is poor, although with new emerging treatment strategies the survival has been improved. AL cardiac amyloidosis has the worst prognosis with more than 50 % mortality within 6 months of the initial diagnosis *(Kumar et al., 2011)*, while ATTR cardiac amyloidosis prognosis is ~3 to 5 years *(Ruberg et al., 2012, Pinney et al., 2013b)*. Interestingly, cardiac ATTR amyloidosis is remarkably gender-specific and almost exclusively occurs in men *(Rapezzi et al., 2008, Pinney et al., 2013b, Ng et al., 2005)*. The reasons for this gender difference are not known.

Amyloid fibrils isolated from hereditary ATTR amyloidosis patients heterozygous for a TTR mutation showed that cardiac deposits *(Dwulet and Benson, 1986)* and deposits in the vitreous body of eye *(Thylen et al., 1993)* consist of wild-type as well as mutated TTR and the mutated protein makes up about two thirds of the ATTR amyloid deposits. Moreover, a major

component of the myocardial and vitreous *ex vivo* ATTR amyloid fibrils is a 49-127 C-terminal fragment of the TTR monomer, regardless of the presence or position of any amyloidogenic mutation *(Dwulet and Benson, 1986, Thylen et al., 1993, Bergstrom et al., 2005)*. These findings and follow up *in vitro* experiments suggested that a selective proteolytic cleavage between amino acids 48-49 of TTR may have an important role in destabilising the TTR tetramers *(Marcoux et al., 2015, Mangione et al., 2014)*. Destabilisation of the TTR tetramer leads to a release of the 49-127 truncated monomers that are highly amyloidogenic *(Marcoux et al., 2015)*.

To date, despite many attempts there is no animal model of cardiac amyloidosis suitable for studying the molecular mechanism of the disease, for testing emerging innovative treatments of cardiac amyloidosis, or new diagnostic imagining technologies.

In the previous chapter, generation and establishment of a new transgenic model expressing a highly amyloidogenic human $TTR^{S52P}$ variant have been presented. Amyloidosis caused by $TTR^{S52P}$ is a devastating disease with a clinical picture of rapidly progressing amyloid cardiomyopathy *(Booth et al., 1993, Mangione et al., 2014)*. Amyloid deposits are also found in the nerves, causing autonomic dysfunction and peripheral neuropathy, in thyroid, spleen, liver, kidneys and adrenal glands. $ATTR^{S52P}$ amyloidosis typically leads to death in early to mid-adult life, within five years of the onset of symptoms *(Booth et al., 1993, Stangou et al., 1998, Mangione et al., 2014)*. The clinical phenotype is among the most severe ever described in ATTR amyloidosis. The S52P variant TTR is the least stable known variant *(Marcoux et al., 2015, Mangione et al., 2014)*. *In vitro* experiments examining the amyloidogenic potential of wild-type TTR and five of the naturally occurring variants – $TTR^{S52P}$, $TTR^{V30M}$, $TTR^{L55P}$, $TTR^{V122I}$ and $TTR^{T119M}$ demonstrated that none of the full-length proteins formed amyloid fibrils under stirring in physiological conditions *(Mangione et al., 2014, Marcoux et al., 2015)*. However, the wild-type protein and all the variants except the non-amyloidogenic $TTR^{T119M}$ were susceptible to trypsin cleavage with the 49-127 fragment being released from

the proteolysed tetramer in each case and typical Congophilic fibrillar structures were rapidly formed *(Marcoux et al., 2015)*. The non-pathogenic $TTR^{T119M}$, expression of which actually protects carriers of amyloidogenic mutations from developing amyloidosis *(Hammarstrom et al., 2001)*, was resistant to proteolysis and did not form amyloid *(Marcoux et al., 2015)*. The $TTR^{S52P}$ was substantially more susceptible to cleavage that all the other variants and wild-type TTR *(Marcoux et al., 2015)*.

The susceptibility to proteolytic cleavage of the $TTR^{S52P}$ and other amyloidogenic variants and the effect of cleavage on conversion to amyloid provide strong evidence that cleavage precedes amyloid formation and is a key pathogenic event, as cleaved TTR is found in cardiac amyloid. Although it is not known yet which protease(s) catalyse the cleavage of TTR, nor the anatomical site at which this cleavage occurs, the hypothesis was that expression of the extremely amyloidogenic $TTR^{S52P}$ in mice may lead to a new model of cardiac ATTR amyloidosis. The $hTTR^{S52P}$ transgenic mice generated and described in the previous chapter present with high serum levels of the human TTR, one of the pre-requisites of amyloid formation *in vivo*, with evidence that fraction of the human protein in these mice has escaped ER-associated degradation, a quality control mechanism that prevents secretion of misfolded proteins suggesting propensity of the $TTR^{S52P}$ in the transgenic mice to misfold and potentially form amyloid.

The aims in support of the hypothesis were to assess spontaneous amyloid deposition in the human $TTR^{S52P}$ transgenic mice in the heart and other tissues in which ATTR amyloid deposition may occur in ATTR amyloidosis, by histological analysis using Congo red staining and immunohistochemistry. $hTTR^{S52P}$ transgenic mice on both, wild-type murine TTR and TTR-KO backgrounds were analysed to evaluate the effect of the mouse TTR on human TTR deposition and amyloid formation in the mice. The possibility of accelerating amyloid deposition by seeding the mice with amyloid-enhancing factor of ATTR amyloid tissue and/or amyloid fibrils was also investigated,

together with determining whether any cleavage of the S52P variant could be detected in the tissues of the transgenic mice.

## 6.2 Results

### 6.2.1 Assessment of spontaneous amyloid deposition in hTTR$^{S52P}$ transgenic mice

In humans, the TTR$^{S52P}$ variant is responsible for the most severe known ATTR amyloidosis with onset as early as the third decade. It is characterised by widespread ATTR amyloid deposits with prominent cardiac involvement and with deposits also found in autonomic and peripheral nerves, liver, spleen, kidney, adrenal and thyroid *(Mangione et al., 2014)*.

In the hTTR$^{S52P}$ transgenic mice, spontaneous amyloid deposition was assessed by Congo red staining of sections of fixed and wax embedded tissue and light microscopy with polarised light. Because of the extremely aggressive amyloidogenicity of the TTR$^{S52P}$ in patients, and the potential for deposition in many sites, the assessment involved a wide variety of tissues. The examined tissues were liver, heart, spleen, kidney, lung, tongue, stomach, gut, thyroid, submandibular gland, sublingual gland, parotid gland, adrenal, lacrymal gland, sciatic nerve, trigeminal ganglion, brain, skin, muscle and fat in hTTR$^{S52P}$ transgenic mice on both, wild-type and TTR-KO backgrounds. Because of the age-dependence in amyloid deposition typical for amyloidosis, the analysis was performed on mice 4 weeks old up to 24 months old. Age-matched non-transgenic wild-type and TTR-KO mice were also analysed as negative controls.

Although the transgenic mice had high levels of the aggressively amyloidogenic TTR$^{S52P}$ variant circulating in the plasma, no spontaneous amyloid deposition was detected in the transgenic mice, despite a thorough search of extensive tissue samples. The results of these analyses are summarised in Table 6.1.

| Spontaneous amyloid deposition | | | | | | | | | |
|---|---|---|---|---|---|---|---|---|---|
| Age | 1-2 months | | 6-12 months | | | 12-18 months | | 18-24 months | |
| Genotype | T/WT | T/KO | T/WT | T/Het | T/KO | T/WT | T/KO | T/WT | T/KO |
| Heart | 0/1 | 0/3 | 0/4 | 0/2 | 0/2 | 0/4 | 0/2 | 0/5 | - |
| Liver | 0/1 | 0/3 | 0/4 | 0/2 | 0/2 | 0/4 | 0/2 | 0/5 | - |
| Spleen | 0/1 | 0/3 | 0/4 | 0/2 | 0/2 | 0/4 | 0/2 | 0/5 | - |
| Kidney | 0/1 | 0/3 | 0/4 | 0/2 | 0/2 | 0/4 | 0/2 | 0/5 | - |
| Lung | 0/1 | 0/3 | 0/4 | 0/2 | - | 0/3 | - | 0/5 | - |
| Tongue | 0/1 | 0/3 | 0/3 | - | 0/1 | 0/3 | 0/2 | 0/5 | - |
| Adrenal | 0/1 | 0/3 | 0/4 | 0/2 | 0/1 | 0/3 | - | 0/5 | - |
| Brain | - | 0/3 | 0/4 | - | 0/1 | 0/3 | - | 0/5 | - |
| Trigeminal g. | - | 0/3 | - | - | - | 0/3 | - | 0/5 | - |
| Sciatic nerve | 0/1 | 0/3 | 0/4 | 0/2 | 0/1 | 0/4 | 0/2 | 0/5 | - |
| Thyroid | - | 0/1 | 0/4 | 0/2 | 0/1 | 0/3 | - | 0/5 | - |
| Salivary gland | 0/1 | 0/3 | 0/4 | 0/2 | 0/1 | 0/3 | - | 0/5 | - |
| (Submandibular) | - | - | 0/4 | 0/2 | 0/1 | 0/3 | - | 0/5 | - |
| (Sublingual) | - | - | 0/4 | - | 0/1 | 0/3 | - | 0/5 | - |
| (Parotid) | - | - | 0/4 | 0/2 | 0/1 | 0/3 | - | 0/5 | - |
| Gut | 0/1 | 0/3 | 0/4 | 0/2 | 0/2 | 0/3 | - | 0/5 | - |
| Stomach | 0/1 | 0/3 | 0/3 | - | 0/1 | 0/3 | - | 0/5 | - |
| Muscle | - | - | 0/4 | 0/2 | 0/1 | 0/3 | - | 0/5 | - |
| Fat | - | - | 0/4 | 0/2 | 0/1 | 0/4 | - | 0/5 | - |
| Skin | - | - | 0/4 | 0/2 | 0/1 | 0/3 | - | 0/5 | - |
| Eye | - | 0/3 | 0/4 | 0/2 | - | 0/1 | - | - | - |
| Lacrymal gland | - | 0/3 | - | - | - | 0/2 | - | 0/5 | - |
| Sex of mice | 0♂ 1♀ | 2♂ 1♀ | 0♂ 4♀ | 0♂ 2♂ | 2♂ 0♀ | 4♂ 0♀ | 1♂ 1♀ | 2♂ 3♀ | - |

***Table 6.1: Analysis of spontaneous amyloid deposition in hTTR$^{S52P}$ transgenic mice***

*Summary of tissue analysed by Congo red in hTTR$^{S52P}$ transgenic mice with both alleles of the murine TTR (T/WT), with one allele of the murine TTR (T/Het) and transgenic mice lacking the endogenous TTR (T/KO) at age groups 1-2 months old, 6-12 months old, 12-18 months old and 18-24 months old. The samples are scored as number of mice with amyloid / number of mice analysed for each tissue analysed. Because the transgenic males have higher concentrations of circulating hTTR than females, the sex of analysed mice in each age group for each genotype is also stated.*

### 6.2.2 TTR deposition in hTTR$^{S52P}$ transgenic mice

In ATTR amyloid patients, non-fibrillar deposits in early stages of disease have been identified *(Sousa et al., 2001)* suggesting that pre-amyloid forms of TTR may play a role in the pathogenesis of amyloidosis. Because no amyloid was found in the hTTR$^{S52P}$ transgenic mice, immunohistochemistry of wax embedded tissue was used to analyse TTR expression and TTR deposition in the transgenic mice on both, wild-type and TTR-KO background.

In the transgenic mice, the TTR$^{S52P}$ variant is expressed in the liver and therefore TTR signal was expected in the liver only. Some signal corresponding to plasma TTR was also expected in the tissues, but a different pattern, or more intensive and localised signal in the extracellular space, would also result from TTR deposition, pre-fibrillar aggregation or small amounts of TTR amyloid.

Because the anti-human TTR antibodies cross-reacted with denatured mouse TTR on Western blots, the specificity of Dako polyclonal anti-human TTR antibody (Table 2.3) to human TTR in fixed and wax embedded tissue was tested. Tissue of 6 months old transgenic mice on both wild-type and TTR-KO background (3 transgenic males and 1 transgenic female on TTR wild-type background, 2 transgenic males and 1 transgenic female on TTR-KO background) was immunostained together with tissues of 1 non-transgenic WT male and 1 non-transgenic TTR-KO male used as negative controls.

No signal was detected in the tissues of non-transgenic WT or TTR-KO mice showing that the antibody did not react with the mouse TTR in the fixed tissue of wild-type mice and thus confirming the specificity of the antibody to human TTR.

In the transgenic mice, strong human TTR signal was detected in the liver as expected. Notably, much stronger TTR signal was observed in the liver of six months old transgenic mice on wild-type background (n=4) in comparison with transgenic mice on TTR-KO background (n=3) and the observed TTR appeared to be localised intracellularly (Figure 6.1).

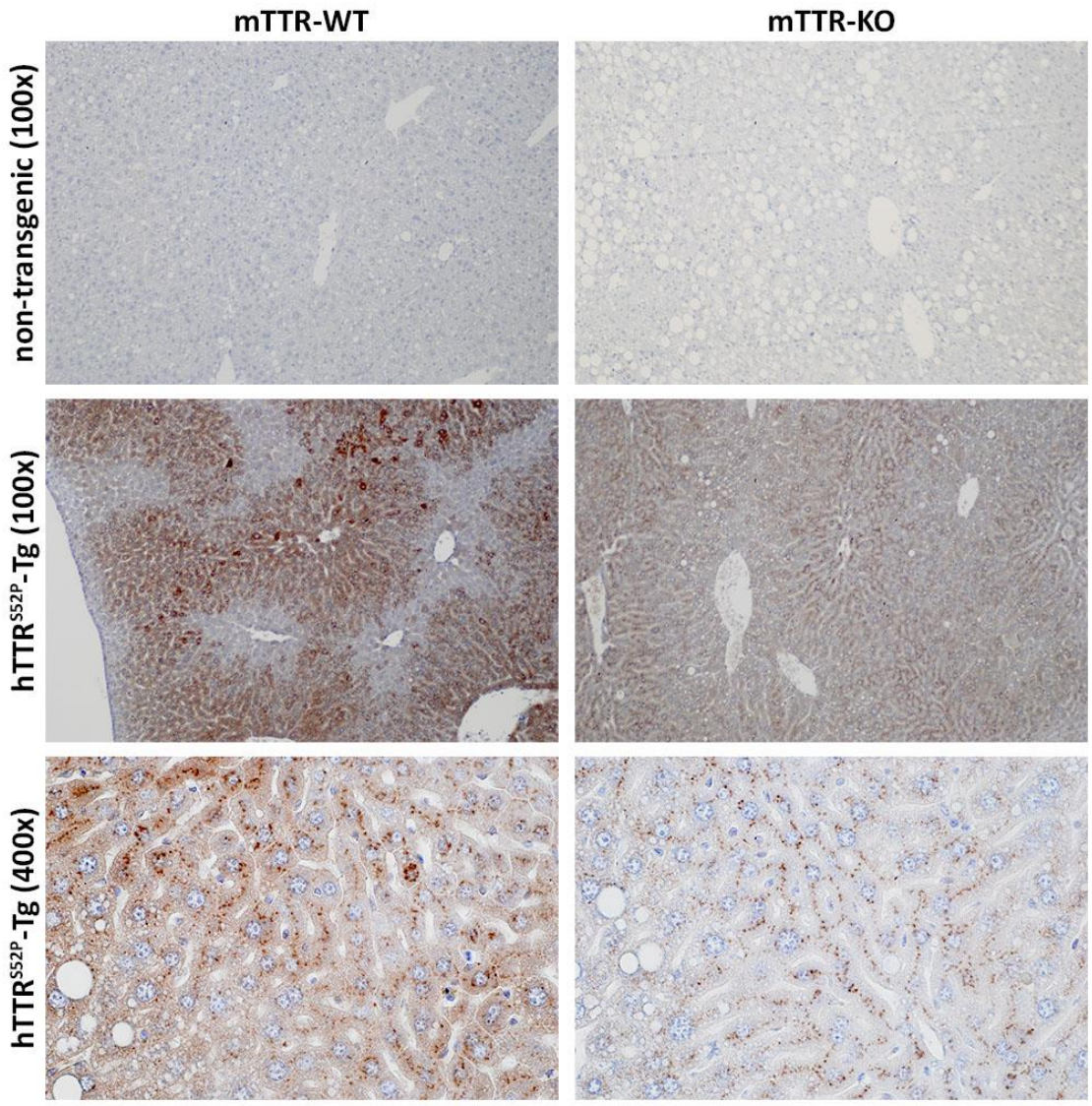


***Figure 6.1: TTR localisation in the liver of hTTR$^{S52P}$ transgenic mice***

*TTR signal in the liver was detected in 6-months old hTTR$^{S52P}$ transgenic mice (hTTR$^{S52P}$-Tg) on both backgrounds, mouse TTR wild-type (mTTR-WT) and mouse TTR knock-out (mTTR-KO), with hTTR$^{S52P}$-Tg/mTTR-WT mice (n=4) showing stronger TTR signal compared to hTTR$^{S52P}$-Tg/mTTR-KO mice (n=3). TTR appears to be localised intracellularly in the hepatocytes. The Dako anti-human TTR antibody used for the immunohistochemical analysis was confirmed to be human TTR-specific in fixed and wax embedded tissue as no TTR reactivity was detected in non-transgenic mTTR-WT mice. Liver of non-transgenic mTTR-KO mouse was used as a negative control. The figure shows representative images of 6 months old mice.*

In the heart of hTTR$^{S52P}$ transgenic mice, it was not possible to clearly distinguish whether the TTR signal observed on the muscle fibres of the heart originated from plasma TTR or whether the signal was due to genuine TTR deposition. However, some non-uniform concentration of signal was observed along the heart muscle fibres in the transgenic mice on both backgrounds. As expected, plasma TTR was detected within the blood vessels of the transgenic mice. (Figure 6.2).

Immunohistochemistry of the kidneys of hTTR$^{S52P}$ transgenic mice suggested that TTR may be depositing around the glomeruli in the transgenics on TTR-KO background, whereas no TTR deposition was detected in the kidneys of the transgenics on wild-type background. As expected, plasma TTR was detected within the blood vessels of the transgenic mice. No signal was observed in the kidneys of non-transgenic mice (Figure 6.3). No TTR deposition was detected in the spleen of transgenic mice. Some background non-specific signal was observed in the spleen of transgenic mice as well as non-transgenic controls (Figure 6.4).

Although none of the TTR deposits were Congophilic, these results suggested that TTR may be accumulating in extracellular spaces. This is consistent with reports of pre-fibrillar aggregates.

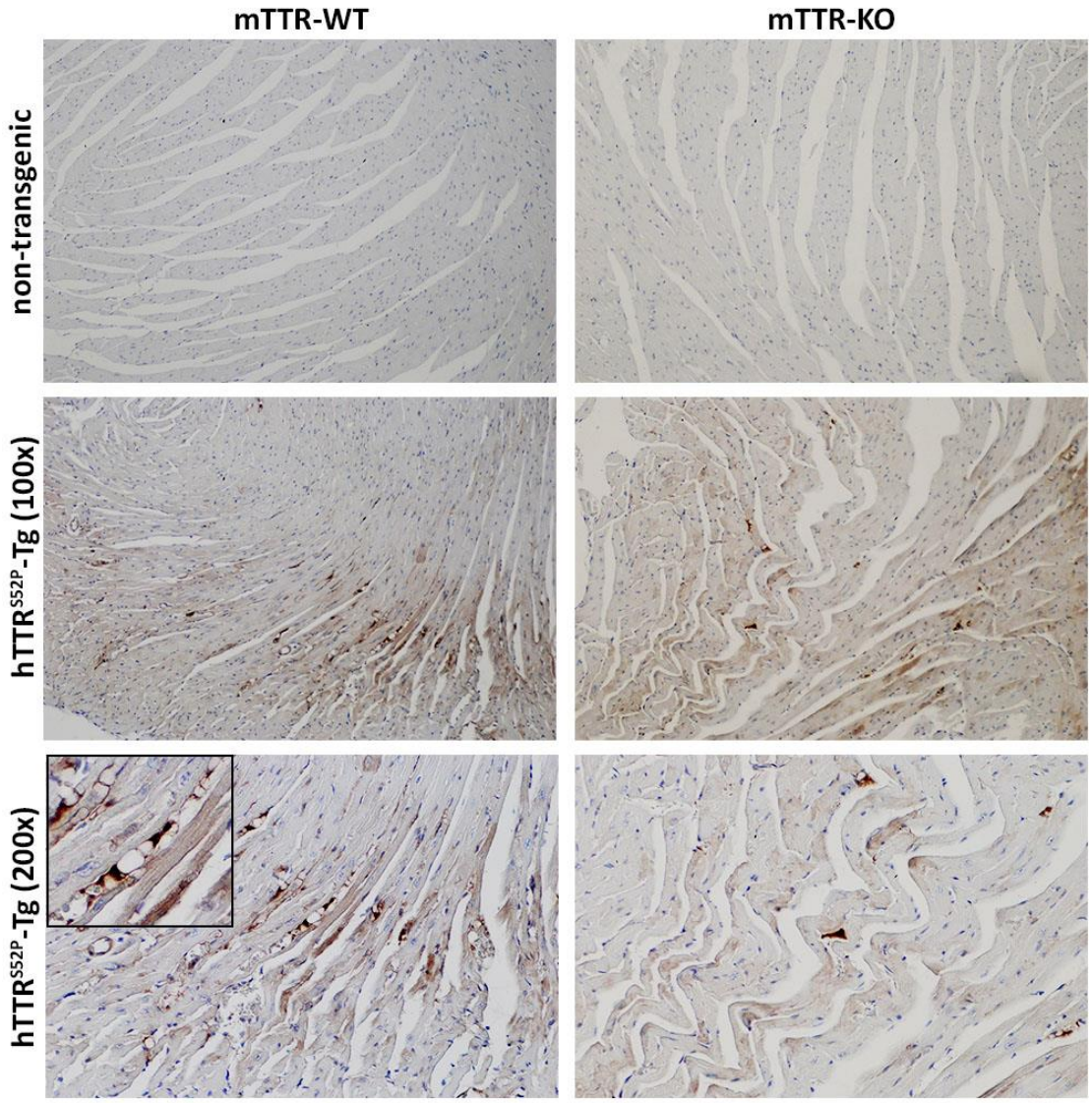


***Figure 6.2: TTR localisation in the heart of hTTR$^{S52P}$ transgenic mice***

*TTR signal in the heart was detected in 6-months old hTTR$^{S52P}$ transgenic mice (hTTR$^{S52P}$-Tg) on both backgrounds, mouse TTR wild-type (mTTR-WT) and mouse TTR knock-out (mTTR-KO) by immunohistochemistry with Dako anti-human TTR antibody. The TTR signal in hTTR$^{S52P}$-Tg/mTTR-KO mice (n=3) seemed more wide-spread than in hTTR$^{S52P}$-Tg/mTTR-WT mice (n=4). TTR signal is also seen in blood vessels within the heart in the hTTR$^{S52P}$-Tg/mTTR-WT mice, shown in the insert (400x). Heart of non-transgenic mTTR-WT mouse and non-transgenic mTTR-KO mouse were used as negative controls. The figure shows representative images of 6 months old mice.*

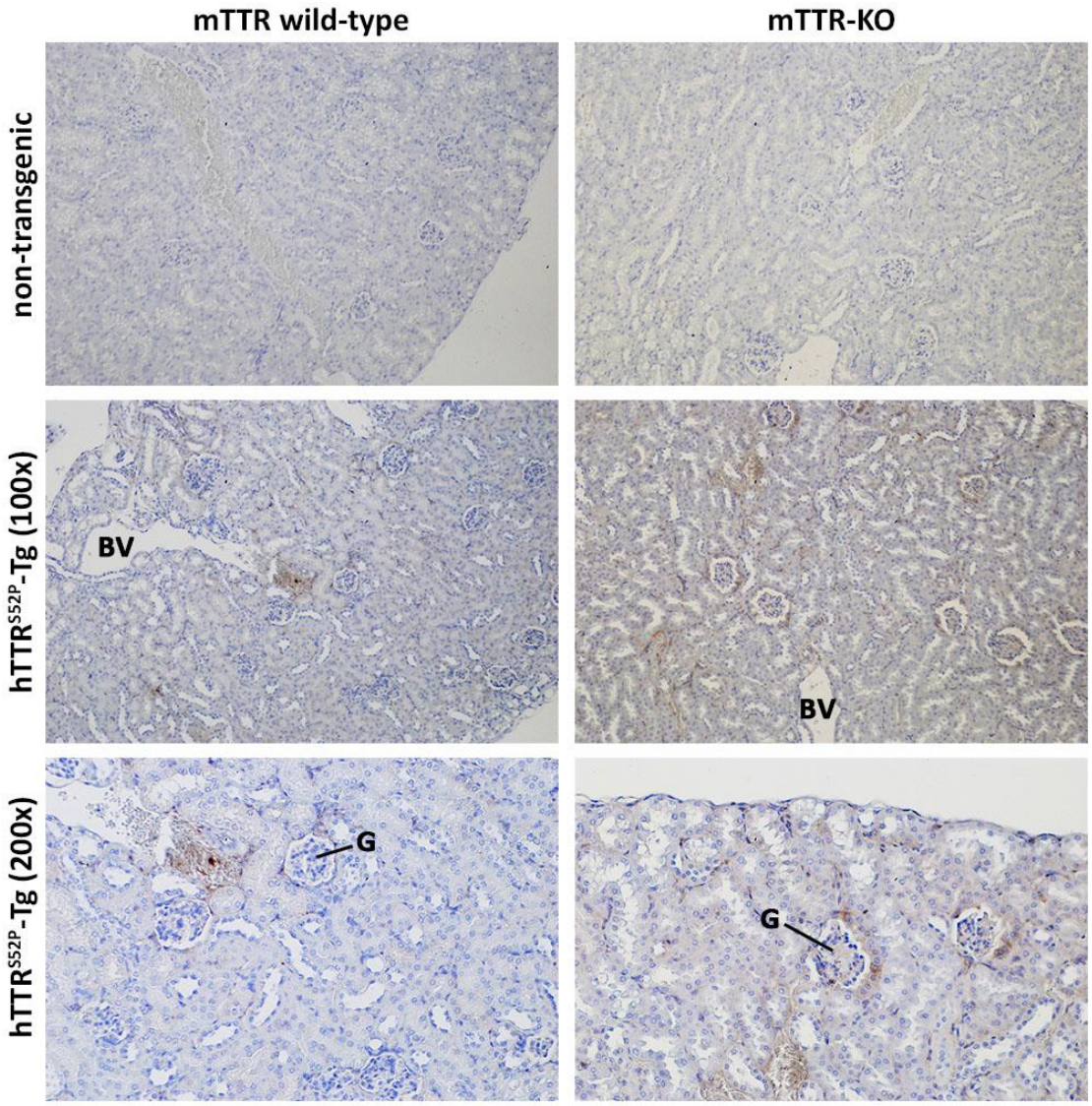


***Figure 6.3: TTR localisation in the kidney of hTTR$^{S52P}$ transgenic mice***

*Immunohistochemistry of the kidney of hTTR$^{S52P}$ transgenic mice (hTTR$^{S52P}$-Tg). TTR signal was detected in the hTTR$^{S52P}$-Tg mice on TTR knock-out (mTTR-KO) background, notably around the glomeruli (G). Plasma TTR was observed within the blood vessels in transgenic mice on both backgrounds. Kidney of non-transgenic wild-type mouse (mTTR-WT) and non-transgenic mTTR-KO mouse were used as negative controls. The figure shows representative images of hTTR$^{S52P}$-Tg/mTTR-WT (n=4) and hTTR$^{S52P}$-Tg/mTTR-KO (n=3) mice.*

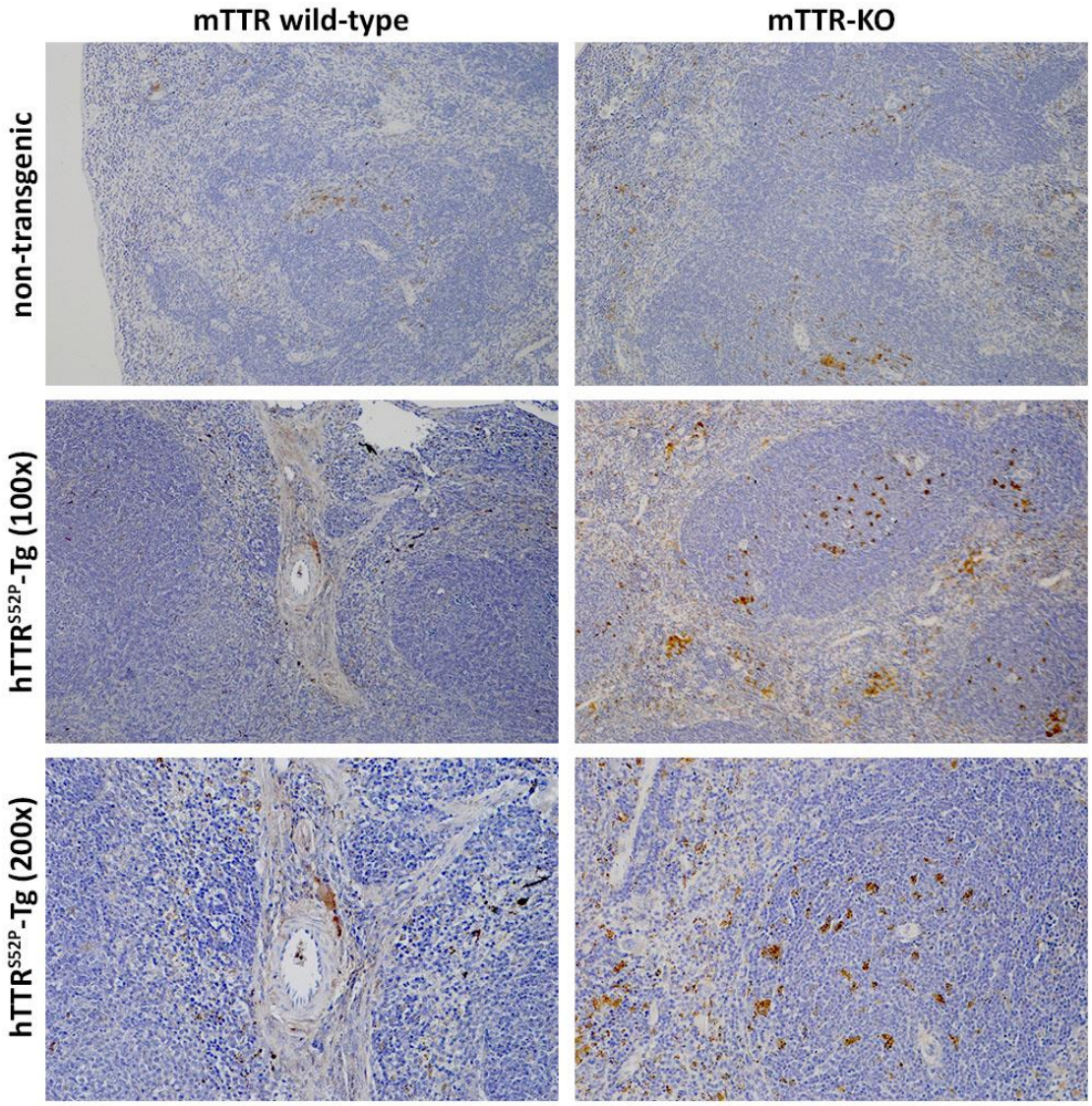


***Figure 6.4: TTR in the spleen of hTTR$^{S52P}$ transgenic mice***

*Immunohistochemistry of the spleen of the hTTR$^{S52P}$ transgenic mice (hTTR$^{S52P}$-Tg). No TTR signal was detected in the hTTR$^{S52P}$-Tg mice as well as in the non-transgenic controls. Some non-specific background staining was seen in the spleens of all mice analysed. The figure shows representative images of hTTR$^{S52P}$-Tg/mTTR-WT (n=4) and hTTR$^{S52P}$-Tg/mTTR-KO (n=3) mice.*

Because amyloid deposition is time dependent, immunohistochemistry for hTTR was performed on tissues of 4-week old $hTTR^{S52P}$ transgenic mice on wild-type background (n=3) and compared with 22-months old $hTTR^{S52P}$ transgenic mice on wild-type background (n=3). Although in most cases the patterns of staining were broadly similar, some consistent differences were evident. The tissues analysed included heart, liver, kidney, spleen, salivary gland, tongue, lung, intestine, adrenal and sciatic nerve. As TTR is expressed in the liver, TTR signal was detected in the hepatocytes of young transgenic mice with the signal evenly distributed throughout the tissue. In the liver of aged mice, the pattern of expression was different from the young mice, with the TTR signal concentrated around portal veins. TTR signal was also detected in the muscle tissue of heart and tongue in both young and aged transgenic mice. However, in the aged mice, the TTR was concentrated around the blood vessels within heart and tongue. Similarly, in the kidney cortex, salivary gland and sciatic nerve, TTR signal was detected around blood vessels in the aged transgenic animals, whereas no TTR signal was detected in the equivalent sites in young transgenic mice. In the kidney, TTR signal was detected in the collecting ducts in both, the young and aged mice. Interestingly, TTR signal was observed in the kidney glomeruli in old transgenic mice on TTR-KO background but not in transgenic mice on wild-type background. Some TTR signal was seen in the adrenal gland of young and aged transgenic mice but no difference in the signal was observed between young and aged animals. No TTR signal was seen in the intestine in either young or old mice. The results are shown in Figures 6.5 and 6.6.

The increased TTR signal in aged transgenic mice was observed mostly around blood vessels, a site of amyloid deposition commonly observed in systemic amyloidosis. As the $TTR^{S52P}$ expression was confirmed exclusively in the liver, the observed increase in TTR signal in the analysed tissues suggested that with advancing age, the TTR was accumulating in the tissues, an observation consistent with very low levels of amyloid deposition and/or pre-fibrillar aggregation.

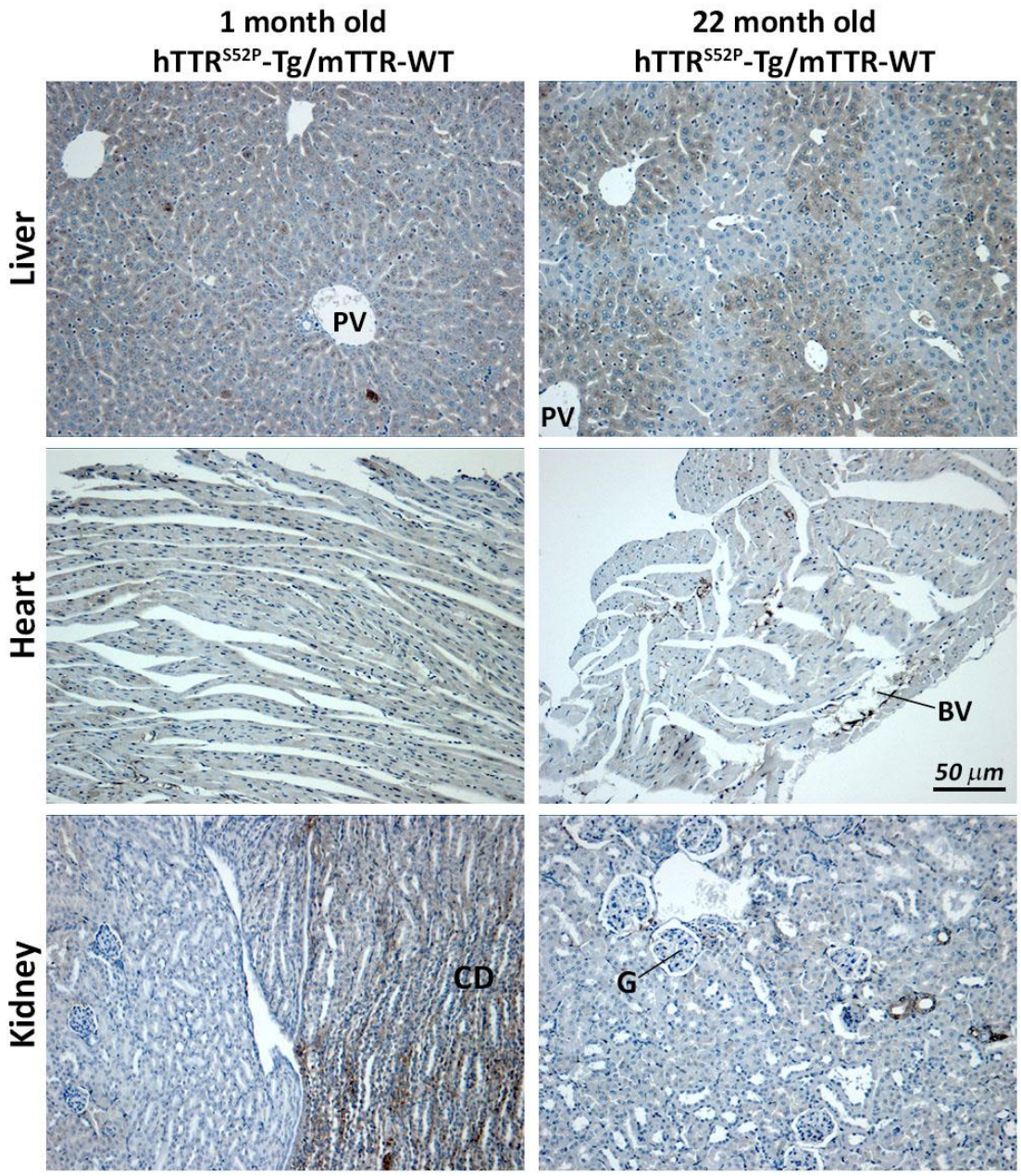


***Figure 6.5: Comparison of hTTR localisation between young and old hTTR$^{S52P}$ transgenic mice***

*Immunohistochemistry of hTTR$^{S52P}$ transgenic mice on wild-type background using Dako anti-human TTR antibody. Representative images of three 4-week old transgenic mice and three 22-months old transgenic mice are shown. In the aged mice, strong hTTR signal was detected around portal veins (PV). In the kidney, hTTR was observed in the collecting ducts (CD) in young and aged mice but no TTR signal was observed in the glomeruli (G). Strong TTR signal was detected around blood vessels (BV) in the heart of aged mice.*

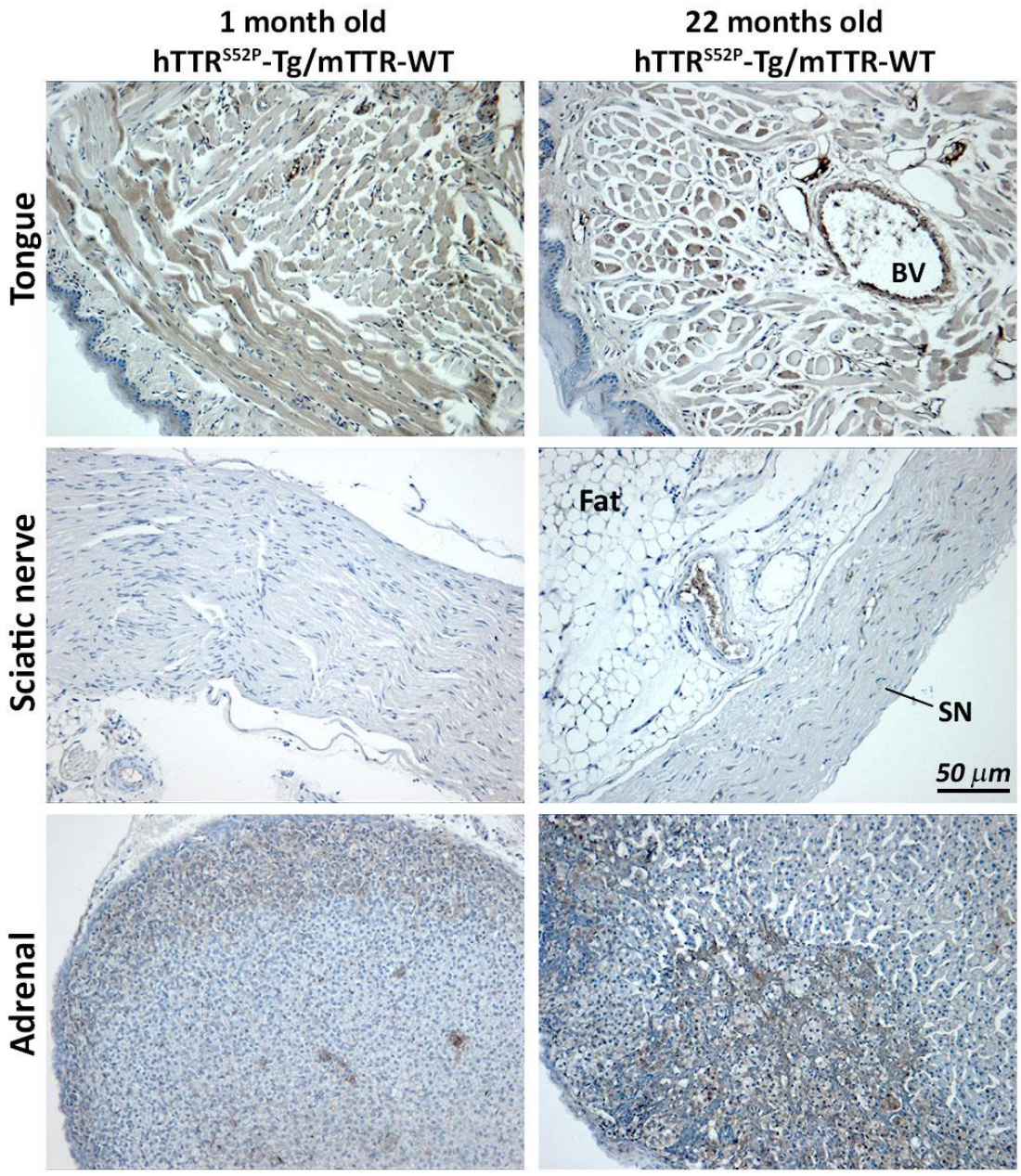


***Figure 6.6: Comparison of hTTR localisation between young and old hTTR$^{S52P}$ transgenic mice***

*Immunohistochemistry of hTTR$^{S52P}$ transgenic mice on wild-type background using Dako anti-human TTR antibody. Representative images of three 4-week old transgenic mice and three 22-months old transgenic mice are shown. Strong TTR signal was detected in the muscle tissue of the tongue in both, young and aged transgenic mice, but the aged mice also showed hTTR localisation around the blood vessels (BV) in the tongue. Some hTTR is also seen around blood vessels in the sciatic nerve (SN).*

### 6.2.3 Priming of amyloid deposition in hTTR$^{S52P}$ transgenic mice

Although no spontaneous ATTR amyloid deposition was observed in the hTTR$^{S52P}$ transgenic mice despite their high concentration of the TTR$^{S52P}$ in the circulation, TTR accumulation in various organs including the heart, a prominent site of ATTR deposition in the TTR$^{S52P}$ patients, was observed. The TTR deposits may represent non-Congophilic pre-fibrillar aggregates of the amyloidogenic variant. In the process of amyloid formation, there is always a lag phase between the first appearance of the potentially amyloidogenic protein and the deposition of clinically significant amyloid. In mice, the lag phase can be significantly shortened by administration of an extract of tissue containing amyloid, called amyloid-enhancing factor (AEF) *(Willerson et al., 1969)*. AEF serves to seed fibril formation and accelerates amyloid deposition of the respective amyloid fibril precursor protein *(Axelrad et al., 1982)*. Amyloid fibrils extracted from amyloidotic tissue and *in vitro* prepared amyloid fibrils have shown to have the same effect *in vivo* as AEF *(Ganowiak et al., 1994, Johan et al., 1998)*. Therefore, the possibility of priming the TTR amyloid deposition in the hTTR$^{S52P}$ transgenic mice by seeding the transgenic mice with an extract of ATTR$^{S52P}$ amyloidotic spleen and/or *ex vivo*-isolated ATTR$^{S52P}$ amyloid fibrils was investigated.

Spleen from an ATTR$^{S52P}$ amyloidosis patient with abundant infiltration of amyloid was provided by Dr Glenys Tennent (Centre for amyloidosis and acute phase proteins, UCL) from Amyloid Research Tissue bank and used to prepared tissue extract for AEF-injections. *Ex-vivo* ATTR$^{S52P}$ fibrils were isolated from the spleen by Dr Patrizia Mangione (Centre for amyloidosis and acute phase proteins, UCL).

3 experimental cohorts of amyloid-seeded mice were set up to evaluate the possibility of accelerating amyloid deposition in the hTTR$^{S52P}$ transgenic mice:

hTTR$^{S52P}$ Cohort I was injected with 10 µg of human ATTR$^{S52P}$ *ex vivo*-isolated amyloid fibrils;

hTTR$^{S52P}$ Cohort II was injected with ATTR$^{S52P}$ AEF prepared from human spleen;

hTTR$^{S52P}$ Cohort III was injected with the combination of both, 10 µg of human ATTR$^{S52P}$ *ex vivo*-isolated amyloid fibrils followed by ATTR$^{S52P}$ AEF.

Outline of the seeding experiments is shown in Figure 6.7.

Similarly like in the hβ2m$^{D76N}$ project (section 4.2.5.2), whole body retention of intravenously administered radiolabelled $^{125}$I-hSAP was carried out in all experimental mice to monitor amyloid deposition *in vivo (Hawkins et al., 1988)*. The injections and counts of radiolabeled material were performed by Dr Stephan Ellmerich (Centre for amyloidosis and acute phase proteins, UCL). The baseline level of $^{125}$I-hSAP retention 48 hours after administration of the radiolabelled tracer in untreated control mice was <10 %.

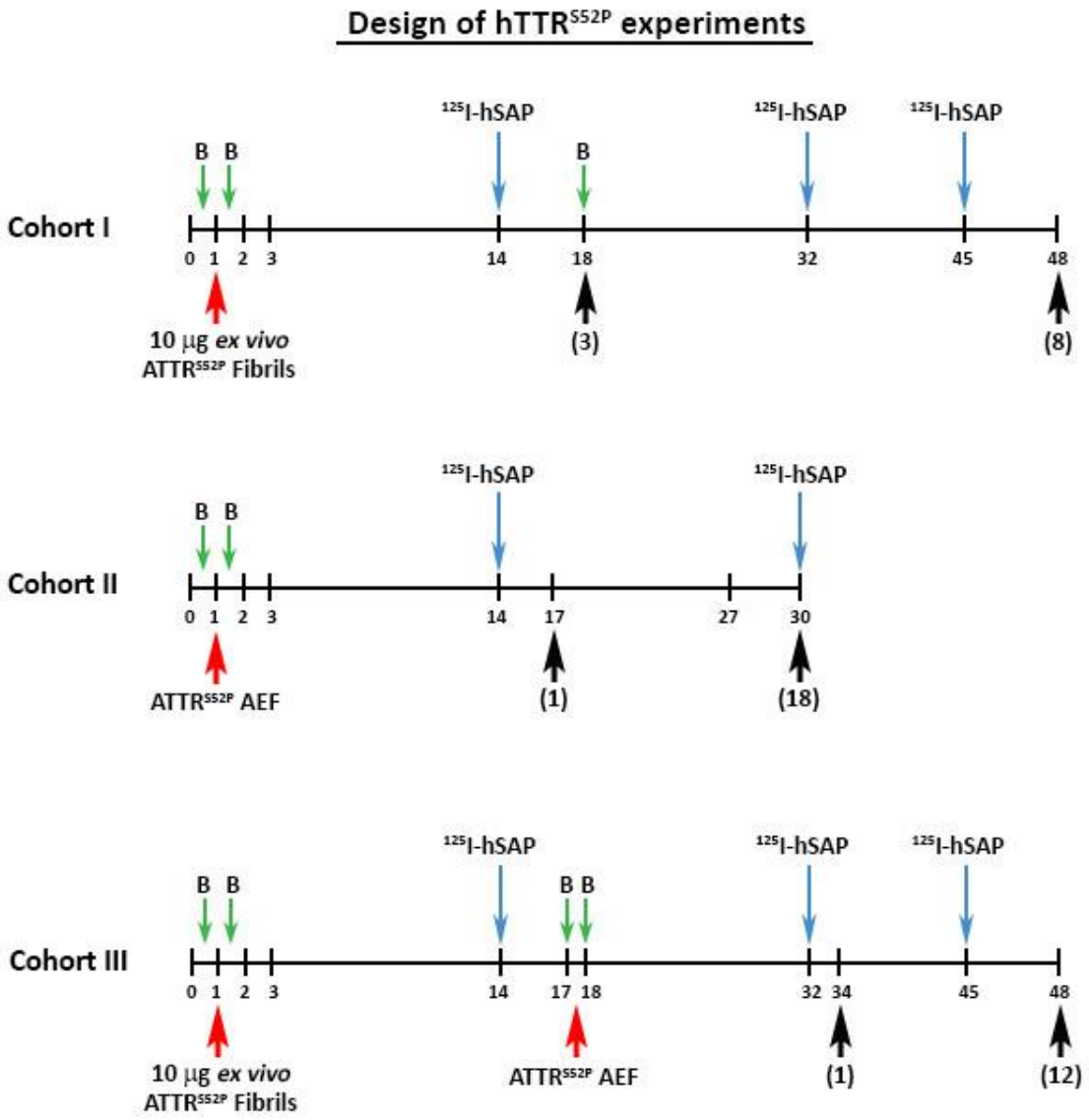


***Figure 6.7: Timeline of seeding experiments of hTTR$^{S52P}$ transgenic mice***

*3 cohorts of hTTR$^{S52P}$ transgenic and control mice were set up to prime amyloid deposition by intravenous injections of 10 µg of human ATTR$^{S52P}$ ex vivo-isolated amyloid fibrils (I), ATTR$^{S52P}$ spleen extract AEF (II) and combination of both, ex-vivo fibrils and AEF (III). The timescale indicates numbers of weeks. Amyloid seeding injections (red arrow), blood sample collection (green arrow), $^{125}$I-human SAP whole body retention assay (blue arrow) and time-point when seeded animals were taken for analysis (black arrow) with the number of animals killed at each time point shown in the brackets are indicated.*

**hTTR$^{S52P}$ Cohort I**

Cohort I consisted of transgenic (T) and non-transgenic mice on mTTR wild-type background (WT), mTTR heterozygous background (Het) and TTR-KO background (KO). The mice were seeded by intravenous injection of 10 µg of human ATTR$^{S52P}$ *ex vivo*-isolated amyloid fibrils when they were 3-4 months old. The group of seeded mice was as follows: 1 T/WT male, 1 T/WT female, 1 T/Het male, 1 T/Het female, 2 T/KO males, 2 T/KO females, with 2 WT females and 1 KO male as non-transgenic controls. Blood samples were collected from all mice prior and 72 hours after the fibril injections to measure plasma SAA concentration to check that the mice did not develop persistent inflammation after the administration of the fibrils. In all mice, no difference in the measured concentrations of SAA was seen between pre- and post-fibril injection time-points (39.43 ± 71.5 µg/ml (n=14), 23.36 ± 43.3 µg/ml (n=14), respectively). 14 weeks after the seeding, the results of the $^{125}$I-hSAP retention assay did not indicate amyloid deposition in the animals. 18 weeks after the seeding, two transgenic females (T/Het and T/KO) and one T/WT male were killed, the tissues were harvested and analysed by histochemistry for amyloid deposition. The analysed tissues included: liver, heart, kidney, spleen, tongue, lung, sciatic nerve, adrenal, thyroid, salivary gland dissected into submandibular, sublingual and parotid glands, lachrymal gland, intestine, stomach, brain, eye, optic nerve, trigeminal ganglion, skin, muscle and fat. Amyloid was found in the tongue of the seeded transgenic male mouse. No amyloid was found in the tissues of transgenic females. The remaining mice were kept and monitored by $^{125}$I-hSAP whole body retention at weeks 32 and 45 after seeding with no amyloid detected by this assay. The experiment was terminated 48 weeks after seeding and liver, heart, kidney, spleen, tongue, sciatic nerve and adrenal were collected for analysis. Congo red staining and polarized light microscopy were used for amyloid detection. In the three remaining fibril-seeded transgenic males, amyloid was detected in the heart (3/3) and tongue (2/3) (Figure 6.8). One T/KO female also had amyloid in the heart and tongue. In one T/WT female, no amyloid was detected. No amyloid

was detected in seeded non-transgenic controls. The numbers and genotypes of the experimental mice, tissues analysed and the outcome of the experiment are summarised in Table 6.2.

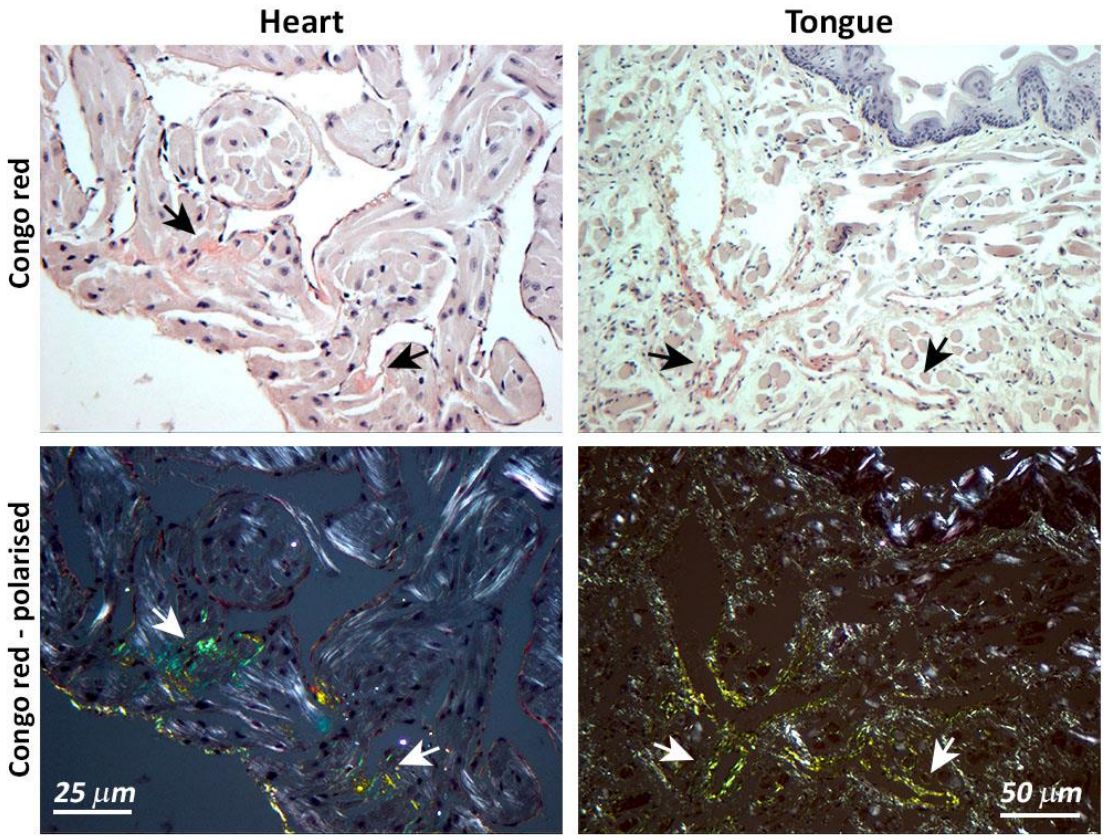


***Figure 6.8: Amyloid deposition in fibril-seeded mice (Cohort I)***

*Amyloid deposits were detected in the heart and the tongue of fibril-seeded hTTR$^{S52P}$ transgenic mice by Congo red. Amyloid (arrows) is stained red and exhibits green birefringence under polarised light. (The figure shows 14 months old transgenic male on mTTR-KO background analysed 11 months after seeding.)*

| | Cohort I - Amyloid deposition | | | | | | | |
|---|---|---|---|---|---|---|---|---|
| **Genotype** | **T/WT** | | **T/Het** | | **T/KO** | | **-ve/KO** | **-ve/WT** |
| **Sex** | ♂ | ♀ | ♂ | ♀ | ♂ | ♀ | ♂ | ♀ |
| **Heart** | 0/1 | 0/1 | **1/1** | 0/1 | **2/2** | **1/2** | 0/1 | 0/2 |
| **Tongue** | **1/1** | 0/1 | **1/1** | 0/1 | **1/1** | **1/2** | 0/1 | 0/2 |
| Liver | 0/1 | 0/1 | 0/1 | 0/1 | 0/2 | 0/2 | 0/1 | 0/2 |
| Kidney | 0/1 | 0/1 | 0/1 | 0/1 | 0/2 | 0/2 | 0/1 | 0/2 |
| Spleen | 0/1 | 0/1 | 0/1 | 0/1 | 0/2 | 0/2 | 0/1 | 0/2 |
| Sciatic nerve | 0/1 | 0/1 | 0/1 | 0/1 | 0/2 | 0/2 | 0/1 | 0/2 |
| Adrenal | 0/1 | 0/1 | 0/1 | 0/1 | 0/2 | 0/2 | 0/1 | 0/2 |
| Brain | 0/1 | - | - | 0/1 | - | 0/1 | - | - |
| Trigeminal g. | 0/1 | - | - | 0/1 | - | 0/1 | - | - |
| Lung | 0/1 | - | - | 0/1 | - | 0/1 | - | - |
| Thyroid | 0/1 | - | - | 0/1 | - | 0/1 | - | - |
| Salivary gland | 0/1 | - | - | 0/1 | - | 0/1 | - | - |
| (Submandibular) | 0/1 | - | - | 0/1 | - | 0/1 | - | - |
| (Sublingual) | 0/1 | - | - | 0/1 | - | 0/1 | - | - |
| (Parotid) | 0/1 | - | - | 0/1 | - | 0/1 | - | - |
| Intestine | 0/1 | - | - | 0/1 | - | 0/1 | - | - |
| Stomach | 0/1 | - | - | 0/1 | - | 0/1 | - | - |
| Muscle | 0/1 | - | - | 0/1 | - | 0/1 | - | - |
| Fat | 0/1 | - | - | 0/1 | - | 0/1 | - | - |
| Skin | 0/1 | - | - | 0/1 | - | 0/1 | - | - |
| Eye | 0/1 | - | - | 0/1 | - | 0/1 | - | - |
| Optic nerve | 0/1 | - | - | 0/1 | - | 0/1 | - | - |
| Lacrymal gland | 0/1 | - | - | 0/1 | - | 0/1 | - | - |

***Table 6.2: Cohort I – Primed amyloid deposition in hTTR$^{S52P}$ transgenic mice***

*Summary of tissues analysed by Congo red in hTTR$^{S52P}$ transgenic (T) mice on mTTR wild-type (WT), mTTR heterozygous (Het) and mTTR-KO background (KO) seeded with 10 µg of human ATTR$^{S52P}$ ex vivo-isolated amyloid fibrils. Amyloid deposition was observed in all 4 seeded transgenic males and in 1 seeded transgenic female. The amyloid deposits were localised in the heart and tongue. 3 non-transgenic controls were injected with the fibrils as negative controls. The samples are scored as number of mice with amyloid / number of mice analysed for each tissue analysed.*

**hTTR$^{S52P}$ Cohort II**

Cohort II consisted of transgenic (T) and non-transgenic mice on mTTR wild-type background (WT), mTTR heterozygous background (Het) and TTR-KO background (KO). 6-8 months old mice were intravenously injected with 200 µl of amyloid enhancing factor (AEF) prepared from a spleen of an ATTR$^{S52P}$ amyloidosis patient (AEF). The group of seeded mice was as follows: 3 T/WT males, 2 T/WT females, 3 T/Het males, 2 T/Het females, 3 T/KO males, 1 T/KO female and 2 KO males and 3 KO females as non-transgenic controls. Blood samples were collected from all mice prior and 72 hours after the AEF injections to measure plasma SAA levels concentration which showed that the mice did not develop persistent inflammation after the administration of the AEF. 14 weeks after the seeding, the results of the $^{125}$I-hSAP retention assay did not indicate amyloid deposition in the animals. 17 weeks after the seeding, one T/WT male and one T/KO female were killed and the tissues were harvested and analysed by histochemistry for amyloid deposition. The analysed tissues included: liver, heart, kidney, spleen, tongue, lung, sciatic nerve, adrenal, thyroid, salivary gland dissected into submandibular, sublingual and parotid glands, lachrymal gland, intestine, stomach, brain, eye, optic nerve, trigeminal ganglion, skin, muscle and fat. Amyloid was detected in the heart and tongue of the seeded transgenic male, no amyloid was detected in the T/KO seeded female.

27 weeks after the AEF injection, the remaining mice were analysed with $^{125}$I-hSAP whole body retention and none of the mice showed retention over the baseline 10 %. At week 30 after the AEF, the experiment was terminated, all mice were killed and heart, liver, kidney, spleen, tongue and sciatic nerve were collected for analysis. Congo red staining and polarized light microscopy were used for amyloid detection. Of the 9 hTTR$^{S52P}$ transgenic males seeded with AEF, 8 had amyloid in the heart and 8 had amyloid in the tongue (Figure 6.9). 2 of the 5 hTTR$^{S52P}$ transgenic females seeded with AEF had amyloid in the tongue. No amyloid was detected in the 5 non-transgenic mice seeded

with AEF. The numbers and genotypes of the experimental mice, tissues analysed and the outcome of the experiment are summarised in Table 6.3.

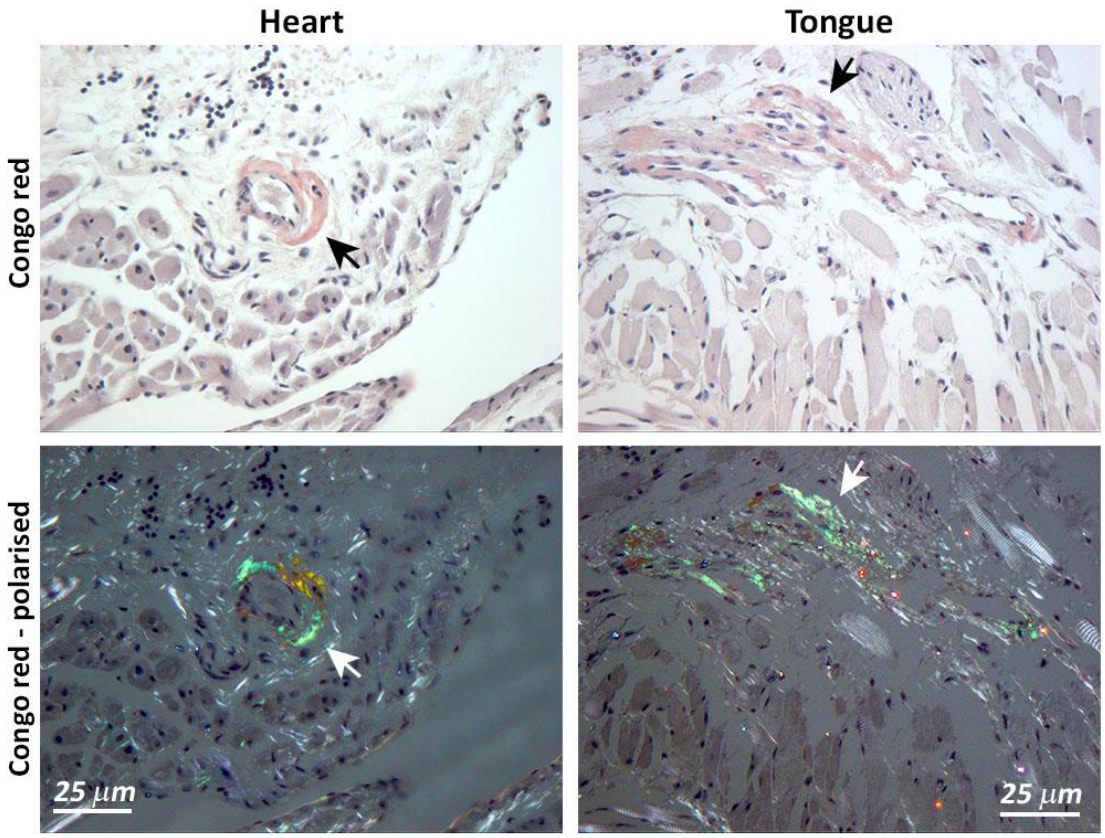


***Figure 6.9: Amyloid deposition in AEF-seeded mice (Cohort II)***

*Amyloid deposits were detected in the heart and the tongue of AEF-seeded hTTR$^{S52P}$ transgenic mice by Congo red. Amyloid (arrows) is stained red and exhibits green birefringence under polarised light. (The figure shows the heart of a 14 months old transgenic male on mTTR-KO background analysed 7 months after seeding, and the tongue of a 10 months old old transgenic male on wild-type background analysed 4 months after seeding).*

| | Cohort II – Amyloid deposition | | | | | | | |
|---|---|---|---|---|---|---|---|---|
| **Genotype** | **T/WT** | | **T/Het** | | **T/KO** | | **-ve/KO** | **-ve/KO** |
| **Sex** | ♂ | ♀ | ♂ | ♀ | ♂ | ♀ | ♂ | ♀ |
| **Heart** | **3/3** | 0/2 | **3/3** | 0/2 | **2/3** | 0/1 | 0/2 | 0/3 |
| **Tongue** | **3/3** | **2/2** | **2/3** | 0/2 | **3/3** | 0/1 | 0/2 | 0/3 |
| Liver | 0/3 | 0/2 | 0/3 | 0/2 | 0/3 | 0/1 | 0/2 | 0/3 |
| Kidney | 0/3 | 0/2 | 0/3 | 0/2 | 0/3 | 0/1 | 0/2 | 0/3 |
| Spleen | 0/3 | 0/2 | 0/3 | 0/2 | 0/3 | 0/1 | 0/2 | 0/3 |
| Sciatic nerve | 0/3 | 0/2 | 0/3 | 0/2 | 0/3 | 0/1 | 0/2 | 0/3 |
| Adrenal | 0/3 | 0/2 | 0/3 | 0/2 | 0/3 | 0/1 | 0/2 | 0/3 |
| Brain | 0/1 | - | - | - | - | - | - | - |
| Trigeminal g. | 0/1 | - | - | - | - | - | - | - |
| Lung | 0/1 | - | - | - | - | 0/1 | - | - |
| Thyroid | 0/1 | - | - | - | - | - | - | - |
| Salivary gland | 0/1 | - | - | - | - | 0/1 | - | - |
| (Submandibular) | 0/1 | - | - | - | - | - | - | - |
| (Sublingual) | 0/1 | - | - | - | - | - | - | - |
| (Parotid) | 0/1 | - | - | - | - | - | - | - |
| Intestine | 0/1 | - | - | - | - | 0/1 | - | - |
| Stomach | 0/1 | - | - | - | - | 0/1 | - | - |
| Muscle | 0/1 | - | - | - | - | 0/1 | - | - |
| Fat | 0/1 | - | - | - | - | 0/1 | - | - |
| Skin | 0/1 | - | - | - | - | - | - | - |
| Eye | 0/1 | - | - | - | - | - | - | - |
| Optic nerve | 0/1 | - | - | - | - | - | - | - |
| Lacrymal gland | 0/1 | - | - | - | - | 0/1 | - | - |

***Table 6.3: Cohort II – Primed amyloid deposition in hTTR$^{S52P}$ transgenic mice***

*Summary of tissues analysed by Congo red in hTTR$^{S52P}$ transgenic (T) mice on mTTR wild-type (WT), mTTR heterozygous (Het) and mTTR-KO background (KO) seeded with ATTR$^{S52P}$ spleen extract (AEF). Amyloid deposition was observed in all 9 seeded transgenic males and 2 seeded transgenic females. The amyloid deposits were localised in the heart and tongue. 5 non-transgenic controls were also injected with the fibrils as negative controls. The samples are scored as number of mice with amyloid / number of mice analysed for each tissue analysed.*

## hTTR$^{S52P}$ Cohort III

In cohort III, 3-4 months old transgenic (T) and non-transgenic mice on mTTR wild-type background (WT), mTTR heterozygous background (Het) and TTR-KO background (KO) were intravenously injected with combination of 10 µg of

human ATTR$^{S52P}$ *ex vivo*-isolated amyloid fibrils, and ATTR$^{S52P}$ spleen AEF. The experimental group consisted of 1 T/WT male, 1 T/WT female, 1 T/Het male, 2 T/Het females, 3 T/KO males, 1 T/KO female and 2 wild-type mice and 2 KO mice as non-transgenic controls. The mice were seeded at week 1 with 10 µg of human ATTR$^{S52P}$ *ex vivo*-isolated amyloid fibrils and bled prior and 72 hours after the fibril injections to measure plasma SAA levels concentration. The SAA concentrations before and after the seeding (33.2 ± 38.6 µg/ml (n=13) and 30.9 ± 31.0 µg/ml (n=13), respectively) showed that the mice did not develop prolonged inflammation after the administration of the fibrils. 14 weeks after the seeding, $^{125}$I-hSAP retention did not indicate amyloid deposition in the animals. At week 17, the mice were seeded again but this time with ATTR$^{S52P}$ spleen AEF. Again, blood samples prior and 72 hours after the AEF injections were collected to measure SAA concentration which confirmed that the mice were not persistently inflamed after the seeding, with the SAA concentrations 22.7 ± 31.5 µg/ml (n=13) prior to AEF seeding and 40.8 ± 38.2 µg/ml (n=13) after AEF seeding. At week 32, $^{125}$I-hSAP retention did not indicate amyloid deposition in the animals. One double-seeded T/KO male was taken for analysis at week 34. The tissue analysed included : liver, heart, kidney, spleen, tongue, lung, sciatic nerve, adrenal, thyroid, salivary gland dissected into submandibular, sublingual and parotid glands, lachrymal gland, intestine, stomach, brain, eye, optic nerve, trigeminal ganglion, skin, muscle and fat. Amyloid deposits were detected in the heart and tongue by Congo red staining. The amounts of amyloid observed in the tissue did not differ from the amounts of amyloid found in the seeded males in the other two cohorts.

45 weeks from the start of the experiment, the remaining mice were analysed with$^{125}$I-hSAP whole body retention and none of the mice showed retention over the baseline 10 %. At week 48, all 12 remaining mice were killed and heart, tongue, liver, kidney, spleen and sciatic nerve were collected for analysis. Congo red staining and polarized light microscopy were used for amyloid detection. All 4 seeded transgenic males had amyloid deposits in the

heart and the tongue (Figure 6.10) and 1 of the 4 seeded transgenic females had amyloid in the tongue only. No amyloid was detected in the seeded non-transgenic controls. The data are summarised in Table 6.4.

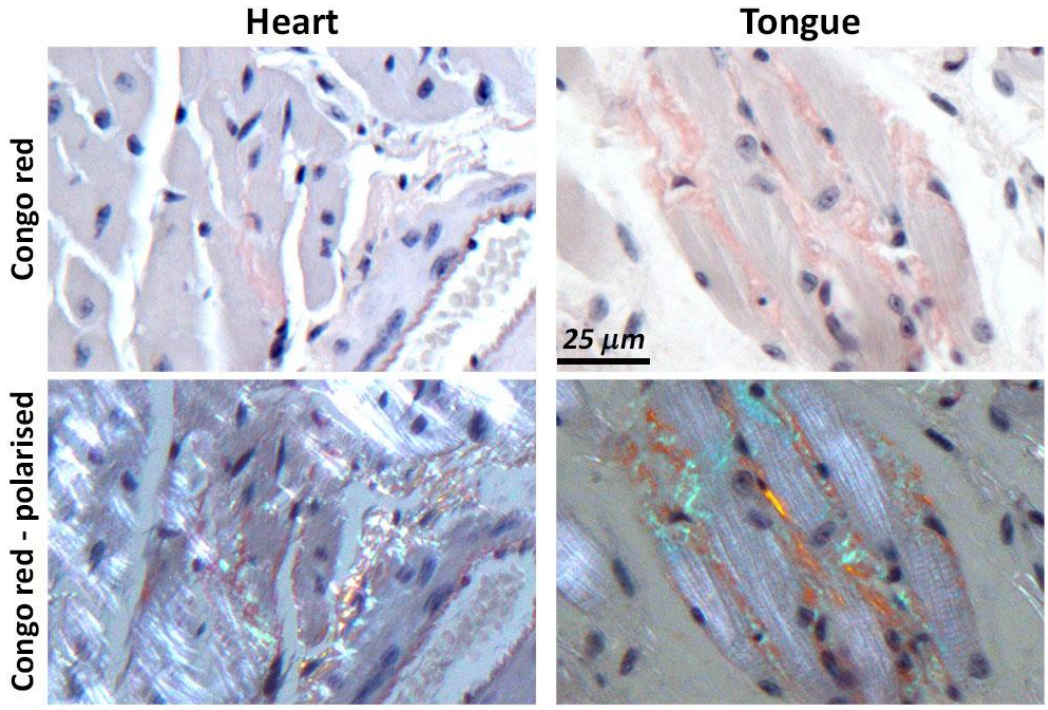


***Figure 6.10: Amyloid deposition in double-seeded mice (Cohort II)***

*Amyloid deposits were detected in the heart and the tongue of double-seeded hTTR$^{S52P}$ transgenic mice by Congo red. Amyloid is stained red and exhibits orange/green birefringence under polarised light. (The figure shows the heart and the tongue of a 13 months old transgenic male on mTTR-KO background analysed 10 months after the first seeding).*

| | Cohort III – Amyloid deposition | | | | | | | |
|---|---|---|---|---|---|---|---|---|
| **Genotype** | **T/WT** | | **T/Het** | | **T/KO** | | **-ve/WT** | **-ve/KO** |
| **Sex** | ♂ | ♀ | ♂ | ♀ | ♂ | ♀ | ♂+♀ | ♂+♀ |
| **Heart** | **1/1** | 0/1 | **1/1** | 0/2 | **3/3** | 0/1 | 0/2 | 0/2 |
| **Tongue** | **1/1** | **1/1** | **1/1** | 0/2 | **3/3** | 0/1 | 0/2 | 0/2 |
| Liver | 0/1 | 0/1 | 0/1 | 0/2 | 0/3 | 0/1 | 0/2 | 0/2 |
| Kidney | 0/1 | 0/1 | 0/1 | 0/2 | 0/3 | 0/1 | 0/2 | 0/2 |
| Spleen | 0/1 | 0/1 | 0/1 | 0/2 | 0/3 | 0/1 | 0/2 | 0/2 |
| Sciatic nerve | 0/1 | 0/1 | 0/1 | 0/2 | 0/3 | 0/1 | 0/2 | 0/2 |
| Adrenal | 0/1 | 0/1 | 0/1 | 0/2 | 0/3 | 0/1 | 0/2 | 0/2 |
| Brain | - | - | - | - | 0/1 | - | - | - |
| Trigeminal g. | - | - | - | - | 0/1 | - | - | - |
| Lung | - | - | - | - | 0/1 | - | - | - |
| Thyroid | - | - | - | - | 0/1 | - | - | - |
| Salivary gland | - | - | - | - | 0/1 | - | - | - |
| (Submandibular) | - | - | - | - | 0/1 | - | - | - |
| (Sublingual) | - | - | - | - | 0/1 | - | - | - |
| (Parotid) | - | - | - | - | 0/1 | - | - | - |
| Intestine | - | - | - | - | 0/1 | - | - | - |
| Stomach | - | - | - | - | 0/1 | - | - | - |
| Muscle | - | - | - | - | 0/1 | - | - | - |
| Fat | - | - | - | - | 0/1 | - | - | - |
| Skin | - | - | - | - | 0/1 | - | - | - |
| Eye | - | - | - | - | 0/1 | - | - | - |
| Optic nerve | - | - | - | - | 0/1 | - | - | - |
| Lacrymal gland | - | - | - | - | 0/1 | - | - | - |

***Table 6.4: Cohort III – Primed amyloid deposition in hTTR$^{S52P}$ transgenic mice***

*Summary of tissues analysed by Congo red in hTTR$^{S52P}$ transgenic (T) mice on mTTR wild-type (WT), mTTR heterozygous (Het) and mTTR-KO background (KO) seeded with combination of ATTR$^{S52P}$ ex-vivo fibrils and ATTR$^{S52P}$ spleen extract (AEF). Amyloid deposition was observed in all 5 seeded transgenic males and 1 seeded transgenic female with the amyloid deposits localised in the heart and tongue. 4 non-transgenic controls were also seeded as negative controls. The samples are scored as number of mice with amyloid / number of mice analysed.*

### 6.2.4 Nature of the amyloid deposits in the hTTR$^{S52P}$ transgenic mice

To identify the amyloid protein co-localised with the amyloid deposits of the hTTR$^{S52P}$ transgenic mice, adjacent sections of the tissues were analysed by immunohistochemistry in all seeded transgenic mice. The amyloid was expected to be human ATTR amyloid and for its identification Dako anti-human TTR antibody was used. In old or inflamed mice, amyloid deposits of ApoAII or SAA, respectively, can be naturally formed *(Higuchi et al., 1991b, Hoffman et al., 1984)*. To analyse whether this was the case in the hTTR$^{S52P}$ transgenic mice, the sections were also immunostained with anti-mouse ApoAII antibody and anti-mouse SAA antibody. One set of the adjacent tissue sections of all seeded transgenic mice was stained with Congo red for exact co-localisation of the amyloid with the amyloid protein.

In the amyloidotic hTTR$^{S52P}$ transgenic mice, in each case (e.g. Figures 6.11 and 6.12) the amyloid in the heart and the tongue was found to be immunoreactive with anti-human TTR antiserum, and negative when stained for ApoAII or for SAA. This shows that the mice have ATTR amyloidosis.

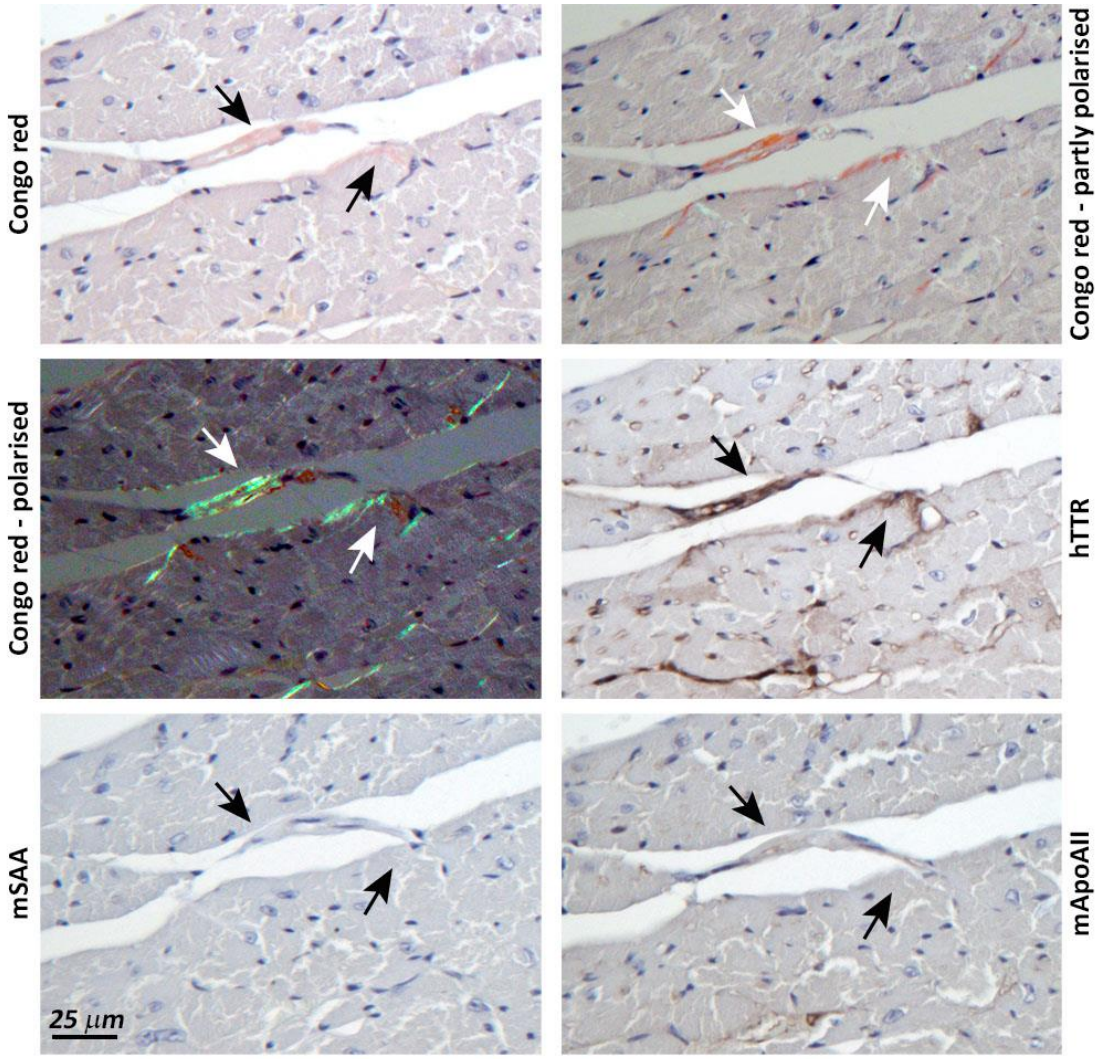


***Figure 6.11: Typing of amyloid deposits in the heart of seeded hTTR$^{S52P}$ transgenic mice***

*Amyloid deposits in the heart of seeded hTTR$^{S52P}$ transgenic mice were localised with Congo red staining, exhibiting green birefringence under polariser light. Co-localisation of the amyloid with human TTR, mouse ApoAII and mouse SAA was analysed on adjacent sections. Positive immunohistochemical staining for human TTR and negative immuno-staining for mApoAII and mSAA confirmed ATTR amyloid deposits in the hearts of amyloidotic mice.*

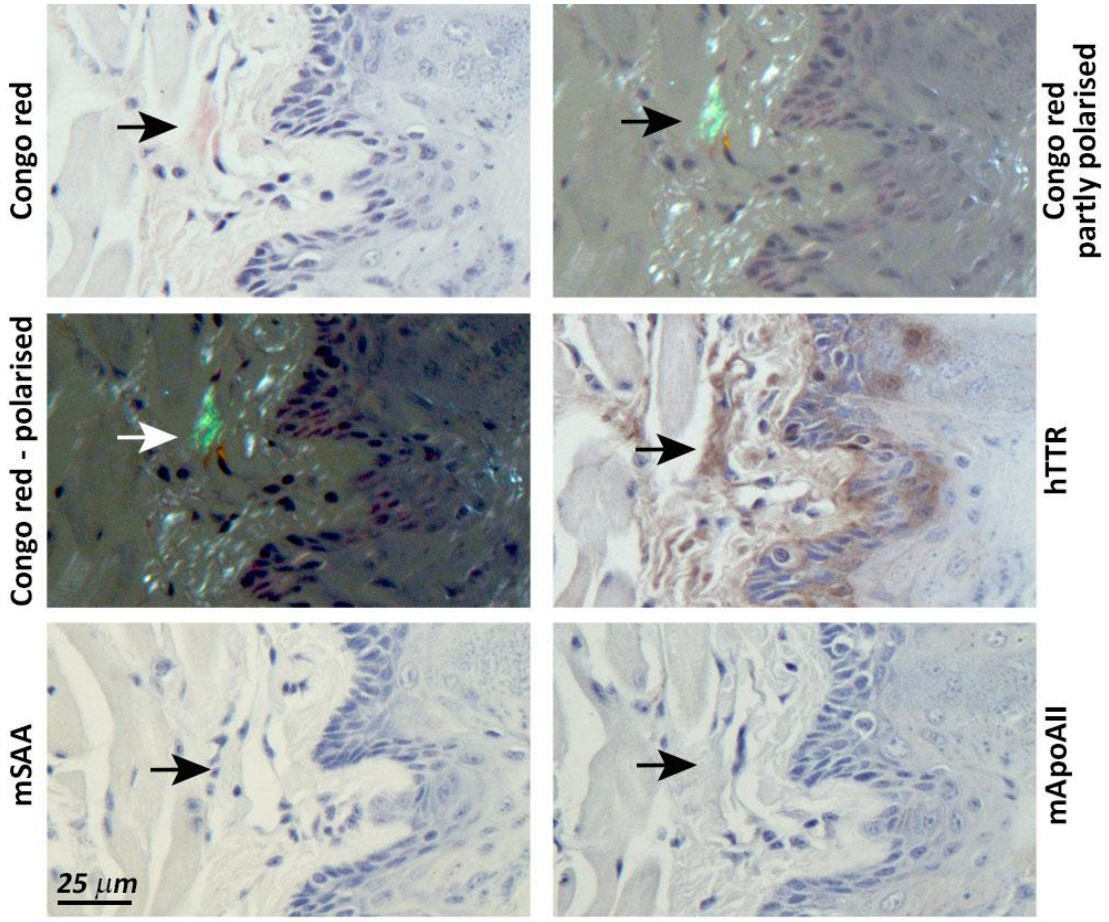


***Figure 6.12: Typing of amyloid deposits in the tongue of seeded hTTR$^{S52P}$ transgenic mice***

*Amyloid deposits in the tongue of seeded hTTR$^{S52P}$ transgenic mice were localised with Congo red staining, exhibiting green birefringence under polariser light. Co-localisation of the amyloid with human TTR, mouse ApoAII and mouse SAA was analysed on adjacent sections. Positive immunohistochemical staining for human TTR and negative immuno-staining for mApoAII and mSAA confirmed ATTR amyloid deposits in the hearts of amyloidotic mice.*

### 6.2.5 Investigation of the presence of cleaved TTR in the cardiac amyloid of hTTR$^{S52P}$ transgenic mice

In ATTR cardiac amyloidosis, the deposits typically contain fragmented TTR *(Cornwell et al., 1988, Bergstrom et al., 2005, Ihse et al., 2013)* which suggests that proteolytic cleavage may be important in the pathogenesis of ATTR amyloidosis. *In vitro* biochemical characterisation of wild-type TTR and pathogenic TTR variants, all associated with ATTR cardiac amyloidosis showed that trypsin-induced proteolytic cleavage results in rapid conversion into amyloid fibrils under physiological conditions, whereas un-cleaved TTR and TTR variants did not form amyloid under the same conditions *(Mangione et al., 2014, Marcoux et al., 2015)*. Moreover, the cleavage occurred between amino acids 48 and 49 of the mature proteins, the same position at which cardiac TTR is cleaved in ATTR cardiac amyloidosis patients *(Marcoux et al., 2015)*. Importantly, the S52P variant was much more susceptible to cleavage at this site than wild-type TTR and any other TTR variant analysed *(Mangione et al., 2014, Marcoux et al., 2015)*.

To determine whether the amyloid in the hTTR$^{S52P}$ transgenic mice contained cleaved TTR, insoluble material from the hearts of two amyloidotic transgenic mice were homogenised, the homogenate was centrifuged to concentrate the insoluble material and washed 4 times to remove all soluble material and the washed pellet was analysed by Western blot. Sheep anti-human TTR antibody (Binding site, UK) was used in the analysis as this antibody recognises the 49-127 fragment of TTR as well as the full-length TTR. Full-length TTR was detected in the soluble supernatant of the tissue homogenate as expected. However, in the insoluble material of both hearts, only full-length TTR was detected and the predicted cleaved fragment of TTR was not detected (Figure 6.13). This finding suggests that the failure to cleave the TTR$^{S52P}$ in the transgenic mice may have limited the spontaneous amyloid deposition in the animals which was only achieved after provision of

exogenous seeds. These observations also suggest that cleavage of the TTR may accelerate the initial formation of amyloid seeds.

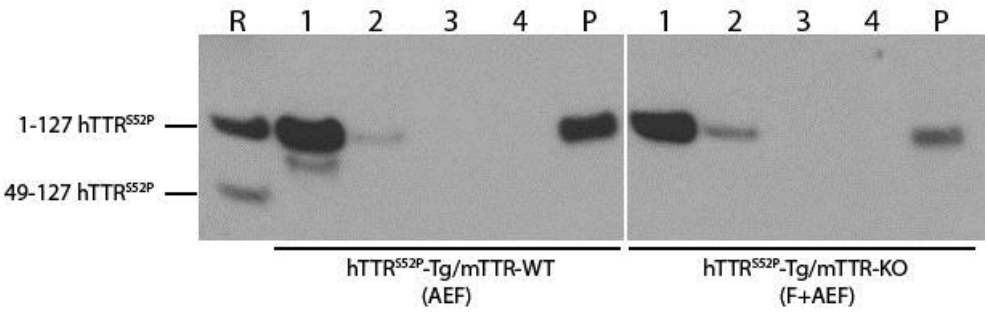


***Figure 6.13: TTR deposited in the heart of amyloidotic hTTR$^{S52P}$ transgenic mice***

*Western blot analysis of insoluble material pelleted from the hearts of two amyloidotic hTTR$^{S52P}$ transgenic mice showed that the TTR deposited in the hearts is un-cleaved full length protein. One transgenic mouse was on mouse TTR wild-type background seeded with AEF and one transgenic mouse was on mouse TTR-KO background seeded with fibrils and AEF. The hearts were homogenised and the supernatant containing the soluble material (lane 1) was removed. The pellet (P) was washed three times to remove the remaining soluble proteins. The supernatants collected from the three washes (lanes 2, 3 and 4 – respectively) were also run on the gel to check no carry-over of soluble proteins in the pellet. Recombinant hTTR$^{S52P}$ cleaved with trypsin (R), showing the full-length hTTR (1-127 hTTR$^{S52P}$) and the released 49-127 fragment (49-127 hTTR$^{S52P}$) which was kindly provided by Dr Riccardo Porcari, was run alongside the samples as a control.*

### 6.2.6 Summary of the results of amyloid deposition in the hTTR$^{S52P}$ transgenic mice

No spontaneous ATTR amyloid was observed in the hTTR$^{S52P}$ transgenic mice despite high levels of plasma human TTR$^{S52P}$ variant and despite thorough search of up to 22 different tissues in which ATTR amyloid may occur in ATTR amyloidosis. However, upon seeding with *ex vivo*-isolated ATTR$^{S52P}$ fibrils and/or AEF of ATTR$^{S52P}$ spleen extract, amyloid was found 4-11 months after seeding in 22 out of 31 transgenic mice analysed, and no amyloid was found in 12 seeded non-transgenic control mice. Strikingly, all 18 seeded males were amyloidotic, in marked contrast to only 4 out of the 13 females having detectable amyloid deposits. Cardiac amyloid was present in 16 of the 18 males, but in only 1 of the 4 amyloidotic females. Amyloid was also detected in the tongue in the seeded mice (16/18 amyloidotic males; 4/4 amyloidotic females). Interestingly, the amyloid deposits developed in mice on all genetic backgrounds – mouse TTR wild-type, heterozygous and knock-out, and no difference was seen in the onset and/or the amount of amyloid deposited in the tissues in these mice. The deposited TTR in two hearts of amyloidotic mice analysed was full-length TTR.

## 6.3 Discussion

Despite many attempts to model ATTR amyloidosis in mice, no or very little, inconsistent ATTR amyloid deposition has been achieved in transgenic mice to date. In this thesis, transgenic mice expressing highly amyloidogenic human $TTR^{S52P}$ variant have been generated and the data presented here demonstrate that the $hTTR^{S52P}$ transgenic mice develop consistent amyloid deposition in the heart, the site of amyloid deposition in cardiac ATTR amyloidosis in humans. Furthermore, $hTTR^{S52P}$ amyloid deposits were found in the tongues of the transgenic mice which were more extensive than those found in the heart. Although amyloid in the tongue has not often been documented in ATTR amyloidosis patients, macroglossia caused by ATTR amyloid has been reported *(Cowan et al., 2011)*. Without macroglossia, the presence of amyloid in the tongue is unlikely to be investigated in the patients.

Although others have reported cardiac amyloid in hTTR transgenic mice, the data presented did not unequivocally demonstrate that the amyloid was TTR amyloid as outlined previously. The analysis reported here demonstrate that the amyloid in this model is composed of hTTR because in adjacent sections the Congo red positive amyloid was coincident with hTTR immunoreactivity and did not react with anti-mouse SAA or anti-mouse ApoAII. Furthermore, recent proteomic analysis of amyloid from the hearts of amyloidotic $hTTR^{S52P}$ transgenic mice by laser-capture microdissection and mass spectrometry confirmed that the amyloid was $hTTR^{S52P}$ (Dr Graham Taylor, Dr Nigel Rendell and Janet Gilbertson – personal communication). No mouse TTR was detected by this assay in the amyloid deposits in a transgenic mouse on mouse TTR wild-type background.

In amyloidosis, pathological amyloid fibrils form from normally soluble proteins which are present in an organism for a long time before the disease develops. In this lag phase, which in case of ATTR amyloidosis can take decades, first amyloid fibril assemblies, “seeds”, are formed *(Jarrett and Lansbury, 1993,*

*Kelly, 1998)* which act as a template for further deposition. This process occurs stochastically *in vivo*. In the hTTR$^{S52P}$ transgenic mice, amyloid deposition was achieved only after a provision of exogenous seeds containing ATTR amyloid fibrils despite high production of the hTTR$^{S52P}$. Together, these observations show that the endogenous formation of amyloid seeds was limiting and therefore spontaneous amyloid deposition was not observed.

In wild-type ATTR amyloidosis patients, the amyloid in the heart contains cleaved TTR as well as full-length protein *(Dwulet and Benson, 1986, Bergstrom et al., 2005)*. The highly amyloidogenic S52P variant was found to be cleaved in the spleen of a patient carrying this variant and *in vitro* cleaved human S52P TTR readily forms amyloid under physiological conditions *(Mangione et al., 2014)*. Against this background, it was expected that any TTR amyloid deposits in the transgenic mice would contain cleaved TTR.

Unexpectedly, in the mice presented here, the cardiac ATTR amyloid deposits consisted of the full-length TTR$^{S52P}$, and the predicted cleaved product was not detected. The best evidence suggests that proteolytic cleavage precedes amyloid deposition in ATTR amyloidosis. However, it is not known yet, which protease(s) catalyse the cleavage of TTR in humans. Differences in the selectivity or efficiency between human and murine proteases in TTR processing or absence of proteases involved in TTR cleavage in mice could explain why ATTR amyloidosis does not naturally occur in mice and why it has been so difficult to model ATTR amyloidosis in mice. The lack of proteolytic cleavage of the hTTR in the hTTR$^{S52P}$ transgenic mice could also explain why the mice did not develop spontaneous amyloid deposits despite very high concentrations of the hTTR$^{S52P}$ in the plasma.

Although fragmented TTR is normally present in cardiac TTR amyloid, in some patients carrying V30M variant TTR, amyloid deposits in the heart are composed of purely full length TTR *(Bergstrom et al., 2005)*, demonstrating that cleavage is not an essential prerequisite for cardiac TTR amyloid.

Amyloid deposits in the hTTR$^{S52P}$ transgenic mice presented here were observed regardless of the presence or absence of murine TTR in these

mice. Other groups that generated hTTR transgenic mice (hTTR$^{V30M}$ or hTTR$^{L55P}$ transgenics) reported that the presence of murine TTR delays deposition of human TTR in the transgenic mice *(Sousa et al., 2002, Tagoe et al., 2007)*. It was then shown that in the transgenic mice in which both, murine and human TTR were present, hybrid TTR heterotetramers composed of mouse and human TTR monomers were formed and that in the presence of mouse TTR, circulating human TTR was much more stable to denaturation *(Tagoe et al., 2007)*. *In vitro* experiments than showed that mouse TTR and mouse/human TTR heterotetramers are much more kinetically stable than human TTR and a subunit exchange that is normally observed in human TTR *in vitro* was not observed between mouse and human TTR over time *(Reixach et al., 2008)*. From these observations, the authors concluded that in transgenic mice expressing human TTR, the presence of mouse TTR may prevent dissociation of the mixed TTR heterotetramers and thus prevent human TTR fibrillogenesis and amyloid deposition. In the hTTR$^{S52P}$ transgenic mice presented here, the expression of mouse TTR did not have a major effect on the onset or the amount of hTTR amyloid deposits in the transgenic mice. This demonstrates that the presence of mouse TTR does not prevent amyloid formation in transgenic mice expressing both human and mouse TTR.

Interestingly, the hTTR$^{S52P}$ transgenic mice recapitulate the yet unexplained male prevalence of clinical cardiac ATTR amyloid *(Rapezzi et al., 2008, Pinney et al., 2013b)*. In people and in the mice presented here, the sex difference in susceptibility to ATTR amyloidosis might reflect the higher TTR concentration in males *(Ingenbleek and De Visscher, 1979, Ingenbleek and Bernstein, 2015)*, although in healthy humans this difference is only modest. The minor difference of TTR abundance suggests that other sex-dependent mechanisms may be involved in the male predisposition to cardiac ATTR amyloidosis. Therefore, the hTTR$^{S52P}$ transgenic mice can be a valuable tool in investigating these differences. One approach to investigate this would be to make the female mice homozygous for the TTR$^{S52P}$ transgene which could

lead to double dose of the $TTR^{S52P}$ variant in the plasma. Hemizygous transgenic males and homozygous transgenic females would then be expected to have similar circulating concentrations of the human TTR variant. If the male prevalence remains despite similar measured serum TTR concentrations, it will be an indicator of sex-difference mechanisms involved in susceptibility to ATTR amyloidosis. If the male prevalence disappears when the measured plasma hTTR concentration is equalised between transgenic males and females, it will be an indicator that the TTR concentration is a critical determinant of susceptibility to ATTR amyloidosis.

# 7 Final Discussion

Two transgenic mouse models have been generated expressing extremely amyloidogenic variants of human proteins associated with severe phenotypes of hereditary systemic amyloidoses in people – Aβ2m$^{D76N}$ amyloidosis and ATTR$^{S52P}$ amyloidosis. Although both variants are highly penetrant in humans with an early onset in mid-adult life, the transgenic mice did not develop spontaneous amyloidosis, despite high plasma concentrations of the variants. It is important to emphasize that phenotypic variations in people exist between individuals and populations due to genetic and environmental factors. In the carriers of V30M variant TTR, the age of onset of the disease is on average 56 years in the Swedish population, whereas the average age of onset is 34 years in the Portuguese population. In addition, at 40 years of age, 5 % of the Swedish and French V30M population will have developed symptomatic disease compared to 55-90 % of the Portuguese V30M population *(Hellman et al., 2008, Sousa et al., 1993, Sousa et al., 1995)*. It was also reported that the penetrance of the V30M variant in Swedish population is higher when the mutation is inherited from the mother than the father *(Hellman et al., 2008)*. This phenomenon was partly explained by an effect of mitochondrial DNA polymorphism on the expression of the TTR mutation *(Bonaiti et al., 2010)* and partly it could be due to DNA imprinting *(Bonaiti et al., 2010)*. Phenotypic variation has even been described between monozygotic twins *(Holmgren et al., 2004)*. These observations indicate that genetic and environmental factors play an important role in amyloidosis. Because such phenotypic variations are seen among humans, it is not surprising that differences exist between humans and mice. Thus, differences between humans and mice, e.g. genetic background, proteome and extracellular matrix will have an effect, at least to some extent, on amyloid protein processing, metabolism, turnover, fibrillogenesis and deposition.

In amyloidosis, concentration of the precursor protein is a limiting factor in amyloid formation in both humans *(Lachmann et al., 2007)* and mice *(Simons et al., 2013)*, affecting the dynamics of the protein deposition as amyloid and amyloid regression. In fact, reducing the concentration of the precursor protein is one of the most important strategies in therapy of amyloidoses *(Lachmann et al., 2007, Comenzo et al., 2012, Weiss et al., 2016, Nakamura, 2011, Adams, 2013)*. In both transgenic mouse models presented here, the plasma concentrations of the human proteins, β2m and TTR, were similar or higher than the concentrations of equivalent proteins seen in patients of $Aβ2m^{D76N}$ and $ATTR^{S52P}$ amyloidoses, respectively, and among the highest ever reported in transgenic mice expressing these human proteins. Although the $hβ2m^{D76N}$ transgenic mice did not develop Aβ2m amyloid deposits, the $hTTR^{S52P}$ transgenic mice did develop ATTR amyloidosis when the amyloid deposition was primed by seeding. Given the background knowledge of the propensity of both variants to aggregate into amyloid fibrils in people and *in vitro*, other factors related to differences between human and murine physiology may have influenced the conversion of the soluble proteins into amyloid fibrils, some of which are discussed below.

The role of proteolysis in protein fibrillogenesis has been intensively studied *(Westermark et al., 1996, Marcoux et al., 2015)*. In cardiac ATTR amyloidosis, cleaved TTR is a major component of ATTR amyloid fibrils *(Dwulet and Benson, 1986, Bergstrom et al., 2005)*, in Aβ2m amyloidosis, truncated species of β2m missing the first six N-terminal residues are a component of Aβ2m amyloid deposits *(Gorevic et al., 1986, Stoppini et al., 2005)*. In AA amyloidosis, the amyloid proteins in the deposits are also fragmented *(Rocken et al., 2005)* and studies have shown that cathepsin B may contribute to the conversion of SAA protein to AA amyloid fibrils *(Yamada et al., 1995, Rocken et al., 2005)*. Interestingly in the same study, while some proteases may contribute to protein fibrillogenesis, other proteases have a protective role over amyloid fibril formation *(Stix et al., 2001, Rocken et al., 2005)*.

In a patient of ATTR$^{S52P}$ amyloidosis, ATTR amyloid deposits in the spleen have been shown to consist of fragmented TTR as well as the full-length protein *(Mangione et al., 2014)* and the S52P variant has been shown to be highly susceptible to proteolytic cleavage *in vitro* and the cleaved variant was readily amyloidogenic *(Marcoux et al., 2015)*. However, in the hTTR$^{S52P}$ transgenic mice presented here, only full-length S52P variant TTR was detected in the cardiac ATTR amyloid deposits. Differences in proteases concentrations, turnover, recognition and inhibition between humans and mice could explain this observation. The fact that cardiac ATTR amyloidosis was achieved in the hTTR$^{S52P}$ transgenic mice only after provision of exogenous seeds and not spontaneously could be explained by the lack of proteolytic cleavage of TTR in the animals, which may have limited the initial formation of endogenous seeds and thus limit the spontaneous development of ATTR deposits. The lack of proteolytic cleavage of TTR observed in the hTTR$^{S52P}$ transgenic mice could also be explained by a difference in protease inhibitors between humans and mice. Interestingly, in the hβ2m$^{D76N}$ transgenic mice, the β2m protein was found to circulate in a complex with a component that has not been identified yet. Complexed β2m has been observed in plasma of mice *(Natori et al., 1976)* and rats *(Nguyen-Simonnet et al., 1982)* but in humans, >98 % of plasma β2m circulates as a free monomer *(Plesner and Bjerrum, 1980)*. Although a fraction of β2m may circulate in the plasma of the transgenic mice complexed with MHC class I heavy chain, as about 2 % of β2m was found to be bound to MHC class I heavy chain in human plasma *(Plesner and Bjerrum, 1980)*, majority of β2m in mouse plasma was found to be complexed with a different, non-identified molecule *(Natori et al., 1976)*. The observation that the β2m is complexed in the plasma of the transgenic mice raises a question whether extracellular chaperones may be the partners of β2m in the plasma of mice. As it was discussed earlier, identification of chaperons and their role in protein fibrillogenesis have been recently studied *(French et al., 2008, Lashley et al., 2006)*.

A common feature in all types of amyloidosis in humans is the presence of SAP in amyloid deposits *(Pepys et al., 1979)*. Although SAP is a plasma protein in both humans and mice, it was shown that human SAP binds much more avidly to amyloid *in vivo than* mouse SAP *(Hawkins et al., 1988)*. Given the stabilising role of SAP on amyloid deposits by preventing proteolysis of the amyloid fibrils *(Tennent et al., 1995)*, the lower affinity of mouse SAP to amyloid deposits may play an important role on the dynamic of the turnover of amyloid in mice, when the amyloid deposition is not exceeding the gradual rate of resorption of the amyloid fibrils. Thus, spontaneous amyloid deposition of a precursor protein in mice may require relatively longer time than in humans, taking the time scale of the life span of both species into consideration. Indeed, in transgenic mice lacking mouse SAP, induced AA amyloid deposition was delayed and the quantity of the deposits was reduced in the SAP knock-out mice compared to mice expressing SAP, despite equal elevated production of SAA *(Botto et al., 1997)*. It would be interesting to see whether expression of human SAP in the two transgenic mouse models presented here would have an effect on amyloid deposition.

Another factor that may influence the aggregation of amyloidogenic proteins is the composition of extracellular matrix. The main components are elastic fibres, fibrillar collagens and glycosaminoglycans and a role of these components on amyloid fibril formation has been studied *in vitro (Stevens and Kisilevsky, 2000, Relini et al., 2006)* as the glycosaminoglycan heparan sulphate is found co-localised with amyloid deposits in humans. *In vivo* evidence that the glycosaminoglycan heparan sulphate can affect the development of amyloidosis was provided in transgenic mice which selectively overexpressed heparanase in the liver and in the kidney, but not in the spleen *(Li et al., 2005)*. The overexpression of heparanase caused shortening of heparan sulphate chains in the liver and the kidney, which led to inhibition of induced AA amyloid deposition in these organs but not in the spleen of the transgenic mice *(Li et al., 2005)*.

Histological identification of amyloid in tissues by green birefringence under cross-polarised light following Congo red staining is the golden standard for confirmation of amyloid deposition *(Puchtler H, 1962)*. Although binding of Congo red to amyloid is specific, it is not very sensitive and requires an adequate amount of amyloid. When patients are diagnosed for presence of amyloid by Congo red staining of tissue biopsy, this usually means that there is a clinical evidence of a disease which suggests that substantial amounts of amyloid may be present within certain tissues. In the $hTTR^{S52P}$ transgenic model presented here, Congophilic amyloid deposits were detected in the heart and the tongue of the seeded transgenic mice. However, no spontaneous amyloid deposition was detected by Congo red in these mice and no amyloid was detected in the $h\beta2m^{D76N}$ transgenic mice. The requirement for an adequate amount of amyloid within the tissue in order to provide a detectable signal by Congo red may not have been met in the non-amyloidotic transgenic mice. However, this does not necessarily mean that amyloid deposits were not present. The deposits may have been of a diffused nature within tissues in amounts in which the bound Congo red dye is of limited quantity to exhibit detectable signal. In fact, a difference in the signal provided by Congo red bound to cardiac amyloid deposits was reported in wild-type ATTR and $ATTR^{V30M}$ amyloidosis patients *(Bergstrom et al., 2005)*. The comparative study revealed that ATTR amyloid seems to occur in two morphologically, histochemically and structurally distinguishable forms in these patients. One form of the amyloid deposits consisted of full-length $TTR^{V30M}$, was more compact and strongly Congophilic and birefringent. The other form of the amyloid deposits consisted of either fragmented wild-type TTR or a mixture of fragmented wild-type TTR and $TTR^{V30M}$, was more diffused, homogeneous and widespread and showed weak Congo red signal and birefringence *(Bergstrom et al., 2005)*. However, for modelling amyloidosis in mice, sufficient amounts of amyloid in the tissues are necessary to resemble the human disease.

To date there are no reports of any animal model of cardiac amyloidosis ideally suited to test the functional efficacy or safety of any treatment for cardiac amyloidosis, or for new diagnostic imaging technologies. Modelling of AA amyloidosis in mice enabled an invention and clinical development of SAP scintigraphy *(Hawkins et al., 1988, Hawkins et al., 1990b, Hawkins et al., 1990a)* for diagnosis and management, which was commissioned by the NHS in 1999. The SAP scan is highly specific and quantitative *in vivo* method which enables to evaluate the visceral amyloid burdens and response to treatment, it is unable to evaluate amyloid in the moving heart. Cardiac MRI has been recently used as a novel tool to monitor amyloid load in the heart showing a high specificity for diagnosis of cardiac amyloidosis *(Maceira et al., 2005, Fontana et al., 2015)*. Recently, 99m-technetium ($^{99m}$Tc) labelled phosphate derivative ($^{99m}$Tc-DPD) used as a nuclear bone scintigraphy tracer was found to localise in hearts of all patients with cardiac ATTR amyloidosis and in a small proportion of patients with AL amyloidosis *(Puille et al., 2002, Perugini et al., 2005, Hutt et al., 2014)*. The mechanisms by which $^{99m}$Tc-DPD localises to amyloidotic hearts and the reason for a difference seen in its reactivity with cardiac amyloid among AL patients are completely unknown which limits the clinical value of this diagnostic technique. The novel hTTR$^{S52P}$ transgenic model of cardiac amyloidosis presented here will be a valuable tool for elucidation of the mechanisms of $^{99m}$Tc-DPD localisation and for investigation of the outcomes of serial monitoring of the course of the disease.

At present, no specific treatment is available for cardiac ATTR amyloidosis. Two small molecules, Tafamidis and non-steroidal inflammatory drug Diflunisal, which kinetically stabilize the native TTR tetramer and thus inhibit its dissociation and TTR amyloid formation, are under investigation in clinical trials *(Bulawa et al., 2012, Coelho et al., 2012, Castano et al., 2012)*. Approaches to reduce TTR production through nucleic acid intervention – anti-sense oligonucleotide targeting TTR *(Ackermann et al., 2012)* and anti-TTR small interfering RNA *(Coelho et al., 2013)* are also in clinical trials.

Both strategies may decrease the rate of amyloid deposition, with potential to slow down or stop disease progression. Indeed, in a mouse model expressing $TTR^{V30M}$, TTR knockdown by small interfering RNA was recently reported to decrease non-fibrillar deposits of transgenic human TTR *(Butler et al., 2016)*. In the $TTR^{V30M}$ mouse model used, the mice were reported to have TTR deposits, however these were not ATTR amyloid deposits *(Santos et al., 2010)*. Although the TTR deposits regressed after the interfering RNA intervention, the influence of pre-formed amyloid deposits in tissues and the regression of amyloid could not be evaluated. In the $hTTR^{S52P}$ transgenic mice presented here, both the gene silencing effect of TTR expression and its effect on amyloid deposits could be investigated. It has been seen in patients *(Gillmore et al., 2001, Lachmann et al., 2007)* and confirmed in transgenic mice *(Simons et al., 2013)* that an increase in concentration of precursor protein after regression of amyloid deposition can lead to a rapid development of amyloid deposits, probably due to remaining templates of amyloid within the tissue. In the inducible AA transgenic model, increased SAA concentrations led to a development of heavy AA amyloid deposits in the liver, the spleen and a minor amyloid deposition in the heart. However, after re-induction of SAA expression in the transgenic mice in which amyloid had previously been induced and spontaneously regressed, renal failure developed very rapidly due to amyloid deposits in kidney *(Simons et al., 2013)*. This response closely resembled the rapid onset of renal failure precipitated by flares of inflammation in some AA amyloidosis patients in remission *(Gillmore et al., 2001, Lachmann et al., 2007)* suggesting that glomeruli amyloid deposits may be responsible *(Simons et al., 2013)*. This observation points out the importance of a different pattern in amyloid re-accumulation following regression, possibly due to different distribution of amyloid template after the regression *(Simons et al., 2013)*.

An immunotherapeutic approach targeting directly amyloid deposits for removal is under investigation in clinical trials. Antibodies to SAP, a universal constituent of human systemic amyloid deposits is used to activate

complement of the deposits thereby attracting and engaging macrophages which have the capability to engulf and destroy amyloid load (Bodin et al., 2010). This approach was tested in AA amyloid mouse model in which the anti-SAP antibody led to clearance of abundant visceral amyloid deposits *(Bodin et al., 2010)*. In fact, the first human phase 1 clinical trial of anti-SAP antibody treatment has shown very promising results *(Richards et al., 2015)*, but cardiac amyloidosis was excluded from the phase 1 trial for safety reasons. Although there is an AA amyloidosis mouse model which presents with minor cardiac amyloid deposits, the mice predominantly develop heavy amyloid deposits in the liver and the spleen *(Simons et al., 2013)*. Although the anti-SAP antibody treatment showed significant reduction of the cardiac amyloid in the heart in the AA mouse model, this was achieved only after a second dose of the treatment because of the abundant amyloid deposits in the liver and the spleen. The overabundance of amyloid in the viscera may complicate the functional studies of the heart and thus the model is not ideally suitable for evaluation of treatment targeting cardiac amyloidosis. The $hTTR^{S52P}$ transgenic mice which closely resemble the amyloid deposition in ATTR cardiac amyloidosis patients provide a great advantage for further testing of the mechanisms and safety of emerging treatments and development of new treatments of cardiac amyloidosis.

# 8 Future work

The established hβ2m$^{D76N}$ and hTTR$^{S52P}$ transgenic mouse models will be further investigated to understand the disease mechanisms, to elucidate some molecular mechanisms of amyloid formation and to test possibilities of inhibition of amyloid formation. This chapter summarises future work discussed in previous sections.

**hβ2m$^{D76N}$ transgenic mouse model:**

- Identification of a molecule complexed with circulating β2m protein.
- Attempt of priming of amyloid deposition by repeated administration of amyloid-fibril seeds.
- Investigation of the effects of amyloid-associated molecules (human SAP, glycosaminoglycans) on the conversion of the β2m$^{D76N}$ protein into amyloid by manipulation of the extracellular environment (e.g. crossing with hSAP transgenic mice).
- Evaluation of β2m protein levels in chronic kidney disease mouse models and the use of such models to increase the concentration of circulating β2m$^{D76N}$ variant which may lead to deposition of the β2m$^{D76N}$ protein as amyloid.
- Breeding of the hβ2m$^{D76N}$ transgenic mice on different backgrounds (e.g. Balb/c background) to investigate whether different mouse strain phenotypes may influence the conversion of the β2m$^{D76N}$ protein into amyloid.

**hTTR$^{S52P}$ transgenic mouse model:**

- Evaluation of the age-effect on amyloid deposition by seeding 2 months old mice and 12-18 months old mice and comparison of the amyloid load in the mice at specific time points.

- Investigation of male preponderance of cardiac ATTR amyloidosis by producing homozygous females which will have a double dose of the transgene and comparing them with hemizygous males. Hemizygous males and homozygous females are expected to produce similar amounts of hTTR. If the male preponderance remains despite the fact that the males and females express similar levels of the hTTR, it will clearly suggest that other gender differences influence ATTR amyloid deposition.
- Investigation of the mechanisms of $^{99m}$Tc-DPD localisation in the heart and other organs of ATTR amyloidotic animals.
- Suppression of TTR (e.g. by RNA inhibition) and its effect on amyloid deposition in the hTTR$^{S52P}$ transgenic mice.

# 9 References


ACKERMANN, E. J., GUO, S., BOOTEN, S., ALVARADO, L., BENSON, M., HUGHES, S. & MONIA, B. P. 2012. Clinical development of an antisense therapy for the treatment of transthyretin-associated polyneuropathy. *Amyloid,* 19 Suppl 1**,** 43-4.

ADAMS, D. 2001. Hereditary and acquired amyloid neuropathies. *J Neurol,* 248**,** 647-57.

ADAMS, D. 2013. Recent advances in the treatment of familial amyloid polyneuropathy. *Ther Adv Neurol Disord,* 6**,** 129-39.

ADAMS, D. & SAID, G. 1996. Ultrastructural immunolabelling of amyloid fibrils in acquired and hereditary amyloid neuropathies. *J Neurol,* 243**,** 63-7.

ADAMS, D., SAMUEL, D., GOULON-GOEAU, C., NAKAZATO, M., COSTA, P. M., FERAY, C., PLANTE, V., DUCOT, B., ICHAI, P., LACROIX, C., METRAL, S., BISMUTH, H. & SAID, G. 2000. The course and prognostic factors of familial amyloid polyneuropathy after liver transplantation. *Brain,* 123 ( Pt 7)**,** 1495-504.

AGUIRRE, M. A., BOIETTI, B. R., NUCIFORA, E., SORROCHE, P. B., GONZALEZ BERNALDO DE QUIROS, F., GIUNTA, D. H. & POSADAS-MARTINEZ, M. L. 2016. Incidence rate of amyloidosis in patients from a medical care program in Buenos Aires, Argentina: a prospective cohort. *Amyloid***,** 1-4.

AITKEN, J. F., LOOMES, K. M., SCOTT, D. W., REDDY, S., PHILLIPS, A. R., PRIJIC, G., FERNANDO, C., ZHANG, S., BROADHURST, R., L'HUILLIER, P. & COOPER, G. J. 2010. Tetracycline treatment retards the onset and slows the progression of diabetes in human amylin/islet amyloid polypeptide transgenic mice. *Diabetes,* 59**,** 161-71.

AL-SHAWI, R., KINNAIRD, J., BURKE, J. & BISHOP, J. O. 1990. Expression of a foreign gene in a line of transgenic mice is modulated by a chromosomal position effect. *Mol Cell Biol,* 10**,** 1192-8.

ALVES, I. L., ALTLAND, K., ALMEIDA, M. R., WINTER, P. & SARAIVA, M. J. 1997. Screening and biochemical characterization of transthyretin variants in the Portuguese population. *Hum Mutat,* 9**,** 226-33.

ANAN, I., EL-SALHY, M., ANDO, Y., TERAZAKI, H. & SUHR, O. B. 2001. Comparison of amyloid deposits and infiltration of enteric nervous system in the upper with those in the lower gastrointestinal tract in patients with familial amyloidotic polyneuropathy. *Acta Neuropathol,* 102**,** 227-32.

ANDERSSON, K., OLOFSSON, A., NIELSEN, E. H., SVEHAG, S. E. & LUNDGREN, E. 2002. Only amyloidogenic intermediates of transthyretin induce apoptosis. *Biochem Biophys Res Commun,* 294**,** 309-14.

ANDERSSON, R. 1976. Familial amyloidosis with polyneuropathy. A clinical study based on patients living in northern Sweden. *Acta Med Scand Suppl,* 590**,** 1-64.

ANDO, Y., COELHO, T., BERK, J. L., CRUZ, M. W., ERICZON, B. G., IKEDA, S., LEWIS, W. D., OBICI, L., PLANTE-BORDENEUVE, V.,

RAPEZZI, C., SAID, G. & SALVI, F. 2013. Guideline of transthyretin-related hereditary amyloidosis for clinicians. *Orphanet J Rare Dis,* 8**,** 31.

ANDO, Y., NAKAMURA, M. & ARAKI, S. 2005. Transthyretin-related familial amyloidotic polyneuropathy. *Arch Neurol,* 62**,** 1057-62.

ANDRADE, C. 1952. A peculiar form of peripheral neuropathy; familiar atypical generalized amyloidosis with special involvement of the peripheral nerves. *Brain,* 75**,** 408-27.

ARAKI, S., MAWATARI, S., OHTA, M., NAKAJIMA, A. & KUROIWA, Y. 1968. Polyneuritic amyloidosis in a Japanese family. *Arch Neurol,* 18**,** 593-602.

ARSHAVSKY, V. Y., LAMB, T. D. & PUGH, E. N., JR. 2002. G proteins and phototransduction. *Annu Rev Physiol,* 64**,** 153-87.

AXELRAD, M. A., KISILEVSKY, R., WILLMER, J., CHEN, S. J. & SKINNER, M. 1982. Further characterization of amyloid-enhancing factor. *Lab Invest,* 47**,** 139-46.

BALDRIDGE, R. D. & RAPOPORT, T. A. 2016. Autoubiquitination of the Hrd1 Ligase Triggers Protein Retrotranslocation in ERAD. *Cell,* 166**,** 394-407.

BALFOUR, W. E. & TUNNICLIFFE, H. E. 1960. Thyroxine binding by serum proteins. *J Physiol,* 153**,** 179-98.

BALTZ, M., CASPI, D., HIND, C. R. K., FEINSTEIN, A. & PEPYS, M. B. 1986a. Isolation and characterization of amyloid enhancing factor (AEF). *In:* GLENNER, G. G., OSSERMAN, E. F., BENDITT, E. P., CALKINS, E., COHEN, A. & ZUCKER-FRANKLIN, D. (eds.) *Amyloidosis.* New York: Plenum Press.

BALTZ, M. L., CASPI, D., EVANS, D. J., ROWE, I. F., HIND, C. R. & PEPYS, M. B. 1986b. Circulating serum amyloid P component is the precursor of amyloid P component in tissue amyloid deposits. *Clin Exp Immunol,* 66**,** 691-700.

BANYPERSAD, S. M., SADO, D. M., FLETT, A. S., GIBBS, S. D., PINNEY, J. H., MAESTRINI, V., COX, A. T., FONTANA, M., WHELAN, C. J., WECHALEKAR, A. D., HAWKINS, P. N. & MOON, J. C. 2013. Quantification of myocardial extracellular volume fraction in systemic AL amyloidosis: an equilibrium contrast cardiovascular magnetic resonance study. *Circ Cardiovasc Imaging,* 6**,** 34-9.

BARDIN, T., ZINGRAFF, J., SHIRAHAMA, T., NOEL, L. H., DROZ, D., VOISIN, M. C., DRUEKE, T., DRYLL, A., SKINNER, M., COHEN, A. S. & ET AL. 1987. Hemodialysis-associated amyloidosis and beta-2 microglobulin. Clinical and immunohistochemical study. *Am J Med,* 83**,** 419-24.

BARREIROS, A. P., POST, F., HOPPE-LOTICHIUS, M., LINKE, R. P., VAHL, C. F., SCHAFERS, H. J., GALLE, P. R. & OTTO, G. 2010. Liver transplantation and combined liver-heart transplantation in patients with familial amyloid polyneuropathy: a single-center experience. *Liver Transpl,* 16**,** 314-23.

BARTON, J. C., EDWARDS, C. Q. & ACTON, R. T. 2015. HFE gene: Structure, function, mutations, and associated iron abnormalities. *Gene,* 574**,** 179-92.

BATEMAN, D. A., TYCKO, R. & WICKNER, R. B. 2011. Experimentally derived structural constraints for amyloid fibrils of wild-type transthyretin. *Biophys J,* 101**,** 2485-92.

BAUER, A., HUTTINGER, R., STAFFLER, G., HANSMANN, C., SCHMIDT, W., MAJDIC, O., KNAPP, W. & STOCKINGER, H. 1997. Analysis of the requirement for beta 2-microglobulin for expression and formation of human CD1 antigens. *Eur J Immunol,* 27**,** 1366-73.

BECKMAN, E. M., PORCELLI, S. A., MORITA, C. T., BEHAR, S. M., FURLONG, S. T. & BRENNER, M. B. 1994. Recognition of a lipid antigen by CD1-restricted alpha beta+ T cells. *Nature,* 372**,** 691-4.

BELLOTTI, V., STOPPINI, M., MANGIONE, P., SUNDE, M., ROBINSON, C., ASTI, L., BRANCACCIO, D. & FERRI, G. 1998. Beta2-microglobulin can be refolded into a native state from ex vivo amyloid fibrils. *Eur J Biochem,* 258**,** 61-7.

BENSON, M. D. 1981. Partial amino acid sequence homology between an heredofamilial amyloid protein and human plasma prealbumin. *J Clin Invest,* 67**,** 1035-41.

BENSON, M. D. & KINCAID, J. C. 2007. The molecular biology and clinical features of amyloid neuropathy. *Muscle Nerve,* 36**,** 411-23.

BENSON, M. D., KLUVE-BECKERMAN, B., ZELDENRUST, S. R., SIESKY, A. M., BODENMILLER, D. M., SHOWALTER, A. D. & SLOOP, K. W. 2006. Targeted suppression of an amyloidogenic transthyretin with antisense oligonucleotides. *Muscle Nerve,* 33**,** 609-18.

BERGGARD, I. & BEARN, A. G. 1968. Isolation and properties of a low molecular weight beta-2-globulin occurring in human biological fluids. *J Biol Chem,* 243**,** 4095-103.

BERGSTROM, J., GUSTAVSSON, A., HELLMAN, U., SLETTEN, K., MURPHY, C. L., WEISS, D. T., SOLOMON, A., OLOFSSON, B. O. & WESTERMARK, P. 2005. Amyloid deposits in transthyretin-derived amyloidosis: cleaved transthyretin is associated with distinct amyloid morphology. *J Pathol,* 206**,** 224-32.

BERK, J. L., SUHR, O. B., OBICI, L., SEKIJIMA, Y., ZELDENRUST, S. R., YAMASHITA, T., HENEGHAN, M. A., GOREVIC, P. D., LITCHY, W. J., WIESMAN, J. F., NORDH, E., CORATO, M., LOZZA, A., CORTESE, A., ROBINSON-PAPP, J., COLTON, T., RYBIN, D. V., BISBEE, A. B., ANDO, Y., IKEDA, S., SELDIN, D. C., MERLINI, G., SKINNER, M., KELLY, J. W., DYCK, P. J. & DIFLUNISAL TRIAL, C. 2013. Repurposing diflunisal for familial amyloid polyneuropathy: a randomized clinical trial. *JAMA,* 310**,** 2658-67.

BERNABEU, C., VAN DE RIJN, M., LERCH, P. G. & TERHORST, C. P. 1984. Beta 2-microglobulin from serum associates with MHC class I antigens on the surface of cultured cells. *Nature,* 308**,** 642-5.

BESSOLES, S., GRANDCLEMENT, C., ALARI-PAHISSA, E., GEHRIG, J., JEEVAN-RAJ, B. & HELD, W. 2014. Adaptations of Natural Killer Cells to Self-MHC Class I. *Front Immunol,* 5**,** 349.

BHATT, L., HORGAN, C. P., WALSH, M. & MCCAFFREY, M. W. 2007. The hereditary hemochromatosis protein HFE and its chaperone beta2-microglobulin localise predominantly to the endosomal-recycling compartment. *Biochem Biophys Res Commun,* 359**,** 277-84.

BIANCHI, C., DONADIO, C., TRAMONTI, G., CONSANI, C., LORUSSO, P. & ROSSI, G. 2001. Reappraisal of serum beta2-microglobulin as marker of GFR. *Ren Fail,* 23**,** 419-29.

BLAKE, C. C., GEISOW, M. J., OATLEY, S. J., RERAT, B. & RERAT, C. 1978. Structure of prealbumin: secondary, tertiary and quaternary interactions determined by Fourier refinement at 1.8 A. *J Mol Biol,* 121**,** 339-56.

BODIN, K., ELLMERICH, S., KAHAN, M. C., TENNENT, G. A., LOESCH, A., GILBERTSON, J. A., HUTCHINSON, W. L., MANGIONE, P. P., GALLIMORE, J. R., MILLAR, D. J., MINOGUE, S., DHILLON, A. P., TAYLOR, G. W., BRADWELL, A. R., PETRIE, A., GILLMORE, J. D., BELLOTTI, V., BOTTO, M., HAWKINS, P. N. & PEPYS, M. B. 2010. Antibodies to human serum amyloid P component eliminate visceral amyloid deposits. *Nature,* 468**,** 93-7.

BOGGS, L. N., FUSON, K. S., BAEZ, M., CHURGAY, L., MCCLURE, D., BECKER, G. & MAY, P. C. 1996. Clusterin (Apo J) protects against in vitro amyloid-beta (1-40) neurotoxicity. *J Neurochem,* 67**,** 1324-7.

BONAITI, B., OLSSON, M., HELLMAN, U., SUHR, O., BONAITI-PELLIE, C. & PLANTE-BORDENEUVE, V. 2010. TTR familial amyloid polyneuropathy: does a mitochondrial polymorphism entirely explain the parent-of-origin difference in penetrance? *Eur J Hum Genet,* 18**,** 948-52.

BONIFACIO, M. J., SAKAKI, Y. & SARAIVA, M. J. 1996. 'In vitro' amyloid fibril formation from transthyretin: the influence of ions and the amyloidogenicity of TTR variants. *Biochim Biophys Acta,* 1316**,** 35-42.

BOOTH, D. R., SOUTAR, A. K., HAWKINS, P. N. & PEPYS, M. B. 1993. Three new amyloidogenic transthyretin gene mutations advantages of direct sequencing. *In:* KISILEVSKY, R., BENSON, M. D., FRANGIONE, B., GAULDIE, J., MUCKLE, T. J. & YOUNG, I. D. (eds.) *Amyloid and Amyloidosis.* New York: Parthenon Publishing.

BOTTO, M., HAWKINS, P. N., BICKERSTAFF, M. C., HERBERT, J., BYGRAVE, A. E., MCBRIDE, A., HUTCHINSON, W. L., TENNENT, G. A., WALPORT, M. J. & PEPYS, M. B. 1997. Amyloid deposition is delayed in mice with targeted deletion of the serum amyloid P component gene. *Nat Med,* 3**,** 855-9.

BRAVERMAN, L. E., INGBAR, S. H. & STERLING, K. 1970. Conversion of thyroxine (T4) to triiodothyronine (T3) in athyreotic human subjects. *J Clin Invest,* 49**,** 855-64.

BRINSTER, R. L., ALLEN, J. M., BEHRINGER, R. R., GELINAS, R. E. & PALMITER, R. D. 1988. Introns increase transcriptional efficiency in transgenic mice. *Proc Natl Acad Sci U S A,* 85**,** 836-40.

BUCCIANTINI, M., CALLONI, G., CHITI, F., FORMIGLI, L., NOSI, D., DOBSON, C. M. & STEFANI, M. 2004. Prefibrillar amyloid protein aggregates share common features of cytotoxicity. *J Biol Chem,* 279**,** 31374-82.

BUKAU, B., WEISSMAN, J. & HORWICH, A. 2006. Molecular chaperones and protein quality control. *Cell,* 125**,** 443-51.

BULAWA, C. E., CONNELLY, S., DEVIT, M., WANG, L., WEIGEL, C., FLEMING, J. A., PACKMAN, J., POWERS, E. T., WISEMAN, R. L., FOSS, T. R., WILSON, I. A., KELLY, J. W. & LABAUDINIERE, R.

2012. Tafamidis, a potent and selective transthyretin kinetic stabilizer that inhibits the amyloid cascade. *Proc Natl Acad Sci U S A,* 109**,** 9629-34.

BUTLER, J. S., CHAN, A., COSTELHA, S., FISHMAN, S., WILLOUGHBY, J. L., BORLAND, T. D., MILSTEIN, S., FOSTER, D. J., GONCALVES, P., CHEN, Q., QIN, J., BETTENCOURT, B. R., SAH, D. W., ALVAREZ, R., RAJEEV, K. G., MANOHARAN, M., FITZGERALD, K., MEYERS, R. E., NOCHUR, S. V., SARAIVA, M. J. & ZIMMERMANN, T. S. 2016. Preclinical evaluation of RNAi as a treatment for transthyretin-mediated amyloidosis. *Amyloid,* 23**,** 109-18.

BUXBAUM, J., ALEXANDER, A., KOZIOL, J., TAGOE, C., FOX, E. & KITZMAN, D. 2010. Significance of the amyloidogenic transthyretin Val 122 Ile allele in African Americans in the Arteriosclerosis Risk in Communities (ARIC) and Cardiovascular Health (CHS) Studies. *Am Heart J,* 159**,** 864-70.

BUXBAUM, J. N., YE, Z., REIXACH, N., FRISKE, L., LEVY, C., DAS, P., GOLDE, T., MASLIAH, E., ROBERTS, A. R. & BARTFAI, T. 2008. Transthyretin protects Alzheimer's mice from the behavioral and biochemical effects of Abeta toxicity. *Proc Natl Acad Sci U S A,* 105**,** 2681-6.

CALABI, F. & MILSTEIN, C. 1986. A novel family of human major histocompatibility complex-related genes not mapping to chromosome 6. *Nature,* 323**,** 540-3.

CALABRESE, M. F. & MIRANKER, A. D. 2009. Metal binding sheds light on mechanisms of amyloid assembly. *Prion,* 3**,** 1-4.

CALERO, M., ROSTAGNO, A. & GHISO, J. 2012. Search for amyloid-binding proteins by affinity chromatography. *Methods Mol Biol,* 849**,** 213-23.

CARDOSO, I. & SARAIVA, M. J. 2006. Doxycycline disrupts transthyretin amyloid: evidence from studies in a FAP transgenic mice model. *FASEB J,* 20**,** 234-9.

CARR, A. S., PELAYO-NEGRO, A. L., EVANS, M. R., LAURA, M., BLAKE, J., STANCANELLI, C., IODICE, V., WECHALEKAR, A. D., WHELAN, C. J., GILLMORE, J. D., HAWKINS, P. N. & REILLY, M. M. 2016. A study of the neuropathy associated with transthyretin amyloidosis (ATTR) in the UK. *J Neurol Neurosurg Psychiatry,* 87**,** 620-7.

CASTANO, A., HELMKE, S., ALVAREZ, J., DELISLE, S. & MAURER, M. S. 2012. Diflunisal for ATTR cardiac amyloidosis. *Congest Heart Fail,* 18**,** 315-9.

CAVALLARO, T., MARTONE, R. L., DWORK, A. J., SCHON, E. A. & HERBERT, J. 1990. The retinal pigment epithelium is the unique site of transthyretin synthesis in the rat eye. *Invest Ophthalmol Vis Sci,* 31**,** 497-501.

CHADA, K., MAGRAM, J., RAPHAEL, K., RADICE, G., LACY, E. & COSTANTINI, F. 1985. Specific expression of a foreign beta-globin gene in erythroid cells of transgenic mice. *Nature,* 314**,** 377-80.

CHAMBERLAIN, J. W., NOLAN, J. A., CONRAD, P. J., VASAVADA, H. A., VASAVADA, H. H., PLOEGH, H. L., GANGULY, S., JANEWAY, C. A., JR. & WEISSMAN, S. M. 1988. Tissue-specific and cell surface expression of human major histocompatibility complex class I heavy

(HLA-B7) and light (beta 2-microglobulin) chain genes in transgenic mice. *Proc Natl Acad Sci U S A,* 85**,** 7690-4.

CHAMPY, M. F., SELLOUM, M., ZEITLER, V., CARADEC, C., JUNG, B., ROUSSEAU, S., POUILLY, L., SORG, T. & AUWERX, J. 2008. Genetic background determines metabolic phenotypes in the mouse. *Mamm Genome,* 19**,** 318-31.

CHAUDHURY, C., MEHNAZ, S., ROBINSON, J. M., HAYTON, W. L., PEARL, D. K., ROOPENIAN, D. C. & ANDERSON, C. L. 2003. The major histocompatibility complex-related Fc receptor for IgG (FcRn) binds albumin and prolongs its lifespan. *J Exp Med,* 197**,** 315-22.

CHITI, F. & DOBSON, C. M. 2006. Protein misfolding, functional amyloid, and human disease. *Annu Rev Biochem,* 75**,** 333-66.

CIBEIRA, M. T., SANCHORAWALA, V., SELDIN, D. C., QUILLEN, K., BERK, J. L., DEMBER, L. M., SEGAL, A., RUBERG, F., MEIER-EWERT, H., ANDREA, N. T., SLOAN, J. M., FINN, K. T., DOROS, G., BLADE, J. & SKINNER, M. 2011. Outcome of AL amyloidosis after high-dose melphalan and autologous stem cell transplantation: long-term results in a series of 421 patients. *Blood,* 118**,** 4346-52.

COELHO, T., ADAMS, D., SILVA, A., LOZERON, P., HAWKINS, P. N., MANT, T., PEREZ, J., CHIESA, J., WARRINGTON, S., TRANTER, E., MUNISAMY, M., FALZONE, R., HARROP, J., CEHELSKY, J., BETTENCOURT, B. R., GEISSLER, M., BUTLER, J. S., SEHGAL, A., MEYERS, R. E., CHEN, Q., BORLAND, T., HUTABARAT, R. M., CLAUSEN, V. A., ALVAREZ, R., FITZGERALD, K., GAMBA-VITALO, C., NOCHUR, S. V., VAISHNAW, A. K., SAH, D. W., GOLLOB, J. A. & SUHR, O. B. 2013. Safety and efficacy of RNAi therapy for transthyretin amyloidosis. *N Engl J Med,* 369**,** 819-29.

COELHO, T., MAIA, L. F., MARTINS DA SILVA, A., WADDINGTON CRUZ, M., PLANTE-BORDENEUVE, V., LOZERON, P., SUHR, O. B., CAMPISTOL, J. M., CONCEICAO, I. M., SCHMIDT, H. H., TRIGO, P., KELLY, J. W., LABAUDINIERE, R., CHAN, J., PACKMAN, J., WILSON, A. & GROGAN, D. R. 2012. Tafamidis for transthyretin familial amyloid polyneuropathy: a randomized, controlled trial. *Neurology,* 79**,** 785-92.

COLBERT, J. D., FARFAN-ARRIBAS, D. J. & ROCK, K. L. 2013. Substrate-induced protein stabilization reveals a predominant contribution from mature proteins to peptides presented on MHC class I. *J Immunol,* 191**,** 5410-9.

COLON, W. & KELLY, J. W. 1992. Partial denaturation of transthyretin is sufficient for amyloid fibril formation in vitro. *Biochemistry,* 31**,** 8654-60.

COLON, W., LAI, Z., MCCUTCHEN, S. L., MIROY, G. J., STRANG, C. & KELLY, J. W. 1996. FAP mutations destabilize transthyretin facilitating conformational changes required for amyloid formation. *Ciba Found Symp,* 199**,** 228-38; discussion 239-42.

COMENZO, R. L., REECE, D., PALLADINI, G., SELDIN, D., SANCHORAWALA, V., LANDAU, H., FALK, R., WELLS, K., SOLOMON, A., WECHALEKAR, A., ZONDER, J., DISPENZIERI, A., GERTZ, M., STREICHER, H., SKINNER, M., KYLE, R. A. & MERLINI, G. 2012. Consensus guidelines for the conduct and reporting of clinical trials in systemic light-chain amyloidosis. *Leukemia,* 26**,** 2317-25.

CONNORS, L. H., DOROS, G., SAM, F., BADIEE, A., SELDIN, D. C. & SKINNER, M. 2011. Clinical features and survival in senile systemic amyloidosis: comparison to familial transthyretin cardiomyopathy. *Amyloid,* 18 Suppl 1**,** 157-9.

CONNORS, L. H., LIM, A., PROKAEVA, T., ROSKENS, V. A. & COSTELLO, C. E. 2003. Tabulation of human transthyretin (TTR) variants, 2003. *Amyloid,* 10**,** 160-84.

CONNORS, L. H., SHIRAHAMA, T., SKINNER, M., FENVES, A. & COHEN, A. S. 1985. In vitro formation of amyloid fibrils from intact beta 2-microglobulin. *Biochem Biophys Res Commun,* 131**,** 1063-8.

COOPER, E. H., FORBES, M. A. & HAMBLING, M. H. 1984. Serum beta 2-microglobulin and C reactive protein concentrations in viral infections. *J Clin Pathol,* 37**,** 1140-3.

CORNWELL, G. G., 3RD, SLETTEN, K., JOHANSSON, B. & WESTERMARK, P. 1988. Evidence that the amyloid fibril protein in senile systemic amyloidosis is derived from normal prealbumin. *Biochem Biophys Res Commun,* 154**,** 648-53.

COSTA, P. P., FIGUEIRA, A. S. & BRAVO, F. R. 1978. Amyloid fibril protein related to prealbumin in familial amyloidotic polyneuropathy. *Proc Natl Acad Sci U S A,* 75**,** 4499-503.

COSTA, R., FERREIRA-DA-SILVA, F., SARAIVA, M. J. & CARDOSO, I. 2008. Transthyretin protects against A-beta peptide toxicity by proteolytic cleavage of the peptide: a mechanism sensitive to the Kunitz protease inhibitor. *PLoS One,* 3**,** e2899.

COWAN, A. J., SKINNER, M., BERK, J. L., SLOAN, J. M., O'HARA, C., SELDIN, D. C. & SANCHORAWALA, V. 2011. Macroglossia - not always AL amyloidosis. *Amyloid,* 18**,** 83-6.

CRESSWELL, P., BANGIA, N., DICK, T. & DIEDRICH, G. 1999. The nature of the MHC class I peptide loading complex. *Immunol Rev,* 172**,** 21-8.

CRESSWELL, P., SPRINGER, T., STROMINGER, J. L., TURNER, M. J., GREY, H. M. & KUBO, R. T. 1974. Immunological identity of the small subunit of HL-A antigens and beta2-microglobulin and its turnover on the cell membrane. *Proc Natl Acad Sci U S A,* 71**,** 2123-7.

CULYBA, E. K., PRICE, J. L., HANSON, S. R., DHAR, A., WONG, C. H., GRUEBELE, M., POWERS, E. T. & KELLY, J. W. 2011. Protein native-state stabilization by placing aromatic side chains in N-glycosylated reverse turns. *Science,* 331**,** 571-5.

DAVIS, P. J., SPAULDING, S. W. & GREGERMAN, R. I. 1970. The three thyroxine-binding proteins in rat serum: binding capacities and effects of binding inhibitors. *Endocrinology,* 87**,** 978-86.

DE LUIGI, A., COLOMBO, L., DIOMEDE, L., CAPOBIANCO, R., MANGIERI, M., MICCOLO, C., LIMIDO, L., FORLONI, G., TAGLIAVINI, F. & SALMONA, M. 2008. The efficacy of tetracyclines in peripheral and intracerebral prion infection. *PLoS One,* 3**,** e1888.

DEGEN, E., COHEN-DOYLE, M. F. & WILLIAMS, D. B. 1992. Efficient dissociation of the p88 chaperone from major histocompatibility complex class I molecules requires both beta 2-microglobulin and peptide. *J Exp Med,* 175**,** 1653-61.

DEMBER, L. M. 2006. Amyloidosis-associated kidney disease. *J Am Soc Nephrol,* 17**,** 3458-71.

DEMBER, L. M., HAWKINS, P. N., HAZENBERG, B. P., GOREVIC, P. D., MERLINI, G., BUTRIMIENE, I., LIVNEH, A., LESNYAK, O., PUECHAL, X., LACHMANN, H. J., OBICI, L., BALSHAW, R., GARCEAU, D., HAUCK, W., SKINNER, M. & EPRODISATE FOR, A. A. A. T. G. 2007. Eprodisate for the treatment of renal disease in AA amyloidosis. *N Engl J Med,* 356**,** 2349-60.

DICKSON, P. W., ALDRED, A. R., MARLEY, P. D., BANNISTER, D. & SCHREIBER, G. 1986. Rat choroid plexus specializes in the synthesis and the secretion of transthyretin (prealbumin). Regulation of transthyretin synthesis in choroid plexus is independent from that in liver. *J Biol Chem,* 261**,** 3475-8.

DICKSON, P. W., HOWLETT, G. J. & SCHREIBER, G. 1985. Rat transthyretin (prealbumin). Molecular cloning, nucleotide sequence, and gene expression in liver and brain. *J Biol Chem,* 260**,** 8214-9.

DIEDRICH, G., BANGIA, N., PAN, M. & CRESSWELL, P. 2001. A role for calnexin in the assembly of the MHC class I loading complex in the endoplasmic reticulum. *J Immunol,* 166**,** 1703-9.

DIOMEDE, L., SORIA, C., ROMEO, M., GIORGETTI, S., MARCHESE, L., MANGIONE, P. P., PORCARI, R., ZORZOLI, I., SALMONA, M., BELLOTTI, V. & STOPPINI, M. 2012. C. elegans expressing human beta2-microglobulin: a novel model for studying the relationship between the molecular assembly and the toxic phenotype. *PLoS One,* 7**,** e52314.

DISPENZIERI, A., SEENITHAMBY, K., LACY, M. Q., KUMAR, S. K., BUADI, F. K., HAYMAN, S. R., DINGLI, D., LITZOW, M. R., GASTINEAU, D. A., INWARDS, D. J., MICALLEF, I. N., ANSELL, S. M., JOHNSTON, P. B., PORRATA, L. F., PATNAIK, M. M., HOGAN, W. J. & GERTZ, M. A. 2013. Patients with immunoglobulin light chain amyloidosis undergoing autologous stem cell transplantation have superior outcomes compared with patients with multiple myeloma: a retrospective review from a tertiary referral center. *Bone Marrow Transplant,* 48**,** 1302-7.

DOYLE, S. M., GENEST, O. & WICKNER, S. 2013. Protein rescue from aggregates by powerful molecular chaperone machines. *Nat Rev Mol Cell Biol,* 14**,** 617-29.

DUBREY, S. W., BURKE, M. M., HAWKINS, P. N. & BANNER, N. R. 2004. Cardiac transplantation for amyloid heart disease: the United Kingdom experience. *J Heart Lung Transplant,* 23**,** 1142-53.

DUBREY, S. W., CHA, K., ANDERSON, J., CHAMARTHI, B., REISINGER, J., SKINNER, M. & FALK, R. H. 1998. The clinical features of immunoglobulin light-chain (AL) amyloidosis with heart involvement. *QJM,* 91**,** 141-57.

DUBREY, S. W., HAWKINS, P. N. & FALK, R. H. 2011. Amyloid diseases of the heart: assessment, diagnosis, and referral. *Heart,* 97**,** 75-84.

DUNGU, J. N., ANDERSON, L. J., WHELAN, C. J. & HAWKINS, P. N. 2012. Cardiac transthyretin amyloidosis. *Heart,* 98**,** 1546-54.

DWULET, F. E. & BENSON, M. D. 1984. Primary structure of an amyloid prealbumin and its plasma precursor in a heredofamilial polyneuropathy of Swedish origin. *Proc Natl Acad Sci U S A,* 81**,** 694-8.

DWULET, F. E. & BENSON, M. D. 1986. Characterization of a transthyretin (prealbumin) variant associated with familial amyloidotic polyneuropathy type II (Indiana/Swiss). *J Clin Invest,* 78**,** 880-6.

EBERL, G., WIDMANN, C. & CORRADIN, G. 1996. The functional half-life of H-2Kd-restricted T cell epitopes on living cells. *Eur J Immunol,* 26**,** 1993-9.

EICHNER, T., KALVERDA, A. P., THOMPSON, G. S., HOMANS, S. W. & RADFORD, S. E. 2011. Conformational conversion during amyloid formation at atomic resolution. *Mol Cell,* 41**,** 161-72.

EPISKOPOU, V., MAEDA, S., NISHIGUCHI, S., SHIMADA, K., GAITANARIS, G. A., GOTTESMAN, M. E. & ROBERTSON, E. J. 1993. Disruption of the transthyretin gene results in mice with depressed levels of plasma retinol and thyroid hormone. *Proc Natl Acad Sci U S A,* 90**,** 2375-9.

ERIKSEN, N., ERICSSON, L. H., PEARSALL, N., LAGUNOFF, D. & BENDITT, E. P. 1976. Mouse amyloid protein AA: Homology with nonimmunoglobulin protein of human and monkey amyloid substance. *Proc Natl Acad Sci U S A,* 73**,** 964-7.

ERIKSSON, M., SCHONLAND, S., YUMLU, S., HEGENBART, U., VON HUTTEN, H., GIOEVA, Z., LOHSE, P., BUTTNER, J., SCHMIDT, H. & ROCKEN, C. 2009. Hereditary apolipoprotein AI-associated amyloidosis in surgical pathology specimens: identification of three novel mutations in the APOA1 gene. *J Mol Diagn,* 11**,** 257-62.

EVRIN, P. E., PETERSON, P. A., WIDE, L. & BERGGARD, I. 1971. Radioimmunoassay of 2 -microglobulin in human biological fluids. *Scand J Clin Lab Invest,* 28**,** 439-43.

FALK, R. H. 2005. Diagnosis and management of the cardiac amyloidoses. *Circulation,* 112**,** 2047-60.

FEDER, J. N., GNIRKE, A., THOMAS, W., TSUCHIHASHI, Z., RUDDY, D. A., BASAVA, A., DORMISHIAN, F., DOMINGO, R., JR., ELLIS, M. C., FULLAN, A., HINTON, L. M., JONES, N. L., KIMMEL, B. E., KRONMAL, G. S., LAUER, P., LEE, V. K., LOEB, D. B., MAPA, F. A., MCCLELLAND, E., MEYER, N. C., MINTIER, G. A., MOELLER, N., MOORE, T., MORIKANG, E., PRASS, C. E., QUINTANA, L., STARNES, S. M., SCHATZMAN, R. C., BRUNKE, K. J., DRAYNA, D. T., RISCH, N. J., BACON, B. R. & WOLFF, R. K. 1996. A novel MHC class I-like gene is mutated in patients with hereditary haemochromatosis. *Nat Genet,* 13**,** 399-408.

FENG, D., EDWARDS, W. D., OH, J. K., CHANDRASEKARAN, K., GROGAN, M., MARTINEZ, M. W., SYED, I. S., HUGHES, D. A., LUST, J. A., JAFFE, A. S., GERTZ, M. A. & KLARICH, K. W. 2007. Intracardiac thrombosis and embolism in patients with cardiac amyloidosis. *Circulation,* 116**,** 2420-6.

FLOEGE, J., BARTSCH, A., SCHULZE, M., SHALDON, S., KOCH, K. M. & SMEBY, L. C. 1991. Clearance and synthesis rates of beta 2-microglobulin in patients undergoing hemodialysis and in normal subjects. *J Lab Clin Med,* 118**,** 153-65.

FLOEGE, J., SCHAFFER, J., KOCH, K. M. & SHALDON, S. 1992. Dialysis related amyloidosis: a disease of chronic retention and inflammation? *Kidney Int Suppl,* 38**,** S78-85.

FOLI, A., PALLADINI, G., CAPORALI, R., VERGA, L., MORBINI, P., OBICI, L., RUSSO, P., SARAIS, G., DONADEI, S., MONTECUCCO, C. & MERLINI, G. 2011. The role of minor salivary gland biopsy in the diagnosis of systemic amyloidosis: results of a prospective study in 62 patients. *Amyloid,* 18 Suppl 1**,** 80-2.

FONTANA, M., PICA, S., REANT, P., ABDEL-GADIR, A., TREIBEL, T. A., BANYPERSAD, S. M., MAESTRINI, V., BARCELLA, W., ROSMINI, S., BULLUCK, H., SAYED, R. H., PATEL, K., MAMHOOD, S., BUCCIARELLI-DUCCI, C., WHELAN, C. J., HERREY, A. S., LACHMANN, H. J., WECHALEKAR, A. D., MANISTY, C. H., SCHELBERT, E. B., KELLMAN, P., GILLMORE, J. D., HAWKINS, P. N. & MOON, J. C. 2015. Prognostic Value of Late Gadolinium Enhancement Cardiovascular Magnetic Resonance in Cardiac Amyloidosis. *Circulation,* 132**,** 1570-9.

FRENCH, K., YERBURY, J. J. & WILSON, M. R. 2008. Protease activation of alpha2-macroglobulin modulates a chaperone-like action with broad specificity. *Biochemistry,* 47**,** 1176-85.

FRIEDMAN, S. & JANOWITZ, H. D. 1998. Systemic amyloidosis and the gastrointestinal tract. *Gastroenterol Clin North Am,* 27**,** 595-614, vi.

FUKUNISHI, S., YOH, K., KAMAE, S. & YOSHIYA, S. 2007. Beta 2-microglobulin amyloid deposit in HLA-B27 transgenic rats. *Mod Rheumatol,* 17**,** 380-4.

GAGNON, R. F., SOMERVILLE, P. & THOMSON, D. M. 1988. Circulating form of beta-2-microglobulin in dialysis patients. *Am J Nephrol,* 8**,** 379-83.

GAL, R., KORZETS, A., SCHWARTZ, A., RATH-WOLFSON, L. & GAFTER, U. 1994. Systemic distribution of beta 2-microglobulin-derived amyloidosis in patients who undergo long-term hemodialysis. Report of seven cases and review of the literature. *Arch Pathol Lab Med,* 118**,** 718-21.

GANOWIAK, K., HULTMAN, P., ENGSTROM, U., GUSTAVSSON, A. & WESTERMARK, P. 1994. Fibrils from synthetic amyloid-related peptides enhance development of experimental AA-amyloidosis in mice. *Biochem Biophys Res Commun,* 199**,** 306-12.

GEJYO, F., HOMMA, N., SUZUKI, Y. & ARAKAWA, M. 1986a. Serum levels of beta 2-microglobulin as a new form of amyloid protein in patients undergoing long-term hemodialysis. *N Engl J Med,* 314**,** 585-6.

GEJYO, F., ODANI, S., YAMADA, T., HONMA, N., SAITO, H., SUZUKI, Y., NAKAGAWA, Y., KOBAYASHI, H., MARUYAMA, Y., HIRASAWA, Y. & ET AL. 1986b. Beta 2-microglobulin: a new form of amyloid protein associated with chronic hemodialysis. *Kidney Int,* 30**,** 385-90.

GEJYO, F., YAMADA, T., ODANI, S., NAKAGAWA, Y., ARAKAWA, M., KUNITOMO, T., KATAOKA, H., SUZUKI, M., HIRASAWA, Y., SHIRAHAMA, T. & ET AL. 1985. A new form of amyloid protein associated with chronic hemodialysis was identified as beta 2-microglobulin. *Biochem Biophys Res Commun,* 129**,** 701-6.

GERTZ, M. A., BENSON, M. D., DYCK, P. J., GROGAN, M., COELHO, T., CRUZ, M., BERK, J. L., PLANTE-BORDENEUVE, V., SCHMIDT, H. H. & MERLINI, G. 2015. Diagnosis, Prognosis, and Therapy of Transthyretin Amyloidosis. *J Am Coll Cardiol,* 66**,** 2451-66.

GHETIE, V., HUBBARD, J. G., KIM, J. K., TSEN, M. F., LEE, Y. & WARD, E. S. 1996. Abnormally short serum half-lives of IgG in beta 2-microglobulin-deficient mice. *Eur J Immunol,* 26**,** 690-6.

GIBSON, D. G., YOUNG, L., CHUANG, R. Y., VENTER, J. C., HUTCHISON, C. A., 3RD & SMITH, H. O. 2009. Enzymatic assembly of DNA molecules up to several hundred kilobases. *Nat Methods,* 6**,** 343-5.

GILBERTSON, J. A., THEIS, J. D., VRANA, J. A., LACHMANN, H., WECHALEKAR, A., WHELAN, C., HAWKINS, P. N., DOGAN, A. & GILLMORE, J. D. 2015. A comparison of immunohistochemistry and mass spectrometry for determining the amyloid fibril protein from formalin-fixed biopsy tissue. *J Clin Pathol,* 68**,** 314-7.

GILLMORE, J. D., LOVAT, L. B., PERSEY, M. R., PEPYS, M. B. & HAWKINS, P. N. 2001. Amyloid load and clinical outcome in AA amyloidosis in relation to circulating concentration of serum amyloid A protein. *Lancet,* 358**,** 24-9.

GILLMORE, J. D., TENNENT, G. A., HUTCHINSON, W. L., GALLIMORE, J. R., LACHMANN, H. J., GOODMAN, H. J., OFFER, M., MILLAR, D. J., PETRIE, A., HAWKINS, P. N. & PEPYS, M. B. 2010. Sustained pharmacological depletion of serum amyloid P component in patients with systemic amyloidosis. *Br J Haematol,* 148**,** 760-7.

GIORGETTI, S., RAIMONDI, S., PAGANO, K., RELINI, A., BUCCIANTINI, M., CORAZZA, A., FOGOLARI, F., CODUTTI, L., SALMONA, M., MANGIONE, P., COLOMBO, L., DE LUIGI, A., PORCARI, R., GLIOZZI, A., STEFANI, M., ESPOSITO, G., BELLOTTI, V. & STOPPINI, M. 2011. Effect of tetracyclines on the dynamics of formation and destructuration of beta2-microglobulin amyloid fibrils. *J Biol Chem,* 286**,** 2121-31.

GLENNER, G. G. & WONG, C. W. 1984. Alzheimer's disease: initial report of the purification and characterization of a novel cerebrovascular amyloid protein. *Biochem Biophys Res Commun,* 120**,** 885-90.

GONZALEZ-DUARTE, A., LEM-CARRILLO, M. & CARDENAS-SOTO, K. 2013. Description of transthyretin S50A, S52P and G47A mutations in familial amyloidosis polyneuropathy. *Amyloid,* 20**,** 221-5.

GOREVIC, P. D., MUNOZ, P. C., CASEY, T. T., DIRAIMONDO, C. R., STONE, W. J., PRELLI, F. C., RODRIGUES, M. M., POULIK, M. D. & FRANGIONE, B. 1986. Polymerization of intact beta 2-microglobulin in tissue causes amyloidosis in patients on chronic hemodialysis. *Proc Natl Acad Sci U S A,* 83**,** 7908-12.

GORSKI, K., CARNEIRO, M. & SCHIBLER, U. 1986. Tissue-specific in vitro transcription from the mouse albumin promoter. *Cell,* 47**,** 767-76.

GOUIN-CHARNET, A., LAUNE, D., GRANIER, C., MANI, J. C., PAU, B., MOURAD, G. & ARGILES, A. 2000. alpha2-Macroglobulin, the main serum antiprotease, binds beta2-microglobulin, the light chain of the class I major histocompatibility complex, which is involved in human disease. *Clin Sci (Lond),* 98**,** 427-33.

GOUIN-CHARNET, A., MOURAD, G. & ARGILES, A. 1997. Alpha 2-macroglobulin protects some of the protein constituents of dialysis-associated amyloidosis from protease degradation. *Biochem Biophys Res Commun,* 231**,** 48-51.

GREGORINI, G., IZZI, C., OBICI, L., TARDANICO, R., ROCKEN, C., VIOLA, B. F., CAPISTRANO, M., DONADEI, S., BIASI, L., SCALVINI, T., MERLINI, G. & SCOLARI, F. 2005. Renal apolipoprotein A-I amyloidosis: a rare and usually ignored cause of hereditary tubulointerstitial nephritis. *J Am Soc Nephrol,* 16**,** 3680-6.

GREIPP, P. R., KATZMANN, J. A., O'FALLON, W. M. & KYLE, R. A. 1988. Value of beta 2-microglobulin level and plasma cell labeling indices as prognostic factors in patients with newly diagnosed myeloma. *Blood,* 72**,** 219-23.

GREY, H. M., KUBO, R. T., COLON, S. M., POULIK, M. D., CRESSWELL, P., SPRINGER, T., TURNER, M. & STROMINGER, J. L. 1973. The small subunit of HL-A antigens is beta 2-microglobulin. *J Exp Med,* 138**,** 1608-12.

GUSSOW, D., REIN, R., GINJAAR, I., HOCHSTENBACH, F., SEEMANN, G., KOTTMAN, A. & PLOEGH, H. L. 1987. The human beta 2-microglobulin gene. Primary structure and definition of the transcriptional unit. *J Immunol,* 139**,** 3132-8.

HAASS, C. & SELKOE, D. J. 1993. Cellular processing of beta-amyloid precursor protein and the genesis of amyloid beta-peptide. *Cell,* 75**,** 1039-42.

HAGEN, G. A. & ELLIOTT, W. J. 1973. Transport of thyroid hormones in serum and cerebrospinal fluid. *J Clin Endocrinol Metab,* 37**,** 415-22.

HAMMARSTROM, P., SCHNEIDER, F. & KELLY, J. W. 2001. Trans-suppression of misfolding in an amyloid disease. *Science,* 293**,** 2459-62.

HAMMER, R. E., KRUMLAUF, R., CAMPER, S. A., BRINSTER, R. L. & TILGHMAN, S. M. 1987. Diversity of alpha-fetoprotein gene expression in mice is generated by a combination of separate enhancer elements. *Science,* 235**,** 53-8.

HANSEN, P. B., KJELDSEN, L., DALHOFF, K. & OLESEN, B. 1992. Cerebrospinal fluid beta-2-microglobulin in adult patients with acute leukemia or lymphoma: a useful marker in early diagnosis and monitoring of CNS-involvement. *Acta Neurol Scand,* 85**,** 224-7.

HARPER, J. D., LIEBER, C. M. & LANSBURY, P. T., JR. 1997. Atomic force microscopic imaging of seeded fibril formation and fibril branching by the Alzheimer's disease amyloid-beta protein. *Chem Biol,* 4**,** 951-9.

HAWKINS, P. N., ANDO, Y., DISPENZERI, A., GONZALEZ-DUARTE, A., ADAMS, D. & SUHR, O. B. 2015. Evolving landscape in the management of transthyretin amyloidosis. *Ann Med,* 47**,** 625-38.

HAWKINS, P. N., LAVENDER, J. P. & PEPYS, M. B. 1990a. Evaluation of systemic amyloidosis by scintigraphy with 123I-labeled serum amyloid P component. *N Engl J Med,* 323**,** 508-13.

HAWKINS, P. N., MYERS, M. J., EPENETOS, A. A., CASPI, D. & PEPYS, M. B. 1988. Specific localization and imaging of amyloid deposits in vivo using 123I-labeled serum amyloid P component. *J Exp Med,* 167**,** 903-13.

HAWKINS, P. N., RICHARDSON, S., MACSWEENEY, J. E., KING, A. D., VIGUSHIN, D. M., LAVENDER, J. P. & PEPYS, M. B. 1993. Scintigraphic quantification and serial monitoring of human visceral

amyloid deposits provide evidence for turnover and regression. *Q J Med,* 86**,** 365-74.

HAWKINS, P. N., WOOTTON, R. & PEPYS, M. B. 1990b. Metabolic studies of radioiodinated serum amyloid P component in normal subjects and patients with systemic amyloidosis. *J Clin Invest,* 86**,** 1862-9.

HECKEL, J. L., SANDGREN, E. P., DEGEN, J. L., PALMITER, R. D. & BRINSTER, R. L. 1990. Neonatal bleeding in transgenic mice expressing urokinase-type plasminogen activator. *Cell,* 62**,** 447-56.

HELENIUS, A. & AEBI, M. 2004. Roles of N-linked glycans in the endoplasmic reticulum. *Annu Rev Biochem,* 73**,** 1019-49.

HELLMAN, U., ALARCON, F., LUNDGREN, H. E., SUHR, O. B., BONAITI-PELLIE, C. & PLANTE-BORDENEUVE, V. 2008. Heterogeneity of penetrance in familial amyloid polyneuropathy, ATTR Val30Met, in the Swedish population. *Amyloid,* 15**,** 181-6.

HIGUCHI, K., KITAGAWA, K., NAIKI, H., HANADA, K., HOSOKAWA, M. & TAKEDA, T. 1991a. Polymorphism of apolipoprotein A-II (apoA-II) among inbred strains of mice. Relationship between the molecular type of apoA-II and mouse senile amyloidosis. *Biochem J,* 279 ( Pt 2)**,** 427-33.

HIGUCHI, K., KOGISHI, K., WANG, J., CHEN, X., CHIBA, T., MATSUSHITA, T., HOSHII, Y., KAWANO, H., ISHIHARA, T., YOKOTA, T. & HOSOKAWA, M. 1998. Fibrilization in mouse senile amyloidosis is fibril conformation-dependent. *Lab Invest,* 78**,** 1535-42.

HIGUCHI, K., KOGISHI, K., WANG, J., XIA, C., CHIBA, T., MATSUSHITA, T. & HOSOKAWA, M. 1997. Accumulation of pro-apolipoprotein A-II in mouse senile amyloid fibrils. *Biochem J,* 325 ( Pt 3)**,** 653-9.

HIGUCHI, K., NAIKI, H., KITAGAWA, K., HOSOKAWA, M. & TAKEDA, T. 1991b. Mouse senile amyloidosis. ASSAM amyloidosis in mice presents universally as a systemic age-associated amyloidosis. *Virchows Arch B Cell Pathol Incl Mol Pathol,* 60**,** 231-8.

HILGERT, I., HOREJSI, V. & KRISTOFOVA, H. 1984. The use of murine monoclonal antibody B2M-01 for detection and purification of human beta 2-microglobulin. *Folia Biol (Praha),* 30**,** 369-76.

HOFFMAN, J. S., ERICSSON, L. H., ERIKSEN, N., WALSH, K. A. & BENDITT, E. P. 1984. Murine tissue amyloid protein AA. NH2-terminal sequence identity with only one of two serum amyloid protein (ApoSAA) gene products. *J Exp Med,* 159**,** 641-6.

HOL, P. R., SNEL, F. W., NIEWOLD, T. A. & GRUYS, E. 1986. Amyloid-enhancing factor (AEF) in the pathogenesis of AA-amyloidosis in the hamster. *Virchows Arch B Cell Pathol Incl Mol Pathol,* 52**,** 273-81.

HOLMGREN, G., STEEN, L., EKSTEDT, J., GROTH, C. G., ERICZON, B. G., ERIKSSON, S., ANDERSEN, O., KARLBERG, I., NORDEN, G., NAKAZATO, M. & ET AL. 1991. Biochemical effect of liver transplantation in two Swedish patients with familial amyloidotic polyneuropathy (FAP-met30). *Clin Genet,* 40**,** 242-6.

HOLMGREN, G., WIKSTROM, L., LUNDGREN, H. E. & SUHR, O. B. 2004. Discordant penetrance of the trait for familial amyloidotic polyneuropathy in two pairs of monozygotic twins. *J Intern Med,* 256**,** 453-6.

HOSHINO, J., YAMAGATA, K., NISHI, S., NAKAI, S., MASAKANE, I., ISEKI, K. & TSUBAKIHARA, Y. 2016. Significance of the decreased risk of dialysis-related amyloidosis now proven by results from Japanese nationwide surveys in 1998 and 2010. *Nephrol Dial Transplant,* 31**,** 595-602.

HSIAO, K., CHAPMAN, P., NILSEN, S., ECKMAN, C., HARIGAYA, Y., YOUNKIN, S., YANG, F. & COLE, G. 1996. Correlative memory deficits, Abeta elevation, and amyloid plaques in transgenic mice. *Science,* 274**,** 99-102.

HUBBARD, R. & KROPF, A. 1959. Molecular aspects of visual excitation. *Ann N Y Acad Sci,* 81**,** 388-98.

HUMPHREYS, D. T., CARVER, J. A., EASTERBROOK-SMITH, S. B. & WILSON, M. R. 1999. Clusterin has chaperone-like activity similar to that of small heat shock proteins. *J Biol Chem,* 274**,** 6875-81.

HURSHMAN, A. R., WHITE, J. T., POWERS, E. T. & KELLY, J. W. 2004. Transthyretin aggregation under partially denaturing conditions is a downhill polymerization. *Biochemistry,* 43**,** 7365-81.

HUTCHINSON, W. L., NOBLE, G. E., HAWKINS, P. N. & PEPYS, M. B. 1994. The pentraxins, C-reactive protein and serum amyloid P component, are cleared and catabolized by hepatocytes in vivo. *J Clin Invest,* 94**,** 1390-6.

HUTT, D. F., QUIGLEY, A. M., PAGE, J., HALL, M. L., BURNISTON, M., GOPAUL, D., LANE, T., WHELAN, C. J., LACHMANN, H. J., GILLMORE, J. D., HAWKINS, P. N. & WECHALEKAR, A. D. 2014. Utility and limitations of 3,3-diphosphono-1,2-propanodicarboxylic acid scintigraphy in systemic amyloidosis. *Eur Heart J Cardiovasc Imaging,* 15**,** 1289-98.

IHSE, E., RAPEZZI, C., MERLINI, G., BENSON, M. D., ANDO, Y., SUHR, O. B., IKEDA, S., LAVATELLI, F., OBICI, L., QUARTA, C. C., LEONE, O., JONO, H., UEDA, M., LORENZINI, M., LIEPNIEKS, J., OHSHIMA, T., TASAKI, M., YAMASHITA, T. & WESTERMARK, P. 2013. Amyloid fibrils containing fragmented ATTR may be the standard fibril composition in ATTR amyloidosis. *Amyloid,* 20**,** 142-50.

INGBAR, S. H. 1958. Pre-albumin: a thyroxinebinding protein of human plasma. *Endocrinology,* 63**,** 256-9.

INGENBLEEK, Y. & BERNSTEIN, L. H. 2015. Plasma Transthyretin as a Biomarker of Lean Body Mass and Catabolic States. *Adv Nutr,* 6**,** 572-80.

INGENBLEEK, Y. & DE VISSCHER, M. 1979. Hormonal and nutritional status: critical conditions for endemic goiter epidemiology? *Metabolism,* 28**,** 9-19.

IONESCU-ZANETTI, C., KHURANA, R., GILLESPIE, J. R., PETRICK, J. S., TRABACHINO, L. C., MINERT, L. J., CARTER, S. A. & FINK, A. L. 1999. Monitoring the assembly of Ig light-chain amyloid fibrils by atomic force microscopy. *Proc Natl Acad Sci U S A,* 96**,** 13175-9.

ISRAEL, E. J., PATEL, V. K., TAYLOR, S. F., MARSHAK-ROTHSTEIN, A. & SIMISTER, N. E. 1995. Requirement for a beta 2-microglobulin-associated Fc receptor for acquisition of maternal IgG by fetal and neonatal mice. *J Immunol,* 154**,** 6246-51.

IVANOVA, M. I., SAWAYA, M. R., GINGERY, M., ATTINGER, A. & EISENBERG, D. 2004. An amyloid-forming segment of beta2-microglobulin suggests a molecular model for the fibril. *Proc Natl Acad Sci U S A,* 101**,** 10584-9.

JACKSON, M. R., COHEN-DOYLE, M. F., PETERSON, P. A. & WILLIAMS, D. B. 1994. Regulation of MHC class I transport by the molecular chaperone, calnexin (p88, IP90). *Science,* 263**,** 384-7.

JACOBSON, D. R., GOREVIC, P. D. & BUXBAUM, J. N. 1990. A homozygous transthyretin variant associated with senile systemic amyloidosis: evidence for a late-onset disease of genetic etiology. *Am J Hum Genet,* 47**,** 127-36.

JACOBSON, D. R., MCFARLIN, D. E., KANE, I. & BUXBAUM, J. N. 1992. Transthyretin Pro55, a variant associated with early-onset, aggressive, diffuse amyloidosis with cardiac and neurologic involvement. *Hum Genet,* 89**,** 353-6.

JACOBSON, D. R., PASTORE, R. D., YAGHOUBIAN, R., KANE, I., GALLO, G., BUCK, F. S. & BUXBAUM, J. N. 1997. Variant-sequence transthyretin (isoleucine 122) in late-onset cardiac amyloidosis in black Americans. *N Engl J Med,* 336**,** 466-73.

JADOUL, M. 1998. Dialysis-related amyloidosis: importance of biocompatibility and age. *Nephrol Dial Transplant,* 13 Suppl 7**,** 61-4.

JADOUL, M., GARBAR, C., NOEL, H., SENNESAEL, J., VANHOLDER, R., BERNAERT, P., RORIVE, G., HANIQUE, G. & VAN YPERSELE DE STRIHOU, C. 1997. Histological prevalence of beta 2-microglobulin amyloidosis in hemodialysis: a prospective post-mortem study. *Kidney Int,* 51**,** 1928-32.

JAHN, T. R., TENNENT, G. A. & RADFORD, S. E. 2008. A common beta-sheet architecture underlies in vitro and in vivo beta2-microglobulin amyloid fibrils. *J Biol Chem,* 283**,** 17279-86.

JANSON, J., SOELLER, W. C., ROCHE, P. C., NELSON, R. T., TORCHIA, A. J., KREUTTER, D. K. & BUTLER, P. C. 1996. Spontaneous diabetes mellitus in transgenic mice expressing human islet amyloid polypeptide. *Proc Natl Acad Sci U S A,* 93**,** 7283-8.

JANSSENS, F., SPAHR, L., RUBBIA-BRANDT, L., GIOSTRA, E. & BIHL, F. 2010. Hepatic amyloidosis increases liver stiffness measured by transient elastography. *Acta Gastroenterol Belg,* 73**,** 52-4.

JARDETZKY, T. S., LANE, W. S., ROBINSON, R. A., MADDEN, D. R. & WILEY, D. C. 1991. Identification of self peptides bound to purified HLA-B27. *Nature,* 353**,** 326-9.

JARRETT, J. T. & LANSBURY, P. T., JR. 1993. Seeding "one-dimensional crystallization" of amyloid: a pathogenic mechanism in Alzheimer's disease and scrapie? *Cell,* 73**,** 1055-8.

JENNINGS, A. S., FERGUSON, D. C. & UTIGER, R. D. 1979. Regulation of the conversion of thyroxine to triiodothyronine in the perfused rat liver. *J Clin Invest,* 64**,** 1614-23.

JIMENEZ, R. E., PRICE, D. A., PINKUS, G. S., OWEN, W. F., JR., LAZARUS, J. M., KAY, J. & TURNER, J. R. 1998. Development of gastrointestinal beta2-microglobulin amyloidosis correlates with time on dialysis. *Am J Surg Pathol,* 22**,** 729-35.

JITSUHARA, Y., TOYODA, T., ITAI, T. & YAMAGUCHI, H. 2002. Chaperone-like functions of high-mannose type and complex-type N-glycans and their molecular basis. *J Biochem,* 132**,** 803-11.

JOHAN, K., WESTERMARK, G., ENGSTROM, U., GUSTAVSSON, A., HULTMAN, P. & WESTERMARK, P. 1998. Acceleration of amyloid protein A amyloidosis by amyloid-like synthetic fibrils. *Proc Natl Acad Sci U S A,* 95**,** 2558-63.

JOHNSON, D., HARRISON, S., PINEDA, N., HEINLEIN, C., AL-SHAWI, R. & BISHOP, J. O. 1995. Localization of the response elements of a gene induced by intermittent growth hormone stimulation. *J Mol Endocrinol,* 14**,** 35-49.

JOHNSON, S. M., CONNELLY, S., FEARNS, C., POWERS, E. T. & KELLY, J. W. 2012. The transthyretin amyloidoses: from delineating the molecular mechanism of aggregation linked to pathology to a regulatory-agency-approved drug. *J Mol Biol,* 421**,** 185-203.

JOOSTEN, M. M., PAI, J. K., BERTOIA, M. L., GANSEVOORT, R. T., BAKKER, S. J., COOKE, J. P., RIMM, E. B. & MUKAMAL, K. J. 2014. beta2-microglobulin, cystatin C, and creatinine and risk of symptomatic peripheral artery disease. *J Am Heart Assoc,* 3.

JUNGHANS, R. P. & ANDERSON, C. L. 1996. The protection receptor for IgG catabolism is the beta2-microglobulin-containing neonatal intestinal transport receptor. *Proc Natl Acad Sci U S A,* 93**,** 5512-6.

JURGENS, C. A., TOUKATLY, M. N., FLIGNER, C. L., UDAYASANKAR, J., SUBRAMANIAN, S. L., ZRAIKA, S., ASTON-MOURNEY, K., CARR, D. B., WESTERMARK, P., WESTERMARK, G. T., KAHN, S. E. & HULL, R. L. 2011. beta-cell loss and beta-cell apoptosis in human type 2 diabetes are related to islet amyloid deposition. *Am J Pathol,* 178**,** 2632-40.

KANAI, M., RAZ, A. & GOODMAN, D. S. 1968. Retinol-binding protein: the transport protein for vitamin A in human plasma. *J Clin Invest,* 47**,** 2025-44.

KANG, S. J. & CRESSWELL, P. 2002. Calnexin, calreticulin, and ERp57 cooperate in disulfide bond formation in human CD1d heavy chain. *J Biol Chem,* 277**,** 44838-44.

KAPOOR, M., ELLGAARD, L., GOPALAKRISHNAPAI, J., SCHIRRA, C., GEMMA, E., OSCARSON, S., HELENIUS, A. & SUROLIA, A. 2004. Mutational analysis provides molecular insight into the carbohydrate-binding region of calreticulin: pivotal roles of tyrosine-109 and aspartate-135 in carbohydrate recognition. *Biochemistry,* 43**,** 97-106.

KARAMANOS, T. K., KALVERDA, A. P., THOMPSON, G. S. & RADFORD, S. E. 2014. Visualization of transient protein-protein interactions that promote or inhibit amyloid assembly. *Mol Cell,* 55**,** 214-26.

KARLSSON, F. A., GROTH, T., SEGE, K., WIBELL, L. & PETERSON, P. A. 1980. Turnover in humans of beta 2-microglobulin: the constant chain of HLA-antigens. *Eur J Clin Invest,* 10**,** 293-300.

KAWAGUCHI, R., YU, J., HONDA, J., HU, J., WHITELEGGE, J., PING, P., WIITA, P., BOK, D. & SUN, H. 2007. A membrane receptor for retinol binding protein mediates cellular uptake of vitamin A. *Science,* 315**,** 820-5.

KELLY, J. W. 1998. The alternative conformations of amyloidogenic proteins and their multi-step assembly pathways. *Curr Opin Struct Biol,* 8**,** 101-6.

KIM, S., POURSINE-LAURENT, J., TRUSCOTT, S. M., LYBARGER, L., SONG, Y. J., YANG, L., FRENCH, A. R., SUNWOO, J. B., LEMIEUX, S., HANSEN, T. H. & YOKOYAMA, W. M. 2005. Licensing of natural killer cells by host major histocompatibility complex class I molecules. *Nature,* 436**,** 709-13.

KISILEVSKY, R. 2000. Review: amyloidogenesis-unquestioned answers and unanswered questions. *J Struct Biol,* 130**,** 99-108.

KISILEVSKY, R., ANCSIN, J. B., SZAREK, W. A. & PETANCESKA, S. 2007. Heparan sulfate as a therapeutic target in amyloidogenesis: prospects and possible complications. *Amyloid,* 14**,** 21-32.

KISS, E., KEUSCH, G., ZANETTI, M., JUNG, T., SCHWARZ, A., SCHOCKE, M., JASCHKE, W. & CZERMAK, B. V. 2005. Dialysis-related amyloidosis revisited. *AJR Am J Roentgenol,* 185**,** 1460-7.

KNITTLER, M. R., ALBERTS, P., DEVERSON, E. V. & HOWARD, J. C. 1999. Nucleotide binding by TAP mediates association with peptide and release of assembled MHC class I molecules. *Curr Biol,* 9**,** 999-1008.

KOCH, K. M. 1992. Dialysis-related amyloidosis. *Kidney Int,* 41**,** 1416-29.

KOLLER, B. H., MARRACK, P., KAPPLER, J. W. & SMITHIES, O. 1990. Normal development of mice deficient in beta 2M, MHC class I proteins, and CD8+ T cells. *Science,* 248**,** 1227-30.

KOPEC, J., GADEK, A., DROZDZ, M., MISKOWIEC, K., DUTKA, J., SYDOR, A., CHOWANIEC, E. & SULOWICZ, W. 2011. Carpal tunnel syndrome in hemodialysis patients as a dialysis-related amyloidosis manifestation--incidence, risk factors and results of surgical treatment. *Med Sci Monit,* 17**,** CR505-9.

KOZIOLEK, M. J., MULLER, G. A., ZAPF, A., PATSCHAN, D., SCHMID, H., COHEN, C. D., KOSCHNICK, S., VASKO, R., BRAMLAGE, C. & STRUTZ, F. 2010. Role of CX3C-chemokine CX3C-L/fractalkine expression in a model of slowly progressive renal failure. *Nephrol Dial Transplant,* 25**,** 684-98.

KRIMPENFORT, P., RUDENKO, G., HOCHSTENBACH, F., GUESSOW, D., BERNS, A. & PLOEGH, H. 1987. Crosses of two independently derived transgenic mice demonstrate functional complementation of the genes encoding heavy (HLA-B27) and light (beta 2-microglobulin) chains of HLA class I antigens. *EMBO J,* 6**,** 1673-6.

KUMAR, S. K., GERTZ, M. A., LACY, M. Q., DINGLI, D., HAYMAN, S. R., BUADI, F. K., SHORT-DETWEILER, K., ZELDENRUST, S. R., LEUNG, N., GREIPP, P. R., LUST, J. A., RUSSELL, S. J., KYLE, R. A., RAJKUMAR, S. V. & DISPENZIERI, A. 2011. Recent improvements in survival in primary systemic amyloidosis and the importance of an early mortality risk score. *Mayo Clin Proc,* 86**,** 12-8.

KUMITA, J. R., POON, S., CADDY, G. L., HAGAN, C. L., DUMOULIN, M., YERBURY, J. J., STEWART, E. M., ROBINSON, C. V., WILSON, M. R. & DOBSON, C. M. 2007. The extracellular chaperone clusterin potently inhibits human lysozyme amyloid formation by interacting with prefibrillar species. *J Mol Biol,* 369**,** 157-67.

KUROSAWA, T., IGARASHI, S., NISHIZAWA, M. & ONODERA, O. 2005. Selective silencing of a mutant transthyretin allele by small interfering RNAs. *Biochem Biophys Res Commun,* 337**,** 1012-8.

KYLE, R. A. & GERTZ, M. A. 1995. Primary systemic amyloidosis: clinical and laboratory features in 474 cases. *Semin Hematol,* 32**,** 45-59.

LACHMANN, H. J., GALLIMORE, R., GILLMORE, J. D., CARR-SMITH, H. D., BRADWELL, A. R., PEPYS, M. B. & HAWKINS, P. N. 2003. Outcome in systemic AL amyloidosis in relation to changes in concentration of circulating free immunoglobulin light chains following chemotherapy. *Br J Haematol,* 122**,** 78-84.

LACHMANN, H. J., GOODMAN, H. J., GILBERTSON, J. A., GALLIMORE, J. R., SABIN, C. A., GILLMORE, J. D. & HAWKINS, P. N. 2007. Natural history and outcome in systemic AA amyloidosis. *N Engl J Med,* 356**,** 2361-71.

LACOUR, A., ESPINOSA, A., LOUWERSHEIMER, E., HEILMANN, S., HERNANDEZ, I., WOLFSGRUBER, S., FERNANDEZ, V., WAGNER, H., ROSENDE-ROCA, M., MAULEON, A., MORENO-GRAU, S., VARGAS, L., PIJNENBURG, Y. A., KOENE, T., RODRIGUEZ-GOMEZ, O., ORTEGA, G., RUIZ, S., HOLSTEGE, H., SOTOLONGO-GRAU, O., KORNHUBER, J., PETERS, O., FROLICH, L., HULL, M., RUTHER, E., WILTFANG, J., SCHERER, M., RIEDEL-HELLER, S., ALEGRET, M., NOTHEN, M. M., SCHELTENS, P., WAGNER, M., TARRAGA, L., JESSEN, F., BOADA, M., MAIER, W., VAN DER FLIER, W. M., BECKER, T., RAMIREZ, A. & RUIZ, A. 2016. Genome-wide significant risk factors for Alzheimer's disease: role in progression to dementia due to Alzheimer's disease among subjects with mild cognitive impairment. *Mol Psychiatry*.

LAI, Z., COLON, W. & KELLY, J. W. 1996. The acid-mediated denaturation pathway of transthyretin yields a conformational intermediate that can self-assemble into amyloid. *Biochemistry,* 35**,** 6470-82.

LARSSON, M., PETTERSSON, T. & CARLSTROM, A. 1985. Thyroid hormone binding in serum of 15 vertebrate species: isolation of thyroxine-binding globulin and prealbumin analogs. *Gen Comp Endocrinol,* 58**,** 360-75.

LASHLEY, T., HOLTON, J. L., VERBEEK, M. M., ROSTAGNO, A., BOJSEN-MOLLER, M., DAVID, G., VAN HORSSEN, J., BRAENDGAARD, H., PLANT, G., FRANGIONE, B., GHISO, J. & REVESZ, T. 2006. Molecular chaperons, amyloid and preamyloid lesions in the BRI2 gene-related dementias: a morphological study. *Neuropathol Appl Neurobiol,* 32**,** 492-504.

LASHUEL, H. A., LAI, Z. & KELLY, J. W. 1998. Characterization of the transthyretin acid denaturation pathways by analytical ultracentrifugation: implications for wild-type, V30M, and L55P amyloid fibril formation. *Biochemistry,* 37**,** 17851-64.

LAVIN, T. N., BAXTER, J. D. & HORITA, S. 1988. The thyroid hormone receptor binds to multiple domains of the rat growth hormone 5'-flanking sequence. *J Biol Chem,* 263**,** 9418-26.

LEDUE, T. B., WEINER, D. L., SIPE, J. D., POULIN, S. E., COLLINS, M. F. & RIFAI, N. 1998. Analytical evaluation of particle-enhanced immunonephelometric assays for C-reactive protein, serum amyloid A

and mannose-binding protein in human serum. *Ann Clin Biochem,* 35 ( Pt 6)**,** 745-53.

LI, J. P., GALVIS, M. L., GONG, F., ZHANG, X., ZCHARIA, E., METZGER, S., VLODAVSKY, I., KISILEVSKY, R. & LINDAHL, U. 2005. In vivo fragmentation of heparan sulfate by heparanase overexpression renders mice resistant to amyloid protein A amyloidosis. *Proc Natl Acad Sci U S A,* 102**,** 6473-7.

LIABEUF, S., LENGLET, A., DESJARDINS, L., NEIRYNCK, N., GLORIEUX, G., LEMKE, H. D., VANHOLDER, R., DIOUF, M., CHOUKROUN, G., MASSY, Z. A. & EUROPEAN UREMIC TOXIN WORK, G. 2012. Plasma beta-2 microglobulin is associated with cardiovascular disease in uremic patients. *Kidney Int,* 82**,** 1297-303.

LINKE, R. P., HAMPL, H., BARTEL-SCHWARZE, S. & EULITZ, M. 1987. Beta 2-microglobulin, different fragments and polymers thereof in synovial amyloid in long-term hemodialysis. *Biol Chem Hoppe Seyler,* 368**,** 137-44.

LIPPINCOTT-SCHWARTZ, J., BONIFACINO, J. S., YUAN, L. C. & KLAUSNER, R. D. 1988. Degradation from the endoplasmic reticulum: disposing of newly synthesized proteins. *Cell,* 54**,** 209-20.

LITVINOVICH, S. V., BREW, S. A., AOTA, S., AKIYAMA, S. K., HAUDENSCHILD, C. & INGHAM, K. C. 1998. Formation of amyloid-like fibrils by self-association of a partially unfolded fibronectin type III module. *J Mol Biol,* 280**,** 245-58.

LIU, Y., CHOUDHURY, P., CABRAL, C. M. & SIFERS, R. N. 1999. Oligosaccharide modification in the early secretory pathway directs the selection of a misfolded glycoprotein for degradation by the proteasome. *J Biol Chem,* 274**,** 5861-7.

LIU, Y., CUI, D., HOSHII, Y., KAWANO, H., UNE, Y., GONDO, T. & ISHIHARA, T. 2007. Induction of murine AA amyloidosis by various homogeneous amyloid fibrils and amyloid-like synthetic peptides. *Scand J Immunol,* 66**,** 495-500.

LIZ, M. A., FARO, C. J., SARAIVA, M. J. & SOUSA, M. M. 2004. Transthyretin, a new cryptic protease. *J Biol Chem,* 279**,** 21431-8.

LIZ, M. A., FLEMING, C. E., NUNES, A. F., ALMEIDA, M. R., MAR, F. M., CHOE, Y., CRAIK, C. S., POWERS, J. C., BOGYO, M. & SOUSA, M. M. 2009. Substrate specificity of transthyretin: identification of natural substrates in the nervous system. *Biochem J,* 419**,** 467-74.

LIZ, M. A., GOMES, C. M., SARAIVA, M. J. & SOUSA, M. M. 2007. ApoA-I cleaved by transthyretin has reduced ability to promote cholesterol efflux and increased amyloidogenicity. *J Lipid Res,* 48**,** 2385-95.

LIZ, M. A., MAR, F. M., FRANQUINHO, F. & SOUSA, M. M. 2010. Aboard transthyretin: From transport to cleavage. *IUBMB Life,* 62**,** 429-35.

LONG, D. A., PRICE, K. L., IOFFE, E., GANNON, C. M., GNUDI, L., WHITE, K. E., YANCOPOULOS, G. D., RUDGE, J. S. & WOOLF, A. S. 2008. Angiopoietin-1 therapy enhances fibrosis and inflammation following folic acid-induced acute renal injury. *Kidney Int,* 74**,** 300-9.

LORENZO, A., RAZZABONI, B., WEIR, G. C. & YANKNER, B. A. 1994. Pancreatic islet cell toxicity of amylin associated with type-2 diabetes mellitus. *Nature,* 368**,** 756-60.

LOZERON, P., THEAUDIN, M., MINCHEVA, Z., DUCOT, B., LACROIX, C., ADAMS, D. & FRENCH NETWORK FOR, F. A. P. 2013. Effect on disability and safety of Tafamidis in late onset of Met30 transthyretin familial amyloid polyneuropathy. *Eur J Neurol,* 20**,** 1539-45.

LU, J. X., QIANG, W., YAU, W. M., SCHWIETERS, C. D., MEREDITH, S. C. & TYCKO, R. 2013. Molecular structure of beta-amyloid fibrils in Alzheimer's disease brain tissue. *Cell,* 154**,** 1257-68.

MACEIRA, A. M., JOSHI, J., PRASAD, S. K., MOON, J. C., PERUGINI, E., HARDING, I., SHEPPARD, M. N., POOLE-WILSON, P. A., HAWKINS, P. N. & PENNELL, D. J. 2005. Cardiovascular magnetic resonance in cardiac amyloidosis. *Circulation,* 111**,** 186-93.

MACHOLD, R. P. & PLOEGH, H. L. 1996. Intermediates in the assembly and degradation of class I major histocompatibility complex (MHC) molecules probed with free heavy chain-specific monoclonal antibodies. *J Exp Med,* 184**,** 2251-9.

MADINE, J., DAVIES, H. A., HUGHES, E. & MIDDLETON, D. A. 2013. Heparin promotes the rapid fibrillization of a peptide with low intrinsic amyloidogenicity. *Biochemistry,* 52**,** 8984-92.

MAETZLER, W., TIAN, Y., BAUR, S. M., GAUGER, T., ODOJ, B., SCHMID, B., SCHULTE, C., DEUSCHLE, C., HECK, S., APEL, A., MELMS, A., GASSER, T. & BERG, D. 2012. Serum and cerebrospinal fluid levels of transthyretin in Lewy body disorders with and without dementia. *PLoS One,* 7**,** e48042.

MAGNUS, J. H., STENSTAD, T., HUSBY, G. & KOLSET, S. O. 1992. Isolation and partial characterization of heparan sulphate proteoglycans from human hepatic amyloid. *Biochem J,* 288 ( Pt 1)**,** 225-31.

MAHER, S. K., WOJNAROWICZ, P., ICHU, T. A., VELDHOEN, N., LU, L., LESPERANCE, M., PROPPER, C. R. & HELBING, C. C. 2016. Rethinking the biological relationships of the thyroid hormones, l-thyroxine and 3,5,3'-triiodothyronine. *Comp Biochem Physiol Part D Genomics Proteomics,* 18**,** 44-53.

MAKOVER, A., MORIWAKI, H., RAMAKRISHNAN, R., SARAIVA, M. J., BLANER, W. S. & GOODMAN, D. S. 1988. Plasma transthyretin. Tissue sites of degradation and turnover in the rat. *J Biol Chem,* 263**,** 8598-603.

MANGIONE, P. P., ESPOSITO, G., RELINI, A., RAIMONDI, S., PORCARI, R., GIORGETTI, S., CORAZZA, A., FOGOLARI, F., PENCO, A., GOTO, Y., LEE, Y. H., YAGI, H., CECCONI, C., NAQVI, M. M., GILLMORE, J. D., HAWKINS, P. N., CHITI, F., ROLANDI, R., TAYLOR, G. W., PEPYS, M. B., STOPPINI, M. & BELLOTTI, V. 2013. Structure, folding dynamics, and amyloidogenesis of D76N beta2-microglobulin: roles of shear flow, hydrophobic surfaces, and alpha-crystallin. *J Biol Chem,* 288**,** 30917-30.

MANGIONE, P. P., PORCARI, R., GILLMORE, J. D., PUCCI, P., MONTI, M., PORCARI, M., GIORGETTI, S., MARCHESE, L., RAIMONDI, S., SERPELL, L. C., CHEN, W., RELINI, A., MARCOUX, J., CLATWORTHY, I. R., TAYLOR, G. W., TENNENT, G. A., ROBINSON, C. V., HAWKINS, P. N., STOPPINI, M., WOOD, S. P., PEPYS, M. B. & BELLOTTI, V. 2014. Proteolytic cleavage of Ser52Pro variant

transthyretin triggers its amyloid fibrillogenesis. *Proc Natl Acad Sci U S A,* 111**,** 1539-44.

MARCELLI, C., PERENNOU, D., CYTEVAL, C., LERAY, H., LAMARQUE, J. L., MION, C. & SIMON, L. 1996. Amyloidosis-related cauda equina compression in long-term hemodialysis patients. Three case reports. *Spine (Phila Pa 1976),* 21**,** 381-5.

MARCOUX, J., MANGIONE, P. P., PORCARI, R., DEGIACOMI, M. T., VERONA, G., TAYLOR, G. W., GIORGETTI, S., RAIMONDI, S., SANGLIER-CIANFERANI, S., BENESCH, J. L., CECCONI, C., NAQVI, M. M., GILLMORE, J. D., HAWKINS, P. N., STOPPINI, M., ROBINSON, C. V., PEPYS, M. B. & BELLOTTI, V. 2015. A novel mechano-enzymatic cleavage mechanism underlies transthyretin amyloidogenesis. *EMBO Mol Med,* 7**,** 1337-49.

MCADAM, K. P. & SIPE, J. D. 1976. Murine model for human secondary amyloidosis: genetic variability of the acute-phase serum protein SAA response to endotoxins and casein. *J Exp Med,* 144**,** 1121-7.

MCCRACKEN, A. A. & BRODSKY, J. L. 1996. Assembly of ER-associated protein degradation in vitro: dependence on cytosol, calnexin, and ATP. *J Cell Biol,* 132**,** 291-8.

MCCUTCHEN, S. L., LAI, Z., MIROY, G. J., KELLY, J. W. & COLON, W. 1995. Comparison of lethal and nonlethal transthyretin variants and their relationship to amyloid disease. *Biochemistry,* 34**,** 13527-36.

MCKINNON, B., LI, H., RICHARD, K. & MORTIMER, R. 2005. Synthesis of thyroid hormone binding proteins transthyretin and albumin by human trophoblast. *J Clin Endocrinol Metab,* 90**,** 6714-20.

MCPARLAND, V. J., KAD, N. M., KALVERDA, A. P., BROWN, A., KIRWIN-JONES, P., HUNTER, M. G., SUNDE, M. & RADFORD, S. E. 2000. Partially unfolded states of beta(2)-microglobulin and amyloid formation in vitro. *Biochemistry,* 39**,** 8735-46.

MELATO, M., ANTONUTTO, G. & FERRONATO, E. 1977. Amyloidosis of the isletes of Langerhans in relation to diabetes mellitus and aging. *Beitr Pathol,* 160**,** 73-81.

MERLINI, G. 2012. CyBorD: stellar response rates in AL amyloidosis. *Blood,* 119**,** 4343-5.

MERLINI, G., COMENZO, R. L., SELDIN, D. C., WECHALEKAR, A. & GERTZ, M. A. 2014. Immunoglobulin light chain amyloidosis. *Expert Rev Hematol,* 7**,** 143-56.

MILLER, S. R., SEKIJIMA, Y. & KELLY, J. W. 2004. Native state stabilization by NSAIDs inhibits transthyretin amyloidogenesis from the most common familial disease variants. *Lab Invest,* 84**,** 545-52.

MONTAGNA, G., CAZZULANI, B., OBICI, L., UGGETTI, C., GIORGETTI, S., PORCARI, R., RUGGIERO, R., MANGIONE, P. P., BRAMBILLA, M., LUCCHETTI, J., GUISO, G., GOBBI, M., MERLINI, G., SALMONA, M., STOPPINI, M., VILLA, G. & BELLOTTI, V. 2013. Benefit of doxycycline treatment on articular disability caused by dialysis related amyloidosis. *Amyloid,* 20**,** 173-8.

MORRICE, N. A. & POWIS, S. J. 1998. A role for the thiol-dependent reductase ERp57 in the assembly of MHC class I molecules. *Curr Biol,* 8**,** 713-6.

MOTOMIYA, Y., ANDO, Y., HARAOKA, K., SUN, X., IWAMOTO, H., UCHIMURA, T. & MARUYAMA, I. 2003. Circulating level of alpha2-macroglobulin-beta2-microglobulin complex in hemodialysis patients. *Kidney Int,* 64**,** 2244-52.

MOURAD, G. & ARGILES, A. 1996. Renal transplantation relieves the symptoms but does not reverse beta 2-microglobulin amyloidosis. *J Am Soc Nephrol,* 7**,** 798-804.

MUCCHIANO, G. I., JONASSON, L., HAGGQVIST, B., EINARSSON, E. & WESTERMARK, P. 2001. Apolipoprotein A-I-derived amyloid in atherosclerosis. Its association with plasma levels of apolipoprotein A-I and cholesterol. *Am J Clin Pathol,* 115**,** 298-303.

MYERS, S. L., JONES, S., JAHN, T. R., MORTEN, I. J., TENNENT, G. A., HEWITT, E. W. & RADFORD, S. E. 2006a. A systematic study of the effect of physiological factors on beta2-microglobulin amyloid formation at neutral pH. *Biochemistry,* 45**,** 2311-21.

MYERS, S. L., THOMSON, N. H., RADFORD, S. E. & ASHCROFT, A. E. 2006b. Investigating the structural properties of amyloid-like fibrils formed in vitro from beta2-microglobulin using limited proteolysis and electrospray ionisation mass spectrometry. *Rapid Commun Mass Spectrom,* 20**,** 1628-36.

NAGATA, Y., TASHIRO, F., YI, S., MURAKAMI, T., MAEDA, S., TAKAHASHI, K., SHIMADA, K., OKAMURA, H. & YAMAMURA, K. 1995. A 6-kb upstream region of the human transthyretin gene can direct developmental, tissue-specific, and quantitatively normal expression in transgenic mouse. *J Biochem,* 117**,** 169-75.

NAKAI, S., ISEKI, K., TABEI, K., KUBO, K., MASAKANE, I., FUSHIMI, K., KIKUCHI, K., SHINZATO, T., SANAKA, T. & AKIBA, T. 2001. Outcomes of hemodiafiltration based on Japanese dialysis patient registry. *Am J Kidney Dis,* 38**,** S212-6.

NAKAMURA, T. 2011. Amyloid A amyloidosis secondary to rheumatoid arthritis: pathophysiology and treatments. *Clin Exp Rheumatol,* 29**,** 850-7.

NAKAO, Y., MATSUMOTO, H., MIYAZAKI, T., WATANABE, S., MASAOKA, T., TAKATSUKI, K., KISHIHARA, M., KOBAYASHI, N., HATTORI, M. & FUJITA, T. 1981. Genetic and clinical studies of serum beta 2-microglobulin levels in haematological malignancies. *Clin Exp Immunol,* 46**,** 134-41.

NAKAZATO, M., KANGAWA, K., MINAMINO, N., TAWARA, S., MATSUO, H. & ARAKI, S. 1984. Revised analysis of amino acid replacement in a prealbumin variant (SKO-III) associated with familial amyloidotic polyneuropathy of Jewish origin. *Biochem Biophys Res Commun,* 123**,** 921-8.

NARITA, M., HOLTZMAN, D. M., SCHWARTZ, A. L. & BU, G. 1997. Alpha2-macroglobulin complexes with and mediates the endocytosis of beta-amyloid peptide via cell surface low-density lipoprotein receptor-related protein. *J Neurochem,* 69**,** 1904-11.

NATORI, T., TANIGAKI, N. & PRESSMAN, D. 1976. A mouse plasma substance carrying beta2-microglobulin activity and lacking in H-2 alloantigenic activity. *J Immunogenet,* 3**,** 123-34.

NELSON, S. R., LYON, M., GALLAGHER, J. T., JOHNSON, E. A. & PEPYS, M. B. 1991. Isolation and characterization of the integral glycosaminoglycan constituents of human amyloid A and monoclonal light-chain amyloid fibrils. *Biochem J,* 275 ( Pt 1)**,** 67-73.

NG, B., CONNORS, L. H., DAVIDOFF, R., SKINNER, M. & FALK, R. H. 2005. Senile systemic amyloidosis presenting with heart failure: a comparison with light chain-associated amyloidosis. *Arch Intern Med,* 165**,** 1425-9.

NGUYEN-SIMONNET, H., VINCENT, C., GAUTHIER, C., REVILLARD, J. P. & PELLET, M. V. 1982. Turnover studies of human beta 2-microglobulin in the rat: evidence for a beta 2-microglobulin-binding plasma protein. *Clin Sci (Lond),* 62**,** 403-10.

NILSSON, M. R. 2004. Techniques to study amyloid fibril formation in vitro. *Methods,* 34**,** 151-60.

NIWA, H., YAMAMURA, K. & MIYAZAKI, J. 1991. Efficient selection for high-expression transfectants with a novel eukaryotic vector. *Gene,* 108**,** 193-9.

NOMENCLATURE-COMMITTEE 1981. Nomenclature Committee of IUB (NC-IUB) IUB-IUPAC Joint Commission on Biochemical Nomenclature (JCBN). Newsletter 1981. *J Biol Chem,* 256**,** 12-4.

NORLUND, L., FEX, G., LANKE, J., VON SCHENCK, H., NILSSON, J. E., LEKSELL, H. & GRUBB, A. 1997. Reference intervals for the glomerular filtration rate and cell-proliferation markers: serum cystatin C and serum beta 2-microglobulin/cystatin C-ratio. *Scand J Clin Lab Invest,* 57**,** 463-70.

OBICI, L., CORTESE, A., LOZZA, A., LUCCHETTI, J., GOBBI, M., PALLADINI, G., PERLINI, S., SARAIVA, M. J. & MERLINI, G. 2012. Doxycycline plus tauroursodeoxycholic acid for transthyretin amyloidosis: a phase II study. *Amyloid,* 19 Suppl 1**,** 34-6.

ORTMANN, B., ANDROLEWICZ, M. J. & CRESSWELL, P. 1994. MHC class I/beta 2-microglobulin complexes associate with TAP transporters before peptide binding. *Nature,* 368**,** 864-7.

ORTMANN, B., COPEMAN, J., LEHNER, P. J., SADASIVAN, B., HERBERG, J. A., GRANDEA, A. G., RIDDELL, S. R., TAMPE, R., SPIES, T., TROWSDALE, J. & CRESSWELL, P. 1997. A critical role for tapasin in the assembly and function of multimeric MHC class I-TAP complexes. *Science,* 277**,** 1306-9.

OTTEN, G. R., BIKOFF, E., RIBAUDO, R. K., KOZLOWSKI, S., MARGULIES, D. H. & GERMAIN, R. N. 1992. Peptide and beta 2-microglobulin regulation of cell surface MHC class I conformation and expression. *J Immunol,* 148**,** 3723-32.

PALHA, J. A., NISSANOV, J., FERNANDES, R., SOUSA, J. C., BERTRAND, L., DRATMAN, M. B., MORREALE DE ESCOBAR, G., GOTTESMAN, M. & SARAIVA, M. J. 2002. Thyroid hormone distribution in the mouse brain: the role of transthyretin. *Neuroscience,* 113**,** 837-47.

PALLADINI, G., RUSSO, P., BOSONI, T., VERGA, L., SARAIS, G., LAVATELLI, F., NUVOLONE, M., OBICI, L., CASARINI, S., DONADEI, S., ALBERTINI, R., RIGHETTI, G., MARINI, M., GRAZIANI, M. S., MELZI D'ERIL, G. V., MORATTI, R. & MERLINI, G. 2009. Identification of amyloidogenic light chains requires the combination of serum-free

light chain assay with immunofixation of serum and urine. *Clin Chem,* 55**,** 499-504.

PATEL, K. S. & HAWKINS, P. N. 2015. Cardiac amyloidosis: where are we today? *J Intern Med,* 278**,** 126-44.

PATROSSO, M. C., SALVI, F., DE GRANDIS, D., VEZZONI, P., JACOBSON, D. R. & FERLINI, A. 1998. Novel transthyretin missense mutation (Thr34) in an Italian family with hereditary amyloidosis. *Am J Med Genet,* 77**,** 135-8.

PEDERSEN, L. O., STRYHN, A., HOLTER, T. L., ETZERODT, M., GERWIEN, J., NISSEN, M. H., THOGERSEN, H. C. & BUUS, S. 1995. The interaction of beta 2-microglobulin (beta 2m) with mouse class I major histocompatibility antigens and its ability to support peptide binding. A comparison of human and mouse beta 2m. *Eur J Immunol,* 25**,** 1609-16.

PEPYS, M. B. 2001. Pathogenesis, diagnosis and treatment of systemic amyloidosis. *Philos Trans R Soc Lond B Biol Sci,* 356**,** 203-10; discussion 210-1.

PEPYS, M. B. 2006. Amyloidosis. *Annu Rev Med,* 57**,** 223-41.

PEPYS, M. B., DYCK, R. F., DE BEER, F. C., SKINNER, M. & COHEN, A. S. 1979. Binding of serum amyloid P-component (SAP) by amyloid fibrils. *Clin Exp Immunol,* 38**,** 284-93.

PEPYS, M. B., GALLIMORE, J. R., LLOYD, J., LI, Z., GRAHAM, D., TAYLOR, G. W., ELLMERICH, S., MANGIONE, P. P., TENNENT, G. A., HUTCHINSON, W. L., MILLAR, D. J., BENNETT, G., MORE, J., EVANS, D., MISTRY, Y., POOLE, S. & HAWKINS, P. N. 2012. Isolation and characterization of pharmaceutical grade human pentraxins, serum amyloid P component and C-reactive protein, for clinical use. *J Immunol Methods,* 384**,** 92-102.

PEPYS, M. B., HERBERT, J., HUTCHINSON, W. L., TENNENT, G. A., LACHMANN, H. J., GALLIMORE, J. R., LOVAT, L. B., BARTFAI, T., ALANINE, A., HERTEL, C., HOFFMANN, T., JAKOB-ROETNE, R., NORCROSS, R. D., KEMP, J. A., YAMAMURA, K., SUZUKI, M., TAYLOR, G. W., MURRAY, S., THOMPSON, D., PURVIS, A., KOLSTOE, S., WOOD, S. P. & HAWKINS, P. N. 2002. Targeted pharmacological depletion of serum amyloid P component for treatment of human amyloidosis. *Nature,* 417**,** 254-9.

PERUGINI, E., GUIDALOTTI, P. L., SALVI, F., COOKE, R. M., PETTINATO, C., RIVA, L., LEONE, O., FARSAD, M., CILIBERTI, P., BACCHI-REGGIANI, L., FALLANI, F., BRANZI, A. & RAPEZZI, C. 2005. Noninvasive etiologic diagnosis of cardiac amyloidosis using 99mTc-3,3-diphosphono-1,2-propanodicarboxylic acid scintigraphy. *J Am Coll Cardiol,* 46**,** 1076-84.

PETERSON, P. A., CUNNINGHAM, B. A., BERGGARD, I. & EDELMAN, G. M. 1972. 2 -Microglobulin--a free immunoglobulin domain. *Proc Natl Acad Sci U S A,* 69**,** 1697-701.

PETERSON, P. A., EVRIN, P. E. & BERGGARD, I. 1969. Differentiation of glomerular, tubular, and normal proteinuria: determinations of urinary excretion of beta-2-macroglobulin, albumin, and total protein. *J Clin Invest,* 48**,** 1189-98.

PETERSON, P. A., RASK, L. & LINDBLOM, J. B. 1974. Highly purified papain-solubilized HL-A antigens contain beta2-microglobulin. *Proc Natl Acad Sci U S A,* 71**,** 35-9.

PETRE, S., SHAH, I. A. & GILANI, N. 2008. Review article: gastrointestinal amyloidosis - clinical features, diagnosis and therapy. *Aliment Pharmacol Ther,* 27**,** 1006-16.

PIAZZA, R., PIERNO, M., IACOPINI, S., MANGIONE, P., ESPOSITO, G. & BELLOTTI, V. 2006. Micro-heterogeneity and aggregation in beta2-microglobulin solutions: effects of temperature, pH, and conformational variant addition. *Eur Biophys J,* 35**,** 439-45.

PICOTTI, P., DE FRANCESCHI, G., FRARE, E., SPOLAORE, B., ZAMBONIN, M., CHITI, F., DE LAURETO, P. P. & FONTANA, A. 2007. Amyloid fibril formation and disaggregation of fragment 1-29 of apomyoglobin: insights into the effect of pH on protein fibrillogenesis. *J Mol Biol,* 367**,** 1237-45.

PINKERT, C. A., ORNITZ, D. M., BRINSTER, R. L. & PALMITER, R. D. 1987. An albumin enhancer located 10 kb upstream functions along with its promoter to direct efficient, liver-specific expression in transgenic mice. *Genes Dev,* 1**,** 268-76.

PINNEY, J. H., SMITH, C. J., TAUBE, J. B., LACHMANN, H. J., VENNER, C. P., GIBBS, S. D., DUNGU, J., BANYPERSAD, S. M., WECHALEKAR, A. D., WHELAN, C. J., HAWKINS, P. N. & GILLMORE, J. D. 2013a. Systemic amyloidosis in England: an epidemiological study. *Br J Haematol,* 161**,** 525-32.

PINNEY, J. H., WHELAN, C. J., PETRIE, A., DUNGU, J., BANYPERSAD, S. M., SATTIANAYAGAM, P., WECHALEKAR, A., GIBBS, S. D., VENNER, C. P., WASSEF, N., MCCARTHY, C. A., GILBERTSON, J. A., ROWCZENIO, D., HAWKINS, P. N., GILLMORE, J. D. & LACHMANN, H. J. 2013b. Senile systemic amyloidosis: clinical features at presentation and outcome. *J Am Heart Assoc,* 2**,** e000098.

PISKUNOV, A., AL TANOURY, Z. & ROCHETTE-EGLY, C. 2014. Nuclear and extra-nuclear effects of retinoid acid receptors: how they are interconnected. *Subcell Biochem,* 70**,** 103-27.

PITKANEN, P., WESTERMARK, P. & CORNWELL, G. G., 3RD 1984. Senile systemic amyloidosis. *Am J Pathol,* 117**,** 391-9.

PLANTE-BORDENEUVE, V., CARAYOL, J., FERREIRA, A., ADAMS, D., CLERGET-DARPOUX, F., MISRAHI, M., SAID, G. & BONAITI-PELLIE, C. 2003. Genetic study of transthyretin amyloid neuropathies: carrier risks among French and Portuguese families. *J Med Genet,* 40**,** e120.

PLANTE-BORDENEUVE, V. & SAID, G. 2011. Familial amyloid polyneuropathy. *Lancet Neurol,* 10**,** 1086-97.

PLESNER, T. & BJERRUM, O. J. 1980. Distribution of 'free' and HLA-associated human beta 2-microglobulin in some plasma membranes and biological fluids. *Scand J Immunol,* 11**,** 341-51.

PRAS, M., NEVO, Z., SCHUBERT, M., ROTMAN, J. & MATALON, R. 1971. The significance of mucopolysaccharides in amyloid. *J Histochem Cytochem,* 19**,** 443-8.

PRAS, M., PRELLI, F., FRANKLIN, E. C. & FRANGIONE, B. 1983. Primary structure of an amyloid prealbumin variant in familial polyneuropathy of Jewish origin. *Proc Natl Acad Sci U S A,* 80**,** 539-42.

PUCHTLER H, S. F., LEVINE M 1962. On the binding of Congo red by amyloid. *J Histochem Cytochem,* 10**,** 355-364.

PUILLE, M., ALTLAND, K., LINKE, R. P., STEEN-MULLER, M. K., KIETT, R., STEINER, D. & BAUER, R. 2002. 99mTc-DPD scintigraphy in transthyretin-related familial amyloidotic polyneuropathy. *Eur J Nucl Med Mol Imaging,* 29**,** 376-9.

QUINTAS, A., VAZ, D. C., CARDOSO, I., SARAIVA, M. J. & BRITO, R. M. 2001. Tetramer dissociation and monomer partial unfolding precedes protofibril formation in amyloidogenic transthyretin variants. *J Biol Chem,* 276**,** 27207-13.

RANDERS, E., ERLANDSEN, E. J., PEDERSEN, O. L., HASLING, C. & DANIELSEN, H. 2000. Serum cystatin C as an endogenous parameter of the renal function in patients with normal to moderately impaired kidney function. *Clin Nephrol,* 54**,** 203-9.

RANDERS, E., KRISTENSEN, J. H., ERLANDSEN, E. J. & DANIELSEN, H. 1998. Serum cystatin C as a marker of the renal function. *Scand J Clin Lab Invest,* 58**,** 585-92.

RAPEZZI, C., MERLINI, G., QUARTA, C. C., RIVA, L., LONGHI, S., LEONE, O., SALVI, F., CILIBERTI, P., PASTORELLI, F., BIAGINI, E., COCCOLO, F., COOKE, R. M., BACCHI-REGGIANI, L., SANGIORGI, D., FERLINI, A., CAVO, M., ZAMAGNI, E., FONTE, M. L., PALLADINI, G., SALINARO, F., MUSCA, F., OBICI, L., BRANZI, A. & PERLINI, S. 2009. Systemic cardiac amyloidoses: disease profiles and clinical courses of the 3 main types. *Circulation,* 120**,** 1203-12.

RAPEZZI, C., PERUGINI, E., SALVI, F., GRIGIONI, F., RIVA, L., COOKE, R. M., FERLINI, A., RIMESSI, P., BACCHI-REGGIANI, L., CILIBERTI, P., PASTORELLI, F., LEONE, O., BARTOLOMEI, I., PINNA, A. D., ARPESELLA, G. & BRANZI, A. 2006. Phenotypic and genotypic heterogeneity in transthyretin-related cardiac amyloidosis: towards tailoring of therapeutic strategies? *Amyloid,* 13**,** 143-53.

RAPEZZI, C., QUARTA, C. C., RIVA, L., LONGHI, S., GALLELLI, I., LORENZINI, M., CILIBERTI, P., BIAGINI, E., SALVI, F. & BRANZI, A. 2010. Transthyretin-related amyloidoses and the heart: a clinical overview. *Nat Rev Cardiol,* 7**,** 398-408.

RAPEZZI, C., RIVA, L., QUARTA, C. C., PERUGINI, E., SALVI, F., LONGHI, S., CILIBERTI, P., PASTORELLI, F., BIAGINI, E., LEONE, O., COOKE, R. M., BACCHI-REGGIANI, L., FERLINI, A., CAVO, M., MERLINI, G., PERLINI, S., PASQUALI, S. & BRANZI, A. 2008. Gender-related risk of myocardial involvement in systemic amyloidosis. *Amyloid,* 15**,** 40-8.

RASK, L., LINDBLOM, J. B. & PETERSON, P. A. 1974. Subunit structure of H-2 alloantigens. *Nature,* 249**,** 833-4.

REIXACH, N., DEECHONGKIT, S., JIANG, X., KELLY, J. W. & BUXBAUM, J. N. 2004. Tissue damage in the amyloidoses: Transthyretin monomers and nonnative oligomers are the major cytotoxic species in tissue culture. *Proc Natl Acad Sci U S A,* 101**,** 2817-22.

REIXACH, N., FOSS, T. R., SANTELLI, E., PASCUAL, J., KELLY, J. W. & BUXBAUM, J. N. 2008. Human-murine transthyretin heterotetramers are kinetically stable and non-amyloidogenic. A lesson in the generation of transgenic models of diseases involving oligomeric proteins. *J Biol Chem,* 283**,** 2098-107.

RELINI, A., CANALE, C., DE STEFANO, S., ROLANDI, R., GIORGETTI, S., STOPPINI, M., ROSSI, A., FOGOLARI, F., CORAZZA, A., ESPOSITO, G., GLIOZZI, A. & BELLOTTI, V. 2006. Collagen plays an active role in the aggregation of beta2-microglobulin under physiopathological conditions of dialysis-related amyloidosis. *J Biol Chem,* 281**,** 16521-9.

RENZULLI, P., SCHOEPFER, A., MUELLER, E. & CANDINAS, D. 2009. Atraumatic splenic rupture in amyloidosis. *Amyloid,* 16**,** 47-53.

RICHARDS, D. B., COOKSON, L. M., BERGES, A. C., BARTON, S. V., LANE, T., RITTER, J. M., FONTANA, M., MOON, J. C., PINZANI, M., GILLMORE, J. D., HAWKINS, P. N. & PEPYS, M. B. 2015. Therapeutic Clearance of Amyloid by Antibodies to Serum Amyloid P Component. *N Engl J Med,* 373**,** 1106-14.

ROBBINS, J. & RALL, J. E. 1955. Thyroxine-binding capacity of serum in normal man. *J Clin Invest,* 34**,** 1324-30.

ROCKEN, C., MENARD, R., BUHLING, F., VOCKLER, S., RAYNES, J., STIX, B., KRUGER, S., ROESSNER, A. & KAHNE, T. 2005. Proteolysis of serum amyloid A and AA amyloid proteins by cysteine proteases: cathepsin B generates AA amyloid proteins and cathepsin L may prevent their formation. *Ann Rheum Dis,* 64**,** 808-15.

ROCKENSTEIN, E., MALLORY, M., MANTE, M., SISK, A. & MASLIAHA, E. 2001. Early formation of mature amyloid-beta protein deposits in a mutant APP transgenic model depends on levels of Abeta(1-42). *J Neurosci Res,* 66**,** 573-82.

ROTHENBERG, B. E. & VOLAND, J. R. 1996. beta2 knockout mice develop parenchymal iron overload: A putative role for class I genes of the major histocompatibility complex in iron metabolism. *Proc Natl Acad Sci U S A,* 93**,** 1529-34.

RUBERG, F. L. & BERK, J. L. 2012. Transthyretin (TTR) cardiac amyloidosis. *Circulation,* 126**,** 1286-300.

RUBERG, F. L., MAURER, M. S., JUDGE, D. P., ZELDENRUST, S., SKINNER, M., KIM, A. Y., FALK, R. H., CHEUNG, K. N., PATEL, A. R., PANO, A., PACKMAN, J. & GROGAN, D. R. 2012. Prospective evaluation of the morbidity and mortality of wild-type and V122I mutant transthyretin amyloid cardiomyopathy: the Transthyretin Amyloidosis Cardiac Study (TRACS). *Am Heart J,* 164**,** 222-228 e1.

SADASIVAN, B., LEHNER, P. J., ORTMANN, B., SPIES, T. & CRESSWELL, P. 1996. Roles for calreticulin and a novel glycoprotein, tapasin, in the interaction of MHC class I molecules with TAP. *Immunity,* 5**,** 103-14.

SANTOS, S. D., FERNANDES, R. & SARAIVA, M. J. 2010. The heat shock response modulates transthyretin deposition in the peripheral and autonomic nervous systems. *Neurobiol Aging,* 31**,** 280-9.

SARAIVA, M. J., BIRKEN, S., COSTA, P. P. & GOODMAN, D. S. 1984. Amyloid fibril protein in familial amyloidotic polyneuropathy, Portuguese type. Definition of molecular abnormality in transthyretin (prealbumin). *J Clin Invest,* 74**,** 104-19.

SASABE, J., SUZUKI, M., MIYOSHI, Y., TOJO, Y., OKAMURA, C., ITO, S., KONNO, R., MITA, M., HAMASE, K. & AISO, S. 2014. Ischemic acute kidney injury perturbs homeostasis of serine enantiomers in the body fluid in mice: early detection of renal dysfunction using the ratio of serine enantiomers. *PLoS One,* 9**,** e86504.

SASAKI, H., TONE, S., NAKAZATO, M., YOSHIOKA, K., MATSUO, H., KATO, Y. & SAKAKI, Y. 1986. Generation of transgenic mice producing a human transthyretin variant: a possible mouse model for familial amyloidotic polyneuropathy. *Biochem Biophys Res Commun,* 139**,** 794-9.

SATO, T., SAKO, Y., SHO, M., MOMOHARA, M., SUICO, M. A., SHUTO, T., NISHITOH, H., OKIYONEDA, T., KOKAME, K., KANEKO, M., TAURA, M., MIYATA, M., CHOSA, K., KOGA, T., MORINO-KOGA, S., WADA, I. & KAI, H. 2012. STT3B-dependent posttranslational N-glycosylation as a surveillance system for secretory protein. *Mol Cell,* 47**,** 99-110.

SCHIFFL, H. 2014. Impact of advanced dialysis technology on the prevalence of dialysis-related amyloidosis in long-term maintenance dialysis patients. *Hemodial Int,* 18**,** 136-41.

SCHNEIDER, F., HAMMARSTROM, P. & KELLY, J. W. 2001. Transthyretin slowly exchanges subunits under physiological conditions: A convenient chromatographic method to study subunit exchange in oligomeric proteins. *Protein Sci,* 10**,** 1606-13.

SCHONLAND, S. O., HEGENBART, U., BOCHTLER, T., MANGATTER, A., HANSBERG, M., HO, A. D., LOHSE, P. & ROCKEN, C. 2012. Immunohistochemistry in the classification of systemic forms of amyloidosis: a systematic investigation of 117 patients. *Blood,* 119**,** 488-93.

SEDIGHI, O., ABEDIANKENARI, S. & OMRANIFAR, B. 2015. Association between plasma Beta-2 microglobulin level and cardiac performance in patients with chronic kidney disease. *Nephrourol Mon,* 7**,** e23563.

SEKIJIMA, Y., DENDLE, M. A. & KELLY, J. W. 2006. Orally administered diflunisal stabilizes transthyretin against dissociation required for amyloidogenesis. *Amyloid,* 13**,** 236-49.

SEKIJIMA, Y., UCHIYAMA, S., TOJO, K., SANO, K., SHIMIZU, Y., IMAEDA, T., HOSHII, Y., KATO, H. & IKEDA, S. 2011. High prevalence of wild-type transthyretin deposition in patients with idiopathic carpal tunnel syndrome: a common cause of carpal tunnel syndrome in the elderly. *Hum Pathol,* 42**,** 1785-91.

SELVANAYAGAM, J. B., HAWKINS, P. N., PAUL, B., MYERSON, S. G. & NEUBAUER, S. 2007. Evaluation and management of the cardiac amyloidosis. *J Am Coll Cardiol,* 50**,** 2101-10.

SERIO, T. R., CASHIKAR, A. G., KOWAL, A. S., SAWICKI, G. J., MOSLEHI, J. J., SERPELL, L., ARNSDORF, M. F. & LINDQUIST, S. L. 2000. Nucleated conformational conversion and the replication of conformational information by a prion determinant. *Science,* 289**,** 1317-21.

SERPELL, L. C., SUNDE, M., BENSON, M. D., TENNENT, G. A., PEPYS, M. B. & FRASER, P. E. 2000. The protofilament substructure of amyloid fibrils. *J Mol Biol,* 300**,** 1033-9.

SHENTAL-BECHOR, D. & LEVY, Y. 2008. Effect of glycosylation on protein folding: a close look at thermodynamic stabilization. *Proc Natl Acad Sci U S A,* 105**,** 8256-61.

SHEPHERD, J. C., SCHUMACHER, T. N., ASHTON-RICKARDT, P. G., IMAEDA, S., PLOEGH, H. L., JANEWAY, C. A., JR. & TONEGAWA, S. 1993. TAP1-dependent peptide translocation in vitro is ATP dependent and peptide selective. *Cell,* 74**,** 577-84.

SHIELDS, M. J., MOFFAT, L. E. & RIBAUDO, R. K. 1998. Functional comparison of bovine, murine, and human beta2-microglobulin: interactions with murine MHC I molecules. *Mol Immunol,* 35**,** 919-28.

SHLIPAK, M. G., SARNAK, M. J., KATZ, R., FRIED, L. F., SELIGER, S. L., NEWMAN, A. B., SISCOVICK, D. S. & STEHMAN-BREEN, C. 2005. Cystatin C and the risk of death and cardiovascular events among elderly persons. *N Engl J Med,* 352**,** 2049-60.

SIMISTER, N. E. & MOSTOV, K. E. 1989. An Fc receptor structurally related to MHC class I antigens. *Nature,* 337**,** 184-7.

SIMONS, J. P., AL-SHAWI, R., ELLMERICH, S., SPECK, I., ASLAM, S., HUTCHINSON, W. L., MANGIONE, P. P., DISTERER, P., GILBERTSON, J. A., HUNT, T., MILLAR, D. J., MINOGUE, S., BODIN, K., PEPYS, M. B. & HAWKINS, P. N. 2013. Pathogenetic mechanisms of amyloid A amyloidosis. *Proc Natl Acad Sci U S A,* 110**,** 16115-20.

SIPE, J. D., BENSON, M. D., BUXBAUM, J. N., IKEDA, S., MERLINI, G., SARAIVA, M. J. & WESTERMARK, P. 2014. Nomenclature 2014: Amyloid fibril proteins and clinical classification of the amyloidosis. *Amyloid,* 21**,** 221-4.

SJOLANDER, D., ROCKEN, C., WESTERMARK, P., WESTERMARK, G. T., NILSSON, K. P. & HAMMARSTROM, P. 2016. Establishing the fluorescent amyloid ligand h-FTAA for studying human tissues with systemic and localized amyloid. *Amyloid,* 23**,** 98-108.

SKINNER, M., SHIRAHAMA, T., BENSON, M. D. & COHEN, A. S. 1977. Murine amyloid protein AA in casein-induced experimental amyloidosis. *Lab Invest,* 36**,** 420-7.

SMALL, T. N., KNOWLES, R. W., KEEVER, C., KERNAN, N. A., COLLINS, N., O'REILLY, R. J., DUPONT, B. & FLOMENBERG, N. 1987. M241 (CD1) expression on B lymphocytes. *J Immunol,* 138**,** 2864-8.

SMITH, F. R. & GOODMAN, D. S. 1971. The effects of diseases of the liver, thyroid, and kidneys on the transport of vitamin A in human plasma. *J Clin Invest,* 50**,** 2426-36.

SMITH, L. K., HE, Y., PARK, J. S., BIERI, G., SNETHLAGE, C. E., LIN, K., GONTIER, G., WABL, R., PLAMBECK, K. E., UDEOCHU, J., WHEATLEY, E. G., BOUCHARD, J., EGGEL, A., NARASIMHA, R., GRANT, J. L., LUO, J., WYSS-CORAY, T. & VILLEDA, S. A. 2015. beta2-microglobulin is a systemic pro-aging factor that impairs cognitive function and neurogenesis. *Nat Med,* 21**,** 932-7.

SNEL, F. W., NIEWOLD, T. A., BALTZ, M. L., HOL, P. R., VAN EDEREN, A. M., PEPYS, M. B. & GRUYS, E. 1989. Experimental amyloidosis in the hamster: correlation between hamster female protein levels and amyloid deposition. *Clin Exp Immunol,* 76**,** 296-300.

SOPRANO, D. R., HERBERT, J., SOPRANO, K. J., SCHON, E. A. & GOODMAN, D. S. 1985. Demonstration of transthyretin mRNA in the

brain and other extrahepatic tissues in the rat. *J Biol Chem,* 260**,** 11793-8.

SOPRANO, D. R., SOPRANO, K. J. & GOODMAN, D. S. 1986. Retinol-binding protein and transthyretin mRNA levels in visceral yolk sac and liver during fetal development in the rat. *Proc Natl Acad Sci U S A,* 83**,** 7330-4.

SOTTRUP-JENSEN, L. 1989. Alpha-macroglobulins: structure, shape, and mechanism of proteinase complex formation. *J Biol Chem,* 264**,** 11539-42.

SOUSA, A., ANDERSSON, R., DRUGGE, U., HOLMGREN, G. & SANDGREN, O. 1993. Familial amyloidotic polyneuropathy in Sweden: geographical distribution, age of onset, and prevalence. *Hum Hered,* 43**,** 288-94.

SOUSA, A., COELHO, T., BARROS, J. & SEQUEIROS, J. 1995. Genetic epidemiology of familial amyloidotic polyneuropathy (FAP)-type I in Povoa do Varzim and Vila do Conde (north of Portugal). *Am J Med Genet,* 60**,** 512-21.

SOUSA, M. M., BERGLUND, L. & SARAIVA, M. J. 2000. Transthyretin in high density lipoproteins: association with apolipoprotein A-I. *J Lipid Res,* 41**,** 58-65.

SOUSA, M. M., CARDOSO, I., FERNANDES, R., GUIMARAES, A. & SARAIVA, M. J. 2001. Deposition of transthyretin in early stages of familial amyloidotic polyneuropathy: evidence for toxicity of nonfibrillar aggregates. *Am J Pathol,* 159**,** 1993-2000.

SOUSA, M. M., FERNANDES, R., PALHA, J. A., TABOADA, A., VIEIRA, P. & SARAIVA, M. J. 2002. Evidence for early cytotoxic aggregates in transgenic mice for human transthyretin Leu55Pro. *Am J Pathol,* 161**,** 1935-48.

SPRIGGS, M. K., KOLLER, B. H., SATO, T., MORRISSEY, P. J., FANSLOW, W. C., SMITHIES, O., VOICE, R. F., WIDMER, M. B. & MALISZEWSKI, C. R. 1992. Beta 2-microglobulin-, CD8+ T-cell-deficient mice survive inoculation with high doses of vaccinia virus and exhibit altered IgG responses. *Proc Natl Acad Sci U S A,* 89**,** 6070-4.

STANGOU, A. J., BANNER, N. R., HENDRY, B. M., RELA, M., PORTMANN, B., WENDON, J., MONAGHAN, M., MACCARTHY, P., BUXTON-THOMAS, M., MATHIAS, C. J., LIEPNIEKS, J. J., O'GRADY, J., HEATON, N. D. & BENSON, M. D. 2010. Hereditary fibrinogen A alpha-chain amyloidosis: phenotypic characterization of a systemic disease and the role of liver transplantation. *Blood,* 115**,** 2998-3007.

STANGOU, A. J., HAWKINS, P. N., HEATON, N. D., RELA, M., MONAGHAN, M., NIHOYANNOPOULOS, P., O'GRADY, J., PEPYS, M. B. & WILLIAMS, R. 1998. Progressive cardiac amyloidosis following liver transplantation for familial amyloid polyneuropathy: implications for amyloid fibrillogenesis. *Transplantation,* 66**,** 229-33.

STEVENS, F. J. & KISILEVSKY, R. 2000. Immunoglobulin light chains, glycosaminoglycans, and amyloid. *Cell Mol Life Sci,* 57**,** 441-9.

STIX, B., KAHNE, T., SLETTEN, K., RAYNES, J., ROESSNER, A. & ROCKEN, C. 2001. Proteolysis of AA amyloid fibril proteins by matrix metalloproteinases-1, -2, and -3. *Am J Pathol,* 159**,** 561-70.

STOPPINI, M., BELLOTTI, V., MANGIONE, P., MERLINI, G. & FERRI, G. 1997. Use of anti-(beta2 microglobulin) mAb to study formation of amyloid fibrils. *Eur J Biochem,* 249**,** 21-6.

STOPPINI, M., MANGIONE, P., MONTI, M., GIORGETTI, S., MARCHESE, L., ARCIDIACO, P., VERGA, L., SEGAGNI, S., PUCCI, P., MERLINI, G. & BELLOTTI, V. 2005. Proteomics of beta2-microglobulin amyloid fibrils. *Biochim Biophys Acta,* 1753**,** 23-33.

STORY, C. M., MIKULSKA, J. E. & SIMISTER, N. E. 1994. A major histocompatibility complex class I-like Fc receptor cloned from human placenta: possible role in transfer of immunoglobulin G from mother to fetus. *J Exp Med,* 180**,** 2377-81.

STURCHLER-PIERRAT, C., ABRAMOWSKI, D., DUKE, M., WIEDERHOLD, K. H., MISTL, C., ROTHACHER, S., LEDERMANN, B., BURKI, K., FREY, P., PAGANETTI, P. A., WARIDEL, C., CALHOUN, M. E., JUCKER, M., PROBST, A., STAUFENBIEL, M. & SOMMER, B. 1997. Two amyloid precursor protein transgenic mouse models with Alzheimer disease-like pathology. *Proc Natl Acad Sci U S A,* 94**,** 13287-92.

SULTAN, A., RAMAN, B., RAO CH, M. & TANGIRALA, R. 2013. The extracellular chaperone haptoglobin prevents serum fatty acid-promoted amyloid fibril formation of beta2-microglobulin, resistance to lysosomal degradation, and cytotoxicity. *J Biol Chem,* 288**,** 32326-42.

SUNDE, M., SERPELL, L. C., BARTLAM, M., FRASER, P. E., PEPYS, M. B. & BLAKE, C. C. 1997. Common core structure of amyloid fibrils by synchrotron X-ray diffraction. *J Mol Biol,* 273**,** 729-39.

SWAIN, S. L. 1983. T cell subsets and the recognition of MHC class. *Immunol Rev,* 74**,** 129-42.

TAGOE, C. E., REIXACH, N., FRISKE, L., MUSTRA, D., FRENCH, D., GALLO, G. & BUXBAUM, J. N. 2007. In vivo stabilization of mutant human transthyretin in transgenic mice. *Amyloid,* 14**,** 227-36.

TAKAHASHI, N., GLOCKNER, J., HOWE, B. M., HARTMAN, R. P. & KAWASHIMA, A. 2016. Taxonomy and Imaging Manifestations of Systemic Amyloidosis. *Radiol Clin North Am,* 54**,** 597-612.

TAKAOKA, Y., TASHIRO, F., YI, S., MAEDA, S., SHIMADA, K., TAKAHASHI, K., SAKAKI, Y. & YAMAMURA, K. 1997. Comparison of amyloid deposition in two lines of transgenic mouse that model familial amyloidotic polyneuropathy, type I. *Transgenic Res,* 6**,** 261-9.

TAKAYAMA, F., MIYAZAKI, S., MORITA, T., HIRASAWA, Y. & NIWA, T. 2001. Dialysis-related amyloidosis of the heart in long-term hemodialysis patients. *Kidney Int Suppl,* 78**,** S172-6.

TAKEDA, T., HOSOKAWA, M., HIGUCHI, K., HOSONO, M., AKIGUCHI, I. & KATOH, H. 1994. A novel murine model of aging, Senescence-Accelerated Mouse (SAM). *Arch Gerontol Geriatr,* 19**,** 185-92.

TAN, S. Y. & PEPYS, M. B. 1994. Amyloidosis. *Histopathology,* 25**,** 403-14.

TANSKANEN, M., PEURALINNA, T., POLVIKOSKI, T., NOTKOLA, I. L., SULKAVA, R., HARDY, J., SINGLETON, A., KIURU-ENARI, S., PAETAU, A., TIENARI, P. J. & MYLLYKANGAS, L. 2008. Senile systemic amyloidosis affects 25% of the very aged and associates with genetic variation in alpha2-macroglobulin and tau: a population-based autopsy study. *Ann Med,* 40**,** 232-9.

TAWARA, S., ARAKI, S., TOSHIMORI, K., NAKAGAWA, H. & OHTAKI, S. 1981. Amyloid fibril protein in type I familial amyloidotic polyneuropathy in Japanese. *J Lab Clin Med,* 98**,** 811-22.

TAWARA, S., NAKAZATO, M., KANGAWA, K., MATSUO, H. & ARAKI, S. 1983. Identification of amyloid prealbumin variant in familial amyloidotic polyneuropathy (Japanese type). *Biochem Biophys Res Commun,* 116**,** 880-8.

TEIXEIRA, A. C. & SARAIVA, M. J. 2013. Presence of N-glycosylated transthyretin in plasma of V30M carriers in familial amyloidotic polyneuropathy: an escape from ERAD. *J Cell Mol Med,* 17**,** 429-35.

TENG, M. H., YIN, J. Y., VIDAL, R., GHISO, J., KUMAR, A., RABENOU, R., SHAH, A., JACOBSON, D. R., TAGOE, C., GALLO, G. & BUXBAUM, J. 2001. Amyloid and nonfibrillar deposits in mice transgenic for wild-type human transthyretin: a possible model for senile systemic amyloidosis. *Lab Invest,* 81**,** 385-96.

TENNENT, G. A., LOVAT, L. B. & PEPYS, M. B. 1995. Serum amyloid P component prevents proteolysis of the amyloid fibrils of Alzheimer disease and systemic amyloidosis. *Proc Natl Acad Sci U S A,* 92**,** 4299-303.

TEPLOW, D. B. 1998. Structural and kinetic features of amyloid beta-protein fibrillogenesis. *Amyloid,* 5**,** 121-42.

THENAPPAN, T., FEDSON, S., RICH, J., MURKS, C., HUSAIN, A., POGORILER, J. & ANDERSON, A. S. 2014. Isolated heart transplantation for familial transthyretin (TTR) V122I cardiac amyloidosis. *Amyloid,* 21**,** 120-3.

THYLEN, C., WAHLQVIST, J., HAETTNER, E., SANDGREN, O., HOLMGREN, G. & LUNDGREN, E. 1993. Modifications of transthyretin in amyloid fibrils: analysis of amyloid from homozygous and heterozygous individuals with the Met30 mutation. *EMBO J,* 12**,** 743-8.

TILGHMAN, S. M. & BELAYEW, A. 1982. Transcriptional control of the murine albumin/alpha-fetoprotein locus during development. *Proc Natl Acad Sci U S A,* 79**,** 5254-7.

TONG, W., TAUROG, A. & CHAIKOFF, I. L. 1951. Non-thyroglobulin iodine of the thyroid gland. I. Free thyroxine and diiodotyrosine. *J Biol Chem,* 191**,** 665-75.

TSOMIDES, T. J., WALKER, B. D. & EISEN, H. N. 1991. An optimal viral peptide recognized by CD8+ T cells binds very tightly to the restricting class I major histocompatibility complex protein on intact cells but not to the purified class I protein. *Proc Natl Acad Sci U S A,* 88**,** 11276-80.

VALLEIX, S., GILLMORE, J. D., BRIDOUX, F., MANGIONE, P. P., DOGAN, A., NEDELEC, B., BOIMARD, M., TOUCHARD, G., GOUJON, J. M., LACOMBE, C., LOZERON, P., ADAMS, D., LACROIX, C., MAISONOBE, T., PLANTE-BORDENEUVE, V., VRANA, J. A., THEIS, J. D., GIORGETTI, S., PORCARI, R., RICAGNO, S., BOLOGNESI, M., STOPPINI, M., DELPECH, M., PEPYS, M. B., HAWKINS, P. N. & BELLOTTI, V. 2012. Hereditary systemic amyloidosis due to Asp76Asn variant beta2-microglobulin. *N Engl J Med,* 366**,** 2276-83.

VAN BENNEKUM, A. M., WEI, S., GAMBLE, M. V., VOGEL, S., PIANTEDOSI, R., GOTTESMAN, M., EPISKOPOU, V. & BLANER, W.

S. 2001. Biochemical basis for depressed serum retinol levels in transthyretin-deficient mice. *J Biol Chem,* 276**,** 1107-13.

VARGA, J., FLINN, M. S., SHIRAHAMA, T., RODGERS, O. G. & COHEN, A. S. 1986. The induction of accelerated murine amyloid with human splenic extract. Probable role of amyloid enhancing factor. *Virchows Arch B Cell Pathol Incl Mol Pathol,* 51**,** 177-85.

VEMBAR, S. S. & BRODSKY, J. L. 2008. One step at a time: endoplasmic reticulum-associated degradation. *Nat Rev Mol Cell Biol,* 9**,** 944-57.

VERDONE, G., CORAZZA, A., VIGLINO, P., PETTIROSSI, F., GIORGETTI, S., MANGIONE, P., ANDREOLA, A., STOPPINI, M., BELLOTTI, V. & ESPOSITO, G. 2002. The solution structure of human beta2-microglobulin reveals the prodromes of its amyloid transition. *Protein Sci,* 11**,** 487-99.

VRANA, J. A., GAMEZ, J. D., MADDEN, B. J., THEIS, J. D., BERGEN, H. R., 3RD & DOGAN, A. 2009. Classification of amyloidosis by laser microdissection and mass spectrometry-based proteomic analysis in clinical biopsy specimens. *Blood,* 114**,** 4957-9.

WALLACE, M. R., DWULET, F. E., CONNEALLY, P. M. & BENSON, M. D. 1986. Biochemical and molecular genetic characterization of a new variant prealbumin associated with hereditary amyloidosis. *J Clin Invest,* 78**,** 6-12.

WALSH, D. M., HARTLEY, D. M., KUSUMOTO, Y., FEZOUI, Y., CONDRON, M. M., LOMAKIN, A., BENEDEK, G. B., SELKOE, D. J. & TEPLOW, D. B. 1999. Amyloid beta-protein fibrillogenesis. Structure and biological activity of protofibrillar intermediates. *J Biol Chem,* 274**,** 25945-52.

WALSH, D. M., KLYUBIN, I., FADEEVA, J. V., CULLEN, W. K., ANWYL, R., WOLFE, M. S., ROWAN, M. J. & SELKOE, D. J. 2002. Naturally secreted oligomers of amyloid beta protein potently inhibit hippocampal long-term potentiation in vivo. *Nature,* 416**,** 535-9.

WALSH, D. M., LOMAKIN, A., BENEDEK, G. B., CONDRON, M. M. & TEPLOW, D. B. 1997. Amyloid beta-protein fibrillogenesis. Detection of a protofibrillar intermediate. *J Biol Chem,* 272**,** 22364-72.

WANG, H. Z., PENG, Z. Y., WEN, X. Y., RIMMELE, T., BISHOP, J. V. & KELLUM, J. A. 2011. N-acetylcysteine is effective for prevention but not for treatment of folic acid-induced acute kidney injury in mice. *Crit Care Med,* 39**,** 2487-94.

WECHALEKAR, A., WHELAN, C., LACHMANN, H., FONTANA, M., MAHMOOD, S., GILLMORE, J. & HAWKINS, P. 2015. Oral Doxycycline Improves Outcomes of Stage III AL Amyloidosis - a Matched Case Control Study. *Blood,* 126**,** 732.

WECHALEKAR, A. D., GILLMORE, J. D. & HAWKINS, P. N. 2016. Systemic amyloidosis. *Lancet,* 387**,** 2641-54.

WECHALEKAR, A. D., SCHONLAND, S. O., KASTRITIS, E., GILLMORE, J. D., DIMOPOULOS, M. A., LANE, T., FOLI, A., FOARD, D., MILANI, P., RANNIGAN, L., HEGENBART, U., HAWKINS, P. N., MERLINI, G. & PALLADINI, G. 2013. A European collaborative study of treatment outcomes in 346 patients with cardiac stage III AL amyloidosis. *Blood,* 121**,** 3420-7.

WEISS, B. M., WONG, S. W. & COMENZO, R. L. 2016. Beyond the plasma cell: emerging therapies for immunoglobulin light chain amyloidosis. *Blood,* 127**,** 2275-80.

WESTERMARK, P., SLETTEN, K., JOHANSSON, B. & CORNWELL, G. G., 3RD 1990. Fibril in senile systemic amyloidosis is derived from normal transthyretin. *Proc Natl Acad Sci U S A,* 87**,** 2843-5.

WESTERMARK, P., SLETTEN, K. & JOHNSON, K. H. 1996. Ageing and amyloid fibrillogenesis: lessons from apolipoprotein AI, transthyretin and islet amyloid polypeptide. *Ciba Found Symp,* 199**,** 205-18; discussion 218-22.

WESTERMARK, P. & STENKVIST, B. 1973. A new method for the diagnosis of systemic amyloidosis. *Arch Intern Med,* 132**,** 522-3.

WHITELAW, C. B., ARCHIBALD, A. L., HARRIS, S., MCCLENAGHAN, M., SIMONS, J. P. & CLARK, A. J. 1991. Targeting expression to the mammary gland: intronic sequences can enhance the efficiency of gene expression in transgenic mice. *Transgenic Res,* 1**,** 3-13.

WILLERSON, J. T., GORDON, J. K., TALAL, N. & BARTH, W. F. 1969. Murine amyloid. II. Transfer of an amyloid-accelerating substance. *Arthritis Rheum,* 12**,** 232-40.

WISNIEWSKI, T. & FRANGIONE, B. 1992. Apolipoprotein E: a pathological chaperone protein in patients with cerebral and systemic amyloid. *Neurosci Lett,* 135**,** 235-8.

WOEBER, K. A. & INGBAR, S. H. 1968. The contribution of thyroxine-binding prealbumin to the binding of thyroxine in human serum, as assessed by immunoadsorption. *J Clin Invest,* 47**,** 1710-21.

XU, Y., SCHNORRER, P., PROIETTO, A., KOWALSKI, G., FEBBRAIO, M. A., ACHA-ORBEA, H., DICKINS, R. A. & VILLADANGOS, J. A. 2011. IL-10 controls cystatin C synthesis and blood concentration in response to inflammation through regulation of IFN regulatory factor 8 expression. *J Immunol,* 186**,** 3666-73.

YAMADA, T., LIEPNIEKS, J. J., KLUVE-BECKERMAN, B. & BENSON, M. D. 1995. Cathepsin B generates the most common form of amyloid A (76 residues) as a degradation product from serum amyloid A. *Scand J Immunol,* 41**,** 94-7.

YAMAMOTO, S. & GEJYO, F. 2005. Historical background and clinical treatment of dialysis-related amyloidosis. *Biochim Biophys Acta,* 1753**,** 4-10.

YAMASHITA, T., ANDO, Y., OKAMOTO, S., MISUMI, Y., HIRAHARA, T., UEDA, M., OBAYASHI, K., NAKAMURA, M., JONO, H., SHONO, M., ASONUMA, K., INOMATA, Y. & UCHINO, M. 2012. Long-term survival after liver transplantation in patients with familial amyloid polyneuropathy. *Neurology,* 78**,** 637-43.

YAMASHITA, T., HAMIDI ASL, K., YAZAKI, M. & BENSON, M. D. 2005. A prospective evaluation of the transthyretin Ile122 allele frequency in an African-American population. *Amyloid,* 12**,** 127-30.

YERBURY, J. J., POON, S., MEEHAN, S., THOMPSON, B., KUMITA, J. R., DOBSON, C. M. & WILSON, M. R. 2007. The extracellular chaperone clusterin influences amyloid formation and toxicity by interacting with prefibrillar structures. *FASEB J,* 21**,** 2312-22.

YERBURY, J. J., RYBCHYN, M. S., EASTERBROOK-SMITH, S. B., HENRIQUES, C. & WILSON, M. R. 2005. The acute phase protein haptoglobin is a mammalian extracellular chaperone with an action similar to clusterin. *Biochemistry,* 44**,** 10914-25.

YEWDELL, J. W., ANTON, L. C. & BENNINK, J. R. 1996. Defective ribosomal products (DRiPs): a major source of antigenic peptides for MHC class I molecules? *J Immunol,* 157**,** 1823-6.

YI, S., TAKAHASHI, K., NAITO, M., TASHIRO, F., WAKASUGI, S., MAEDA, S., SHIMADA, K., YAMAMURA, K. & ARAKI, S. 1991. Systemic amyloidosis in transgenic mice carrying the human mutant transthyretin (Met30) gene. Pathologic similarity to human familial amyloidotic polyneuropathy, type I. *Am J Pathol,* 138**,** 403-12.

YILMAZ, B., KOKLU, S., YUKSEL, O. & ARSLAN, S. 2014. Serum beta 2-microglobulin as a biomarker in inflammatory bowel disease. *World J Gastroenterol,* 20**,** 10916-20.

YUAN, H. T., LI, X. Z., PITERA, J. E., LONG, D. A. & WOOLF, A. S. 2003. Peritubular capillary loss after mouse acute nephrotoxicity correlates with down-regulation of vascular endothelial growth factor-A and hypoxia-inducible factor-1 alpha. *Am J Pathol,* 163**,** 2289-301.

ZHANG, P., FU, X., SAWASHITA, J., YAO, J., ZHANG, B., QIAN, J., TOMOZAWA, H., MORI, M., ANDO, Y., NAIKI, H. & HIGUCHI, K. 2010. Mouse model to study human A beta2M amyloidosis: generation of a transgenic mouse with excessive expression of human beta2-microglobulin. *Amyloid,* 17**,** 50-62.

ZHAO, G., LI, Z., ARAKI, K., HARUNA, K., YAMAGUCHI, K., ARAKI, M., TAKEYA, M., ANDO, Y. & YAMAMURA, K. 2008. Inconsistency between hepatic expression and serum concentration of transthyretin in mice humanized at the transthyretin locus. *Genes Cells,* 13**,** 1257-68.

ZIJLSTRA, M., BIX, M., SIMISTER, N. E., LORING, J. M., RAULET, D. H. & JAENISCH, R. 1990. Beta 2-microglobulin deficient mice lack CD4-8+ cytolytic T cells. *Nature,* 344**,** 742-6.

ZINGRAFF, J. J., NOEL, L. H., BARDIN, T., ATIENZA, C., ZINS, B., DRUEKE, T. B. & KUNTZ, D. 1990. Beta 2-microglobulin amyloidosis in chronic renal failure. *N Engl J Med,* 323**,** 1070-1.